Chemical Engineering Methods and Technology

Chemistry and Chemical Engineering Research Progress

A. K. Haghi
Editor

NOVA

CHEMICAL ENGINEERING METHODS AND TECHNOLOGY

CHEMISTRY AND CHEMICAL ENGINEERING RESEARCH PROGRESS

CHEMICAL ENGINEERING METHODS AND TECHNOLOGY

Additional books in this series can be found on Nova's website under the Series tab.

Additional E-books in this series can be found on Nova's website under the E-books tab.

CHEMICAL ENGINEERING METHODS AND TECHNOLOGY

CHEMISTRY AND CHEMICAL ENGINEERING RESEARCH PROGRESS

A.K. HAGHI
EDITOR

Nova Science Publishers, Inc.
New York

LIBRARY OF CONGRESS CATALOGING-IN-PUBLICATION DATA
Chemistry and chemical engineering research progress / editor, A.K. Haghi.
p. cm.
Includes index.
ISBN 978-1-61942-237-7 (eBook)
1. Composite materials. 2. Chemistry. 3. Chemical engineering. I.
Haghi, A. K.
TA418.9.C6C444 2009
660--dc22
2010015594

Published by Nova Science Publishers, Inc. ✣ New York

CONTENTS

PREFACE

The collection of topics in this book aims to reflect the diversity of recent advances in chemistry and chemical engineering with a broad perspective which may be useful for scientists as well as for graduate students and engineers. This new book presents leading-edge research from around the world in this dynamic field.

Diverse topics published in this book are the original works of some of the brightest and well-known international scientists.

The book offers scope for academics, researchers, and engineering professionals to present their research and development works that have potential for applications in several disciplines of engineering and science. Contributions ranged from new methods to novel applications of existing methods to gain understanding of the material and/or structural behavior of new and advanced systems.

Contributions are sought from many areas of science and engineering in which advanced methods are used to formulate (model) and/or analyze the problem. In view of the different background of the expected audience, readers are requested to focus on the main ideas, and to highlight as much as possible the specific advantages that arise from applying modern ideas. A chapter may therefore be motivated by the specific problem, but just as well by the advanced method used which may be more generally applicable.

I would like to express my deep appreciation to all the authors for their outstanding contribution to this book and to express my sincere gratitude for their generosity. All the authors eagerly shared their experiences and expertise in this new book. Special thanks go to the referees for their valuable work.

Professor A. K. HAGHI
Montréal, CANADA
Haghi@Canada.com

In: Chemistry and Chemical Engineering Reserch Progress ISBN: 978-1-61668-502-7
Editor: A.K. Haghi

Chapter 1

USING ACCELERATED AGEING PROCESS TO PREDICT THE ARCHIVAL LIFE OF CELLULOSE NITRATE BASED MATERIALS AND HISTORICAL OBJECTS

A. Hamrang*
Consultant to the Polymeric Industries, England, UK

ABSTRACT

Accelerated ageing process was used to estimate the useful lives of cellulose nitrate based materials in archival conditions. Samples in glass containers were aged at 15-50% relative humidity conditions and at different temperatures. The extent of degradation was measured by the time for cellulose nitrate to lose 20% of its relative viscosity. The data obtained were plotted against the reciprocal temperature using the Arrhenius relationship. Extrapolation of the data to room temperature (20^oC) gave approximate archival lives of samples. Even at temperatures below their second glass transition temperatures (T_g), cellulose nitrates deteriorated significantly in humid environments; the degree of which depended on the level of humidity. The importance of these results in relation to the archival conditions is discussed.

INTRODUCTION

Problems regarding decomposition of cellulose nitrate based historical objects in museums and various collections are quite serious. These problems are characterised by the release of plasticiser deposits on the surface of objects as well as loss of colour, surface crazing, etc. The loss of plasticiser is evident as a heavy liquid / crystalline deposit.

The properties and applications of the cellulose nitrate materials are dependent on their degrees of nitration. For plastic grade nitrates [1], the nitrogen content is between 10.7-11.1 percent and their degrees of esterification are between 1.9-2.0. Cellulose nitrate with a nitrogen content of less than 11.1 percent is the least flammable and is used for production of

* Email: hamrang1@yahoo.com

celluloid. Celluloid is the cellulose nitrate which is plasticized with camphor. Celluloid was the first man made plastic to be used by artists [2]. The first recorded use of celluloid in sculpture (Constructed Head No.3, 1917-20) is now in the Museum of Modern Art, New York. The most popular period of use for celluloid was between 1900-1935. The material was used because of its characteristics such as rigidity, toughness, transparency of basic composition as well as forming multi coloured sheets. The history of celluloid invention and usage are described elsewhere [3-4].

Several studies have been carried out on the decomposition of cellulose nitrates at elevated temperatures [5-7] and a few of them with emphasis on hydrolysis [8-9]. However these studies have been carried out mainly at high temperatures (>100^{o}C) which museum objects and other collections will not be kept at. The thermal sensitivity of nitrate esters is such that they are readily cleaved at ambient temperatures to generate nitrogen oxide. Nitrogen oxide is highly oxidising and an odd electron molecule which can initiate highly exothermic, free radical reactions [10]. This oxidising atmosphere will result in the production of carboxylic acid groups which may then undergo oxidative decarboxylation, particularly in the presence of metal ions.

Due to thermal sensitivity of cellulose nitrates, in this work accelerated ageing was carried out at temperatures below 90^{o}C (i.e. 50-80^{o}C) and at four different levels of humidity (i.e. 15-50%). The effect of ageing process on samples was monitored by viscometric analyses.

EXPERIMENTAL

Materials

The original samples used in this work were in the form of uniform plastic sheet of tortoiseshell effect and 1.2 mm in thickness. No information was available on the history of production or the plasticizer used in the sample. No visible signs of degradation such as stickiness, surface crazing, loss of colour or odour were noticed. The original samples were characterised by various methods. Direct solution method [11] was used to isolate the plasticiser from the polymer matrix and analysed. The plasticizer content was measured at about 29% which is a usual amount for fabricated cellulose nitrate materials. FTIR studies revealed that natural camphor was the plactiser used for these samples. The second glass transition temperature (T_g) of the samples was also measured by Differential Scanning Calorimetry (DSC) technique, which was found to be about 53^{o}C. This corresponded well with the T_g of undegraded cellulose nitrate materials mentioned in references [12].

Ageing Conditions

The samples were aged in all glass containers with the desired environments simulated within them. The ageing processes were carried out at temperatures of 50, 60, 70, 80^{o}C and

in15, 30, 40, 50% relative humidity conditions. The samples were taken out periodically for analysis.

Viscometry

Viscometric analyses were carried out for the original samples and the aged samples in order to examine if degradation is taking place and at what rate. Viscometric measurements were performed by determining the flow times using an Ostwald Viscometer type BS/U/M2. Flow times of a fixed volume of both a polymer solution and pure solvent were determined from which the relative viscosity could be found. A 1% solution of cellulose nitrate sample in acetone was prepared, for all viscometric analyses. All the calculations are based on the average of 3 tests for each sample. A modified Arrhenius approach was adopted and the time taken for 20% loss in relative viscosity determined rather than a rate constant.

RESULTS AND DISCUSSION

Arrhenius Treatment

In order to extrapolate the high temperature ageing results to normal archival conditions the data were treated by the Arrhenius approach. The rate constant for a first order reaction from classical kinetics is given by:

$$K = \frac{2.3}{t}\log\left[\frac{a}{a-x}\right]$$

Here 'a' is the initial concentration of the reactant and 'x' is the decrease in the concentration of the reactant after time 't'. It is assumed that the reaction is first order [13-14]. In this work 'a' is the initial physical property of the sample (viscosity retention), 'a-x' is the remaining property after a given time, 't'. The rate constant for a first order reaction can be calculated from the time required for the property to decrease to half the original value (half-time life, t_{half}) by the equation shown below.

$$t_{\text{half}} = \frac{2.3\log 2}{K}$$

Using Arrhenius relationship, extrapolation of the reaction rates to other temperatures can be made as shown below.

$$\frac{d\ \ln K}{d\ T} = \frac{E}{RT^2}$$

where '*E*' is the activation energy, '*T*' is the absolute temperature and '*R*' is the gas constant. The rate constants obtained at two or more temperatures are plotted as ln *K* against $\frac{1}{T}$. In this way a straight line is obtained which then it can be extrapolated to the desired temperature.

Archival Predictions

Figures 1 to 4 show the times for a 20% loss in relative viscosity of cellulose nitrate materials at a series of elevated temperatures (50-80^{o}C). In these figures reciprocal temperatures were plotted versus number of days taken for a sample to lose 20% of its original relative viscosity value at a particular relative humidity condition. Reciprocal temperatures were calculated as (1 / T+273) where T is the four ageing temperatures of 50, 60, 70 and 80^{o}C. At each relative humidity condition and at each ageing temperature one value was obtained for example in Figure 1, at 15% relative humidity and at 50, 60, 70, 80^{o}C, it took 111, 56, 20 and 5 days respectively for nitrates to lose 20% of their relative viscosity values. For Figures 2 to 4 the same procedures were followed.

Prediction of life under archival conditions can be made by extrapolating the plots. Figures 1 to 4 examine the effects of ageing on cellulose nitrate materials at 15, 30, 40 and 50% relative humidity conditions, respectively. Linear plots were obtained and as expected the rate of degradation increasing with increasing temperatures. One significant result is that the degradation rate is greater at higher humidity levels. This effectively illustrates the hydrolytic effect of moisture in the degradation mechanism even at a relatively lower temperature of 50^{o}C. It is evident that changes took place in the polymer structure as a result of exposure to different temperatures and humidity levels.

Temperatures greater than 50^{o}C are likely to be above the T_g of cellulose nitrate materials. Above the T_g penetration of moisture into the polymer structure will occur more easily. In addition the T_g of cellulose nitrate polymer will be lower in the presence of moisture due to the swelling of the polymer. This will facilitate the penetration of water and its chemical reaction with the polymer.

From the data, it is possible to determine the approximate lifetime for cellulose nitrate made objects through modification of the Arrhenius expression assuming that the rate of degradation follows the first order kinetics. It should be pointed out that the rate controlling step in the degradation of the plastic grade nitrates may be more complex than first order as there may be interactions between the main polymer and the additives used. In this work the time taken for the nitrate samples to achieve 20% loss in relative viscosity are plotted against the reciprocal temperature in K and the data extrapolated to 20^{o}C (i.e. $\frac{1}{273+20} = 0.0034$). The least squares method was used in each case to obtain the best fit for the points.

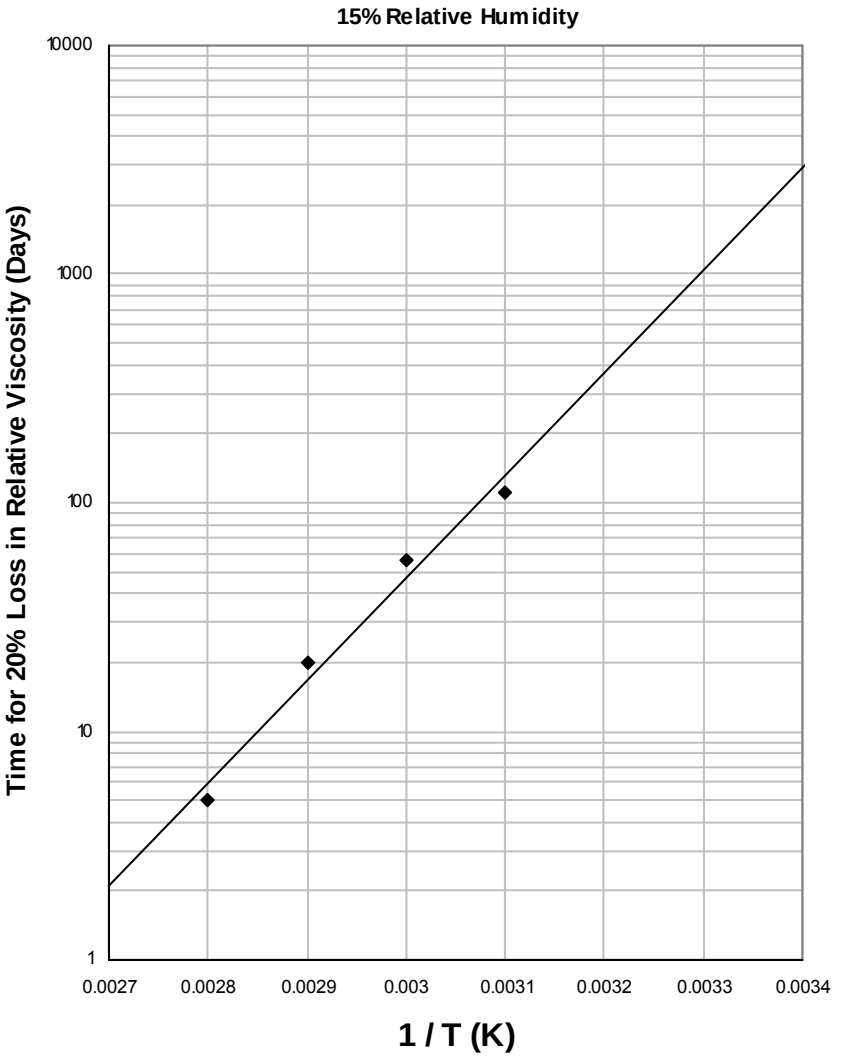

Figure 1. Time for 20% loss in relative viscosity of cellulose nitrates versus the reciprocal temperature of ageing (K) at 15% relative humidity condition.

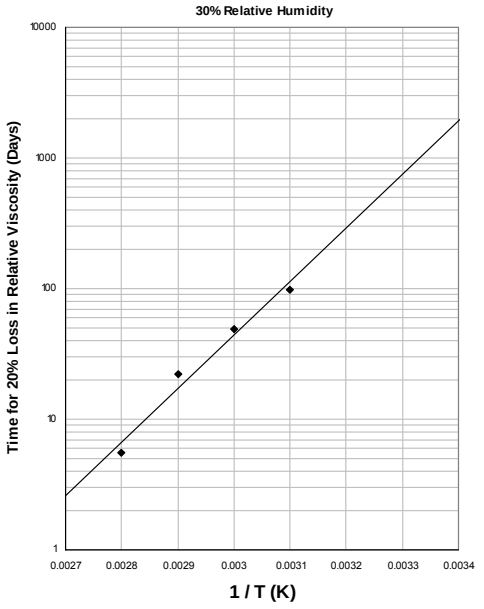

Figure 2. Time for 20% loss in relative viscosity of cellulose nitrates versus the reciprocal temperature of ageing (K) at 30% relative humidity condition.

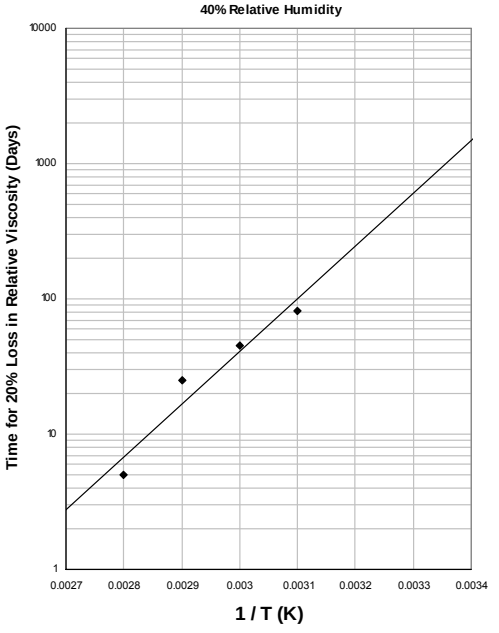

Figure 3. Time for 20% loss in relative viscosity of cellulose nitrates versus the reciprocal temperature of ageing (K) at 40% relative humidity condition.

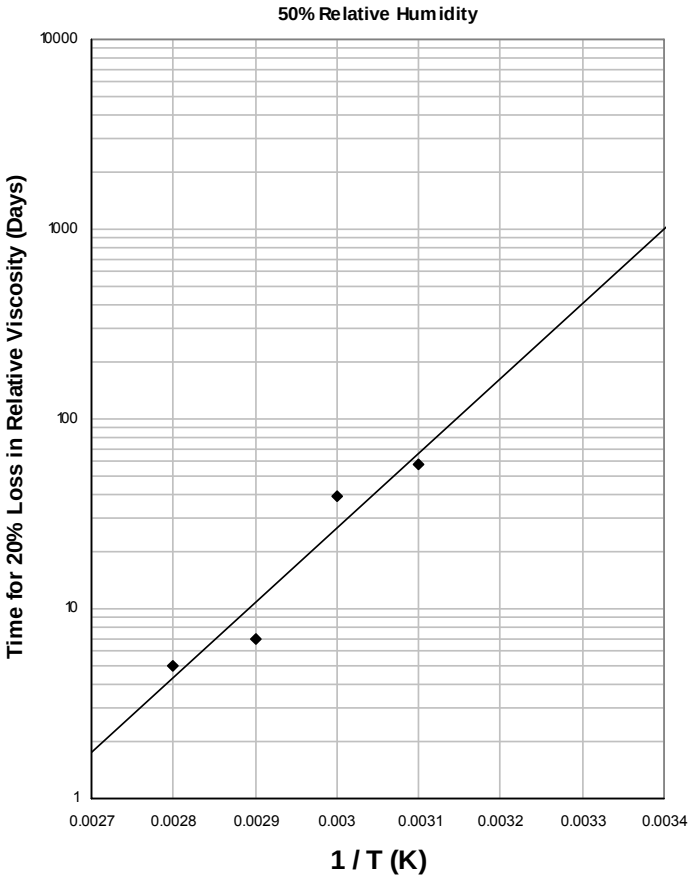

Figure 4. Time for 20% loss in relative viscosity of cellulose nitrates versus the reciprocal temperature of ageing (K) at 50% relative humidity condition.

From figures 1 to 4, it is estimated that at 20^{o}C (0.0034 on X axis), the cellulose nitrate based object will lose 20% of its property after 8.22, 5.45, 4.11 and 2.74 years at 15, 30, 40 and 50% relative humidity conditions, respectively. According to the above data, it is clear that cellulose nitrate polymers are sensitive to temperature. Humidity also affects cellulose nitrate materials even at ambient temperatures.

CONCLUSION

The conditions that the cellulose nitrate based objects are kept in play a vital role in their archival longevity. By means of accelerated ageing trials, the useful lives of these objects can be estimated. Predicting the archival lives of cellulose nitrate objects by using modified Arrhenius expression can only be taken as approximations. Whilst considering the effect of plasticizer and the environmental conditions, accelerated ageing results indicated that

humidity plays an important part in the degradation process of cellulose nitrate based materials and objects. As the level of humidity increased, degradation process occurred at a faster rate. Therefore, according to the data obtained in this study, it would be necessary to minimise the level of humidity as low as possible in order to prolong the useful life of the cellulose nitrate based objects in actual archival conditions.

REFERENCES

[1] Saunders, K. J., Organic Polymer Chemistry, Chapman & Hall Ltd., 1973, P255.
[2] Katz, S., Plastics / Designs and Materials, Macmillan Publishing Co. Inc., 1978, P42-44.
[3] Kaufman, M., The first Century of Plastics, Crown Press, 1963.
[4] Worden, E. C., Nitrocellulose Industry, Van Nostrand, Vols. 1 and 2, 1911.
[5] Philips, L., *Nature*, 160, 753, (1947)
[6] Miles, F. D., Cellulose Nitrate, *Interscience*, 1955, P253.
[7] Adams, G. K., and Bawn, C. E. H., The Homogeneous Decomposition of Ethyl Nitrate, Transactions of the Faraday Society, 45, (1949), P494.
[8] Miles, F. D., Cellulose Nitrate, Oliver & Boyd, 1955, P286.
[9] Ott, E., Spurlin, H. M., and Grafflin, M. W., Cellulose and Cellulose Deravatives, 2nd ed., Part II, Interscience Publishers, 1954, P1052.
[10] Miles, F. D., Cellulose Nitrate, Oliver & Boyd, 1955, P263-4.
[11] Crompton, T. R. Chemical Analysis of Additives in Plastics, 2nd ed., Pergamon Press, 1977, Chapter 1.
[12] Brydson, J. A., Plastic Materials, 3rd ed., Butterworth Group, 1975, P493-494.
[13] Adelstein, P. Z., McCrea, J. L., *J. Soc. Photog. Sci and Eng*., 7, (1981), 6.
[14] Ram, A. T., McCrea, J. L., Presented at the 129th SMPTE Technical Conference, Los Angeles, CA, (1987).

In: Chemistry and Chemical Engineering Reserch Progress ISBN: 978-1-61668-502-7
Editor: A.K. Haghi

Chapter 2

DEGRADATION STUDIES OF CELLULOSE ESTERS USING PEAK RATIO MEASUREMENT TECHNIQUE

A. Hamrang*
ASenior Consultant of Polymer Industries,
4 Heswall Avenue, Withington, Manchester, M20 3ER, UK

ABSTRACT

Aspects of degradation of plastic grade cellulose esters have been investigated with work concentrating on cellulose nitrate and cellulose acetate. The original samples were characterized and used as controls for subsequent ageing studies. Relative rates of degradation for samples aged in various temperatures and relative humidities were evaluated using FTIR studies, with emphasis on Peak Ratio Measurements (PRM) technique. In this study for nitrates the peak ratios corresponding to C=O (1730 cm^{-1}) / NO_2 (1650 cm^{-1}) and OH (3400 cm^{-1}) / NO_2 (1650 cm^{-1}) were measured. For acetates C=O (1750 cm^{-1}) / CH_3 (1370 cm^{-1}) and OH (3490 cm^{-1}) / CH_3 (2935 cm^{-1}) were measured. The results obtained from this technique along with visual observations of samples indicated that the rate of deacetylation / denitration (de-esterification) depended on moisture concentration. These reactions are largely characteristics of surrounding relative humidity and temperature of cellulose esters. The results indicated that for nitrates, denitration is accompanied by the formation of carbonyl impurities whilst for acetates carbonyl impurities and deacetylation did not occur together and deacetylation is the major process of degradation.

INTRODUCTION

Plastic grade cellulose esters are susceptible to degrading processes as a consequence of the chemical nature of the cellulose chain molecules and the substituents along the chain. The rate of degradation is dependent upon the type and degree of substitution of the individual polymer. Primary decomposition processes slowly produce degradation products and if they

* Email: hamrang1@yahoo.com

are not removed, they can (catalytically) cause a faster and more extensive degradation. Autocatalytic oxidation and hydrolysis reactions occur in cellulose esters. For cellulose nitrates, it has been suggested that auto-oxidation is the more likely degradation mechanism. [1] They are readily cleaved at ambient temperatures to generate nitrogen oxide, which is highly oxidising and acts as an odd electron molecule capable of initiating highly exothermic free radical reactions. It is indicated in some other studies [2-4] that the highly oxidising atmosphere produced by the release of nitrogen oxide will eventually result in the production of carboxylic acid groups and these can undergo oxidative decarboxylation, particularly in the presence of metal ions. Although degradation would proceed faster in the presence of oxygen than in an inert atmosphere, the change of atmosphere would have no influence on the nature of volatile products.

In contrast to cellulose nitrates, cellulose acetates are much more stable to thermal degradation. Cellulose acetate is quite resistant to oxidative degradation, even at rather high temperature of 90^{o}C, but if the temperature is sufficiently high, for instance 160^{o}C, then it will oxidise and as a result, a loss of strength, change of colour and solubility changes occur. [5]. Various studies [6-9] have indicated that primary decomposition products are environmentally dependent. In the presence of oxygen a different degradation mechanism is involved, since the first evolved degradation product in air is carbon dioxide, but in inert atmosphere (i.e. Helium), it is acetic acid.

The reaction of cellulose acetate with acetic acid and water has been investigated and the results showed a slow and complex reaction of two simultaneous reversible second order processes taking place. [10] It was concluded that in the system, degradation occur as a result of acetic acid hydrolysis. It was also found that the rate of the reaction is temperature dependent and under ambient conditions the acetylation of the C6 acetyl group in the polymer chain is one of the primary decomposition processes.

Most of the degradation studies carried out by various researchers on cellulose esters are at temperatures above 100^{o}C. In view of this finding, degradation studies in this work were carried out at temperatures near the T_g of the samples (i.e. 50-60^{o}C for nitrates and 100^{o}C for acetate samples) and at 0, 100% humidities. The effect of degradation on samples was monitored by FTIR using PRM technique.

EXPERIMENTAL

Materials

The original samples used in this work included fabricated cellulose nitrate (CN, manufacturer not known) and cellulose acetate (CA, manufactured by Courtaulds, UK) plastic sheets, with no visible signs of degradation on them. The thickness of CN and CA sheets was measured at 1.2 and 3 mm respectively. The original samples were characterized and used as controls for subsequent ageing processes.

Ageing Conditions

Strips of samples were aged in all glass containers with the desired environments simulated within them. Anhydrous calcium chloride and distilled water were used to produce 0% and 100% relative humidity (RH) conditions, respectively. The lids were put on tightly and the containers then placed in constant temperature ovens at 50-60^{o}C for CN and 100^{o}C for CA samples. Samples were taken out periodically and analysed.

Sample Characterization

All control samples were found to be soluble in acetone. Later on it was revealed that severely degraded samples particularly those aged in high humidity and temperatures became insoluble in acetone. Differential Scanning Calorimetry (DSC) was used to measure the second glass transition temperature (T_g) of the control samples in air. A Mettler furnace with a TC10TA processor was used for this purpose (a sample of about 20mg was used at a constant rate of 15^{o}C). In these analyses, the T_g of CN and CA control samples were measured at 53^{o}C and 117^{o}C, respectively which corresponded well with the figures reported in references [11-12] for undegraded samples. FTIR spectroscopy was also used for characterizing samples, the details of which are described below.

FTIR Analyses – PRM Technique

All control and aged samples were dissolved in acetone and thin films cast at < 0.01 mm thickness. A Nicolet Magna 560 FTR Spectrometer was used to record all spectra (spectra obtained using 64 scans at a resolution of 4 cm^{-1}). The effects of ageing on samples were monitored by FTIR-PRM technique and the changes, which took place, were recorded. The affected bands of the aged samples were compared against the control samples. In this technique, peak heights were measured, because if bands overlap, using peak heights may give more reproducible results since only the centre positions of the bands are used.

RESULTS AND DISCUSSION

There are several regions of interest in the characteristic transmittance bands at 4000-400 cm^{-1} for CN and CA samples. These bands occurred mainly due to the vibrations produced by the cellulose ring, ether linkages and substituent groups, details of which are discussed elsewhere. [13] A few of these regions are of prime importance with respect to degradation. These are associated with denitration / deacetylation (de-esterification) reactions. For CN samples, these IR regions correspond to C6-nitroester (NO_2; at 1650 cm^{-1}), carbonyl impurities (C=O at 1730 cm^{-1}) and OH (at 3400 cm^{-1}) vibrations. For CA samples these regions of interest correspond to CH_3 (of $COCH_3$ occurring at 1370 cm^{-1}, 2935 cm^{-1}), (C=O at 1750 cm^{-1}) and (OH at 3490 cm^{-1}).

In this study for nitrates, the peaks which corresponded to C=O / NO_2 and OH / NO_2 ratios were chosen for measurement. For acetates peak ratios of OH / CH_3 and C=O / CH_3 were measured. Figures 1 to 5 show the results of peak ratio measurements carried out for CN and CA samples aged in both dry and humid conditions at various temperatures. Figures 1 and 2 examine the effects of ageing on CA samples at 0, 100% relative humidity (RH) and 100^{o}C.

The results in Figure 1 corresponding to peak ratio OH / CH_3 for CA samples showed a progressive increase in values as the severity of ageing process increased. This could be due to the formation of acetic acid (CH_3COOH) inside the ageing containers. The rate of acid formation occurred at a faster rate in humid conditions. This was also evident by the strong vinegary smell detected for acetate samples, particularly for those aged in humid environments. As a result of this very rapid reaction, the samples aged in humid conditions became insoluble in acetone in a much shorter period (i.e. about 20 weeks), compared with those aged in dry conditions (i.e. more than 80 weeks). The most significant result here is that the degradation rate is greater at 100% RH, rather than 0% RH and effectively illustrates the hydrolytic effect of moisture in the degradation mechanism.

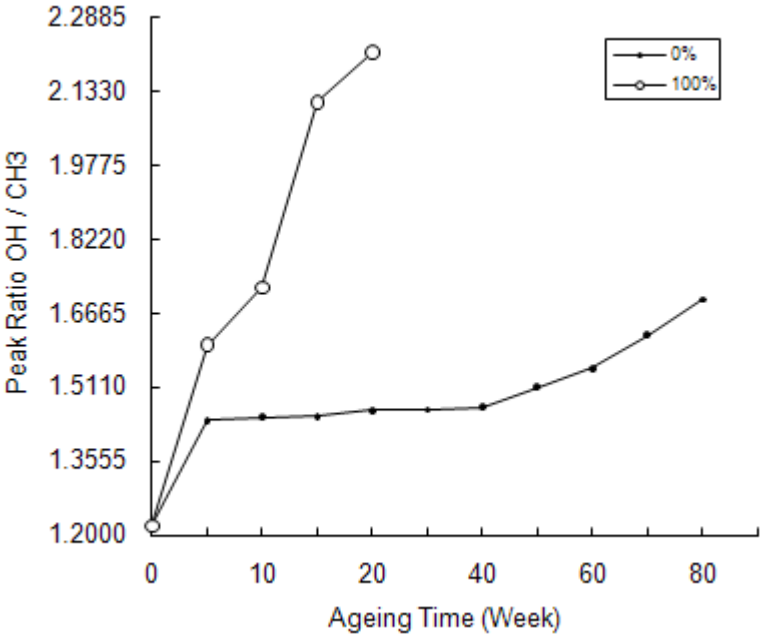

Figure 1. Values measured for peak ratio of OH / CH_3 versus ageing time for CA samples aged at 0, 100^{o}C & 0% RH.

The results of measurements for peak ratio of C=O / CH_3 are presented in Figure 2. These results indicated that as the ageing time increased the measured values decreased. This may indicate that carbonyl impurities are not formed in this case. Also these results may be the indication that the losses in acetyl groups may be occurring as a result of deacetylation. This could also indicate that deacetylation and the formation of carbonyl impurities may not be happening together and deacetylation is the major degradation process.

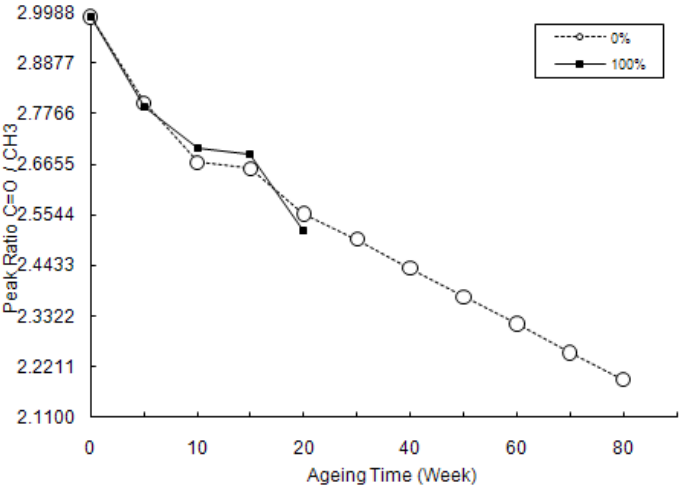

Figure 2. Values measured for peak ratio C=O / CH_3 versus ageing time for CA samples aged at 100°C & 0% and 100% RH.

Figures 3 to 5 examine the effects of ageing on CN samples at 0, 100% relative humidity and 50-60°C. Figures 3 and 5 show the results of the measurements carried out for the OH / NO_2 ratio. Figure 3 shows the effect of temperature and Figure 5, the effect of moisture on CN samples. As the severity of ageing conditions increased, the values for the measured ratio decreased. This may be due to the reduction of OH and NO_2 groups. In humid environments the reduction in values occurred at a much faster rate, indicating that the loss of covalent nitrate groups in the presence of moisture accelerated. This could be responsible for changes in solubility characteristics and loss of properties for CN samples, as the samples aged in humid conditions became insoluble in acetone (i.e. in less than 10 weeks of ageing), whilst samples aged in dry conditions retained their solubility characteristics and most of their useful properties even after a long ageing process (i.e. over 60 weeks of ageing).

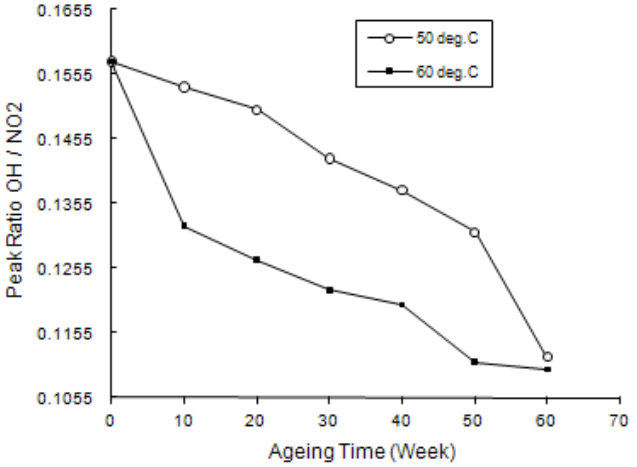

Figure 3. Values measured for peak ratio of OH / NO_2 versus ageing time for CN samples aged at 50, 60°C and 0% RH.

Figures 4 and 5 show the results of the peak measurements carried out for C=O / NO_2 ratio. Here the measured values increased for samples aged in both dry and humid conditions. The increase in values was larger for samples aged in humid environments. These results showed a progressive increase in the carbonyl / nitroester ratio, as the samples became more degraded. This indicated that as denitration occurred (decrease in OH / NO_2 ratio), the rate of formation of carbonyl impurities increased (increases in C=O / NO_2 ratio).

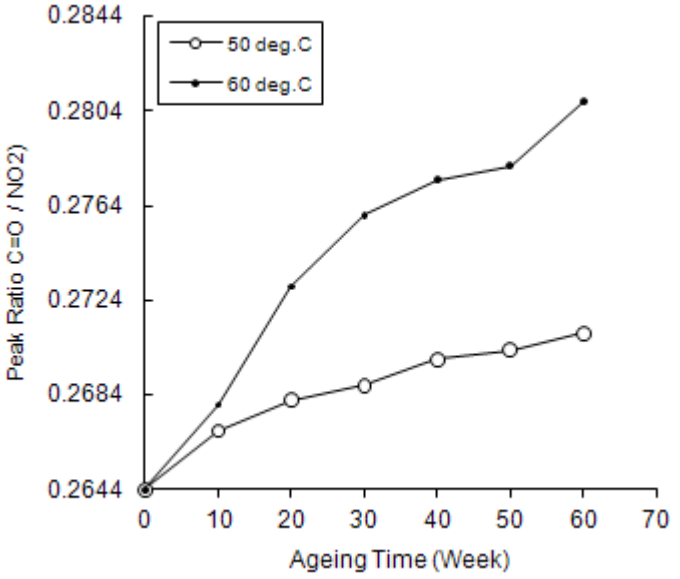

Figure 4. Values measured for peak ratio of C=O / NO_2 versus ageing time for CN samples aged at 50, 60^{o}C and 0% RH.

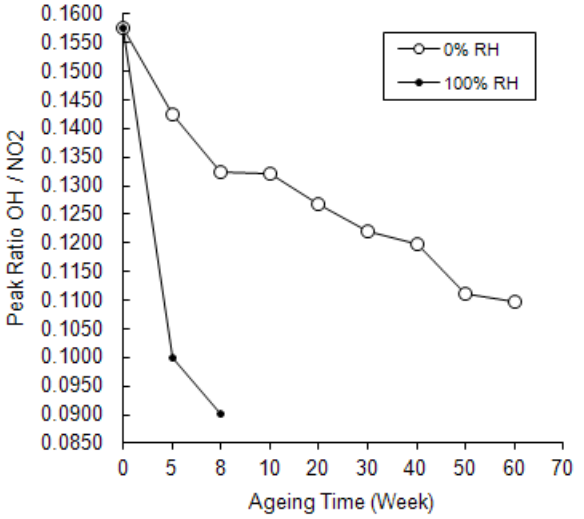

Figure 5. Values measured for peak ratio of OH / NO_2 versus ageing time for CN samples aged at 60^{o}C & 0% and 100% RH.

CONCLUSION

The results obtained in this study indicated that the peak ratio measurement technique could be used to monitor the changes in polymeric systems of cellulose esters, which may occur as a result of degradation. The rate of degradation of cellulose acetates and cellulose nitrates are environmentally dependent. The increase in moisture concentration can increase the rate of degradation. The results showed that the degradation process for acetates is accompanied by the loss in acetyl groups which may be occurring as a result of deacetylation. These results also indicated that the formation of carbonyl impurities did not occur together with deacetylation. Therefore, deacetylation is the major process of degradation for cellulose acetates. In contrast to acetates, for cellulose nitrates, denitration is accompanied by the formation of carbonyl impurities.

REFERENCES

[1] Miles, F. D., Cellulose Nitrate, Oliver & Boyd, 1955, P263-264.
[2] Hon, D. N. S. & Gui, T. L., Photodegradation of Cellulose Nitrate, *Polymer Photochemistry*, 7 (1986), P299-310.
[3] Ott, E. & Spurlin, H. M., Cellulose and Cellulose Derivatives, Vol. V, Part II, Interscience Publishers, 1954, P1036.
[4] Miles, F. D., Cellulose Nitrate, Oliver & Boyd, 1955, P158-9.
[5] Evans, E. F. & McBurney, L. F., *Ind. Eng. Chem*., 41 (1949), P1260.
[6] Zitomer, F., Anal. Chem., 40 (1968), P1091-5.
[7] Scotney, A., The thermal Degradation of Cellulose Triacetate-I, The Reaction Products, *Europ. Polym. J.*, 8 (1972), P163-174.
[8] Scotney, A., The thermal Degradation of Cellulose Triacetate-II, The Carbonaccous Residues, *Europ. Polym. J.*, 8 (1972), P175-184.
[9] Scotney, A., The thermal Degradation of Cellulose Triacetate-III, The Degradation Mechanism, *Europ. Polym. J*., 8 (1972), P185-193.
[10] Hiller, L. A., The Reaction of Cellulose Acetate With Acetic Acid and Water, *J. Polymer. Sci*., 10 (1953), P385-423.
[11] Brydson, J. A., Plastic Materials (3rd ed.), Butterworth Group, 1975, P493-4.
[12] Brydson, J. A., Plastic Materials (2nd ed.), Iliffe Books Ltd. 1969, P369.
[13] Haslam, J. & Willis, H. A. & Squirrell, D. C. M., Identification and Analysis of Plastics (2nd ed.), Iliffe Books, 1972, P534-6.

In: Chemistry and Chemical Engineering Reserch Progress ISBN: 978-1-61668-502-7
Editor: A.K. Haghi

Chapter 3

HIPING OF ENCAPSULATED ELECTRICALLY CONDUCTIVE ZrO_2-BASED COMPOSITES

Sedigheh Salehi[1], Omer Van der Biest[1], Jef Vleugels[1], Marc De Prez[2], Alfons Bogaerts[2], and Patrick Jacquot[2]

[1]Department of Metallurgy and Materials Engineering, K.U.Leuven, Kasteelpark Arenberg 44, B-3001 Leuven, Belgium

[2]Bodycote HIP, Industriepark Noord 7, B-9100 Sint-Niklaas, Belgium

ABSTRACT

Yttria-stabilised ZrO_2 can be pressureless sintered in air at 1450°C. The addition of 40 or 50 vol % electrically conductive secondary phases however makes it impossible to reach closed porosity by means of pressureless sintering under protective atmosphere, whereas full density can be obtained by hot pressing or pulsed electric current sintering at 1450°C. Densification at higher temperature strongly reduces the toughness and consequently strength of the composite material due to ZrO_2 grain growth, eventually leading to spontaneous phase transformation and material degradation. Therefore, as an alternative, the possibility of post HIPing and encapsulated HIPing of ZrO_2-based composites with 40 or 50 vol % WC, NbC or TiN is investigated.

Encapsulated HIPing of ceramics at temperatures above 1550°C is commonly performed using quartz encapsulation. The target temperature of 1420°C however is below the softening point of SiO_2, rendering this type of material unsuitable. Moreover, glass compositions with a suitable softening point are not commercially available. In order to find a solution, two potential encapsulation approaches were investigated. The first was to coat the cold isostatically pressed ZrO_2-based composite powder compacts with a 1-2 mm thick ZrO_2 powder coating prior to sinter-HIP. The ZrO_2 coating reaches closed porosity at a temperature of about 1300°C before applying the pressure. This approach allowed full densification of the ZrO_2-based composites at 1420°C. The main problem however was to remove the ZrO_2 coating from the sample. A solution was found in using a very thin layer of boron nitride powder in-between the composite powder compact and the external ZrO_2 powder coating, resulting in a spontaneous coating degradation during cooling. In another approach, low carbon steel was used for vacuum encapsulation, using Al_2O_3 powder to fill the gap between the powder compact and the steel tube capsule.

The microstructures and mechanical properties of the HIPed samples (1420°C, 30min, 170 MPa) are compared with those after hot pressing (1450°C, 1h, 30MPa).

1. INTRODUCTION

ZrO_2 ceramics are known for their high fracture toughness due to the transformation toughening mechanis [1] Addition of hard, conductive secondary phases such as TiN [2], NbC [3] or WC [4] increases the modest hardness of ZrO_2 whilst keeping the high toughness and excellent strength. The addition of hard secondary phases allows engineering a new generation of ceramics with mechanical properties that fill the gap between those of the tough and strong cermets (ceramic-metal composites) and the high hardness carbides, nitrides or borides, as schematically presented in Figure 1.

The large-scale production of complex shaped ceramic parts that can not be densified by pressureless sintering, however is challenging due to the difficulty in creating a homogeneous high temperature and pressure during densification. Hot Isostatic Pressing (HIP) however can be used as a solution. In HIP, rigid tools with limited strength and simple geometry (like graphite dies in hot pressing) are avoided since high isostatic pressures (~100-300 MPa) are established by an applied gas pressure. Due to the applied high pressure during sintering, it is possible to densify materials at temperatures lower than during conventional hot pressing. The reduced sintering temperature allows to control and avoid grain growth [5-7], increasing the material's strength[8]. Amongst the advantages of HIPing are: increased density, healing of major processing flaws, achieving more reproducible properties, improving or even producing novel microstructures, elevated material strength and in general the possibility to process large and complex parts at reduced cost.

Conventional HIPing usually involves a post HIPing of moulded or sintered parts. An essential requirement for this method is that the component should have closed porosity [9]. In the case of ZrO_2 based composites, post HIPing can result in ZrO_2 grain growth and consequently tetragonal to monoclinic phase transformation that is accompanied by microcrack formation. In ZrO_2-based ceramic composites, there is a tendency to keep the yttria stabilizer content as low as possible, because a tetragonal ZrO_2 with lower yttria content allows obtaining a higher toughness. This however makes ZrO_2 ceramics more sensitive to a post heat treatment. The post HIPing method is verified in this paper.

An alternative HIP technique is sinter-HIPing, a two-step process involving sintering at low pressure or in vacuum to closed porosity, immediately followed by a HIP process at elevated pressure. In this method, no intermediate cooling and manipulation is necessary between the sintering and HIP treatment. A series of pressureless sintering tests on ZrO_2-based composites with 40 vol% NbC, WC or TiN revealed that the minimum temperature needed to achieve closed porosity was 1550°C for ZrO_2-TiN and 1650°C for ZrO_2-NbC or ZrO_2-WC. These high temperatures however are not appropriate because a sintering temperature above 1500°C increases the risk of ZrO_2 grain growth and crack formation due to ZrO_2 phase transformation.

Another way of direct HIPing of green ceramic parts uses encapsulation. Capsules prevent pressurizing gas from entering pores and components with open porosity. The important issue is to find a suitable capsule that can fulfil the requirement of being plastically deformable at the HIP temperature in order to transfer the gas pressure uniformly to the

sample, being thermally stable at the HIP temperature. Quartz encapsulation is commonly used for HIPing above 1500°C.

A final method is the sinter-canning technique, which involves applying a coating of highly sinterable powder mixture to the green component [10]. The powder coating should reach closed porosity during heating up in vacuum before applying the isostatic pressure. The powder mixture should have a good matching thermal expansion with that of the component, to avoid cracking during heating.

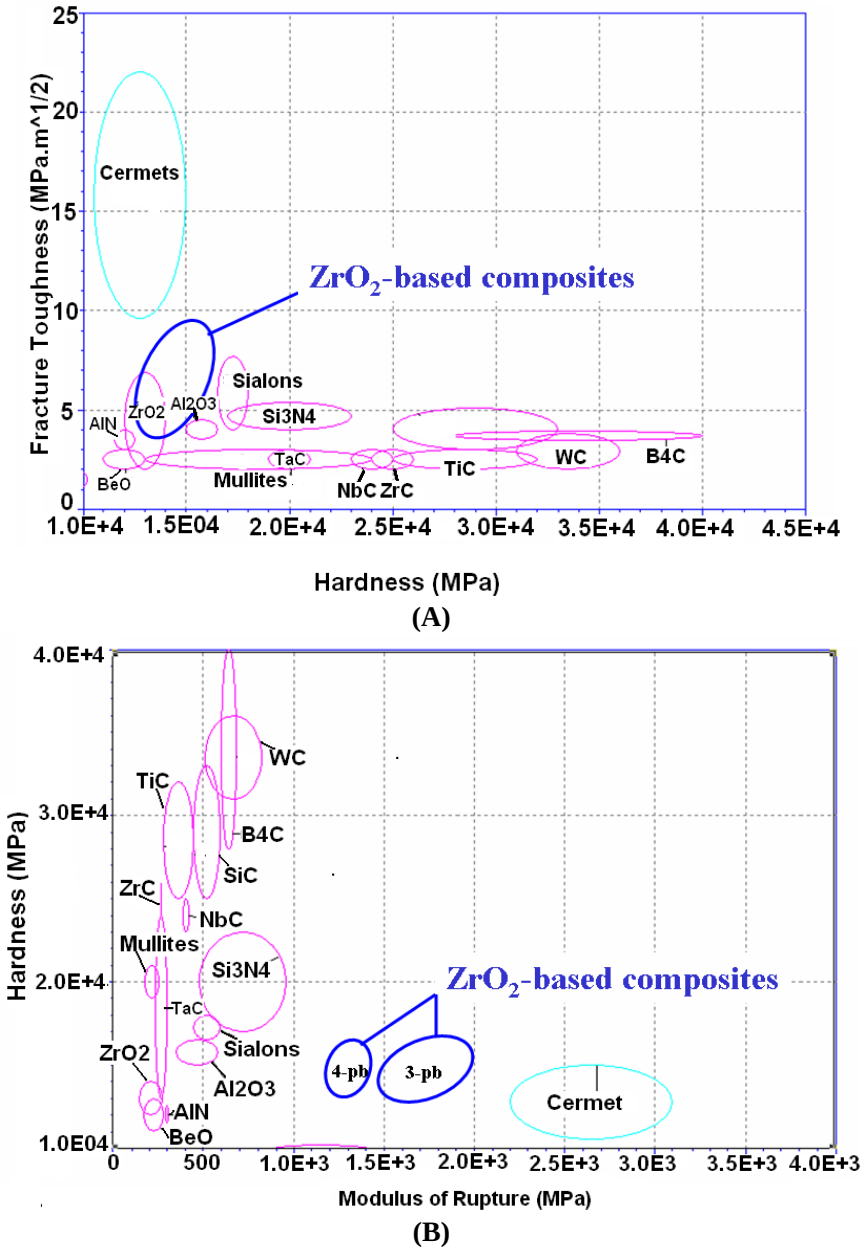

Figure 1. Fracture toughness versus hardness (a) and hardness versus modulus of rupture (b) for the ZrO_2 based composites and a range of common ceramic classes [2, 4, 13].

This work focuses on the encapsulation and sinter-canning techniques. With respect to encapsulation, two types of materials are widely used. Sheet metal containers of mainly mild steel, stainless steel or nickel based alloys are used at low temperatures. Stainless steel for example can be used as capsule to HIP alumina nanopowder at 1350°C [11]. At higher temperatures, e.g. 1500-2000°C, glass encapsulation is commonly used [12].

In a preliminary set of experiments, commercially available quartz and borosilicate glass were used to encapsulate ZrO_2-based composites for HIPing at 1420°C. Quartz however did not deform at this temperature and the melting point of borosilicate glass was too low resulting in a very low capsule viscosity. As a possible solution, yttria-stabilised ZrO_2 powder was chosen as coating material (sinter-canning technique) due to the relatively low onset point of densification (~1300°C, pressureless). CIPed (Cold Isostatically Pressed) composite powder compacts were coated with a 1-2 mm thick ZrO_2 powder coating prior to sinter-HIP. The ZrO_2 coating reaches closed porosity at about 1400°C, before applying the pressure, allowing to fully densify ZrO_2-based composites with 40 vol % secondary hard phases at 1420°C. In a further attempt, a boron nitride coating was added to the ZrO_2 coating, to facilitate coating removal. In another approach, low carbon steel was used for vacuum encapsulation, using Al_2O_3 powder to fill the gap between the powder compact and the steel tube capsule.

2. EXPERIMENTAL PROCEDURE

Three ZrO_2-based compositions were chosen for HIPing experiments, i.e., 1.75 mol% yttria stabilized ZrO_2-TiN (60/40 vol%), 2 mol% yttria stabilized ZrO_2-WC (60/40 vol%) and 2 mol% yttria stabilized ZrO_2-NbC with 40 or 50 vol% NbC. Details on the starting powders and powder preparation method are provided elsewhere [2-4].

The powder mixtures were sieved (315 mesh) prior to cold isostatically pressing in a cylindrical mould (ϕ~3 cm, H~4 cm) at 300 MPa (EPSI, Temse, Belgium). In case of sinter canning, ZrO_2 powder (Tosoh grade TZ-3Y, Japan) with a thickness of 1-2 mm was applied to the green compact by means of a second CIP treatment. After initial composite sample CIPing, the compacted powder was removed from the mould, reinserted in a ZrO_2 powder bed and CIPed at 300 MPa.

To facilitate application of a double boron nitride (BN) + ZrO_2 coating, a spherical sample geometry was used (Figure 2). The composite powder mixture was poured in a self-made mould using silicone moulding rubber (Castaldo, MA, USA) with spherical shape. After filling the mould with powder, the two parts of the rubber mould were sealed with a banderol, packed in a balloon and CIPed at 300 MPa.

Figure 2. Rubber mould and balloon used for making spherical BN+ZrO_2 coated samples.

The CIPed composite was plunged in BN (HeboFill, Henze, Germany) powder before immersion into the ZrO_2 powder bed prior to the second CIP cycle.

Steel encapsulation was realised by encapsulating spherical CIPed composite samples in a low carbon steel tube using Al_2O_3 powder as protective bed around the sample inside the tube.

All steel encapsulated, ZrO_2 and BN+ZrO_2 coated compacts were HIPed at Bodycote (Sint-Niklaas, Belgium) in a molybdenum heated HIP furnace. The HIP cycle is presented in Figure 3. In step 1, the compacts are heated at 5°C/min in an argon pressure of 0.2-0.3 MPa (2-3 bar) up to 1250°C. In step 2, the pressure is decreased to 2×10^{-3} MPa (2E-2 bar) at 1250°C and the samples are heated further at 5°C/min. In order to allow the ZrO_2 coating to reach closed porosity, the samples were soaked at 1420°C for 1 h at 2×10^{-3} MPa before applying 170 MPa argon gas pressure. The dwell time at maximum temperature and pressure is 30 minutes. The samples were naturally cooled under reduced pressure during the cooling step (step 3).

After removal of the encapsulation, the microstructure and mechanical properties of the ceramics were investigated and compared with those of hot pressed samples. Hot pressing was always performed at 1450ºC for 1 h under 30 MPa pressure. Microstructural investigation was performed by scanning electron microscopy (SEM, XL-30FEG, FEI, Eindhoven, The Netherlands). The density of the samples was measured in ethanol, according to the Archimedes method (BP210S balance, Sartorius AG, Germany). The Vickers hardness, HV_{10}, was measured (Model FV-700, Future-Tech Corp., Tokyo, Japan) with an indentation load of 98 N and a dwell time of 10 s. The indentation toughness, K_{IC}, was calculated according to the formula of Anstis et al. [3] based on the radial crack pattern produced by Vickers HV_{10} indentations. The reported values are the mean and standard deviation of 5 measurements.

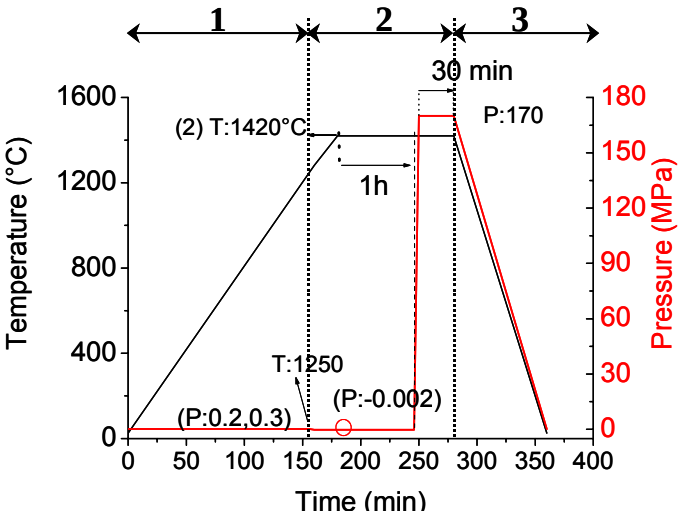

Figure 3. Applied HIP cycle for the powder coated composites.

3. RESULTS AND DISCUSSION

3.A. Post HIPing

As a start, hot pressed (1450°C, 30 MPa, 1h) 1.75 mol % yttria stabilized ZrO_2-TiN (60/40 vol %) composites were additionally hot isostatically pressed (1390°C, 20 min, 140 MPa Ar) to investigate the influence of the additional heat treatment on the microstructure and mechanical properties. The mechanical properties are summarised in Table 1 and the microstructures are shown in Figure 4, revealing that the post HIPing resulted in a significant grain growth of the TiN phase. Therefore, the softer ZrO_2 phase will also show substantial grain growth. ZrO_2 grain growth is accompanied with microcrack formation due to tetragonal to monoclinic phase transformation and consequently leads to decreasing hardness (see Table 1). Microcracking is a toughening mechanism that can be added to the other active toughening mechanisms, i.e., transformation toughening and crack deflection, explaining the increased fracture toughness. Due to the substantial grain growth and associated microcracking and loss of hardness, it was concluded that post HIPing, even at temperature of 1390ºC is not an option to pursue.

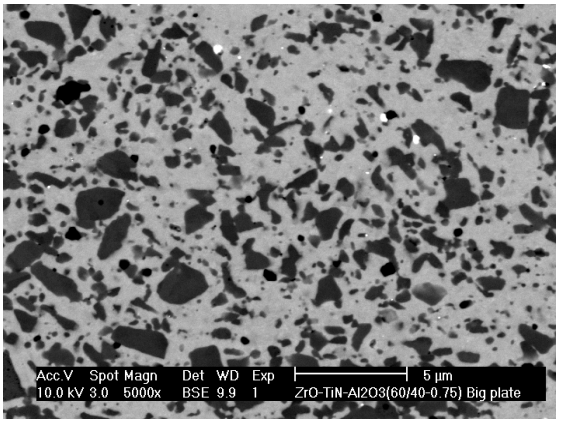

(A)

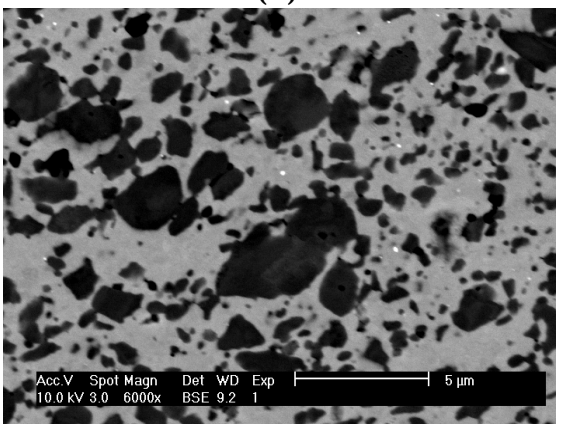

(B)

Figure 4. Hot pressed (1450°C, 1h, 30 MPa) ZrO_2-TiN (60/40), before (left) and after (right) HIP. TiN = dark, ZrO_2 = grey, WC = white (originating from the milling medium).

Table 1. Mechanical properties of hot pressed (1450°C, 30MPa, 1h) ZrO_2-TiN before and after HIPing

	Before HIP	After HIP
Hardness (GPa)	13.29 ± 0.13	12.49 ± 0.09
Toughness (MPa.$m^{0.5}$)	6.0 ± 0.3	6.5 ± 0.4

3.B. Powder Coating Encapsulation

3.B.1. ZrO_2 Coating

The HIPed 2 mol% yttria stabilized ZrO_2-NbC (60/40 vol%) samples before and after capsule removal are shown in Figure 5. The ZrO_2 capsules, were removed by Electro Discharge Machining (EDM). A necessary condition for a material to be electro-erodable is a low enough electrical resistivity (< 5μΩ.m). ZrO_2 is an electrical insulator (10^9 Ω.m) and can not be processed by ED [14]. Hence, in order to be able to remove the capsule by EDM, a

rotating diamond wheel was used to make a groove in the ZrO_2 coating down to the electro-conductive ZrO_2-based composite material. Wire-EDM allowed to machine a cylindrical shape and cut-off the cracked coating. The ZrO_2 coating is cracked because of the higher thermal expansion coefficient of the ZrO_2 compared to the composite, resulting in a stronger shrinkage of the ZrO_2 coating during cooling and the concomitant formation of too high tensile stresses in the coating. Although these tensile stresses are substantial, the coating does not delaminate due to the excellent bonding between the coating and the composite substrate.

Although the ZrO_2-based composites with 40 vol% TiN or NbC could be successfully densified by HIPing at 1420°C in 170 MPa argon (see Figure 6. d and f), the ZrO_2-NbC ceramic with 50 vol% NbC could not (see Figure 6.b). The microstructure of the HIPed and hot pressed ZrO_2-NbC and ZrO_2-TiN (60/40) grades are similar, as shown in Figure 6.c-f).

Figure 5. HIPed ZrO_2 powder coated composites before and after capsule removal; the ZrO_2 coating cracked during cooling.

Table 2. Mechanical properties of HIPed (1420°C, 170 MPa, 30 min) and Hot pressed (1450°C, 1h, 30MPa) 2 mol% yttria stabilized ZrO_2-NbC (50/50 and 60/40) and 1.75 mol% yttria stabilized ZrO_2-TiN (60/40) composites

Material grade	Hot pressed		HIPed	
	HV_{10} (GPa)	KIC_{10} ($MPa.m^{0.5}$)	HV_{10} (GPa)	KIC_{10} ($MPa.m^{0.5}$)
ZrO_2-NbC (50/50)	15.66 ± 0.08	5.6 ± 0.3	porous	/
ZrO_2-NbC (60/40)	13.74 ± 0.19	5.0 ± 0.3	14.99 ± 0.26	5.7 ± 0.4
ZrO_2-TiN (60/40)	13.70 ± 0.07	5.6 ± 0.1	13.45 ± 0.12	5.3 ± 0.1

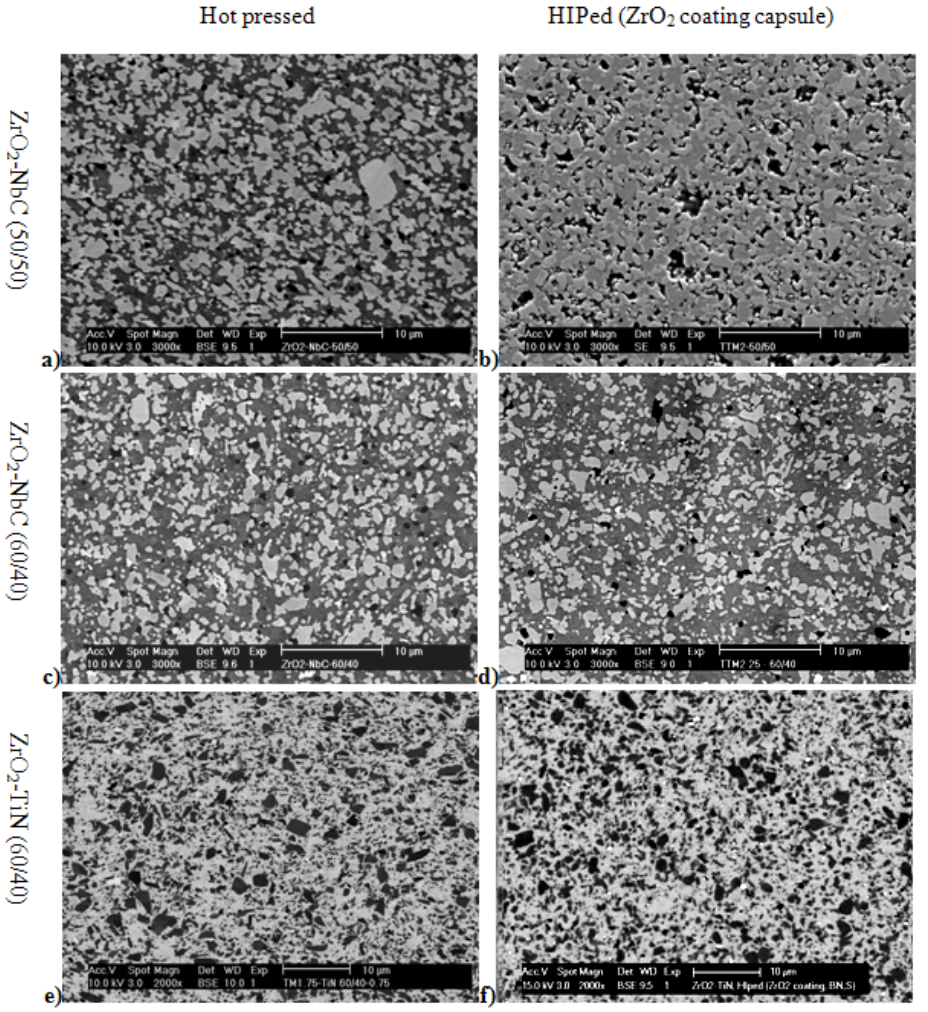

Figure 6. SEM microstructures of Hot pressed (left) and HIPed (ZrO_2 coating capsule) (right) 2 mol% yttria stabilized ZrO_2-NbC (50/50) (a,b), 2 mol% yttria stabilized ZrO_2-NbC (60/40) (c,d) and 1.75 mol% yttria stabilized ZrO_2-TiN (60/40) (e,f) composites. The ZrO_2 phase is dark in the ZrO_2-NbC and bright in the ZrO_2-TiN composites. Black phase is Al_2O_3 which was added to all compositions (0.75 wt %) as ZrO_2 grain growth inhibitor.

3.B.2. BN+ZrO_2 coating

Because of the difficulty in removing the cracked ZrO_2 coating, a dual BN + ZrO_2 coating was tested. The idea was to weaken the interfacial strength between the ZrO_2 coating and the composite substrate resulting in a spontaneous coating delamination during cooling. The HIPed BN+ZrO_2 coated ZrO_2-WC (60/40) composite before and after coating removal are shown in Figure 7. The ZrO_2 capsule could be easily manually removed with a spatula. The hardness, toughness and density of the HIPed and hot pressed grades are similar, as shown in Table 3, proving that the dual BN+ZrO_2 coating technique is quite suitable for sinter-HIPing of ZrO_2-based composites at 1420°C.

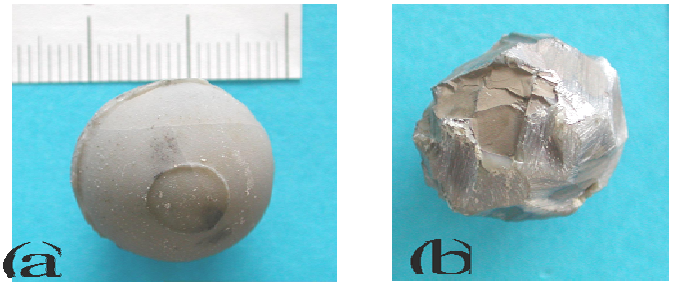

Figure 7. HIPed ZrO_2 + BN coated 2 mol% yttria stabilized ZrO_2-WC (60/40) before (a) and after (b) ZrO_2 capsule removal.

Table 3. Mechanical properties of 1.75 mol% Y_2O_3 stabilized ZrO_2-TiN (60/40) and 2 mol% Y_2O_3 stabilized ZrO_2-WC (60/40) composites, hot pressed at 1450°C for 1 h under 30 MPa and HIPed at 1420°C under 170MPa for 30 min

Material grade	Hot pressed			HIPed		
	density (g/cm^3)	HV_{10} (GPa)	KIC_{10} ($MPa.m^{0.5}$)	density (g/cm^3)	HV_{10} (GPa)	KIC_{10} ($MPa.m^{0.5}$)
ZrO_2-TiN (60/40)	5.81	13.77 ± 0.20	5.4 ± 0.3	5.83	13.41 ± 0.13	5.6 ± 0.2
ZrO_2-WC (60/40)	9.80	16.53 ± 0.20	7.5 ± 0.3	9.77	16.18 ± 0.16	7.5 ± 0.2

3.C. Steel Encapsulation

In another attempt, the CIPed spherical composite samples were encapsulated in a low carbon steel tube using alumina powder as protective bed around the sample inside the tube. The HIPed steel encapsulated and cross-sectioned sample are shown in Figure 8. The mechanical properties of steel encapsulated HIPed (1420°C, 170 MPa, 30 min) and hot pressed (1450°C, 1 h, 30 MPa) 2 mol% Y_2O_3 stabilised ZrO_2-WC (60/40) composites were found to be the same, as summarized in Table 4.

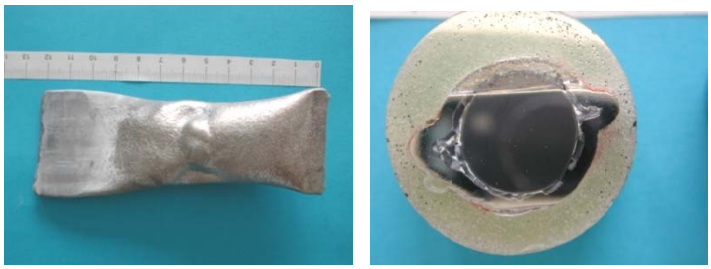

Figure 8. Overview (a) and cross-section (b) of the steel encapsulated HIPed 2 mol% yttria stabilized ZrO_2-WC (60/40) composite.

Table 4. Mechanical properties of hot pressed (1450°C, 1 h, 30 MPa) and HIPed (1420°C, 170 MPa, 30 min, using low carbon steel encapsulation) 2 mol% Y_2O_3 stabilised ZrO_2-WC (60/40) composites

	Hot pressed			HIP		
	density (g/cm^3)	HV_{10} (GPa)	KIC_{10} ($MPa.m^{0.5}$)	density (g/cm^3)	HV_{10} (GPa)	KIC_{10} ($MPa.m^{0.5}$)
ZrO_2-WC (60/40)	9.80	16.53 ± 0.20	7.5 ± 0.3	9.81	16.03 ± 0.14	7.1 ± 0.4

4. CONCLUSION

ZrO_2-based composites with 40 vol% TiN, NbC or WC addition could be successfully HIPed (sinter canning) using a ZrO_2 coating. In order to facilitate the ZrO_2 capsule removal after HIPing, a thin BN powder coating was applied in-between the composite compact and the ZrO_2 powder coating. The result was successful, since the capsule could be manually removed easily and the mechanical properties of the HIPed materials (90 min at 1420°C of which 30 min at 170 MPa Ar) were similar to those of hot-pressed grades (60 min at 1450°C and 30 MPa).

Alternatively, low carbon steel encapsulation using Al_2O_3 powder as a protective powder bed around the CIPed composite sample can be used. The mechanical properties of the steel encapsulated HIPed and hot pressed grades were the same.

Post HIPing of hot pressed ZrO_2-TiN (60/40) at 1390°C was resulted to a decrease in hardness due to ZrO_2 grain growth and associated microcracking; therefore post HIPing option was not further investigated.

ACKNOWLEDGMENTS

S. Salehi expresses her thanks to the Research Council of K.U.Leuven for a doctoral scholarship (DB/07/012). This work was supported by the Commission of the European Communities within the Framework 6 Program under project No. STRP 505541-1.

REFERENCES

[1] R. H. J. Hannink, P. M. Kelly, and B. C. Muddle, Transformation toughening in Zirconia-Containing ceramics, *J. Amer. Ceram. Soc*., 83 (2000) 461-487.

[2] S. Salehi, O. Van der Biest and J. Vleugels, Electrically conductive ZrO_2-TiN composites, *J. Europ. Ceram. Soc*., 26 (2006) 3173–3179.

[3] S. Salehi, J. Verhelst, O. Van der Biest, J. Vleugels, Electro-conductive ZrO_2-NbC composites using NbC nanopowder made by carbo-thermal reduction, Proceedings of 30th International conference on advanced ceramics and composites, Daytona Beach, Jan 2007.

[4] G. Anné, S. Put, K. Vanmeensel, D. Jiang, J. Vleugels, O. Van der Biest, Hard, tough and strong ZrO_2-WC composites from nanosized powders., *J. Europ. Ceram. Soc*., 25 (2005) 55-63.

[5] R. Widmar, Future prospect for Hot isostatic pressing; Proceedings of the Third International Conference Osaka, Japan, June 1991, p. 3.

[6] N. Hoo, F. H. Fores, Synthesis of a 8-TiAl alloy by mechanical alloying and hot isostatic pressing, Proceedings of the International Conference on Hot Isostatic Pressing, 20-22 May 1996, Andover, Massachusetts, USA, p. 91.

[7] L. Delaey, H. Tas; Proceedings of the International Conference on Hot Isostatic Pressing- HIP '93 Antwerp, Belgium, 21-23 April 1993.

[8] Seong-Min Choi, Hideo Awaji, Nanocomposites - a new material design concept; *Science and Technology of Advanced Materials*, 6 (2005) 2–10.

[9] R. Davidge, J. Sleurs and L. Buekenhout; HIPing of technical ceramics: A synopsis; Proceedings of International Conference on Hot Isostatic Pressing of Materials: Application and developments, Antwerp 25th-27th April 1988. p. 5.1

[10] Sheehan, J. E., Cermet fabrication with thermal spraying and hot isostatic pressing, *Ceramic Engineering Science Proc*., 4 (1983) 695.

[11] P. Weimar, R. Knitter, D. V. Szabo, Densification of nanosized alumina powders by Hot Isostatic Pressing, Proceedings of The International Conference on Hot Isostatic Pressing, 20-22 May 1996, Andover, Massachusetts, USA, p. 105.

[12] H. V. Atkinson and B. A. Rickinson; Hot isostatic pressing, The Adam Hilger series on new manufacturing processes and materials, imprint by IOP publishing Ltd, Bristol, UK, 1991.

[13] Cambridge Materials Selector, CMS version 2.05, Granta Design Ltd., UK, 1994.

[14] R. Morrell, *Handbook of properties of technical & engineering ceramics*, 1985, p. 95-166.

In: Chemistry and Chemical Engineering Reserch Progress ISBN: 978-1-61668-502-7
Editor: A.K. Haghi

Chapter 4

NANOPARTICLE FINISHES INFLUENCE ON COLOR MATCHING OF COTTON FABRICS

G. Rosace[1*], V. Migani[1], C. Colleoni[1], M.R. Massafra[2], and E. Sancaktaroglu[3]

[1] Dipartimento di Ingegneria Industriale - Università degli Studi di Bergamo - viale Marconi, 5 - 24044 Dalmine (BG) – Italy

[2] Stazione Sperimentale per la Seta - via G. Colombo, 83 - 20133 Milano – Italy

[3] Department of Textile Engineering – Uludag University – Gorukle Campus, 16059 Bursa – Turkey

ABSTRACT

Color change is one of the most important side effects of textile treatments to be considered. This research focuses on color modifications occurring ondyed cotton fabrics due to the nanoparticle sized dendrimer (DWR), dendrimer-fluorocarbon (DWOR) and fluorocarbon (FWOR) finishing. A remarkable influence of finishing onto ΔR (reflectance difference) and ΔE (color difference) of fabrics was observed. Roughness of treated surfaces also plays a relevant role in determining the reflectance and colour changes. In fact, roughness increases the scattering of light thus decreasing surface reflectance. Finishes particle sizes designate the distribution and orientation of surface roughness and the overlay of their absorbance values in the short wavelength results in color differences. Thanks to the nanoparticle size, the highest performances are achieved in some typical textile finishing applications: water and oil repellency induced by finishing on cotton textile and mechanical characteristics of the fabric have been here deeply investigated.

1. INTRODUCTION

Cotton is one of the major textile fibers and it has a unique combination of properties, including softness, durability, high strength, good dyeability and biodegradability, and for

* Corresponding author: phone +39 035 2052021; fax +39 035 2052077 e-mail: giuseppe.rosace@unibg.it

many centuries it has found use in textile production [1].Reactive dyes with vinylsulphone groups are widely used to dye cotton fibers, because of the simplicity of application, the great choice of commercial products and their cheapness.Even though a long tradition has given a solid and an in-depth knowledge of cotton textile fibers and of dyeing processes, the new research borders are moving to a development of the inherent textile materials properties: for this purpose, chemical finishing procedures are widely used. Textile materials can be treated with different functional finishes, such as water and oil repellent, durable press, soil-release, flame retardant, antistatic, and antimicrobial [2,3]. Water repellent finishing on fabrics is mostly imparted by the incorporation of low surface energy compounds, accompanied by the increase of the contact angle of liquids on its surface. The most recent approaches to improverepellency are based on the use of nanoparticles, such ashighly branched 3D surface functional macromolecules called dendrimers, whose effect mechanism depends on being in a position to build-up crystal structures in nano-range, which produce wash-permanent, water-repellent and highly abrasion resistant effects. When combined with fluoropolymers, dendrimers force them to co-crystallize leading to a self-organization of the whole system and to an enrichment of the fluoro polymers on the most outer layer of the textile [3]. Functionality and properties of dendrimers can be changed by filling their cavities or modifying the core and chain-ends [4]. Conformational flexibility of branches is capable of placing dendrimers hydrophilic interior in contact with aqueous subphase and extending their chains into the air above the air–water interface [5]. Particle size of these repellent finishes plays a vital role because, when the inorganic particle size is reduced, the surface area is increased; this leads to good interaction with the matrix polymer, and a highest performance is achieved [6]. Alteration of surface properties by textile finishing applications and creation of a smoother reflection surface by a reduced superficial particle size could also give a color change [7].In this study the effect of particle sizes on surface roughness and color assessment after finishing of cotton fabrics was evaluated by surface reflectance, absorbance of finishes and color coordinates measurement. For this purpose, three types of commercially available dendrimer water repellent (DWR), fluorocarbon included dendrimer water-oil repellent (DWOR) and fluorocarbon water-oil repellent (FWOR) reagents were impregnated to dyed cotton fabrics and polymerized under optimum conditions. The dyeing of the fabric samples was carried out by three different colors commercial dyes. The reflectance and color coordinates of treated and untreated samples were measured by reflectance spectrophotometer according to the CIELAB, a CIE defined color space, that supports the accepted theory of color perception based on three separate color receptors in the eye (red, green and blue) and is currently one of the most popular color spaces [8].Finally, water and oil repellency performances, treated-substrate characterization and fabrics mechanical properties were extensively investigated to estimate if finishing agents application gives rise to other changes, besides color alterations [9].

2. EXPERIMENTAL

2.1. Fabrics

Scoured and bleached woven cotton fabrics (68 g/m^2) were employed in this study. Each sample (10 g) was immersed for 30 minutes at 60°C in 5 g/L ECE solution (adetergent free from fluorescent brightening agent, used in the ISO 105 series of color fastness test) with 0.5 g/L soaking agent, in a conical flask with a continuous shaking. The samples were then thoroughly rinsed and dried at room temperature and stored at laboratory conditions (25 ± 2 °C and 65 ± 2% relative humidity).

2.2. Dyes

Three different colors commercial Remazol (Dystar) reactive dyes with vinylsulphone groups (Table1) were used. The dyes selection has been made according to the behaviour of finishing chemicals in their maximum reflectance intervals.

Table 1. Reactive dyes used

Commercial name	**λ_{max}**	**C.I. generic name**
Remazol Yellow Gold RNL	413	Reactive Orange 107
Remazol Red F3B	541	Reactive Red 180
Remazol Black B	600	Reactive Black 5

The molecular structures are reported in Figure 1. All dyes were of commercial grade and were used as received.

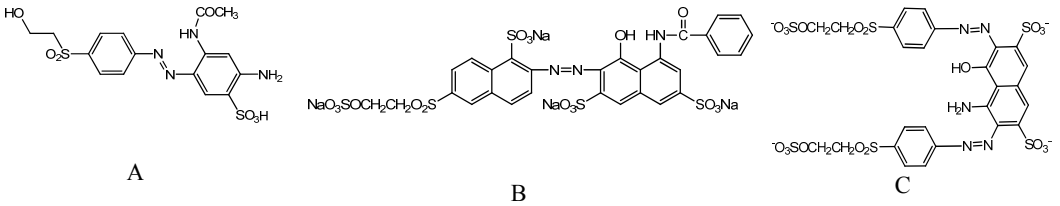

Figure 1. A: Reactive Orange 107 (Remazol Yellow Gold RNL). B: Reactive Red 180 (Remazol Red F3B). C: Reactive Black 5 (Remazol Black B).

2.3. Dyeing Agents

For level and consistent dyeing of cotton fabrics Bersol CM (1g/L), Berdet WF(1g/L) (sequestering and wetting agents, respectively, supplied by Europizzi - Urgnano, Italy), Depsolube ACA (1g/L) (anti-creasing agent supplied by Basf - Italy) were used. All chemicals were commercial products.

2.4. Repellents

Patented dendrimer water repellent (density = 1.1 g/cm^3), fluorocarbon/dendrimer water-oil repellent (density = 1.03 g/cm^3) and also fluorocarbon water-oil repellent (density = 1.03 g/cm^3) provided by Rudolf Chemie (Turkey and Italy) were used as finishing agents and coded as DWR, DWOR and FWOR respectively (Table 2).

Table 2. Finishing agents codes

Textile finish	Code
Dendrimer Water Repellent	DWR
Fluorocarbon/Dendrimer Water-Oil Repellent	DWOR
Fluorocarbon Water-Oil Repellent	FWOR

2.5. Buffer

The pH 5.5 buffer used for neutralization after dyeing and finishing application comprised acetic acid (9.60 g dm^{-3}) and sodium acetate (3.56 g dm^{-3}). Chemicals were obtained from Sigma-Aldrich, in analytical grade.

2.6. Dyeing

Untreated fabrics were dyed using method depicted in Figure 2, according to selected dyes. Reactive dyeing was carried out using a liquor ratio of 10:1. Samples were then washed, rinsed and neutralized at proper temperature levels, to be finally left to dry under laboratory conditions.

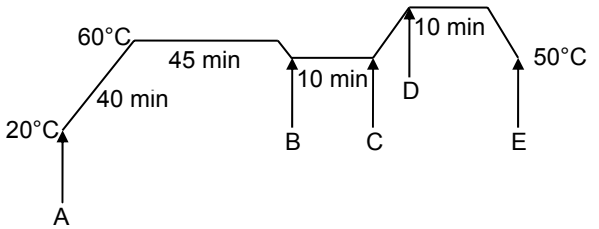

A= LR 10:1; 1% dye shade; 10 g fabric; 1 g/L Bersol CM; 50 g/L NaCl; 12 g/L Na_2CO_3; 1 g/L Berdet WE; 1 g/L Depsolube ACA
B= rinsing
C= 0,7 ml buffer solution (pH= 5,5)
D= 1 g/L soaping
E= rinsing

Figure 2. Dyeing profile method for reactive dye used.

2.7. Application of Dendrimers

Dyed cotton samples were padded separately in aqueous baths with finishing chemicals (DWR, DWOR and FWOR). All products were applied to the fabrics with the pad-cure method, including full immersion into the bath to a wet pick-up of 60-80% at 20°C and were cured at 140-150 °C for 120 seconds. The application conditions for the three tested finishes are reported in Table 3: for allproducts two different concentrations were investigated, taking into account the concentration ranges recommended by supplier.

Table 3. Dendrimer and fluorocarbon application conditions

Conditions	DWR		DWOR		FWOR	
Concentrations (g/l)	100	125	30	50	30	50
Pick up (%)	60-80		60-80		60-80	
pH	5-5.5		5-5.5		5-5.5	
Fixation temp (°C)	150		150		150	
Fixation time (min)	2		2		2	

2.8.Particle Size Measurement

The finishes particle size measurements were performed with a Malvern Instruments Mastersizer 2000. During the laser diffraction measurement, particles were passed through a focused laser beam and scattered light at an angle that was inversely proportional to their size. The angular intensity of the scattered light was then measured by a series of photosensitive detectors. The number and positioning of these detectors in the Mastersizer 2000 have been optimized to achieve maximum resolution across a broad range of sizes.

2.9.Textile Testing

GSM (Grams per square: the standard measurement of the gravitational force acting on fabrics), TS (Tensile strength: the resistance of a material to rupture when subject to tension) and ELB (Elongation at break: the increase in length when the last component of the specimen breaks) properties of cotton fabrics were also measured for all applications.GSM is a standard measurement of fabric weight per unit area carried out for all samples as follows: the weight of samples with the size of 20 square cm was measured by Mettler balance (± 10^{-4}g). The percentage change of fabric weight was calculated with (1).

$$Weight\ change\ (\%) = \frac{W_1 - W_0}{W_0} X\ 100 \quad (1)$$

where W_1 is the weight of the substrate after treatment and W_0 is the initial weight of the untreated substrate. Tensile strength and breaking elongation were measured according to ISO 13934-1, using standard test methods on dynamometer Instron Tensile Tester model 4501

(CRE). Ten specimens were prepared for testing, five for warp direction and five for weft direction. The standard deviations of all experimental results were lower than ± 2,5%.To thoroughly evaluate both water and oil repellency, above mentioned performances were measured after abrasion, washing and iron treatments. The samples were conditioned at 20 ± 2 °C and 65 ± 4 % RH for 24 hours before textile testing, according to standard ISO 139:2005. All measurements were repeated for the three equally treated samples and then averaged. Water and oil repellency tests were reformulated after 5 and 15 repeated home launderings carried out at 40° C, as described in the ISO 6330, followed by tumbler drying at 80° C for 20 min. Half of the samples were also ironed at 150° C for 60 seconds for observation of heat effect on recovery of repellency. The abrading cycles of the treated and control fabric samples were performed on a Nu-Martindale abrasion tester (Mesdan Italy) according to ISO 12947-3 with two different abrasion cycles (150 and 300). Water resistance test measures the resistance to surface wetting, water absorption and penetration. To determine the extent of surface wetting, the ISO 4920 spray test was used. The substrate was held taut within a 15 cm diameter ring at a 45° angle, and 250 mL of water at a temperature of 23 ± 1°C was lightly dropped onto the substrate from a distance of 15.2 cm, to remove excess water. A rating of 80 or higher is desirable, because it indicates better water repellency. Oil repellency was measured according to ISO 14419. In this test, oily drops were deposited onto substrate, allowed to remain for 30 seconds, and removed by wicking or wiping with a paper tissue. Eight different challenge liquids with different liquid tensions are numbered by a rating increasing from 1 in the case of vaseline, the easiest to repel, to 8 in the case of n-heptane, the most difficult to repel (Table 4). Oil repellency is reported as the maximum rating of the liquid that does not wet the substrate. For detailed comparisons, multiple drops of each liquid were tested. In general, an oil repellency rating of 5 or higher is desirable.

Table 4. Definition of oil repellency

Oil repellency rating	Test liquid	γ_L, mN/M
8	n-heptane	19.8
7	n-octane	21.4
6	n-decane	23.5
5	n-dodecane	24.7
4	n-tetradecane	26.4
3	n-hexadecane	27.3
2	35/65 mix n-hexadecane/vaseline	29.6
1	vaseline	31.5

2.10. Surface Reflectance and Roughness Measurement

The reflectance of non-dyed samples (untreated and treated) was measured with a Lambda 950 Perkin Elmer apparatus, equipped with an RSA-PE-150 Labsphere accessory for reflectance measurements. Each reflectance value R (%) was determined as the average of four measurements, with an experimental error of about 1-2%. For a randomly rough surface

having a Gaussian type surface heights distribution, the reflectance can be expressed as follows:

$$Rr = Rs \exp[- (4\pi\sigma\cos i/\lambda)^2] \quad (2)$$

where Rs and Rr are specular reflectances of perfectly smooth and rough surfaces, respectively; σ is the standard deviation of the surface from its mean level, function of the surface roughness; i and λ are the incident angle and wavelength of light, respectively.Changes in surface roughness of treated fabrics were expressed as differences in the root-mean-square of the vertical Z dimension values within the examined areas, which were calculated using the following equation:

$$RMS_{xy} = \sqrt{\sum_{xy=1}^{N} \frac{(Z_{xy} - Z_{average})^2}{N^2}} \quad (3)$$

2.11. Absorbance Measurement

The ultraviolet–visible absorption spectra of finishes were recorded on a Thermo Nicolet Evolution UV–Vis 500 spectrophotometer Vision 32 software, using a 1 cm path length cell. All spectra were recorded at room temperature in the wavelength range from 350 to 750 nm at the rate of 300 nm min^{-1}. Finish/dye solutions were evaluated from the change of absorbance at the λ_{max} of the dye in the UV-Vis spectra of the sample solution.

2.12. Color Difference Assessment

Color difference evaluation was based on the surface reflectance in the visible waveband: indeed, any effects that change the reflectance cause a color difference. The color coordinates of dyed cotton (untreated and treated) samples dyestuffs selected for dyeing cotton fabrics were measured on the same spectrophotometer used for absorbance measurements, equipped with an integrating sphere with a 10mm opening, under a $D65/10^0$ illuminant according to ISO 105 J01. The spectrophotometer measurements were made using the L*a*b* system. The evaluation of the overall color difference (ΔE), obtained before and after finishing, in the 3D color space is given by:

$$\Delta E^* = \sqrt{(\Delta L^*)^2 + (\Delta a^*)^2 + (\Delta b^*)^2} \quad (4)$$

where ΔL* represents the lightness difference; Δa and Δb, the differences in a and b values, wherein a* is a measure of redness/greenness, and b* is a measure of yellowness/blueness.The a* and b* coordinates approach to zero for neutral colors (white, greys) and increase in magnitude for more saturated or intense colors. The advantage of the CIE-lab system is that color differences can be expressed in units that can be related to visual perception and clinical significance [8]. Four reflectance measurements were made on each sample; the samples were rotated 90° before each measurement, and the averages of the

reflectance values (%) at wavelengths between 400 and 700 nm were recorded.A white Thermo Nicolet Electronic calibration plate was used.

3. RESULTS AND DISCUSSION

3.1. Particle Size and Surface Roughness Measurements

The results of nano particle sizes for DWR, DWOR and FWOR finishing agents are depicted in Figure 3.DWR presents the greatest particle size and volume (%) values are about the half of the ones observed for the two other finishes. Besides, DWR shows a second low concentration peak in the particles size range of 10-100 nm, probably due toa self-assembling of dendrimers [10]. From these results, specific surface areas of nanoparticles were determined: 6.6 m^2/g, 38.0 m^2/g and 40.1 m^2/g for DWR, DWOR and FWOR respectively.

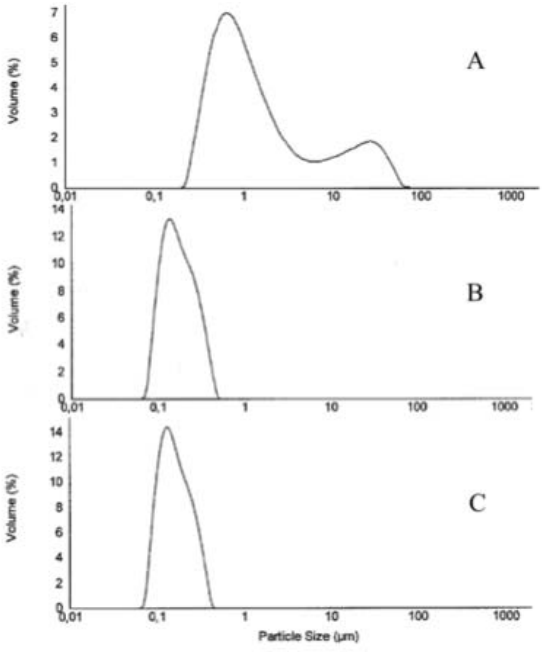

Figure 3. Particle size of DWR (A), DWOR (B) and FWOR (C) finishes.

Table 5 compares treated to untreated samples concentrations and RMS_{xy} values, the latter computed using (3). For the selected chemicals concentrations, the smaller the particle size the smoother the polymer over the textile surface, as expected. Particle surface area, in fact,increases as the particle size decreases: the highest particle surface area is achieved when there is a high concentration of nanometer or sub-nanometer sized particles. This is the reason why a higher concentration of DWR product is required to obtain the same repellency effects of DWOR and FWOR. Surface roughness reduces the specular reflectance of a wavelength of light, especially at high angle of incidence, and increases the scattering of light while decreasing the surface reflectance. Textile samples treated with small particle sized

chemicals, having a higher surface area, give a more uniform dispersion, a smoother reflecting surface and thus higher reflectance values (%) [8].With the application of finishing agent, it was believed that such treatment increased the inter-yarn and inter-fiber frictional force, as confirmed by the roughening effect on the textile surface.

Table 5. Surface characterization of untreated and treated samples

Samples	Concentrations (g/l)	RMS (Root-mean-square) nm
Untreated	0	25.41
DWR	125	13.7
DWOR	50	6.9
FWOR	50	6.9

3.2. Repellency Measurements

It was observed (Figure 4) that high water repellency degrees of dendrimers have a tendency to improve, when they are combined with fluorocarbon polymers. It was also observed that untreated fabrics showed no repellency behaviour and that, for all different treatments, water repellency was initially the same. After abrasion and washing processes a performance decrease was observed, particularly for lower finishing concentrations. In addition, the binding properties of dendrimers to textile surface had acceptable fastnesses.

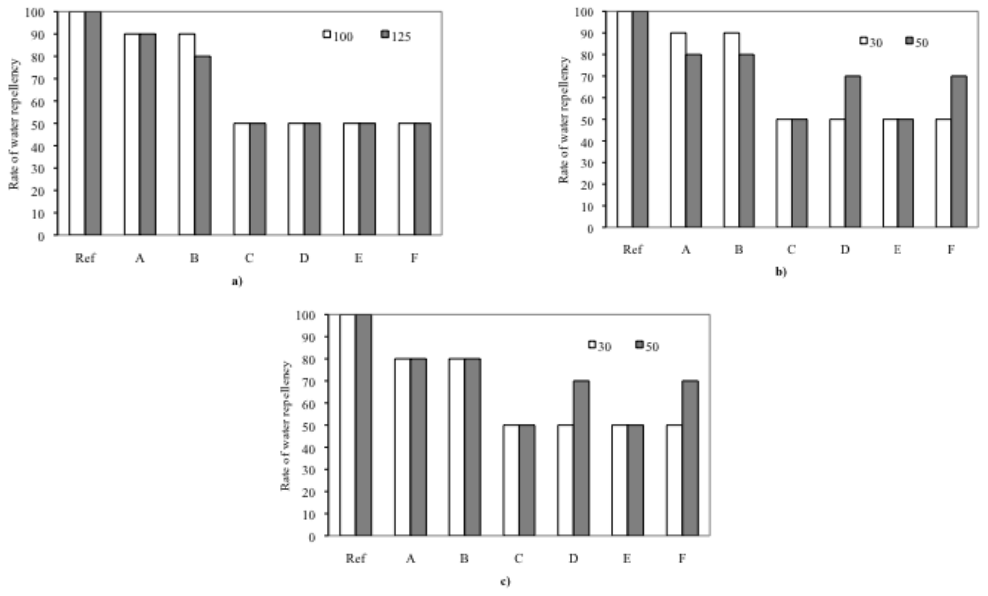

Figure 4. Water repellency a) after DWR finish at 80 g/L and 125 g/L concentrations, b) DWOR finish at 30 g/L and 50 g/L concentrations and c) FWOR finish at 30 g/L and 50 g/L concentrations after: application alone (ref); 150 cycles of abrasion (A); 300 cycles of abrasion (B); laundering (5 cycles) (C); laundering (5 cycles) and ironing (D); laundering (15 cycles) (E); laundering (15 cycles) and ironing (F).

After oil repellency testing of DWR finishing, no repellency effect was observed. The possible reason is related to the high DWR finishing surface energy in comparison with surface tension of oil (20-35 mN/m). For fluorocarbon groups supplied DWOR and FWOR, a very low critical energy of 6 mN/m can be achieved [11]. The change in oil repellency was shown in Figure 5. The effect of concentration is evident on FWOR products in comparison with DWOR products, probably due to the orientation of fluorocarbon chains achieved by dendrimers. For this reason lower concentrations of DWOR are more efficient than FWOR products, which do not include dendrimers [12].

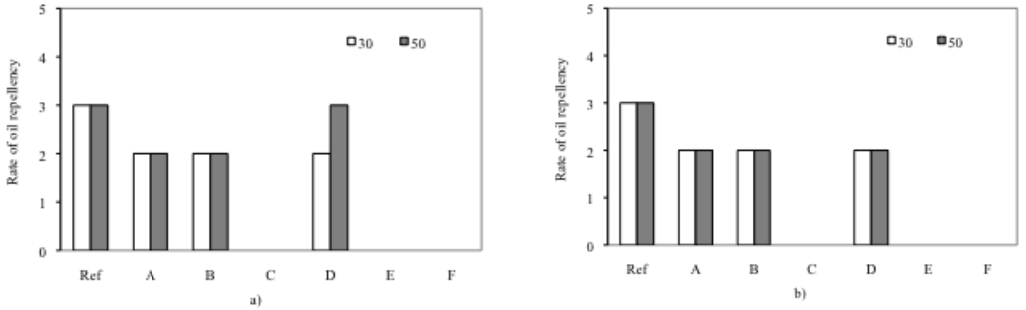

Figure 5. Oil repellency after a) DWOR finish at 30 g/L and 50 g/L concentrations and b) FWOR finish at 30 g/L and 50 g/L concentrations after: application alone (ref); 150 cycles of abrasion (A); 300 cycles of abrasion (B); laundering (5 cycles) (C); laundering (5 cycles) and ironing (D); laundering (15 cycles) (E); laundering (15 cycles) and ironing (F).

Despite sufficient fixation, textiles finished with fluorocarbon suffer from a clear loss in effect after washing, caused by the unfavourable conditions prevailing in the washing machine. Surface-active surfactants, the extremely polar medium (water), the elevated temperature (at least 40°C) in combination with the mechanical influence, lead the orientated fluorocarbon chains "diving away" from the edge or being very much disturbed. After drying the polymer is still on the substrate, however, but the side chains are in disorder, and for this reason no oil and water repellent effects are apparent. Since the fluorocarbon chains melting temperature is80-90°C, the fluorocarbon finish is not able to spontaneously regenerate at room or drying temperature.

Table 6. Mechanical properties of treated fabrics

Cotton		Untreated	DWR		DWOR		FWOR	
Concentration (g/l)		0	100	125	30	50	30	50
GSM (g/m²)		66.80	70.84	70.79	69.29	71.39	69.00	70.05
Weight change (%)		0.0	6.0	6.0	3.7	6.9	4.0	6.7
TS (N)	Warp	223.1	212.2	204.5	235.8	219.3	237.7	220.4
	Weft	144.6	85.5	112.7	152.7	192.3	154.1	189.3
ELB (%)	Warp	7.6	4.5	3.6	4.6	5.5	4.7	5.3
	Weft	14.1	15.8	18.0	23.2	26.0	23.1	25.0

A simple ironing and thus the heating up of the textile over the melting temperature of the fluorocarbon chains would be however sufficient to reorganize the finishing and to reproduce the performance level [11].In our opinion the change in water repellency after washing and abrasion seen on DWR products is also probably related to this reason. Anyway, samples before and after dendrimer and fluorocarbon finishing treatment have very similar mechanical properties as indicated in Table 6 and in a range that is intrinsic to the raw material.

3.3. Color Difference Measurements

Color-difference evaluation in the visible waveband (400-700 nm) computed on the basis of (4) is depicted in Figure 6 for the three tested finishes on the cotton fabric samples. It was observed that the application of three finishing products have an effect on color change in any color, whether in hue, chroma, or lightness (AATCC). Color difference trends are comparable for all colors, and always show the highest ΔE value for DWR, while the lowest for FWOR finishing. Besides, distinctive behaviours are observed for red color, which presents the highest ΔE for all finishings, and for blue one, whose attitude is decidedly opposing. Color matching as depicted in Figure 6 and *ΔL,* Δa*, Δb** values of dyestuffs selected for dyeing in Table 7 show a remarkable influence of finishing onto color difference of textile.

Table 7. ΔL,* Δa*, Δb* values of reactive dyestuffs used on cotton fabrics

Colour	*ΔL**			*Δa**			*Δb**		
	DWR	DWOR	FWOR	DWR	DWOR	FWOR	DWR	DWOR	FWOR
Yellow	0.40	0.84	0.80	0.78	0.30	0.25	0.38	-0.30	-0.29
Red	-0.77	0.37	0.25	-1.86	-1.29	-1.15	-1.01	-1.03	-0.59
Blue	0.34	0.28	-0.39	-0.46	-0.36	0.88	-0.22	-0.15	-0.46

3.4. Reflectance Difference Measurements

One of the major effects on color difference after finishing can be related with surface roughness change, seen as reflectance difference ΔR between the percentage reflectance of treated fabrics from the one of control fabrics, as indicated in Figure 7. As Figure 7 shows, the DWR, DWOR and FWOR finishes have similar curves of reflectance which stabilize after 530 nm around an almost constant level.It is shown that the finishing treatment changes the percentage reflectance values of the fabric, depending on the chemical type: samples treated with chemicals that are smaller in particle size (DWOR, FWOR)generally give higher reflectance (%) values for λ>530nm; DWOR and FWOR finishes increase their refractive index, in comparison with the fabric itself, and this behaviour is opposite to the one of DWR. Samples treated with DWR finishing, having greater particle size, exhibit in fact a significant decrease in reflectance (%), especially for short wavelengths, if compared with control fabrics.This pronounced decrease may be related to the height of the surface roughness, which can scatter wavelength of the visible spectrum. The contribution of the particle size

distribution and the assignment of the height profile of a treated fabric surface may be correlated to the profile of the reflectance difference plots of the samples [13].

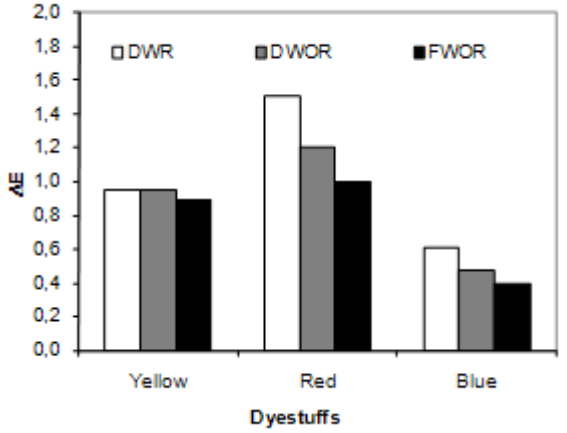

Figure 6. Color differences on cotton fabrics.

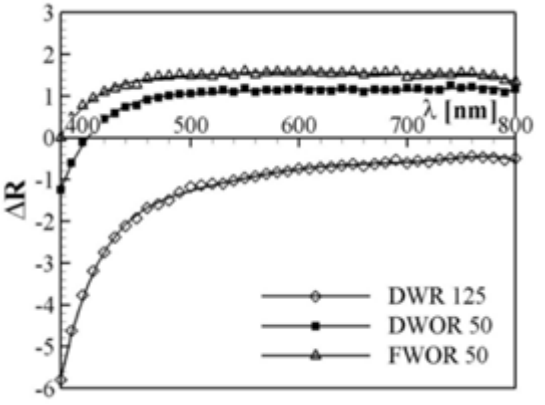

Figure 7. Reflectance differences of three finishing agents at the best concentration selected according to water and oil repellency performance results.

3.5. Absorbancemeasurements

Another effect of finishing agents on color difference could be explained by the absorbance plots in the visible range as shown in Figure 8. The concentrations selected for the measurement are related with the application concentrations of the products over the textile surface.As shown in Figure 8 there are two distinct zones for each absorbance curve. The first one is approximately 350-500 nm, in which stronger adsorption of products and a higher difference between each finishing agent occur. The rate of absorbance gradually reduces and so the difference becomes smaller. This is valid under the same concentrations conditions (B, C, D: 0.50 g/L). The absorbance increases for the same product with concentration increasing (e.g. DWR A: 1.25 g/L, D: 0.50 g/L), as expected.The adsorption differences for the three

products are depicted in Figure 9, 10 and 11 for different colors of the same dyestuff group. Equal ratios of the dyestuff and water/product solutions were carried out for each measurement.

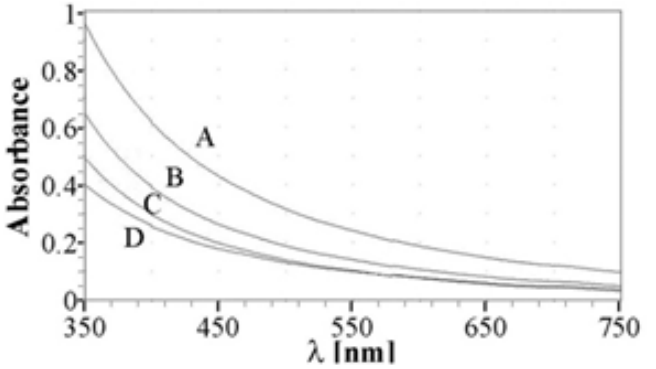

Figure 8. Absorbance spectrum of DWR (A: 1.25 g/L; D:0,5 g/L), DWOR (B: 0.50 g/L), FWOR (C: 0.50 g/L) solutions in the visible range.

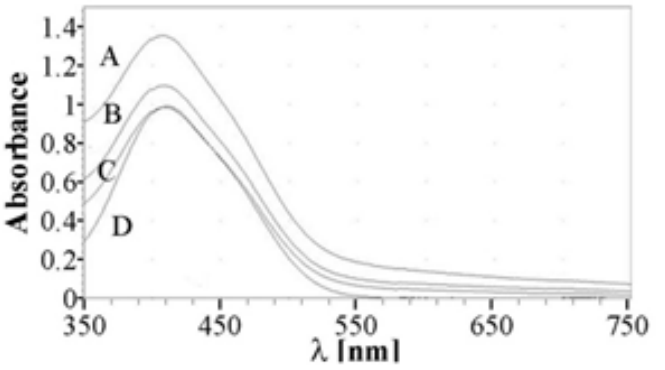

Figure 9. Absorbance spectrum of Yellow Remazol RNL in water solution (D) and in solution with DWR (A: 1.25 g/L), DWOR (B: 0.50 g/L), FWOR (C: 0.50 g/L) products in the visible range.

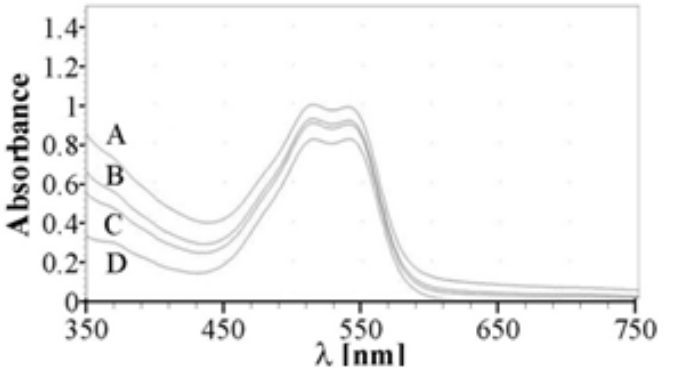

Figure 10. Absorbance spectrum of Red Remazol F3B in water solution (D) and in solution with DWR (A: 1.25 g/L), DWOR (C: 0.50 g/L), FWOR (B: 0.50 g/L) products in the visible range.

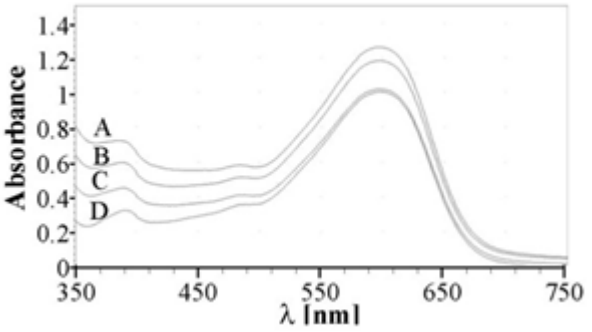

Figure 11. Absorbance spectrum of Black Remazol B in water solution (D:0,1 g/L) and in solution with DWR (A: 1.25 g/L), DWOR (C: 0.50 g/L), FWOR (B: 0.50 g/L) products in the visible range.

For all colors there is no change in theabsorbance spectrum profile of dyestuff solution with finishing agents, but an overlay of the absorbance values in the short wavelength. This means that the dyestuffs do not interact with finishing agents but show a small variation of the λ_{max} which results with ΔE. Absorbance values at λ_{max} of dyestuff with water/product solutions on measurement concentrations are reported in Table 8.

Table 8. Absorbance values of dyestuff with water/product solutions at λ_{max}

Absorbance	Dyestuff	DWR	DWOR	FWOR
Yellow Remazol RNL	0.98	1.34	0.98	1.09
Red Remazol F3B	0.82	0.98	0.90	0.92
Black Remazol B	1.00	1.26	1.02	1.18

It was evaluated that red dyestuff has a lower absorbance at λ_{max} than the other two colors. When combined with the finishing products, red dyestuff has lower influence on the increase of λ_{max}, too. The absorbance effect of DWR is the best for all the colors, while DWOR and FWOR show similar absorbance effect except in the case of Black Remazol B. This can be related with the lower adsorption of dendrimer in comparison with fluorocarbon polymers at the same concentration. When fluorocarbon polymers dendrimers are applied, the percentage of fluorocarbon in the product decreases because the same effect of oil and water repellency is achieved with the help of the only dendrimers. That is why absorbance value is always the lowest for DWOR. Looking at absorbance values of FWOR (having only fluorocarbons)fluorocarbons polymers increase the λ_{max} of dyestuff alone more than with dendrimers, and dendrimers alone have the lowest effect onλ_{max}.

3.6. Color Difference Evaluation

Color difference evaluation for the three tested finished, as depicted in Figure 6, could be also estimated on the base of absorbance and reflectance values considerations.For yellow (λ = 413 nm) dyed and finished cotton fabrics, the effect of absorbance for DWR is the highest,

when compared with all other colors. This effect is compensated for DWR lower reflectance at its wavelength, and this results in a ΔE similar to the DWOR one. FWOR finishing presents an absorbance value similar to DWOR and the highest reflectance one, so ΔE is lower.For red (λ = 541 nm) dyed and finished cotton fabrics, the absorbance effect is the lowest for all finishes, when compared with other colors. Reflectance of DWR is still quite low but absorbance is lower than the yellow case, so ΔE is the highest and decidedly higher than in yellow dyeing. For all finishes, absorbance values are quite similar, but DWOR and FWOR have an increment of ΔE, due to the reflectance contribution enhancement.For blue (λ = 600 nm) dyed and finished cotton fabrics, absorbance values are intermediate between yellow and red dyeing while reflectance values are the highest for all finishes.This provokes a fall in DWR, DWOR and FWOR ΔE values. In synthesis, for yellow and blue colors, having high values of absorbance, ΔE increases if reflectance is low, while ΔE decreases with high reflectance values. For red color, having for all finishes the lowest absorbance value and a quite high reflectance value for all finishes, a ΔE enhancement is observed.

4. CONCLUSION

Textile fabrics are subjected to various treatments for water/oil repellency, for crease recovery and for a large number of different functionalities, but one of the most innovative effects could be ascribed to the color change induced by finishing operations.Hitherto, the use of dendrimers as textile dyeing auxiliaries is quite unexplored and their application is still to be optimized; in this context, dendrimer influence on color assessment is worthy of exploration.This paper has given new results associated with the evaluation of colour assessment of cotton fabric due to nanoparticle sized finishing. Color matching of dyed samples before and after repellency treatments shows an influence of finishing onto color difference.This can be due to three possible reasons: a change on the surface roughness, an influence of finishing agents concentration and a dyeing agent/dendrimer interaction or reaction. DWR, DWOR and FWOR finishes particle sizes designate the distribution and orientation of surface layer roughness and this results with color difference.The reflectance change of the treated cotton fabric seems to be related to the particle size and to the distribution of the chemical applied. In addition, it should be also taken into consideration the absorbance of finishing agents, that in the visible range influences the dyestuff λ_{max}.Effect of surface roughness of DWR ishigher than DWOR and FWOR on color difference because of particle size distribution on the fabric surface. So it was expected to observe the highest ΔE for DWR, if taking into consideration only this major factor. As the absorbance level of DWR is not same for three colors it was clearly seen the positive effect of absorbance increasing on color difference. Increasing of λ_{max}after finishing chemicals application is always positive (or there is no effect) because of an additional absorbance after applying additives over the textile surface. Although the amount of additives over the cotton surface influences additional absorbance, no interaction with dyes results with the increase on λ_{max}. With a concentration and particle size increasing, the distribution of chemicals over the fabric causes higher surface roughness, so reflectance directly effects on concentration. Because the ability of the human eye to appreciate differences in color differs from individual to individual (as it is a combination of eye characteristics and skill of the operator), for the three different finishes

used ΔE<1 values indicated that the color changes were appreciable only byinstrumental equipment. Dendrimers finishing on cotton textiles is confirmed as good device for water and oil repellency treatments, and its performances can be compared to the commonly used fluorocarbon products. Finally, mechanical characteristics of the fabric are not considerably altered by finishing treatments:no significant differences were observed in the mechanical properties between treated and control samples.

REFERENCES

[1] Nakamura A. (2000) *Fiber science and technology*. Science, USA.

[2] Cerne L. &Simoncic, B.,(2004)Influence of Repellent Finishing on the Free Surface Energy of Cellulosic Textile Substrates.*Textile Research Journal, 74,* 426.

[3] Schindler W. D. & Hauser P. J,(2004)Chemical Finishing of Textiles.*Woodhead Publishing in Textiles, Cambridge England,* 6 *,* 79-81.

[4] Tully D. C.& Fréchet, J. M. J.,(2001)Dendrimers at Surfaces and Interfaces: Chemistry and Applications., *Chem. Commun.,*1229-1239.

[5] Menger F. M., Peresypkin A. V. &Wu, S., Do (2001)Dendritic Amphiphiles Self-Assemble in Water? A Fourier Transform Pulse-Gradient Spin-Echo NMR Study, *J. Phys. Org. Chem., 14* 392-399.

[6] Mani G., Fan Q., Ugbole S., &Eiff, I.M.,(2003)Effect of Nanoparticle Size and Its Distribution on the Dyeability of Polypropylene *„AATCC Rev,* 3, 22.

[7] Qian, L., (2004) Nanotechnology in Textiles: Recent Development and Future Prospect *„AATCC Rev,* 4, 14.

[8] Jang J., Jeong Y.,(2006) Nano roughening of PET and PTT fabrics via continuous UV/O_3 irradiation. *Dyes Pigments,* 69 137.

[9] Rosace G, Massafra MR, Iskender A & Sancaktaroglu E. (2008) "Influence of dendrimer finishing on color assessment of CO/PES blended fabrics" Proceedings of the 21st IFATCC International Congress, 6-9/05/2008 Barcellona.

[10] Dykes G.M. (2001) Dendrimers: A Review of Their Appeal and Applications. *Chem. Technol. Biotechnol.,* 76 , 903-918.

[11] Duschek G. (2001) Low-emission and APEO-free Fluorocarbon Finishing, *Melliand English,* 7-8.

[12] Duschek Gunther (2004) "Bionic Finish" *Revista de Quimica Textil* 170, 20-35

[13] Cem G., Dilek K. & Mehmet O., (2007) Effect of the Particle Size of Finishing Chemicals on the Color Assessment of Treated Cotton Fabrics, *J. of Applied Polymer Science 104*, 2587-2594.

In: Chemistry and Chemical Engineering Reserch Progress ISBN: 978-1-61668-502-7
Editor: A.K. Haghi

Chapter 5

REMOVAL OF CHROMIUM(VI) ION FROM AQUEOUS SOLUTIONS USING ACID MODIFIED RICE HUSK

S. M. Mirabdolazimi, A. Mohammad-Khah, R. Ansari, and M. A. Zanjanchi
Department of Chemistry, University of Guilan, Rasht 41635-19141, Iran

ABSTRACT

Rice husk, an agricultural solid waste was used as sorbent for the removal of chromium(VI) from aqueous solution after modification with HCl. The results of the experiments showed that acid treatment of rice husk can improve the sorption efficiency considerably. Effects of pH, contact time, initial Cr(VI) concentration and adsorbent dosage were studied. Removal of chromium ion was found to be highly dependent on pH and initial concentration of Cr(VI) solution. Sorption isotherm investigation showed that equilibrium sorption data were better represented by Freundlich model than the Langmuir model. Our finding in this paper has indicated that very low cost abundant material of the rice husk modified with HCl can be effectively used for removal of Cr(VI) ion from effluents such as textile waste waters.

1. INTRODUCTION

Heavy metals are toxic and environmentally harmful substances. Especially those accumulated within the living organisms as well as in human body are more dangerous. Therefore, they have to be removed from the wastewaters before they are given to the receiving medium [1]. One of the most dangerous metal ions for human life is Cr(VI) ion which is found in industrial wastewater because of the extensive use of chromate and dichromate in electroplating, leather tanning, metal finishing, nuclear power plant, textile industries and chromate preparation. Chromium(VI) is a powerful carcinogenic agent that modifies the DNA transcription process causing important chromosomic aberrations. Cr(VI) may also cause epigastric pain, nausea, vomiting, severe diarrhea and hemorrhage. Portable

waters containing more than 0.05 mg/L of chromium are considered to be toxic. Thus, the removal of chromium ions from wastewaters is very important [2, 3].

Various methods including reverse osmosis, ion exchange, adsorption, chemical precipitation and electro deposition have been used for removal of chromium(VI) [4]. Most of these methods are highly expensive and cost effective. Therefore, numerous approaches have been studied for the development of low cost adsorbents [4]. Agricultural materials particularly those containing cellulose shows potential metal biosorption capacity. Agricultural waste materials are usually composed of lignin and cellulose as the main constituents. Other components are hemicellulose, extractives, lipids, Proteins, simple sugars, starches, water, hydrocarbons, ash and many more compounds that contain a variety of functional groups present in the binding process. Agricultural waste materials being economic and ecofriendly due to their unique chemical composition, availability in abundance, renewable, low in cost and more efficient are seem to be viable option for heavy metal remediation. Studies reveal that various agricultural waste materials such as rice bran, rice husk, wheat bran, weat husk, saw dust of various plants, bark of the trees, ground nut shells, coconut shells, black gram husk, hazelnut shells, walnut shells, cotton seed hulls, waste tea leaves, maize corn cob, jatropha deoiled cakes, sugar cane bagasse, apple, banana, orange peels, soybean hulls, grapes stalks, water hyacinth, sugar beet pulp, sunflower stalks, coffee beans, arjun nuts, cotton stalks etc has been tried [5].

In this work, we investigated HCl treated rice husk as a sorbent for the removal of Cr(VI) in this paper. Rice husk consists of cellulose, hemicellulose, lignin, and mineral ash. It is insoluble in water, has good chemical stability and high mechanical strength. Rice husk possesses a granular structure, making it a good adsorbent material for treating heavy metals from wastewater [6]. The aim of the present investigation is to detect the performance of HCl treated rice husk on Cr(VI) removal and to investigate the effect of various parameters on adsorption of Cr(VI) from aqueous solution. The information gained from these studies will elucidate whether the treated rice husk have the potential to be used for the removal of Cr(VI) ions from wastewater.

2. METHODS

2.1. Preparation of Cr(VI) solution

$K_2Cr_2O_7$ was obtained from Merck. A stock solution (1000 mg/L) of Cr(VI) was prepared by dissolving required quantity of $K_2Cr_2O_7$ in distilled water. For the experiments, Cr(VI) solution having 10-100 mg/L was prepared and used.

2.2. Preparation of Rice Husk

The rice husk used was obtained from the north part of Iran. It was crushed and sieved through the following sizes: 90-180, 180-300, 300-500, 500-600 μm. 180-300 μm fractions was used in all experiments. Then the husks were thoroughly washed with distilled water and then were dried at 110 °C. The dried husk was stored in desiccator before use.

2.3. Modification of the Rice Husk

5.0 g of rice husk was mixed with 500 mL of the HCl 0.10M and agitated for 24h. After acid treatment, it was filtered, washed with distilled water and dried in an oven at 80 °C for 6h.

2.4. Batch Adsorption Experiments

All experiments were carried out at room temperature. The adsorbent was added to 50 mL of test solution in a 100 mL conical flask. Batch adsorption studies were carried out at the desired pH value, contact time and adsorbent dosage level. Different initial concentration of Cr(VI) solutions was prepared by proper dilution from stock 1000 ppm Cr(VI). The pH of the solution was monitored by adding 0.1 M HCl and 0.1 M NaOH solution as required. The suspension was shaken for some time which is required for reaching the equilibrium condition estimated by drawing samples at regular intervals of time till equilibrium was reached. The contents of the flask were filtered through filter paper and the filtrate was analyzed for remaining Cr(VI) concentration in the sample using Perkin-Elmer UV-visible spectrophotometer with 1,5-diphenylcarbazide in acid medium by following APHA, AWWA standard methods for examination of water and wastewater [7]. The removal percentage (R%) of chromium(VI) was calculated by following expression:

$$R(\%) = \left[\frac{(C_i - C_e)}{C_i} \right] \times 100 \tag{1}$$

And amount of Cr(VI) adsorbed by adsorbent (q) in the adsorption system was calculated using the mass balance:

$$q = \frac{V(C_i - C_e)}{m} \tag{2}$$

where V is the solution volume (L), m is the amount of sorbent (g), and Ci and Ce (mg/L) are the initial and equilibrium metal concentration, respectively.

3. RESULTS AND DISCUSSION

3.1. Effect of Chemical Treatment on Sorption

The chemical modification resulted in increasing the Cr(VI) uptake of rice husk. Pretreatment of plant wastes can extract soluble organic compounds and enhance chelating efficiency [6]. The effect of physical and chemical pretreatment processes appeared to enhance the metal (usually cations) sorption capacity [8]. Pretreatment of rice husk can remove lignin, hemicellulose, reduce cellulose crystallinity and increase the porosity or

surface area. In general, chemically modified or treated rice husk exhibited higher adsorption capacities on heavy metal ions that unmodified rice husk. When rice husk is treated with hydrochloric acid, adsorption sites on the surface of rice husk will be protonated, leaving the heavy metal ions in the aqueous phase rather than being adsorbed on the adsorbent surface [6].

3.2. Effect of pH on Cr(VI) Removal

The pH of the medium has a significant effect on the sorption of on metal ions on different adsorbents. For adsorption of Cr(VI), experiments were carried out by varying pH from 2 to 8. The results presented in Fig .1 indicate that Cr(VI) removal is considerably affected by the pH. The maximum adsorption of chromium(VI) metal ions was observed at pH value of 2.0. At initial pH value of 2.0, the adsorbent surfaces might be highly protonated which favor the uptake Cr(VI) in the predominant anionic form ($HCrO_4^-$). With increase in pH, the degree of protonation of the surface reduces gradually and hence adsorption is decreased [9]. Further decrease in percent removal at alkaline pH is due to the competition of OH^- ions and chromate ions for the adsorption sites [3]. Adsorption of Cr(VI) on the adsorbent was not significant at greater pH values due to dual competition of both the anions (CrO_4^{-2} and OH^-) for adsorbtion on the surface of the adsorbent of which OH^- predominant.

Furthermore, the removal of Cr(VI) is also dependent on the redox between the sorbent surface groups and sorbate [10]. Cr(VI) oxyanion is readily reduced to Cr(III) ions due to the presence of electron donors of rice hulls according to the following reaction:

$$HCrO_4^- + 7H^+ + 3e- \rightleftharpoons Cr^{3+} + 4H_2O$$

This can be observed that the reduction of Cr(VI) oxyanion is accompanied by proton consumption in the acidic solution, confirming the role played by H^+ in the Cr(VI) removal [11]. A significant portion of Cr(VI) in solution can be reduced to Cr(III) depending on the conditions such as PH, temperature and time [3]. In such studies, some important kinetic and thermodynamic evaluations have been made on the basis of Cr(VI) removal without considering reduction effects which can lead to erroneous conclusions.

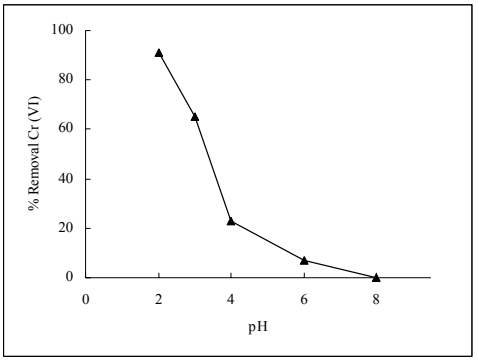

Figure 1. Effect of pH on the adsorption of Cr(VI); Initial Cr(VI) concentration 10 mg/L, adsorbent dosage 1g /50 mL, contact time 2 h.

4. Effect of Adsorbent Dosage

One of the parameters that strongly affect the sorption capacity is the dosage of the adsorbent in the liquid phase. The adsorbent was used at dosage ranging from 0.2 g/50 mL to 1.2g/50mL in a batch adsorption technique. The effect of adsorbent dosage is depicted in Figure 2. As our data show, increase in adsorbent results in an increase in percent removal of Cr(VI). With increasing adsorbent dosage more surface area is available for adsorption due to increase in active sites on the adsorbent [9]. After certain adsorbent dosage the removal efficiency is not increased so significantly. At 1.0 g/50mL of adsorbent dosage maximum Cr(VI) removal was observed. Therefore, the experiments were carried out at adsorbent concentration of 1.0 g/50 mL.

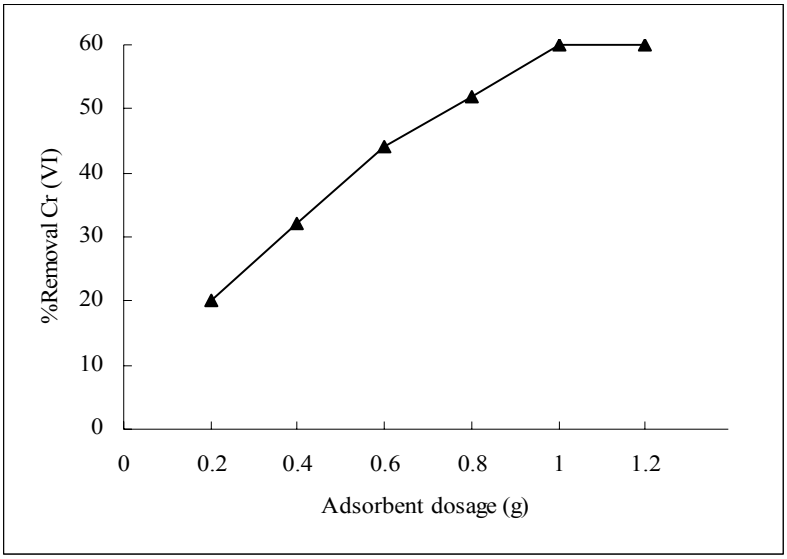

Figure 2. Effect of adsorbent dosage on adsorption of Cr(VI); pH 2, initial Cr(VI) concentration 100 mg/L, contact time 2 h.

5. Effect of Initial Metal Ion Concentration

For performing this experiment, fixed amounts of adsorbent (1.0 g) was treated with 50 mL of Cr(VI) solutions containing various concentrations (10-100 mg/L). Experiments were also carried out at contact time of 2 h and pH value of 2.0. According to the results obtained in this experiment (Figure 3), it was found that the efficiency of Cr(VI) removal is affected by the initial Cr(VI) concentration. Removal percentage is decreased as the initial concentration of Cr(VI) is increased.

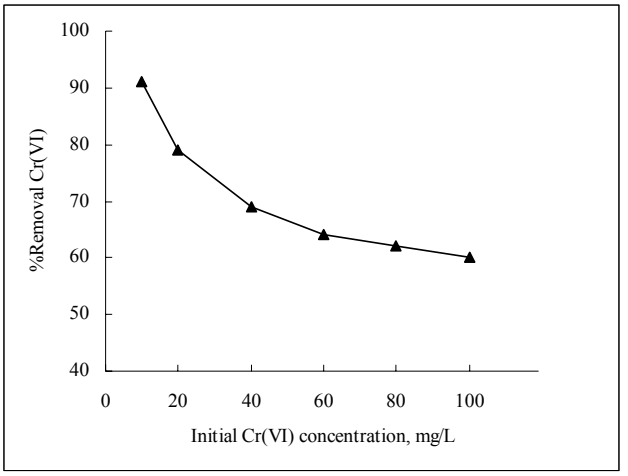

Figure. 3. Effect of initial concentration on the adsorption of Cr(VI); pH 2, adsorbent dosage 1 g/50 mL, contact time 2 h.

At low metal ion/adsorbent ratios, metal ion adsorption involves higher energy sites. As the metal ion/adsorbent ratio increases, the higher energy sites are saturated and adsorption begins on lower energy sites, resulting in decreases in the adsorption efficiency [12].

6. Effect of Contact Time

The experimental runs measuring the effect of contact time on the batch adsorption of Cr(VI) and at initial pH value 2 and initial Cr(VI) concentration of 100 mg/L is shown in Figure 4. It is obvious that increase in contact time from 0.5 to 2.0 h enhanced the percent removal of Cr(VI) significantly and thereafter, it remains almost constant. Therefore a contact time of 2 h was needed for equilibrium to be established.

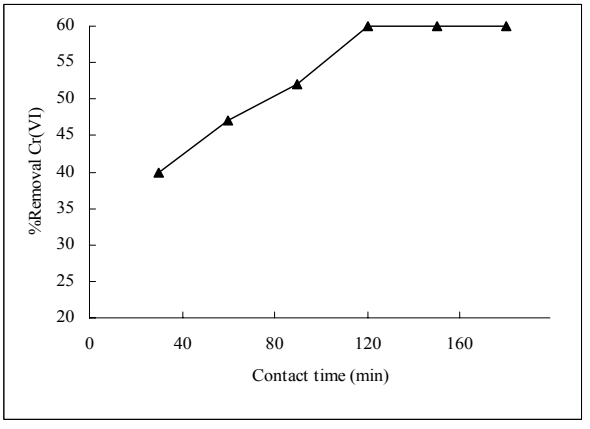

Figure. 4. Effect of contact time on the adsorption of Cr(VI); initial Cr(VI) concentration 100mg/L, adsorbent dosage 1 g/50 mL and pH 2.

7. ADSORPTION MODELS

Two well-known adsorption models, Langmuir and Freundlich, were applied for the analysis of sorption data obtained at different initial concentrations [8]. The Langmuir equation is applicable for the adsorption on homogeneous surfaces and it depends on the assumptions which can be summarized as there are constant numbers of active sites having the uniform energy on adsorbent surface and adsorption energy is constant. Further, it is assumed that adsorption is a monolayer adsorption and the maximum adsorption occurs when molecules adsorbed on the surface of adsorbent form a saturated layer. Langmuir isotherm is valid for the cases where adsorption is a monolayer coverage processes, therefore, it is expected that adsorption value reach to a maximum value at high pressure or concentrations [1, 8]. Langmuir isotherm may be written as the following:

$$q_e = \frac{Q_{\max} b C_e}{1 + b C_e} \text{ (nonlinear form)} \tag{3}$$

$$\frac{1}{q_e} = \frac{1}{Q_{\max}} + \frac{1}{b Q_{\max} C_e} \text{ (linear form)} \tag{4}$$

where C_e is the residual Cr(VI) concentration (mg/L), q_e is the amount of metal adsorbed (mg/g), Q_{max} (mg/g) and b (L/mg) are the Langmuir constant showing the maximum amount of metal ion adsorbed per unit weight of adsorbent to form a complete monolayer on the surface bound at high equilibrium metal ion concentration and the energy of adsorption, respectively [13]. Langmuir isotherm showed linear plot and values of Langmuir constant (Q_{max} and b) calculated from the slope and the intercept of the plot (Figure 5).

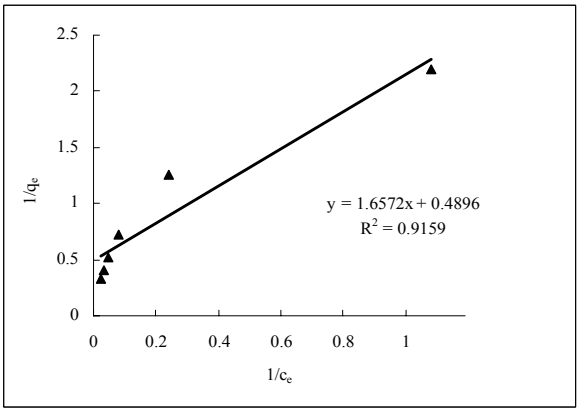

Figure. 5. Langmuir adsorption isotherm for the adsorption of Cr(VI) ions on to adsorbent.

The essential characteristics of the Langmuir isotherm may be expressed in terms of a dimensionless constant separation factor or equilibrium parameter, R_L, which is defined as

$$R_L = \frac{1}{1 + bC_0} \tag{5}$$

Where b is the Langmuir constant (L/mg) and C_0 is the initial concentration (mg/L). The R_L value lying between 0 and 1 indicate favorable adsorption [8].

Values	Types of isotherm
$R_L>1$	Unfavorable
$R_L=1$	Linear
$0<R_L<1$	Favorable
$R_L<0$	Irreversible

The values of R_L for the HCl treated rice husk are listed in Table 1. The data represented a favorable uptake of Cr(VI) by modified rice husk.

Table 1. Separation factor for the adsorption of Cr(VI) on to modified rice husk

R_L	Initial concentration of chromium(VI)
0.25	10
0.15	20
0.08	40
0.05	60
0.04	80
0.03	100

Although Freundlich isotherm is generally used for the adsorption from liquid solutions, it is used for the gas adsorption as well. The empirical Freundlich adsorption isotherm is obtained on the assumption that the sorption takes place on a heterogeneous adsorbent surface where the sorption energy distribution decreases exponentially. This equation is also applicable to multilayer adsorption. According to this model, initially amount of adsorbed compound increases rapidly, this increase slow down with the increasing surface coverage [14, 15]. Freundlich isotherm may be written as the following:

$$q_e = K_f C_e^{1/n} \text{ (nonlinear form)} \tag{6}$$

$$\log q_e = \frac{1}{n}\log C_e + \log k_f \text{ (linear form)} \tag{7}$$

where K_f and n are the Freundlich constant which represent the adsorption capacity and the adsorption intensity of the sorbent, respectively [8, 13]. The value of n between 1 and 10 represent a favorable adsorption [16]. Freundlich isotherm showed linear plot and values of Freundlich constant (K_f and n) calculated from the slope and the intercept of the plot (Figure

6) are presented in table 2. The value of n lies between 1 and 0 for HCl treated rice husk, which represents a favorable adsorption.

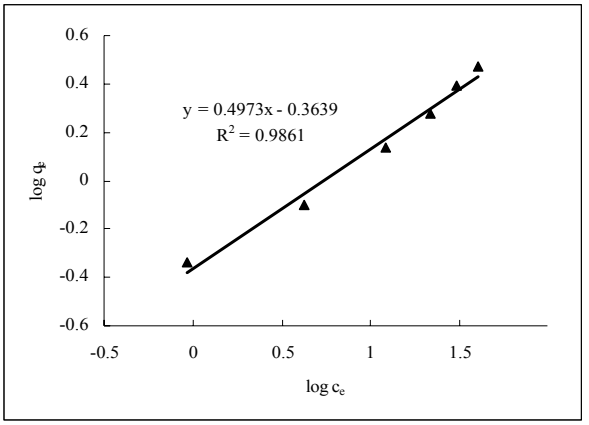

Figure 6. Freundlich adsorption isotherm for the adsorption of Cr(VI) ions on to adsorbent.

The calculated results of the Langmuir and Freundlich isotherm constants are also given in Table 2. Comparison of experimental values and Langmuir and Freundlich isotherms showed that Freundlich isotherm confirms very well with the experimental data. Regression coefficient values also support this observation. This observation suggests that the adsorption of chromium ion on HCl treated rice husk is a multilayer adsorption.

Table 2. Freundlich and Langmuir isotherms regression constants

Freundlich isotherm			Langmuir isotherm		
R^2	K_f (L g^{-1})	n	R^2	Q_{max}(mg g^{-1})	b(L mg^{-1})
0.98	0.43	2.01	0.91	2.04	0.29

CONCLUSION

The pH variation studies showed that the adsorption process for the adsorbent is highly pH dependent. The optimum pH range for the removal was found to be 2. HCl treated rice husk could be suitable adsorbent for the removal of Cr(VI) from dilute aqueous solutions. The adsorption data of HCl treated rice husk have been found to be better fitting to Freundlich isotherm. Therefore, it may be regarded that HCl treated rice husk has a heterogeneous surface.

REFERENCES

[1] Uysal, M., & Ar, I. (2007). Removal of Cr(VI) from industrial wastewaters by adsorption Part I: Determination of optimum conditions. *Journal of Hazardous Materials,* 149, 482–491.

[2] Bayramoglu, G., Celik, G., Yalcın, E., Yılmaz, M., & Arıca, M. Y. (2005). Modification of surface properties of Lentinus Sajor-caju mycelia by physical and chemical methods: evaluation of their Cr^{6+} removal efficiencies from aqueous medium. *Journal of Hazardous Materials,* B119, 219–229.

[3] Namasivayam, C., & Sureshkumar, M. V. (2008). Removal of chromium(VI) from water and wastewater using surfactant modified coconut coir pith as a biosorbent. *Bioresource Technology,* 99, 2218-2225.

[4] Kumar, U., & Bandyopadhyay, M. (2006). Sorption of cadmium from aqueous solution using pretreated rice husk. *Bioresource Technology,* 97, 104-109.

[5] Sud, D., Mahajan, G., & Kaur, M.P. (2008). Agricultural waste material as potential adsorbent for sequestering heavy metal ions from aqueous solutions - A review. *Bioresource Technology,* 99, 6017-6027.

[6] Wan Ngah, W. S., & Hanafiah, M. A. K. M. (2008). Removal of heavy metal ions from wastewater by chemically modified plant wastes as adsorbents: A review. *Bioresource Technology,* 99, 3935-3948.

[7] Clesceri, L. S, Greenberg, A. E., & Eaton, A. D. (1998). *Standard Methods for the Examination of Water and Wastewater. 20th ed*. New York, United states: APHA, AWWA.

[8] Bingol, A., Aslan, A., & Cakici, A. (2009). Biosorption of chromate anions from aqueous solution by a cationic surfactant-modified lichen (cladonia rangiformis (L)). *Journal of Hazardous Materials,* 161, 747-752.

[9] Bansal, M., Garg, U., Singh, D., & Garg, V. K. (2009). Removal of Cr(VI) from aqueous solutions using pre-consumer processing agricultural waste: A case study of rice husk. *Journa of Hazardous Materials,* 162, 312-320.

[10] Guo, Y., Qi, J., Yang, S., Yu, K., Wang, Z., & Xu, H. (2002). Adsorption of Cr(VI) on micro- and mesoporous rice husk-based active carbon. *Materials Chemistry and Physics,* 78, 132-137.

[11] Kurniawan, T.A., Chan, G.Y.S., Lo, W., & Babel, S. (2006). Comparisons of low-cost adsorbents for treating wastewaters laden with heavy metals. *Science of the Total Environment,* 366, 409-426.

[12] Bhattacharya, A. K., Naiya, T. K., Mandal, S. N., & Das, S. K. (2008). Adsorption, kinetics and equilibrium studies on removal of Cr(VI) from aqueous solutions using different low-cost adsorbents. *Chemical Engineering Journal*, 137, 529-541.

[13] Mohan, D., & Pittman Jr, C.U. (2006). Activated carbons and low cost adsorbents for remediation of tri- and hexavalent chromium from water. *Journa of Hazardous Materials,* B137, 762-811.

[14] Aoyama, M., & Tsuda, M. (2004). Removal of chromium(VI) from aqueous solutions by larch bark. *Wood Science and Technology,* 35, 425-434.

[15] Sharma, A., & Bhattacharyya, K.B. (2004). Adsorption of chromium(VI) on *Azadirachta indica* (neem) leaf powder. *Adsorption,* 10, 327-338.

[16] Bhattacharya, A.K., Mandal, S.N., & Das, S.K. (2006). Adsorption of Zn(II) from aqueous solution by using different adsorbents. *Chemical Engineering Journal*, 123, 43-51.

In: Chemistry and Chemical Engineering Reserch Progress ISBN: 978-1-61668-502-7
Editor: A.K. Haghi

Chapter 6

LATTICE PARAMETERS OF CALCITE IN THE PT-PLANE TO 7.62 KBAR AND 533°C

Michael J. Bucknum[1] and Eduardo A. Castro[2*]

[1] Department of Chemistry, Baker Laboratory, Cornell University, Ithaca, New York 14853, USA

[2] INIFTA, Theoretical Chemistry Division, Suc.4, C.C. 16, La Plata 1900, Buenos Aires, Argentina

ABSTRACT

Calcite lattice parameters have been measured at simultaneous pressure and temperature using a newly designed hydrothermal diamond anvil cell capable of 1200°C and 25 kbar. Real-time energy dispersive diffraction patterns were obtained from a gasketed sample of powdered calcite immersed in water using white synchrotron radiation. A path of constant density was followed in the PT-plane of water as the sample chamber volume remained constant. Temperature was directly measured from chromel-alumel thermocouples cemented to the upper and lower diamond anvils, and the pressure was calculated from the equation of state of water using the temperature (115 ± 3ºC) at which the vapour phase disappeared to mark the isochore (0.950 ± 0.005 gm/cm^3) followed. Least squares regression of eight calcite reflections from a room pressure-tempeature pattern obtained at the Cornell High Energy Synchrotron Source (CHESS) yielded a_o = 4.988 ± 0.001 Å and c_o = 17.088 ± 0.001 Å.

A high temperature diffractometer on a conventional source was used to measure lattice parameters of the calcite to 524ºC. From a linear least squares fit to these data, the thermal anisotropy previously reported for calcite was confirmed as a/a_o changed by -3.63x10^{-6}/°C, while in contrast changed by +3.26x10^{-5}/°C. At CHESS, diffraction data were collected in the PT-plane from calcite immersed in water, and each pattern was least squares refined for the calcite lattice parameters. Along the 0.950 gm/cm^3 isochore of water, the thermal anisotropy in the calcite lattice parameters changed slightly with the application of water pressure. From a linear fit on the calcite data obtained at CHESS, a/a_o changed by -5.196x10^{-6}/°C and c/c_o changed by +2.872x10^{-5}/°C along the 0.950 gm/cm^3 isochore of water. Because the expansion of the c-lattice parameter of calcite is

* Corresponding author (eacast@gmail.com, castro@quimica.unlp.edu.ar)

nearly an order of magnitude greater than the contraction of the a-lattice parameter, the unit cell volume of calcite expands along the temperature axis and along this water isochore to 7.62 kbar water pressure at 533°C.

INTRODUCTION

Carbonate minerals have been the subject of many crystallographic studies owing to the curious anisotropy observed in the temperature and pressure responses. High-temperature diffractometer studies of calcite (Markgraf and Reeder, 1985) and Rao et al., 1968) indicate a/a_o *decreases* by 10^{-6}/°C while c/c_o *increases* by 10^{-5}/°C with increasing temperature. With pressure, the compressibility of a/a_o is 3/5 as great as that of c/c_o, up to 20 kbar (Fiquet et al., 1993).

Bivariant changes of the calcite lattice parameters in the PT-plane have been proposed as a basis for a double internal X-ray standard for simultaneous pressure and temperature measurements by Hazen and Finger (1982). The monogram shown in Figure 1 of Hanzen and Finger (1982, p.72) and corrected by us for switched axes, shows proposed contours of constant a/a_o and c/c_o in the PT-plane. Because data on calcite in the PT-plane are determined only along the pressure and temperature axes, these contours lines are only a proposal. The main purpose of the research reported in this paper is to fill in these contour lines based on simultaneous pressure-temperature measurements.

Through the use of a recently designed hydrothermal diamond anvil cell (Bassett et al., 1993) it is now possible to carry out hydrothermal experiments to temperatures above 1000°C while simultaneously applying water pressure up to 20 kbar and beyond. Synchrotron radiation experiments can be performed to obtain real-time energy dispersive X-ray diffraction patterns of the gasketed sample of powdered calcite in water at an accurately measured temperature and pressure. The intervening points along the contour lines in the calcite monogram can be determined from calcite diffraction patterns obtained in this way.

As is described in this paper, diffraction patterns of powdered calcite were obtained in the PT-plane along the 0.950 gm/cm^3 isochore of water. Pressure was calculated by the equation of state of water (Shen et al., 1992) using as primary reading the temperature measured from chromel-alumel thermocouples cemented in contact with the diamonds. Least-squares refinement of the calcite patterns (Burnham, 1965) at each pressure-temperature point resulted in refined a(P,T) and c(P,T) values along the water isochore that was followed.

EXPERIMENTAL

Specimens

Icepand Spar was obtained from the Mineral Collection of Cornell University, Department of Geological Sciences, #11.41-231. Several centimetre-size calcite crystals were ground in an alumina mortar and pestle to a fine-grained powder. Part of the fine-grained sample was carefully transferred to a 500 μm diameter sample chamber made from a laser machined Re foil with a 125 μm thickness.

The Re gasket was centered and mounted on the lower diamond anvil face which was approximately 1000 μm across. A droplet is distilled and deionized water was applied to the upper diamond anvil face. By surface tension, the droplet adhered to the upper diamond as it was brought into contact with the gasketed calcite sample and sealed by driving the anvil faces together with the driver nuts. At room temperature, the gasketed sample appeared as white powdered calcite immersed in water in contact with a bubble of water-saturated air.

Data Collection

A fixed volume was attained inside the 500 micrometer gasket hole by bringing the diamond from the upper platen in contact with the gasket containing the calcite in water sample. As has been verified in separate experiments (Shen et al., 1992), the thickness of the Re gasket undergoes only minor change in the hydrothermal cell to well over 1000°C; during cooling there is usually no change in the thickness of the gasket hence the volume of the sample chamber is usually constant during cooling (Bassett, 1993).

After sealing off the sample, the hydrothermal cell was mounted on a white X-ray beamline at CHESS. The incident white beam was centered and normal to the gasketed sample and was directed at the sample using a pinhole with a diameter of 300 μm. An intrinsic Ge detector and a multi-channel analyzer (MCA) program were used to collect the actual energy dispersive diffraction pattern.

From a pattern collected at room temperature, the presence of calcite reflections and the absence of Re reflections indicated when the X-ray beam passé through the sample. From this criterion alone, the centering of the white beam within the sample was verified. At room temperature and normal pressure, the pattern was collected with the calcite reflections labelled on the inset.

There are eight reflections in this room-temperature pattern intense enough for an accurate peak fitting to be performed. From comparison against published powder diffraction data on calcite (Swanson and Fuyat, 1953) at room temperature and pressure, the room pressure-temperature reflections were used to refine the conversion factor Ed, where E is the energy of the peak in keV, and d is the spacing of lattice planes, in Å, that produced the peak. The value 64.790 ± 0.005 keV-Å corresponds to a 2θ of 10.989 ± 0.021°.

As explained by Bassett et al., (1993), heating of the gasketed sample was accomplished by resistance heaters consisting of molybdenum wire wound around each WC diamond anvil seat. The extremely high thermal conductivity of the diamond anvils is exploited in this design, and from calibration of the thermocouples against the room pressure melting points of sodium nitrate, sodium chloride and the triple point of water, it is apparent that the difference in the temperature is registered at the thermocouple and that corresponding to these phase changes are within 4ºC of each other (Shen et al., 1993).

Typically the gasket changes thickness to some extent during the heating of the sample, while following a cooling curve, the thickness of the gasket is maintained (Bassett, 1993). Observation of the homogenization temperature before the diffraction experimented yielded 113°C to 117°C. After collecting the diffraction data along the heating curve, the homogenization temperature was observed to 112°C to 115°C indicating that the volume of the sample chamber had not changed significantly during heating and cooling. Therefore to

0.950 ± 0.005 gm/cm^3 isochore was followed for the diffraction data collected in this experiment.

From the room pressure-temperature pattern, the shift in the Bragg peaks and their relative intensities in subsequent patterns collected along the heating curve in the experiment indicated that the calcite sample did not transform by decomposition or by chemical reaction to other phases.

Along the temperature axis, powder diffraction data were collected to 524°C on an conventional source using a Scintag θ-θ diffractometer with a high temperature attachment. These data were then employed in a linear interpolation of the temperature response on the lattice parameters of calcite, as is described below.

Refinement Procedures

Each of the energy dispersive diffraction patterns was comprised of peaks of diffracted intensity at the wavelengths satisfying the Bragg equation at a fixed angle of 10.989 ± 0.021º. In each pattern, from six to eight such peaks due to calcite were of sufficient intensity above background so that a Gaussian-Lorentzian curve fitting algorithm could be applied to reduce the pattern to a set of d-spacings.

A least squares program (Burnham, 1965) was used to refine the calcite lattice parameters, a and c, from the peaks for each pressure-temperature point at which a calcite pattern was collected. The algorithm which this program is based upon is Cohen´s least-squares method (Cohen, 1935 and Klug and Alexander, 1954). The refinement procedure involves iteratively minimizing the sum of the random observational errors for the reflections in the pattern with respect to the lattice parameters on the unit cell. A Smith-Snyder figure of merit (Smith and Snyder, 1968) was used as the convergence criterion for each refinement. Each of the patterns was refined after fewer than three cycles.

RESULTS

Lattice Parameters of Calcite to 533°C and 7.62 kbar

Least squares refined values of the calcite lattice parameters were collected using a high temperature attachment on a θ-θ powder diffractometer. The data indicate anisotropy in the thermal expansivity of the calcite lattice parameters. Since the volume of the hexagonal unit cell of calcite is proportional to a^2c, and c/c_o increases by 10^{-5}/°C while a/a_o decreases by 10^{-6}/°C, the unit cell in calcite expands with temperature despite the fact that the a-axis is contracting. The linear interpolation is used to provide the $a/a_o(T)$ and $c/c_o(T)$ scale for the temperature axis. Results are shown in Table 1.

Table 1. Lattice parameters of Calcite and a/ao and c/co of calcite along the temperature axis at 1 bar pressure using high temperature ◘-◘ diffractometer data.

Temperature, °C	a(Å)	c(Å)	a/a_o	c/c_o
28.0	5.016(3)	17.167(3)	1.0000	1.0000
50.0	5.016(4)	17.173(6)	1.000(0)	1.000(4)
100.0	5.013(7)	17.209(7)	0.999(5)	1.002(5)
158.0	5.012(5)	17.238(8)	0.999(2)	1.004(2)
200.0	5.011(8)	17.262(4)	0.999(1)	1.005(5)
254.0	5.011(7)	17.283(4)	0.999(1)	1.006(8)
400.0	5.008(9)	17.364(6)	0.998(5)	1.011(5)
432.0	5.007(9)	17.393(0)	0.998(3)	1.013(2)
524.0	5.007(4)	17.449(4)	0.998(2)	1.016(4)

Along the pressure axis, the powder diffraction data of Fiquet et al. (1993) can be plotted as a/a_o and c/c_o versus pressure. The room temperature compressibility curve of a/a_o is about 3/5 as great as that of c/c_o up to 20 kbar. A linear interpolation of these data is used to provide the $a/a_o(P)$ scale for for the pressure axis in the a/a_o contours. For the calcite sample used in the compressibility study by Fiquet et al. (1993) at zero pressure and room temperature, a_o = 4.990(4) Å and c_o = 17.064(7) Å, which agree with the values of a_o = 4.988(3) Å and c_o = 17.088(5) Å from the powder data collected at CHESS in the diamond anvil cell at room temperature and pressure.

In the PT-plane, the calcite lattice parameters were determined from energy dispersive X-ray diffraction. The energy dispersive diffraction patterns collected at about 150°C intervals along the 0.950 gm/cm^3 isochore of water indicate that the calcite sample did not transform to another phase during heating along this isochore of water.

Lattice parameters of calcite along the 0.950 gm/cm^3 isochore of water are given in Table 2. The values of a/a_o and c/c_o along this isochore versus temperature along the bottom axis and versus pressure along the top axis based on least squares fits of the data to linear functions provide smooth functions of the temperature and pressure dependences, respectively, of a/a_o and c/c_o along the 0.950 gm/cm^3 isochore of water. By interpolating along the smooth functions of temperature, the corresponding pressures can be calculated using the equation of state of water (Haar, 1984). The interpolated pressure-temperature points are then used for constructing the contour points.

The linear interpolation performed to obtain $a/a_o(P,T)$ and $c/c_o(P,T)$ points along the 0.950 gm/cm^3 isochore of water was then combined with corresponding interpolated points along the pressure and temperature axes. Lines of constant a/a_o could be constructed from the sets of related a/a_o points along the temperature axis, along the 0.950 gm/cm^3 isochore of water and along the pressure axis. From the points along the temperature axis and along the isochore of water followed in the experiment, lines of constant c/c_o could be constructed. These lines of constant a/a_o and c/c_o in the PT-plane can be compared to the calcite nomogram of Hazen and Finger mentioned before.

Table 2. Lattice parameters of calcite and a/a_o and c/c_o of calcite along the 0.950 gm/cm^3 water isochore

Temperature, ºC	Pressure, kbar	a(Å)	c(Å)	a/a_o	c/c_o
25.5	0.00	4.988(3)	17.088(5)	1.0000	1.0000
51.5	0.00	4.986(9)	17.102(8)	0.999(7)	1.000(8)
76.5	0.00	4.986(2)	17.114(3)	0.999(6)	1.001(5)
103.0	0.00	4.987(3)	17.113(9)	0.999(8)	1.001(5)
133.0	0.36	4.986(8)	17.134(0)	0.999(7)	1.002(7)
161.5	0.86	4.985(5)	17.147(9)	0.999(4)	1.003(5)
176.0	1.13	4.984(8)	17.152(3)	0.999(3)	1.003(7)
199.0	1.57	4.983(5)	17.160(5)	0.999(0)	1.004(2)
231.5	2.18	4.984(3)	17.171(2)	0.999(2)	1.004(5)
249.5	2.53	4.983(0)	17.182(7)	0.998(9)	1.005(5)
279.5	3.12	4.982(9)	17.198(9)	0.998(9)	1.006(5)
298.0	3.46	4.983(9)	17.201(1)	0.999(1)	1.006(6)
318.0	3.84	4.980(9)	17.228(0)	0.998(5)	1.008(2)
350.5	4.46	4.979(5)	17.242(2)	0.998(2)	1.009(0)
374.5	4.90	4.981(6)	17.235(7)	0.998(6)	1.008(6)
394.5	5.24	4.980(4)	17.257(5)	0.998(4)	1.009(9)
411.0	5.55	4.976(4)	17.309(7)	0.997(6)	1.012(9)
533.0	7.62	4.976(4)	17.309(6)	0.997(6)	1.012(9)

DISCUSSION

Contour Diagrams of $a/a_o(P,T)$ and $c/c_o(P,T)$

Up to 533ºC and 7.62 kbar, the c-axis expands with temperature and along the 0.950 gm/cm^3 isochore of water, while the a-axis contracts. The contours of a/a_o in the PT-plane can be derived from data in Table 3. Since a/a_o decreases along the temperature axis and also along the pressure axis, contour lines are expected to join a/a_o points of the same value along the pressure and temperature axes through the PT-plane. In order for the a/a_o points along the temperature and pressure axes to pass through the corresponding $a/a_o(P,T)$ isochore points, the contour lines for a/a_o are constrained to have convex-upward curvature.

This experimental result is in contrast to the predicted shape of the a/a_o contours shown in the calcite nomogram in Figure 1 from Hazen and Finger (1982). Our experimentally observed convex-upward curvature for the a/a_o contours corresponds to a decrease in the compressibility of the a-axis of calcite compared to the room temperature compressibility along this axis. Such a decrease in the slope of the compressibility along the a-axis refers to compressibility curves above room temperature in which the a/a_o ratios are offset to values less than one along the room temperature axis.

Table 3. Contour lines of calcite a/a_o in the PT-plane interpolated from least squares fits to the calcite lattice parameters along the temperature-axis, the pressure-axis and along the 0.950 gm/cm^3 water isochore

Temperature, °C	Pressure, kbar	a/a_o
25.5	0.00	1.0000
153.1	0.00	0.9995
25.0	1.39	0.9995
138.6	0.46	0.9995
178.6	0.00	0.9994
25.0	1.66	0.9994
158.4	0.80	0.9994
204.1	0.00	0.9993
25.0	1.94	0.9993
178.2	1.17	0.9993
229.6	0.00	0.9992
25.0	2.21	0.9992
198.0	1.55	0.9992
255.1	0.00	0.9991
25.0	2.49	0.9991
217.8	1.93	0.9991
280.6	0.00	0.9990
25.0	2.77	0.9990
237.7	2.31	0.9990
306.2	0.00	0.9989
25.0	3.05	0.9989
257.5	2.68	0.9989
331.7	0.00	0.9988
25.0	3.33	0.9988
277.3	3.06	0.9988
357.2	0.00	0.9987
25.0	3.60	0.9987
297.1	3.45	0.9987
382.7	0.00	0.9986
25.0	3.88	0.9986
316.9	3.82	0.9986
408.2	0.00	0.9985
25.0	4.16	0.9985
336.7	4.20	0.9985
433.7	0.00	0.9984
25.0	4.43	0.9984
356.5	4.55	0.9984
459.2	0.00	0.9983
25.0	4.71	0.9983

Table 3 (Continued)		
376.3	4.92	0.9983
484.8	0.00	0.9982
25.0	4.99	0.9982
396.1	5.28	0.9982
510.3	0.00	0.9981
25.0	5.26	0.9981
415.9	5.62	0.9981
535.8	0.00	0.9980
25.0	5.54	0.9980
435.7	5.99	0.9980

The sets of corresponding points used in constructing the contours plots of $c/c_o(P,T)$ are listed in Table 4. Contours of c/c_o in the PT-plane can be derived using data from Table 4. Because c/c_o increases with temperature but decreases with pressure, the contours in the pressure-temperature plane will not join the temperature and pressure axes. These contours have slight upward curvature to about 2 kbar then gradually level off to straight parallel lines with slight positive slopes. Their shape is in agreement qualitatively with the predicted c/c_o contours in the corrected calcite nomogram shown in Figure 1 from Hazen and Finger (1982).

Table 4. Contour lines of calcite c/c_o in the PT-plane interpolated from least squares fits to the calcite lattice parameters along the temperature-axis and along the 0.950 gm/cm3 water isochore

Temperature, °C	Pressure, kbar	c/c_o
25.5	0.00	1.0000
60.1	0.00	1.0010
91.0	0.00	1.0020
122.1	0.18	1.0020
121.9	0.00	1.0030
156.2	0.77	1.0030
152.9	0.00	1.0040
190.4	1.40	1.0040
183.9	0.00	1.0050
224.5	2.05	1.0050
214.8	0.00	1.0060
258.6	2.70	1.0060
245.8	0.00	1.0070
292.7	3.37	1.0070
276.8	0.00	1.0080
326.8	4.01	1.0080
307.7	0.00	1.0090
360.9	4.64	1.0090
338.7	0.00	1.0100

395.1	5.26	1.0100
369.6	0.00	1.0110
429.2	5.86	1.0110
400.6	0.00	1.0120
463.3	6.45	1.0120
431.5	0.00	1.0130
497.4	7.03	1.0130
462.5	0.00	1.0140
531.5	7.60	1.0140
493.4	0.00	1.0150
565.6	8.15	1.0150

The room temperature compressibility curve of the c-axis will pass through values of c/c_o less than one, while at temperatures above room temperature the compressibility curves have shallower slopes but refer to compressibility from c/c_o which are offset to ratios greater than one along the pressure axis. The shallower slopes of these higher temperature compressibility curves correspond to a decrease in the compressibility of the c-axis at higher temperatures.

Contour Diagrams of c/a(P,T) and V/V_o(P,T

Least squares refined values for c/a(P,T) and V/V_o(P,T) are shown in Table 5 from the diffraction data collected to 533ºC and 7.62 kbar. A linear interpolation was performed to obtain c/a(P,T) and V/V_o(P,T) points along the 0.950 gm/cm^3 isochore of water which had the corresponding interpolated points along the temperature axis, in a manner previously described for the c/c_o contour plot. From these interpolated sets of points, contour lines were constructed for c/a and V/V_o in the PT-plane by joining together points of the same value at the temperature axis with the corresponding point in the PT-plane along the 0.950 gm/cm^3 isochore of water.

Table 5. V/V_o and c/a ratios of calcite measured along the 0.950 gm/cm^3 water isochore

Temperature °C	Pressure, kbar	V, Å^3	V/V_o	c/a
25.5	0.00	368.23(5)	1.0000	3.425(7)
51.5	0.00	368.33(6)	1.000(3)	3.429(6)
76.5	0.00	368.48(2)	1.000(7)	3.432(3)
103.0	0.00	368.63(5)	1.001(1)	3.431(5)
133.0	0.36	369.00(0)	1.002(1)	3.435(9)
161.5	0.86	369.09(3)	1.002(3)	3.439(6)
176.0	1.13	369.08(8)	1.002(3)	3.440(9)
199.0	1.57	369.07(5)	1.002(3)	3.443(5)
231.5	2.18	369.42(4)	1.003(2)	3.445(1)
249.5	2.53	369.47(9)	1.003(4)	3.448(3)
279.5	3.12	369.81(6)	1.004(3)	3.451(6)
298.0	3.46	370.00(1)	1.004(8)	3.451(4)

Table 5 (Continued)				
318.0	3.84	370.14(6)	1.005(2)	3.458(8)
350.5	4.46	370.24(2)	1.005(5)	3.462(6)
374.5	4.90	370.40(7)	1.005(9)	3.459(9)
394.5	5.24	370.70(2)	1.006(7)	3.465(1)
411.0	5.55	371.22(9)	1.008(1)	3.478(3)
533.0	7.62	371.22(9)	1.0087(1)	3.478(3)

The V/V_o contours of calcite can be constructed from the data listed in Table 6. Each of these contours is estimated to be nearly linear with a positive slope. Compression curves are shown to decrease in slope with temperature slightly. Along the temperature axis the thermal curves are of shallower slope. This corresponds to passing through higher temperatures than in the room pressure thermal expansion curve than in the room thermal expansion curve, to pass through the same values of V/V_o. From the V/V_o contour diagram, it is evident that the crystallographic data supports the thermodynamically expected behaviour for the calcite unit cell in the PT-plane.

Table 6. Contour lines of calcite V/V_o in the PT-plane interpolated from least squares fits to the calcite lattice parameters along the temperature-axis and along the 0.950 gm/cm3 water isochore

Temperature, °C	Pressure, kbar	V/V_o
25.0	0.00	1.0000
83.8	0.00	1.0010
123.4	0.00	1.0020
153.7	0.73	1.0020
162.9	0.00	1.0030
202.5	0.00	1.0040
258.7	2.72	1.0040
242.0	0.00	1.0050
311.2	3.71	1.0050
281.6	0.00	1.0060
363.6	4.68	1.0060
321.1	0.00	1.0070
416.1	5.64	1.0070
360.7	0.00	1.0080
468.6	6.56	1.0080
400.2	0.00	1.0090
521.0	7.42	1.0090
439.7	0.00	1.0100
573.5	8.27	1.0100

The c/a contours can be constructed from the data listed in Table 7. These contours are estimated to be linear with very slight, positive slope. The flatness of these contours is remarkable and indicates that the c/a ratio has a very slight dependence on pressure and a

strong dependence on temperature. According to the shape of the c/a contours, at room pressure at a given temperature, the ratio of the c-axis to the a-axis is defined in the calcite unit cell such that subsequently applying pressure, up to about 8 kbar, will cause very slight change in this ratio.

Table 7. Contour lines of calcite c/a in the PT-plane interpolated from least squares fits to the calcite lattice parameters along the temperature-axis and along the 0.950 gm/cm3 water isochore

Temperature, °C	Pressure, kbar	c/a
25.0	**0.00**	**3.4200**
90.8	0.00	3.4300
131.0	0.00	3.4350
132.1	0.34	3.4350
171.1	0.00	3.4400
174.5	1.10	3.4400
211.3	0.00	3.4450
216.8	1.91	3.4450
251.2	0.00	3.4500
259.2	2.72	3.4500
291.6	0.00	3.4550
301.5	3.54	3.4550
331.8	0.00	3.4600
343.9	4.33	3.4600
372.0	0.00	3.4650
386.2	5.10	3.4650
412.2	0.00	3.4700
428.6	5.86	3.4700
452.3	0.00	3.4750
470.9	6.60	3.4750
492.5	0.00	3.4800
513.3	7.29	3.4800

Use of Calcite as a Double Internal X-ray Standard

Calcite has been proposed as a double internal X-ray standard by Hazen and Finger (1982). One of the objectives of this work is to assess the usefulness of calcite for this purpose. We conclude that it will be possible to develop calcite diffraction data for this purpose, but that the contours would have to be more closely defined both above and below the 0.950 gm/cm^3 isochore.

The differences between data presented in Table 7 and Table 1 suggest that more study will be required to understand the behaviour of the lattice parameters of calcite in the PT-plane. There is marked disagreement between the shape of the a/a_o contours of calcite determined in this high temperature-high pressure X-ray diffraction work (contours

constrained to be convex shaped, bowing upward) and the predicted contours of calcite of Hazen and Finger (1982) shown in their Figure 1 (the a/a_o contours are predicted with negative slopes, bowed downward). Contours of c/c_o based upon the experimental calcite diffraction data conform qualitatively to the shape proposed by Hazen and Finger (1982) in their Figure 1. Predicted c/c_o contours of calcite are linear with positive slope, while c/c_o contours based upon the calcite diffraction data bow upward from zero pressure to become linear with shallower slope than predicted by Hazen and Finger (1982).

The hydrothermal diamond anvil cell (Bassett et al., 1993) has been applied to measuring these contours quantitatively to 533ºC and 7.62 kbar using the equation of state of water from Haar et al. (1984) to calculate the pressure. A calcite nomogram that is quantitatively accurate can be constructed as more crystallographic data on calcite are collected.

REFERENCES

Bassett, W. A., Chen, A. H., Bucknum, M. J., Chou, I. M. (1993), A new diamond anvil cell for hydrothermal studies at 2.5 Gpa and from -190 to 1200ºC, *Review of Scientific Instruments*, 64, 2340-2345.

Burnham, C. W. (1965), Refinement of lattice parameters using systematic correction terms, *Carnegie Institution of Washington Yearbook*, 64, 200-202.

Cohen, M. U. (1935), Precision lattice constants from X-ray powder photographs, *Review of Scientific Instruments,* 6, 68-74.

Fiquet, G., Guyot, F., Andrault, D., Itie, J. P. (1993), High-pressure X-ray diffraction study of carbonates $MgCO_3$, $MgCa(CO_3)_2$ and $CaCO_3$, *American Mineralogist* (in press).

Haar, L., Gallagher, J. S., Kell, G. S. (1984), NBS/NRC Steam Tables: Thermodynamic and Transport Properties and Computer Programs for Vapour and Liquid States of Water in SI Units, Hemisphere Publishing Corporation, New York.

Hazen, R. M., Finger, L. W. (1982), Comparative Crystal Chemistry, John Wiley & Sons, New York, 72-73.

Klug, H. P., Alexander, L. E. (1974), X-ray Diffraction Procedures, 2nd Edition, John Wiley & Sons, New York.

Markgraf, S. A., Reeder, R. J. (1985) , High-temperature structure refinements of calcite and magnesite, *American Mineralogist,* 70, 590-600.

Rao, K., Naidu, S. V., Murthy, K. (1968), Precision lattice parameters and thermal expansion of calcite, *Journal of Physical Chemistry of Solids*, 29, 245-248.

Shen, A. H., Bassett, W. A., Chou, I. M. (1992), Hydrothermal studies in the diamond anvil cell: Pressure determination using the equation of state of water, in High-Pressure Research: Application to Earth and Planetary Sciences, Editors Y. Syono, M. H. Manghnani, 61-68, Terra Science Publishers, Tokyo/AGU, Washington, D.C.

Smith, G. S., Snyder, R. L. (1979), A criterion for rating powder diffraction patterns and evaluating the reliability of powder-pattern indexing, *Journal of Applied Crystallography*, 12, 60-65.

In: Chemistry and Chemical Engineering Reserch Progress ISBN: 978-1-61668-502-7
Editor: A.K. Haghi

Chapter 7

A CLOSER PERSPECTIVE OF PROCESSING AND PROPERTIES OF SWING THREADS

Akshay Kumar[1] and M.Subramanian Senthil Kannan[2]
[1] Department of Textile Technology, Indian Institute of Technology, New Delhi -110016, India
[2] Department of Textile Technology, PSG College of Technology,Coimbatore,Tamilnadu, India

ABSTRACT

Clothing manufacture is the last link in a long and complicated process by which two-dimensional fabric is transforms into three-dimensional garments by sewing the fabric pieces together. However, whatever the quality of the fabric, if the sewing operation is not performed appropriately, the resultant garment will be second-rate. Hence the sewing operation is most important in clothing manufacture and the sewing threads play a very important role in this operation. Generally, sewing threads are manufactured from either natural or manmade fibres in either staple or filament form. Sewing threads are primarily used in garments, upholstery, air-supported fabric structures and geotextiles to join different components by forming a seam. Different kinds of sewing threads are manufactured depending upon their specific field of application. A number of factors should be considered when choosing the sewing thread: to achieve good sewing performance, sewing thread must be chosen according to the fabric characteristics and end-use of the material. In this paper a glimpse on processing & properties of sewing threads is given.

1. INTRODUCTION

According to the definition given by ASTM, sewing thread is a flexible small diameter yarn or strand usually treated with a surface coating, lubricant or both, intended to be used to

[1] E-mail: akshay.sardana@gmail.com
[2] E-mail: senthilkannan@gmail.com

stitch one or more pieces of material or an object to a material. It may be defined as smooth, evenly spun, hard-twisted ply yarn, treated by a special finishing process to make it resistant to stresses in its passage through the eye of a needle and through material involved in seaming and stitching operations [1].

Sewing threads are used in garments, upholstery, air-supported fabric structures and geotextiles to join different components by forming a seam. The primary function of a seam is to provide uniform stress transfer from one piece of fabric to another, thus preserving the overall integrity of the fabric assembly.

Seam can be formed by the following techniques:

- **Mechanical**: stapling, sewing.
- **Physical:** welding or heat-setting.
- **Chemical:** by means of resins. [2]

The formation of seams by physical and chemical methods is restricted to a few specialized applications, as these processes tend to alter certain properties of the textile material. Among mechanical sewing techniques, sewing maintains its prevailing position by virtue of its simplicity, sophisticated and economical production methods and the controllable elasticity of the seam produced.

2. HISTORICAL BACKGROUND

Sewing thread is considered to be the first textile material excavated. Archaeologists concluded that caveman made the first sewing threads some 25,000 years ago. Caveman or jungle-man prepared them by rubbing and twisting together either fur fibres from skin of animals or bast fibres. These were single twisted yarns, which were unbalanced and snarly, making stitching difficult. The difficulty was overcome by plying single threads to balance torque. Out of the natural fibres, cotton and silk were extensively used for stitching purposes. Until the middle of 19^{th} century, all the threads were used for hand sewing. However, Isaac Singer, who invented sewing machine in 1850, brought about a considerable change in the field. James and Patric Clark, who were engaged in manufacture of loom, produced Cotton thread in 1812 in Paisley. The technology of Clark was further developed to a great extent by James Coat and became leading sewing thread manufacturer as M/s. J & P Coats of Scotland.

In India, Calico Mills commissioned India's first sewing thread plant in 1922 and introduced 100% polyester sewing thread in 1968. During pre-independence period M/s. J & P Coats were manufacturing most of the sewing threads in India for a long period. [2] Then M/s Madura Coats (in collaboration with M/s. J & P Coats) and M/s Modi Threads were the leading sewing thread manufacturers in India. At present M/s. Madura and M/s. Vardhman are the two leading sewing thread manufacturers of India.

3. DIFFERENT TYPES OF SEWING THREADS

Usually, sewing threads are manufactured from either natural or manmade fibres in either staple or filament form [3]. A broad classification of different types of sewing threads is given below:

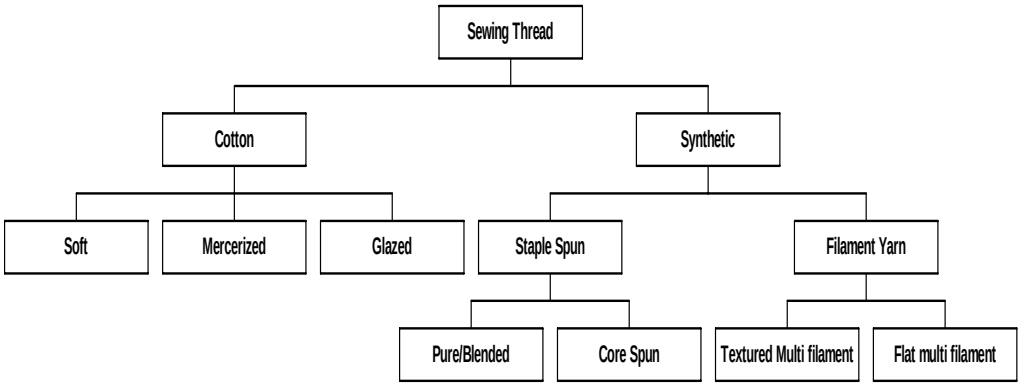

Figure 1.

3.1. Cotton Threads

Cotton is still used for sewing thread. High quality fibres are used for the manufacture of sewing threads. The very good resistance to heat of cotton is responsible for its high duty performance. Cotton threads are however susceptible to acid damage, mildew and certain forms of bacterial attack, and have relatively low extensibility and abrasion resistance compared to synthetic threads.

The spinning process including combing provides yarns of highest strength and quality. These singles yarn generally have an S- twist direction and are next twisted together in the Z-direction, the twist being balanced to eliminate snarling. In case of cotton sewing threads, wet folding is usually used on ring system to lay-in the surface fibres and thereby obtain smoother, stronger and more compact yarn than could be obtained by dry processing; the single cotton yarns are passed are passed over the surface of rotating conditioning roller on folding machine before they are combined together with twist insertion. Cabled yarns may be used with various twist combinations. Frequently three two-fold yarns are cabled together with Z cabling twist following S spinning twist or vice-versa, with folding twist approximate 1.5 x spinning twist, cabling twist about 1.3 x spinning twist if a balanced yarn is required. Spinning twist has only a minor influence on the cabled yarn properties; the cabling twist has a major influence on cabled yarn strength, extension, torque and yarn length contraction during cabling. The proportion of cabled yarn used in sewing has reduced largely because of the higher cost of production and because strong folded synthetic yarns are now available; nevertheless cabled yarns may still be required for applications such as buttonholes and decorative topstitching [4].

A medium thickness (size 50) is available in a wide range of colors, and is used for sewing on light and medium weight cottons, rayons and linens. Cotton thread is usually mercerized a finishing process that makes it smooth and lustrous, also helping it to take dye better.

The highest quality cotton threads are mercerized to make them lustrous and to improve strength. The alkali treatment is done after twisting and before dyeing.

Some cotton yarns are supplied as glace or polished sewing threads; these are often used when severe condition is encountered during sewing and in use such as with heavy fabrics; and for decorative stitching. The yarn has a mixture of size and lubricants added to it before being polished by high speed rotating brushes while under tension. The surface finish is not permanent and is removed by subsequent wet treatments.

3.1.1. Process for 2, 3 and 4 Cord Sewing Threads (Ply Yarn)

Ring Frame – steaming- cone winding- cheese winding- doubling (wet) – cheese winding – steaming – singing – reeling (if necessary) – wet processing (bleaching/ mercerizing/ dyeing) – rewinding (hank to cheese) – spooling (finish application) – labeling – packing.

3.1.2. Process for Embroidery Threads

Final twisted yarn (grey yarn) – cone winding (never on hanks) – ball warping/ singing – warp mercerizing – quilling (operation in which the mercerized warp is separated into individual threads) – rewinding on perforated stainless steel cones – package bleaching – package dyeing (vat, reactive, naphthol, i.e. fast colours- never direct dyes) – rewinding on spools (sewing finish application, which gives a protective surface coating to the thread that minimizes thread or needle friction and hence reduces thread breakage during sewing operations. Generally, yarns here pass through two/three waxing units or silicone finish in liquid form) – labeling – packing.

3.2. Spun Synthetic Threads

Modern high-speed sewing machines, imposing very high strains on the threads, require sewing thread of high toughness for satisfactory performance. Synthetic fibres, with very high strength and durability, have therefore become popular. However, the thermoplastic nature of these fibres makes them susceptible to change in their properties when they heated either during sewing or in subsequent processing or use. Stabilization treatment at suitable temperature and stretch during manufacture is therefore essential. To improve the threads gliding and cooling properties, special finishes are also used.

The fibres used for these threads are normally polyester with a staple length similar to that of cotton fibres so they can be spun and twisted on the same machinery. Polyester yarn and multifilament threads have almost replaced cotton-sewing threads in the market [5]. The main reason for the increasing demand for polyester threads is their higher breaking force, low degree of shrinkage while washing, and good wearing properties in comparison to cotton threads. Polyester sewing threads have one negative feature: at high sewing speeds and high friction with the metal parts of a sewing machine, these threads heat up and start melting at ~250°C. Due to their high strength, good chemical properties, acceptable elasticity and good dye fastness, polyester multifilament yarns are considered a perfect raw material for sewing threads. Due to its even surface and circular cross-section, polyester is more lustrous than natural threads. Synthetic yarns are also produced with fibres of long staple length. Special machines are used for processing and generally higher strength is achieved.

The essential differences between cotton and synthetic threads are illustrated in Table 1.

Table 1.

Cotton threads	Synthetic threads
Good strength	High strength
Low extensibility	High, adjustable extensibility
Low laundry shrinkage	Very low laundry shrinkage
Low dry-heat shrinkage	Very low dry-heat shrinkage
Do not melt	Melt
Good abrasion resistance	High abrasion resistance

3.3. Core Spun Threads

To achieve the optimum strength to fineness ratio of continuous filament threads together with the sewing performance and surface characteristics of spun fibre threads, core spun threads are produced in two main versions. In one version, polyester filament threads are covered and protected by cotton fibres; strength provided by the core and the heat resistance of the sheath permitting high sewing speed.

In the other, known as poly. / poly. polyester filament threads are covered by polyester fibres. The filaments are brought together with the fibres in the yarn spinning operation, these composite yarns being then twisted to form 2, 3 or 4 ply threads.

As with all synthetic threads core spun threads require a setting and stabilizing process and special dyeing technique is needed to obtain the same shade on both core and sheath where cotton is used. Because of their cotton cover, it is possible to produce glace core spun threads by polishing in a similar way to the 100% cotton threads. Mercerized core spun threads are also very popular.

3.4. Silk Threads

Although they are not widely used, some sewing threads are made from spun silk. An important feature of such yarns is the high extent at break of about 20%, along with a high breaking load. Some continuous filament silk yarns are used for buttonholes and decorative stitching because of their attractive appearance and smoothness.

3.5. Monofilament Threads

Monofilament is not a conventional thread, as it comprises only a single filament, suitably lubricated. Monofilaments are produced by melt spinning (as are continuous multifilament yarns), but the spinneret has only one aperture which is much larger than for conventional yarns.

3.6. Multifilament Threads

Plied or corded threads produced from 100% synthetic (polyamide or polyester) filaments are used as continuous filament threads. Where flexible threads are required, the filaments are twisted, set, dyed and lubricated only.Where optimum sewing performance and abrasion resistance are required, the plied threads are treated with synthetic co-polymer, which bonds the individual filaments together. Plied continuous filament multilobal polyester threads are favored for embroidery applications on account of its superior lusture.

Very fine threads are produced from a single ply of multifilament polyester yarn, suitably twisted and then treated with a light bonding finish - just sufficient to consolidate the individual filaments without stiffening the final product.

3.7. Bonded Continuous Multifilament Threads

The continuous multifilament threads are low twisted and uniformly coated with suitable bonding agent to form bonded filament threads. The bonding agent protects the thread from possible heat damage in sewing, prevents cut ends from fraying and also prevents run-back of twist. Bonding of threads makes them easier to sew and retain their tensile strength during the sewing operation. Additional UV inhibitors are often applied during the bonding process by incorporating them into the bonding resins. The bonding of nylon is comparatively easier than that of the polyester. Most nylon-bonded threads are hot-stretched to give high modulus together with low extension at break. Bonded nylon thread is an ideal choice for footwear, luggage, upholstery, wet suits, seat belts, leather goods, canvas, heavy-duty fabrics and similar materials.

3.8. Textured Threads

Texturing is a general term to describe modifications to the appearance and surface characteristics of flat synthetic filament yarns, obtained by various means such as false twisting, air jet, stuffer box etc. depending on the application for which the thread is intended, the degree of crimp rigidity can be varied. Textured threads have a soft handle and are used primarily as under threads where a particularly soft seam is required. Texturing is the process where filaments are entangled by various methods, which impart softness and bulk to the product. Loops made in this manner may be fixed by thermo-setting depending on the origin of the raw material processed, i.e. if a thermoplastic polymer is under texturing. Non-thermoplastic polymers are not fixed by thermo-setting. For each polymer, an adequate thermo-setting temperature must be selected.

It is ideal for very extensible seams in knitwear, underwear, swimwear, foundation wear and tights. Textured sewing threads are most economical sewing threads available today. The textured threads can be used in most of the stitches except for the lock stitches. A German patent gives a method for producing low shrinkage bulky air jet textured yarns for sewing thread from synthetic POY. J & Protection Coats Ltd. reported a method of producing sewing thread that consists in passing two drawn continuous filament yarns, to an air jet-texturing device to form a single bulked yarn in which the filaments are intermingled and looped [5].

3.9. Direct Spun Sewing Threads

Tow to yarn 'direct spun' sewing threads are made by feeding a continuous filament tow into a stretch breaking zone and inserting twist into the strand of fibres so produced, with delivery on to a ring spinning package. Compared with yarn spun from staple fibre, direct spun yarns are more uniform, compact, strong have a lower extension at break, a better abrasion resistance, and are free of defects such as neps. Unless high temperature setting is used on the direct spun thread, it will have a greater relaxation in subsequent hot wet processing than an equivalent spun yarn. Because of their characteristics, direct spun yarns may be used to advantage in some critical applications, but only when the higher cost can be justified.

The tow produced in this purpose is relatively thin compared with tow produced for staple fibre production and consequently it usually costs well over twice the cost of staple fibre; hence relatively expensive.

4. ESSENTIAL PROPERTIES REQUIRED FOR SEWING THREADS

Industrial sewing techniques make specific and often very exacting demands on the threads involved in the sewing process. The sewability of sewing threads is of major importance [6], having a very profound effect on seam quality and production costs. The sewing and the seam performance of a sewing thread are largely influenced by the material to be sewn, the sewing technique and the end-use for which the sewn material is intended. These requirements can be defined as:

- The ability of the sewing thread to meet the functional requirements of producing the desired seam effectively.
- The ability of the sewing thread to provide the desired aesthetics and serviceability in the seam.
- The cost of sewing thread and that associated with producing the desired seam.

The different important properties required by a sewing thread are discussed below:

1) Needle thread must pass freely through the small eye of the needle; consequently they must be uniform, knot-free, non-torque and fault free.
2) Tensile strength / breaking strength is one of the essential properties of the thread. It must be capable of withstanding several kinetic/ lateral movements during sewing. The strength of the sewing thread must be higher than that of the fabric so that the thread does not rupture during use. During sewing at high speeds, the needle thread is subjected to repeated tensile stresses at very high rates. The thread also comes under the influence of heat, bending, pressures, torsion and wearing. The value of these stresses depends on the sewing speed, machine settings and the thread used. The stresses created within the thread have a negative effect on the processing and functional characteristics of the thread, and there is significant reduction in the thread strength after sewing.

This is a function of the dynamic and thermal loading of the thread and is influenced by the thread frictional properties, thread tensioning during sewing, needle size, stitch length and number of fabric layers in the seam. The thread should therefore possess adequate strength and elongation in order to perform satisfactorily during sewing and in seam. [7]

3) For good performance in sewing machine moderate to low extension-at-break of the thread is usually preferred. Needle thread with different elongation-at-break has been found to behave quite differently during stitch formation. The determinants of success of sewing a thread with certain elongation percent without any problem are the machine setting and special properties of the sewing thread itself [6].
4) The elasticity of the sewing thread must be uniform along its length in order to enable equal length stitches to be formed, and it must closely match the elasticity of the fabric being sewn; otherwise either seam thread fracture, or tearing of the adjacent fabric may arise during garment use. Clearly the requirements of woven and knitted fabrics will be different.
5) The forces that are developed in the sewing thread are mostly due to the friction between the thread and machine parts, the most severe action taking place between:

- The thread and the needle.
- The thread and the fabric being sewn.

A controlled level of both static and dynamic friction is required; this must not be too high, which could cause lack of thread control. High static friction values are necessary to allow the stitches to lock and prevent "run-back" of seams. Spun threads are particularly good in this respect when compared with filament thread. The worst is the monofilament threads. The frictional properties are affected by lubrication. The factors that influence the frictional properties are:

- Uniform application of lubricating agents.
- Adhesion of the finishing agent on the thread.

The quantity and quality of finishes are very important. Special finishes like silicone compounds have been found to exhibit clear advantage over standard paraffin wax.

6) Good abrasion resistance is essential for good sewing performance. The thread is under tension condition, especially when the stitch is being set. The thread must be resilient enough to return to shape after the distortions, and then must maintain its physical properties to provide good performance in the seam after the sewing process is complete. Nylon and polyester offer the best resistance to abrasion.
7) Good resistance to heat is a very important requirement of a sewing thread. The temperature reached by the sewing needle during sewing very much depends on:

- the nature of the fabric to be sewn (density, thickness, finish)
- the speed of the sewing machine
- the type of needle used (size, shape, surface finish)

- size and finish of the sewing thread.

The needle temperature is especially critical for fabrics and sewing threads of thermoplastic fibres, where it may exceed their melting temperature. Needle heating causes sewing thread breakage, cross-thread, skipped stitches, seam damage and physical damage to the needle.

Various studies show that the sewing thread influences the needle temperature significantly. Its movement through the needle reduces the needle temperature by an average of 21- 45%, the amount of reduction depends on the sewing condition and the structure, fineness and composition of sewing thread.

Lubrication of sewing thread with a mixture of wax, emulsions with synthetic resins, and silicon based products may minimize heat generation, and the fibres surface of spun yarns may be an advantage in that a thin layer of the surrounding air will move with the thread and promote needle cooling.

8) The hairiness of sewing thread also affects the appearance of the seam. Sewing thread for decorative seams are singed, squeezed and gloss-brushed.
9) The final direction of twist insertion may be important to enable the stitch forming mechanism of the sewing machine to perform correctly; most sewing machine require Z twist, but there are a few where performance is better with S twist.
10) Colour Fastness is a general requirement for sewing thread. It is important that the selected shade retain its colour throughout the life of the garment. Two aspects of fastness are important:

- the thread must not change colour.
- The thread must not stain any material adjacent to the seam.

11) Low shrinkage during washing and ironing is required. Shrinkage due to fibre swelling causes seams to pucker, especially if the fabric exhibits less shrinkage than threads. Synthetic threads suffer less from this problem than cotton threads owing to their much lower moisture absorbency; however they are liable to residual shrinkage problems if unsuitable manufacturing processes are employed. Synthetic threads can suffer from the problem of thermal shrinkage during ironing but this difficulty can be solved by the use of high temperature setting, which stabilizes the thread at temperature above those normally encountered during the ironing process.
12) The sewing threads should possess better evenness and should contain minimal number of knots, faults and neps etc. Thread should have very low level of imperfections and classimat faults.
13) Good luster in the thread improves appearance of the seam.
14) Threads must be uniformly dyed in a good match to the materials being sewn and also the dyed thread should have properties like colourfastness to washing, light, perspiration, and sublimation.
15) The ability of the thread to perform efficiently in the sewing machine is defined sewability. It can be assessed by the number of breaks that occur during the sewing of a certain number of stitches. However, owing to the generation of needle heat in

high-speed sewing, the threads could be damaged without breaking. The long knot free evenner yarns in case of rotor and air-jet can give better sewability.

16) The characteristics of properly constructed seam are strength, elasticity, durability, stability and appearance. The relative importance of these qualities is determined by the end-use of the sewn product. The factors that govern these properties are seam and stitch type, thread strength and elasticity, stitches per unit length of seam, thread tension, seam efficiency of the material. The hairiness of sewing thread is important to decide seam appearance. The shrinkage potential of the thread and hence the seam is also major importance for proper seam appearance. The serviceability of a garment depends not only on the quality of the fabric but also on that of the seam. The seam quality is measured by stitching parameters of the threads and seam parameters such as size, slippage and strength.

    The failure of seam produced by traverse loading can generally be classified as: Type I: the failure due to thread breakage, Type II: the failure due to fabric breakage, Seam breakage: the failure due to the slippage of cloth yarns at right angle to the seam.

    Seam slippage is the most probable cause for seam failure that leads to garment rejection in wear. The durability of a seam depends largely on its strength and its relationship with elasticity of the material. It is measured in terms of seam efficiency, where Seam Efficiency = (Seam tensile strength/fabric tensile strength) x 100, generally ranges between 85 to 90 %. The minimum loop strength correlate well with the stitch breaking strength. Further resistance to abrasion and wear of the seam during everyday use, including laundering is also essential for the longer seam.

17) Seam pucker can be defined as a differential shrinkage occurring along the line of a seam and is mainly caused due to seam instability, due to high tension imposed during sewing. Though currently available threads have a certain amount of controlled elasticity and elongation they get over-stretched when the sewing tensions are high. During relaxation the thread recovers its original length thus gathering up the seam. Threads for use in apparel are also required to have good stability to laundering, ironing and other treatments since differential shrinkage between the sewing thread and the fabric of a garment can cause puckering.

    Further, Seam pucker can be determined by measuring the differences in fabric and seam thickness under a constant compressive load. The seam-thickness strain is calculated by using the formula:

Thickness strain (%) = (seam thickness – 2 x fabric thickness) x 100 / 2x fabric thickness {ref}

5. PROCESS FLOW CHART OF SEWING THREAD

The process flow chart for the manufacture of sewing threads is shown in the flowchart given below.

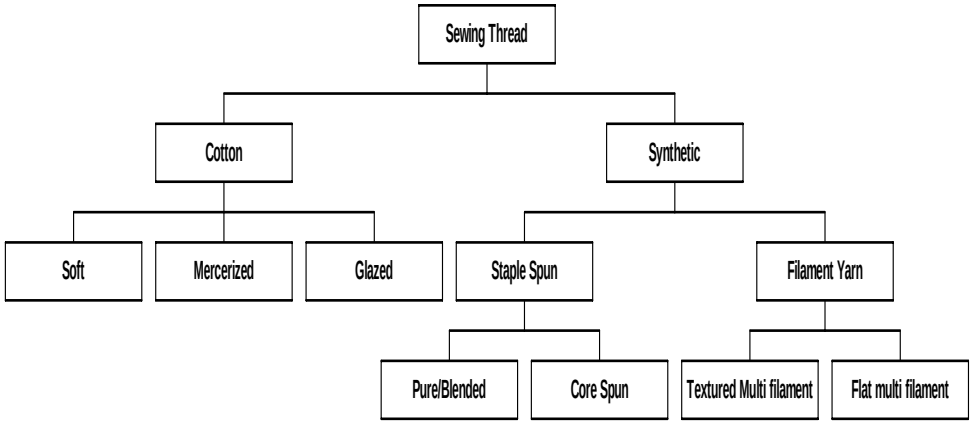

Figure 2.

6. FUNCTION OF VARIOUS MACHINES IN SEWING THREAD MANUFACTURING PROCESS

6.1. Yarn Singeing

Sewing thread must be singed to ensure that the projecting fibers do not interfere with downstream processing. Percentage of singeing can be achieved varied by varying the yarn collection speed. Hair removal efficiency at singeing machine is normally 30-50%. Flame temperature is around 800°C. Singeing is mainly done in Cotton Sewing Threads.

6.1.1. Features

- The heart of the machine - the burner, serves to singe reliably the projecting fibres of yarn running through at high speed, without inflicting burns on yarn itself. There is a choice between the gas burner and the electric burner. Gas burner are widely used. The gas burner consumes about 55 gm of natural, propane or butane gas an hour, depending on singeing rate and yarn type.
- Speed: 300-1200 m/min.

6.2. Hank to Cone Winding

- Conversion of hank in to cone of suitable weight
- Waxing for reducing co-officient of friction in sewing thread .
- Features of new machines:
- Twin Input Rollers: At the front of the head are the twin-input rollers, set to a fixed speed but proportional to the winding speed. The main functions of this unit are to eliminate unwanted tensions prior to yarn entering waxing unit.
- The speed of machine ranging from 400-700 mpm, with possible traverse from150-200mm.

6.3. Polishing

Some threads for special end uses like leather industries, bag stitching, kite flying are treated with starch, softeners, whitener etc. on this machine. Cooked starch is mixed with other chemicals and different recipes are made for different qualities depending on the end uses.

Main objectives of polishing are:

- Extra ordinary smooth surface
- Thread becomes round.
- Stiffness increases.
- Increase in tensile strength (7-10%).

6.4. Cross Winding and Lubrication

- Winding in various types of sewing thread packages like cone, cop , tube, ball, vicone and spool.
- Threads are treated with special waxes for achieving best workability during sewing operation.
- Lick roller lubrication is applied on industrial sewing thread where thread has to run on high speed sewing machine; the basic ingredient of the most of the lubricants is parafin wax. Although silicones are also used because of their stability to heat and various additives are also included to give some special properties.

7. GEOMETRY OF PACKAGES

Threads are wound in many forms. Small length spools are employed in retail store distribution, whereas somewhat larger spools are used to a limited extent industrially. Some of the very fine soft threads are wound on cones, very coarse soft threads are in skein form, but the largest proportion by far is wound on the one headed tube with base or straight tubes. These packages in some instances are put on a weight basis; however, the larger percentage is marked on a length basis. Ready-wound bobbins in a number of styles to accommodate the various sewing machines employed are also available.

Cross winding threads are generally laid in with traverse ratio 1: 6 (one double traverse = six spindle revolution) and 1: 4 for coarser counts.

Following types of packages are used in sewing threads (with commonly used dimensions) .

7.1. Spool

Spools are small flanged plastic or wooden bobbins, they are both with tapered (so-called Diabolo spools) and straight flanges. Mainly parallel winding (because side unwinding is

easy) is done. Cross-windings are also possible on the spools. They contain relatively short length of 100-500 meter thread. The length of traverse on spool is 2.9-3.8 cm.

End uses: Upholstery, footwear, leather goods manufacturing, and in hand sewing operations.

1.7/3.6 cm
2.3/3.2 cm
3.8/4.3 cm
3.2/5.2 cm

7.2. Cop

Cops are small cylindrical flangeless spools, with precision cross winding. They are mostly made of paper and plastic. They are of two types, small Cop (Tube) and medium Cop (Cop). The lack of flanges facilitates regular off winding on industrial sewing machines although their small diameter makes them less well suited to the faster thread take off machines. Smaller Cops are popular make-up in fashion trades, where a variety of shades are used and production runs for any one colour or style of garments. The length of thread wound ranges from 100-2000m on small cop and 400-4000m on cop. The length of traverse on small cop is 5 - 6.3 cm and on cop is10 cm.

End uses: Kite flying, Upholstery, ready-made garment, tailoring, hosiery, umbrella, and shoe stitching

11.5/6.5 cm

7.3. Cone

This is self-supporting, cross wound conical package. It is easier to withdraw yarn over end from a cone than from a cheese and because of this, cone is more widely used. They contain relatively long lengths 1000-25000m with length of traverse ranging from 10-15cm. They give trouble free thread unwinding at intermittent or continuous high speeds. Cones are the most economical packages for conventional sewing threads in situations where thread consumption is high and production runs are long.

End uses: ready made garment, tailoring, hosiery, leather stitching, Upholstery, shoe stitching, denim, embroidery, and kite flying.

φ = 3.6 cm
φ = 2.1 cm
11.5 cm

7.4. Vicone or King Spool

Vicones are parallel tubes or low angled cones with an additional base in the form of a raised flange, which may incorporate a small tip. The build of vicone depends on the exact conformity of the taper with the angle of vicone's base. Coarse yarns require a large traverse for the taper - fine yarn a small one. They contain lengths of 1000-5000m with length of traverse 6.5-9cm.

End uses: embroidery, core-spun, and filament threads.

φ = 4.3/7.6 cm
φ = 1.1/2.95 cm
5.6/8.2 cm
7.5/10.8 cm

7.5. Prewound Bobbin

Prewound Bobbins are precision parallel wound thread package designed to replace metal bobbins on a variety of lock stitch machines.

7.6. Skein

A very small hank of soft twisted plied thread (around 8 m) of coarse count, is parallel wound with the help rotating flyer, which withdraws the thread from the supply package cone.

End uses: embroidery.

7.7. Ball

A typical ball like structure, wound with the help of four types of different winding. They are: Rough base winding, form winding, surface layer winding, and circumference winding. The initial winding provides firmness at the base. Next winding process makes space for placing the identification ticket. The third stage of winding provides firm gripping of the ticket. The last stage of winding makes a band over the ball, which retains its shape. An easy unwinding of thread is possible.

End uses: embroidery, fishing net and bag closing.

7.8. Cocoon

Cocoons are self-supporting i.e. center-less thread package specially designed for the insertion in the shuttle of multi needle quilting and some types of embroidery. Cocoons are used in the shuttle of multi needle quilting and some types of embroidery machines.

Skein
Pre wound bobbin
Cocoon
Ball

8. DIFFERENT TYPES OF WINDING SYSTEM

8.1. Precision Winding

- constant winding ratio
- winding angle reduces with increasing diameter
- No pattern areas
- Good off-winding characteristics
- High package density

8.2. Step Precision or Digicone Winding

- almost constant winding angle
- the wind ratio is reduced in steps
- combines the advantage of random and precision winding
- no pattern areas
- higher consistent package density
- perfect unwinding characteristics
- straight sided packages

8.3. Random Winding

- winding angle is kept constant since the winding ratio reduces with increasing diameter
- stable packages
- even density

8.4. Pineapple Winding

- winding traverse reduces to produce packages with tapered edges
- required for filament winding operations
- all three types of winding applicable

8.5. Parallel Winding

- very high package density
- thread vertical to package axis
- relatively short lengths of thread
- suitable for side unwinding
- no pattern areas [5,6]

8.6. Ball Winding

- very easy unwinding
- winding takes place in 4 stages:
  1) rough base winding
  2) form winding
  3) surface layer winding
  4) circumferencial winding

8.7. Skein Winding

- easy unwinding
- Very small parallel strand of soft twisted thread.

9. PROPER SELECTION OF SEWING THREAD

A number of factors should be considered when choosing the sewing thread: to achieve good sewing performance, sewing thread must be chosen according to the fabric characteristics and end-use of the material. The choice of sewing threads according to fabric characteristics can be classified as in Table 2.

Table 2

Fabric properties	**Sewing thread**
Fabrics and garments that are not tumble-dried	Sewing thread shrinkage must be less than 1%. To dry at the same time with the fabric, moisture absorption of the thread must be low.
Fabrics and garments that can be ironed	Sewing thread must be resistant to high temperature (ironing and pressing), and must not give its colour. If it is cellulosic, the thread must be little thicker.
Water resistant fabrics	Texturised or core-spun yarns must be preferred to fill the needle holes in the fabric.
Fabric that are dried under tension	The threads' extensibility must be equal to the fabric's.

9.1. Selection According to Seam Type

9.1.1. Lock Stitch

If cotton yarn is to be used in this type of seam, 50% extensibility can be achieved and this ratio is enough for the comfort of the garments. If standard synthetic sewing thread is used, extensibility value reach 60% and no slacking occur when the seam is under tension. If plied nylon thread is used as bobbin thread, 20% more extensibility can be achieved. Cotton thread must be preferred for normal lock stitches. When fabric with 30% to 100% extensibility are to be sewn, synthetic threads or blended plied threads must be used.

9.1.2. Chain Stitch

As this kind of seam is generally used on elastic fabrics, synthetic or blended threads are preferable to cotton. As looper thread, nylon threads or filled give better results.

9.2. Selecting the Right Size

The ticket number system (related to Ne, Nm and denier) is now generally used by most thread manufacturers and industrial thread consumers to describe approximately the threads of the finished product. The ticket number of cotton threads are generally based on cotton system Ne, these ticket numbers being approximately equal to three times the cotton count of the thread. The ticket number of synthetic threads are based on the metric count system Nm ; approximately three times the metric count of the thread.

Selecting the correct size of thread for a particular application is very important to the thread performance during sewing and afterwards in the seam. However the choice is not always easy. It depends on many factors, including seam strength, fabric weight and type, end use, stitch type, seam type, needle size and many others.

In general, the heavier the fabric, the thicker the thread is. The ultimate choice lies with garment designer and the garment technologist, taking account of aesthetic and technical considerations.

9.3. Colour Selection

There are many hazards to be avoided when visually matching samples, and especially:

- **Dichroism:** An apparent change of colour as the direction of viewing is changed. This tends to occur more with fabrics than with threads, but can affect the judgement of thread colour.
- **Metamerism:** A change of shade which occurs when lighting conditions are changed. For colour matching this is a serious problem because while two samples may match in daylight, they may not change colour under artificial light to the same degree.

9.4. Colourfastness

When a suitable shade of thread is chosen that matches the fabric to be sewn, there remains a very important factor: it is important that the selected shade retain its colour fast through the life of the finished article. It must not stain any article adjacent to the seam. The colour fastness is affected not only by washing and light but by chlorinated water, rubbing/ crocking, dry cleaning, hot pressing, bleaching and sublimation. So before selection all these things are to be considered.

10. APPLICATIONS OF SEWING THREADS

Approximately 80% of all sewing threads produced are used by the clothing industries. The main classes of clothing requiring threads are as shown in Table 3 and 4**.**

Table 3.

Class	Approximate percentage of all threads produced
Dresses and blouses	13
Shirts and nightwear	5
Suits, coats and other outwear	
Underwear	28
	16
Knitwear	
Work clothing	
Sportswear	
Footwear	
Other clothing	21
accessories	

10.1. Sewing Threads for Technical Applications

Different kinds of sewing threads are manufactured depending upon their specific field of application. Threads for use in apparel are required to have good stability to laundering and ironing, with better seam appearance. The threads are also required to perform satisfactorily during high speed sewing operations [8]. However, for technical applications sewing threads are engineered to meet certain critical requirements. Sewing thread characteristics are required to be different for their use in flame retardant garments, clothing for extreme weather conditions etc. for different application, the types of sewing thread and their characteristics vary widely.

Table 4. End uses of different types of sewing threads

Cotton	**Spun Polyester**	**Core Spun**	**Textured Threads**	**Airjet Textured**	**Bonded Fil.(nylon)**	**Bonded Fil.(PET)**
Garment Embroidery	Shirts Blouses	All apparel (lingerie to jeans)	Slacks	Jeans	Automotive	Rainwear
Selvage Threads Tea bag Strings Bag closing	Lingerie Slacks Knits Jeans Mattresses Embroidery	Furniture Shoes Tents	Home furnishing Shirts Blouses Jeans T-shirts Brief Fleece	Mattresses Slacks Mops Flags Caps	Interiors Seat belts Air-bags Footwear Leather Canvass goods Luggage Sporting goods	Furniture Tents Footwear Mattresses Sporting goods Embroidery

10.2. High-Temperature Applications

Threads for high-temperature applications are required to hold the seam and secure it in extreme temperature conditions (between 260 and 1100^{o}C). Threads are usually made from quartz, glass, carbon, polytetrafluoroethylene, steel and aramide fibres. Military requirements and growing demands of safety legislation have built a viable market for high-temperature threads in spite of their higher cost.

Table 5. Sewing Threads for Technical Applications

Generic type	**Availability**	**Applications**
p-Aramide	Staple fibre	Heat protection clothing, personal protection clothing, welder's clothing etc.
PTFE	Monofilament	Awnings, sun protection shades, boat covers, filter bags etc.
Polyester(Normal tenacity)	Multifilament	High load seams, safety belts, tents, suitcases etc.
Polyester(High tenacity)	Multifilament	Safety belts, cargo slings, tarpaulins, air bags, geotextiles, convertible car hoods etc.
m- Aramides	Multifilament	High temperature fields
Polyester/cotton	Spun yarn	Tents, tarpaulins, flags and bunting, book binding, convertible car hoods etc.
Polypropylene	Multifilament	Filtration, binder twine for agriculture use etc.
Polyamides(4.6& 6.6)	Multifilament	Safety belts and cargo slings, car seatings, tarpaulins, air bags, footwear, tents, geotextiles, sails, rucksacks, convertible car hoods etc.

The most commonly used and comparatively cheap threads are manufactured from glass fibre, Nomex and Kevlar. Threads from carbon and quartz fibres are quite expensive and are produced exclusively for military and aerospace applications. Nomex threads are widely used in the filtration of hot gases and in thermal protection clothing. Quartz fibre is also used in atomic plants since it does not contaminate the atmosphere and can withstand temperature as high as 1093 ^{o}C.

10.3. Geo-Textile Applications

In many geotechnical and air-supported fabric structures, the seam constitutes one of the most critical components in forming a wider fabric from the available narrow fabrics. Sewing is generally performed because of its simplicity and its ability to maintain the elasticity of the fabric structure.

Polyester and polypropylene fibre threads are the most used threads, since these are the principal materials used for geotextiles. For demanding applications, high tenacity fibres such as Kevlar are used.

CONCLUSION

The sewing thread is of considerable importance and playing a major role in retaining the fabric appearance, look, and life of the garment in the long run, even though it usually represents much less than 1% by mass of a garment.

Now-a- days, a numerous variety of sewing threads are prevailing in the market due to diverse demands from the sewing industry, increasing use of different types of fibres in the garment industry and expanding application of textile materials in various fields like apparels, technical applications as well. Better understanding of the sewing process and its requirements as obtained through studies by modern instrumentation techniques has also greatly contributed to the development of new threads. It is also very much required & appreciable to have different types of sewing threads which can suit various applications, since various end-uses demand specific property requirements.

It's beyond anybody's doubt that the success of garment manufacturing process majorly depends upon the operation of sewing, though a very better quality of fabric is selected for the garment manufacturing process. Again, the sewing threads play a vital role in the success of sewing operation, since a wrong thread may collapse a very high quality fabric & even a best sewing machine used for the sewing, the whole process will be failed. It can add to waste of both time & money. Hence it is very much imperative to select a right type of sewing thread which can suit one's requirements exactly. This is possible by the correct understanding of the type of fibre used to manufacture, manufacturing processing sequence & properties of different types of sewing threads existing on earth, which was touched upon in this technical article to a greater extent.

REFERENCES

[1] J.O. Ukponmwan, A.Mukhopadhyay and K.N.Chatterjee, " Sewing Threads", Textile Progress, *The Textile institute*, Volume 30, No. 3 /4, Page 1.

[2] S. D. Pai, V. G. Munshi & A. V. Ukidue, "Cotton and synthetic sewing thread- I", *The Indian Textile Journal*, August 1984, page 63-75.

[3] Alan Crook (information updated by Ron Lioyd), "Sewing threads", *Textiles*, Issue No. 2, 1991, page 14-16.

[4] K. N. Krishna Swamy, "Prerequisites for manufacturing sewing thread- I", *The Indian Textile Journal*, March 1982, page 103- 111.

[5] H. U. Bhonde, "Sewing thread: types and some recent developments", MANTRA Bulletin, Manmade Textiles Research Association, Vol. 19/11, November 2001, page-5-10.

[6] Pradip V. Mehta, satish K. Bharadwaj, "Managing Quality in the Apparel Industry", National Institute of Fashion Technology, New delhi, India, New Age Publihers, 1998.

[7] K. R. Salhotra, P. K. Hari & G. Sundaresan, "Sewing thread properties", *Textile Asia*, September 1994, page 46-57.

[8] Walter Fung, Mike Hardcastle, "Textiles in Automotive Engineering" Woodhead Publishing, 2001.

In: Chemistry and Chemical Engineering Reserch Progress ISBN: 978-1-61668-502-7
Editor: A.K. Haghi

Chapter 8

IMPACT OF DIFFERENT STAGES OF YARN SPINNING PROCESS ON FIBRE ORIENTATION AND PROPERTIES OF RING, ROTOR AND AIR-JET YARNS

Akshay Kumar and S. M. Ishtiaque
Department of Textile Technology, Indian Institute of Technology,
New Delhi- 110 016, India

1. INTRODUCTION

The economic situation of the textile industry and the extremely sharp worldwide competition has forced the textile mills to use all possibilities of cutting costs. In this context, the question of higher productions at each spinning sequence of machine gains importance. This demands a strict observance of spinning process variables on fibre orientation and properties of products produced out of these machines.

Since last 60 years, numerous concepts have been introduced to characterize fibre orientation, namely, straightness, fibre extent, helix angle, coefficient of relative fibre parallelization, proportion of curved fibre ends, migration parameters etc. Several methods of investigating fibre orientation were also developed, such as the direct method, [1] in which tracer fibres are viewed through a projection microscope and the indirect method, such as Lindsley [2], modified Lindsley [3] method in which the orientation and parallelization in sliver and roving are quantified in terms of weight ratios. But, the orientation parameters measured with the direct method takes into account the behaviour of a single fibre and extrapolate the characteristics of sliver or roving or yarn from it, which is, infact, not a realistic measure. This is due to the fact that the fibrous assembly contains a larger number of fibres whose laying and overlapping each other is of greater significance. Furthermore, both these methods are quite old and need a thorough review or modifications.

Overall, this paper gives a brief review of work done by some of the researchers for studying the effect of spinning process variables on fibre orientation and quality parameters of sliver, roving, and ring, rotor and air-jet yarns.

2. MEASUREMENT OF FIBRE ORIENTATION

The earliest method for the study of fibre orientation was direct method, which was based on the use of optical tracer fibre technique and ultraviolet rays for study of hooks. In optical tracer fibre technique [1, 5], 0.1% to 0.3% of tracer fibres are dyed with any dark colour dye. These tracer fibres are further mixed with parent fibre preferably during fibre mixing just before blowroom opening. Further, in optical tracer fibre technique sliver, roving or yarn is immersed in a solution, which is having same refractive index as of parent fibres. This makes the grey parent fibres to optically dissolve while profile of coloured tracer fibres can easily be seen under a microscope. The optical tracer fibre technique can be used for the measurement of fibre orientation parameters like fibre extent, type of hooks, hook extent etc. in sliver, roving and yarn. The schematic view of a fibre seen under microscope for the study of extent study is shown in Figure 1. But, this technique is very tedious and time consuming. As the parameters like fibre extent and hook extent are dependent on the length of fibre used, these parameters can not be compared in different samples prepared from different fibre lengths.

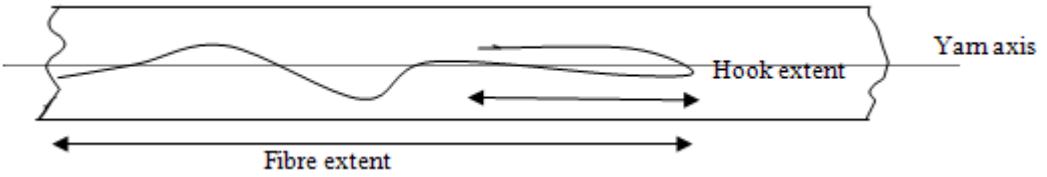

Figure 1. Outline of a hooked tracer fibre seen under microscope.

Further, the study of fibre-overlap is a new approach to study the longitudinal behaviour of fibre in yarn. It was measured in terms of two newly proposed parameters viz. fibre-overlap index (FOI) and fibre-pair-overlap length (FPO). The objective of measuring fibre-overlap indices was to get a direct interpretation of total contact length between the fibres which has earlier been interpreted from the fibre extent [6].

However, in the UV tracer fibre technique fibres are dyed with any commercial fluorescent dye and this technique can only be used to study the fibre orientation in the web delivered by the card, drawframe and intermediate frame after collecting the web on the black boards. In both of the above techniques, the dyeing of fibres changes the surface characteristics of the fibres. These fibres are thus expected to behave differently during processing in the spinning process. Further, both of them are quite old. Recently, a new index, named Fibre Straightness Index (FSI), which can give information about fibre straightness and is comparable for different samples made from different fibre type and length was also being used. FSI is a ratio of total axial projected length of a fibre to the actual length of that fibre in a section of length observed directly with the microscope [6]. The actual photograph of fibre used for FSI study is shown in Figure 2.

FSI = n x P / (L_1+L_2+L_3+…+L_n), where n – no.of.fibres, p and L_1, L_2 are fibre extent and actual length of the fibre in the section observed

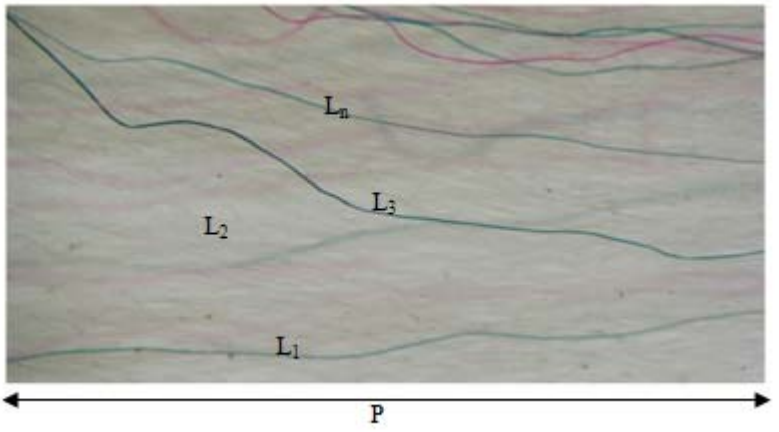

Figure 2. Section of sliver seen under stereomicroscope at 20 magnification.

Further, this tracer fibre technique in yarn is also used to study the fibre migration in the yarn in terms of few mathematical formulae. These formulae specify over-all tendency of a fiber to be near the centre or surface of the yarn, termed as mean fibre position (MFP); the rate of change of radial position, termed as mean migration intensity (MMI); and the magnitude of the deviations from the mean position or the amplitude of the migration, termed as root mean square deviation (RMSD) [7, 8]. The schematic view of a fibre seen under microscope for fibre migration study in yarn is shown in Figure 3. The formulae used for the calculation of the migration parameters were those provided by Hearle *et. al.* and are given below:

Mean Fibre Position

$$(Y) = 1/Z_n \int_0^{Z_n} y.dz = (\sum_{1=1}^{n} y_i)/n$$

where, n observations of *Y*, made over a length Z_n

Mean Migration Intensity

$$I = [1/Z_n \int_0^{Z_n} (dY/dz)^2 dz]^{1/2} = \{[\sum_{i=2}^{n} (y_i - y_{i-1})^2 /(z_i - z_{i-1})^2]/n\}^{1/2}$$

Root mean square deviation

$$(T) = [1/Z_n \int_0^{Z_n} (y - Y)^2 dz]^{1/2} = \{\sum_{i=1}^{n} (y_i - Y)^2 / n\}^{1/2}$$

where, R_i & r_i are ith value of yarn radius and helix radius, z_i is corresponding values of length along the yarn and $y_i = (\frac{r_i}{R_i})^2$

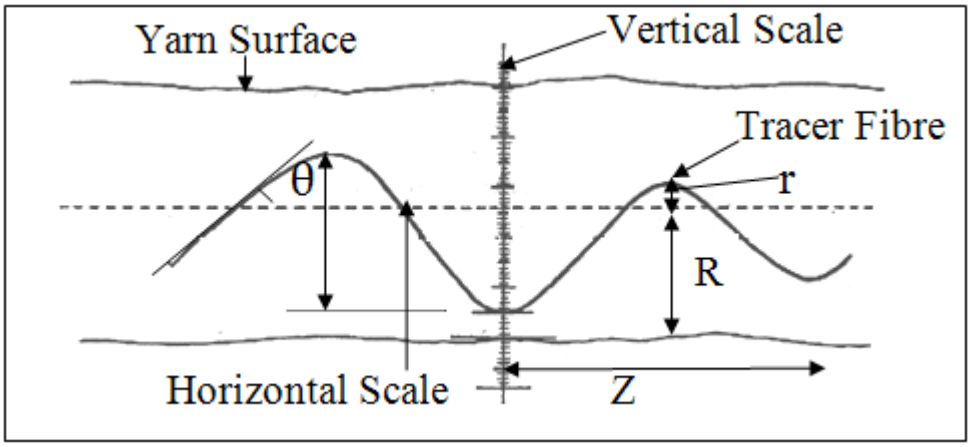

Figure 3. Schematic view of a tracer fibre seen under projection microscope.

Later on, indirect methods, like Lindsley and modified Lindsley, which gives an indirect measure of fibre orientation in terms of few coefficients, were widely being used. In this category Lindsley [2] or Modified Lindsley [3] devices are used for indirect measurement of fibre orientation in the sliver and roving. Initially, three indices were used to measure fibre orientation in sliver and roving. These were cutting ratio, combing ratio and orientation index. But, these indices fail to supply an explanation of the physical sense of these coefficients. Therefore, Lindsley's coefficients were replaced by Leon'teva by two new coefficients known as proportion of curved fibre ends 'ρ' and coefficient of relative fibre parallelization 'K_{rp}'. Where, 'ρ' indicates curved fibre ends as well as their length and 'K_{rp}' represent degree of fibre parallelization and straightening in sliver/roving. Very recently, the equation of 'K_{rp}' is being modified to 'K_{rpm}' for better measure of fibre parallelization and straightness in the sliver and roving [6]. The schematic view of the instrument used for the study of fibre orientation by indirect method is shown in Figure 4.

However, it was stated that the above indices are relative measures of fibre hooks and dependent on the width of the plate used in making the measurement and on the fibre length distributions of the material being measured. The projected mean length measured with a special clamping technique similar to the modified Lindsley apparatus was found to be a good absolute measure of fibre parallelization [9]. The various coefficients used by several previous researchers for the study of indirect method of fibre orientation in sliver and roving are given in Table 1.

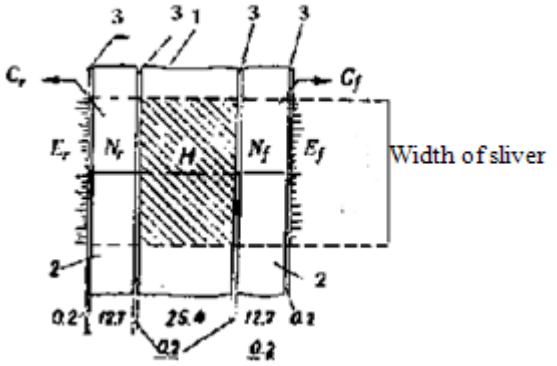

Figure 4. Schematic view of instrument for indirect method of study of Fibre Orientation.

Table 1. Coefficient used to measure fibre orientation in sliver and roving, indirectly

Orientation Parameter	**Formula**
Cutting ratio	E/N
Combing Ratio	C/(E+N)
Proportion of curved fibre ends (ρ)	E/ (E+N) x 100 %
Orientation index	(1-E/N) x 100 %
Coefficient of relative fibre parallelization (K_{rp})	(1-C/(C+N+E)) x 100 %
Modified coefficient of relative fibre parallelization (K_{rpm})	{1-(C+E)/(C+N+E)} x 100 %
Projected mean Length (PML), inches	$2x\ (W_f + W_r)/(C_f+C_r+N_f+N_r+E_f+E_r)+M$

where, C= weight of the combed out portion under the side plates (1 and 3), E = weight of projected portion from the edge of the side plate after combing, N = weight of the material after combing and cutting under the side plates, M= weight of the material under the middle plate, W = weight of the material clamped by the edge plate after initial combing, and t= width of the clamp in inches (2").

Overall, the indirect method of measuring fibre orientation involves lot of manual operations on fibres which alters the actual state of fibres in tested sample and gives only an approximate measure of fibre orientation. The direct methods can be used for the study of fibre orientation in sliver, roving and yarn, whereas, indirect methods are mainly used for the study of fibre orientation in sliver and roving only. Furthermore, few researchers have also tried to measure fibre orientation in the sliver and roving by classical fibrogram analysis with the use of specially designed clamp. The fibrogram measure of span lengths and mean lengths are shown in Figure 5. The beards in majority and minority hooks directions are scanned and measurements were taken of 66.7 %, 50 %, 5.5 % and 2.5 % span lengths. It was concluded

that the Fibrograph technique is faster than other techniques and as it also gives measure of fibre configuration comparable with the spinning process, this technique can be used to determine the fibre configuration in a sliver [4].

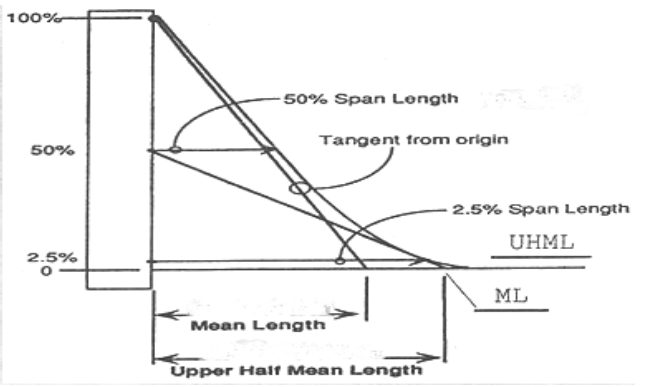

Figure 5. Fibrograph length measurement in terms of mean lengths and span lengths.

Further, when 2.5 %, 50 %, and 66.7 % span lengths were measured in direction of majority and minority hooks in the sliver. The span length readings from majority-hook beards were greater than minority-hook beards. The excess span length from majority-hook beards over span length from minority hook-beards was more clearly shown for the 50% and 66.7 % span lengths than for the 2.5% span length [10]. For constant staple length material and for fibres with low length variability the maximum span length difference between the fibrograms in the two directions becomes equal to differential hook extent in the sliver. Also shape of the fibrogram is dependent upon the number and extent of hooks in reverse and forward direction. When length variability is more the maximum span length difference is found to be different but is still closely related to the differential hook extent [11].

A study was conducted by Iyer *et al.* for comparing different methods of measuring fibre orientation during the processing of six selected varieties of cottons. When Classical Optical tracer fibre technique, UV tracer fibre technique, Modified Lindsley technique, and Digital Fibrograph clamp technique were compared by using card and drawframe slivers and rovings, both in forward and reverse directions. It was found that these methods were closely related with one another, inspite of differences in the concepts of measurement of fibre hooking and orientation [4]. A similar comparison revealed that multiple correlation of %E, %C, %N with % hooks by visual method is 0.9534 [12]. It was also proved that conclusion based on the evidence of combing ratio's, the quality of yarn is better when the majority of hooks fed to ring frame were trailing brought out distinctly by the data on the hooks measured by tracer fibre technique [13].

The yarn cross-sectional study was also done by several researchers [14,15,16]. Hearle *et al.*[8] derived a formula to calculate yarn specific volume based on the yarn twist and count and which was further used to calculate the packing density of the yarn. The formula is as given below:

Packing coefficient = fibre specific volume/yarn specific volume = $\frac{v_f}{v_y} = v_f / (\tan^2 \alpha / 4\pi . C . T^2 x 10^5)$

where, α is twist angle, T is number of turns of twist per centimeter, C= yarn count, in tex

However in similar context, Ishtiaque [17] proposed a formula to calculate packing density of the yarn, which is more realistic and based on helix angle, actual number of fibres in yarn cross section and helix twist. The formula is as given below:

Packing density of yarn $\mu = 2\pi nFZ^2 / (\sqrt{1 + (\pi D Z)^2} - 1)$

where, D = 2R= yarn diameter (in mm); d = 2r =helix diameter (in mm); θ = helix angle (in degrees) = $\tan^{-1}$ (π d Z / 25.4); Z = number of turns of twist in fibre helix per inch; Z (per mm) = Z (per inch)/25.4; n = actual number of fibres in the yarn cross-section obtained by multiplying theoretical number of fibres by cosine of helix angle (θ); The theoretical number of fibres in yarn cross section was calculated by {5315/ (yarn count (Ne) x fibre denier)}.F' the cross sectional area of fibre (mm^2);

One can conclude from the above discussion that although there are number of ways to measure fibre orientation in sliver, roving and yarn but the data generated in each technique is unique. Thus the selection of technique is entirely dependent on the objective of the study that needs to be carried out.

3. Impact of Different Spinning Stages on Fibre Orientation and Quality of Sliver, Roving and Yarn

In order to understand the role of different spinning stages on fibre orientation and quality parameters, a significant research work has already been carried out by several researchers. In subsequent sections a brief account of those contributions has been discussed.

3.1. Role of Blowroom Process

In cotton fibre the purpose of the blowroom is to open the hard pressed bales in to small tufts which provide new surface for cleaning the material. Whereas, in manmades, blowroom is mainly responsible for efficient opening of compact fibre mass in the bale form so that it can be processed smoothly on subsequent process stages. The efficient opening at blow room stage not only improves fibre cleaning but also improves yarn properties like; yarn tenacity and total imperfections but with excessive fibre openness these parameters deteriorate sharply. The increase in imperfections at higher openness is due to over beating than is necessary, fibres are stressed and damaged which then buckle and tend to form neps. The changes in fibre openness at blowroom do not appreciably influence the yarn irregularity. The yarn hairiness remains almost unchanged initially with the increase in openness at blowroom,

but at higher level of openness it increases sharply. This is attributed to the overstressing of fibres at high values of openness with staple shortening and generation of short fibres. These short fibres could be the cause of increase in hairiness in yarn [18, 19, 20]. However, in a normal range of blowroom treatment the degree of opening in the blowroom greatly affects the cleaning and lint loss at carding. But it does not appear to have a significant effect on yarn quality and in particular, yarn strength, evenness and performance [21]. A high degree of opening out in the blowroom reduces shortening of staple at the cards [22]. Furthermore, the opening of fibres in the blowroom is essential to properly carry out the subsequent process of carding for fibre individualization which in turn is essential for smooth drafting at the drawframe, roving frame and ring frame. Thorough opening of fibres is also essential toward achieving a homogenous blend at the yarn stage [23]. Also, the operation of blowroom to be controlled depending upon the quality characteristics desired in yarn and the role of blowroom process on it. Further, consistency in yarn count depends on the degree of mixing or uniformity of the lap or batt produced [20].

The opening at blow room is primarily dependent on linear density of the lap processed. The reduction in throughput rate/or thickness of the feed material to any machines improves the opening capability of that machine [20]. The heavier lap causes excessive beating at the card causing lap-ups in the card cylinder and formation of too many neps [23]. However, a good quality of sliver can be produced from a heavy lap by using high draft at card [24]. Further, the fibre parallelization is always high, initially, when heavier lap is fed to the card. This is due to more carding force generated on the heavy fibre layer present on the cylinder. But, final yarn quality in terms of evenness and hairiness deteriorates [6].

Overall the blowroom machine influence the opening, blending, cleaning, parallelization and distribution of the mass in the subsequent products like sliver, roving and yarn. In turn, have influence on the quality of the final yarn also [25, 26].

3.2. Effect of Carding Process

Carding is the most important process responsible for fibre individualization and straightness. In turn, affecting the fibre orientation in sliver, roving and yarn. Several researchers have studied the effect of carding process parameters on fibre orientation and quality of sliver, roving and yarn. Carding is the first process where fibre hooks are formed. The type of hooks and their amount plays a vital role in deciding the fibre orientation and properties of sliver, roving and yarn and their properties. The majority of fibres are hooked at one or both ends in the card sliver, and fibres having their trailing end hooked are dominant. The leading hooks are not only fewer in number than the trailing hooks, but also they are appreciably smaller [5]. Initially, configurations of fibres were classified in five groups. These were; I: fibres whose leading ends are hooked, II: fibres whose trailing ends are hooked, III: fibres with both ends are hooked, IV: fibres of which neither end was hooked but which were not necessarily straight, V: Fibres which assumed any other shape unclassifiable under groups, I – IV: i.e. knotted fibres, looped fibres, etc [1].

Further, the mechanism of these different types of hook formation was classified accordingly. Basically, the fibres on the cylinder lies in two types a) those which are held in the position by their leading end being hooked round the cylinder wires, and b) those which are not hooked around the cylinder wires but held in position with the contact and

entanglement with the hooked fibres. Further when type a) reaches the doffer, transfer takes place with relatively straight trailing ends lashed into the doffer wire point more firmly than the hooked end is held by the cylinder. Otherwise, the fibres would be drawn past the doffer, merely having their tails brushed once again. The probability of such effective lashing into the doffer wire, however, seems to be very remote. The class b) type of fibres on reaching the doffer will arrested at its projecting part most probably by actual contact with a doffer wire. The rest of its length will immediately swept downwards by the rapidly rotating cylinder forming a trailing hook by carding its leading end. Thus due to the above two types of fibre transfer in carding leads to majority of hooks in carding sliver as a trailing hook. The third group of the hooks may form in card sliver possibly due to three mechanisms. First, the downward trailing ends of the fibre immediately below the doffer setting point may have their extremities slipped in to the form of a hook by the rapid passage of the cylinder wires. Second possibility is that the hooking of the leading ends is accomplished at the doffer comb. The majority of the fibres on the doffer may approach the doffer comb with relatively straightened ends projecting forward and with its downward stroke be bent forward to form hook. Thirdly, the leading hooked ends at cylinder immediately after leaving the flats, if they are held loosely on cylinder surface may dislodge from the cylinder under the influence of air-current especially below the bottom edge of the front plate. These fibres after dislodging from the cylinder approaches to the doffer with hooked ends leading and lying close to the cylinder surface though detached from it. Such leading ends conceivably passed intact through cylinder and doffer [1]. Overall, it was observed that the majority of fibres change their configuration during transfer. Hooks are formed and previously formed hooks are removed. Transfer of fibres takes place both with and without reversal of ends. Those fibres that transfer without reversal change their configurations more. Thus, the number or the percentage of leading and trailing hooks in the web depend on the balance of three factors: a) number of fibres with hooks transferred from the cylinder to the doffer with or without reversal; b) number of straight ends hooked during transfer and transferred with or without reversal; and c) number of hooked ends straightened out due to carding action between the cylinder and the doffer. Further, the magnitudes of a, b and c-and, hence, the number of hooks- are likely to influenced by fibre, process and machine factors.

Further, an increase in load on the operational layer of the cylinder would decrease the magnitude of positive control that cylinder wires have over individual fibres. In such a state, fibre transfer will take place more easily without reversal, leaving the leading hooks as leading hooks on the doffer surface. It was also postulated that the formation of a leading hook on the doffer during transference is caused by buckling of the front end of a fibre. When the front end of a fibre moving with the velocity of the cylinder comes in contact with the relatively slower moving doffer surface, it buckles, and if the fibre is loosely held by the cylinder, it gets transferred without reversal. When conditions for buckling of front ends are satisfied, the probability of a fibre transferring from the cylinder to the doffer without reversal of ends would depend largely on the nature and extent of positive control exercised by the cylinder on the rest of the fibre [27]. Quantitatively, in card sliver 50 % are trailing hooks, about 15 % are leading hooks and about 15 % are double hooks and less than 20 % of fibres are not hooked at all [22].

Further, several researchers have studied the effect of carding process parameters on fibre orientation and quality of sliver, roving and yarn. There are various processing factors

affecting the quality of carding operation. The effects of these factors are described briefly in next few sections.

3.2.1. Influence of Card Sliver Weight

The sliver weight is changed either by changing linear density of lap feed for constant card draft or by changing card draft for a constant linear density of lap. The nature of change in the orientation of fibres in sliver shows that increase in sliver weight, either through lap hank or through card draft, decreases the proportion of curved fibre ends, and increases relative coefficient of fibre parallelization and projected mean length. This was explained on the basis of deposition of operational layers over cylinder. As coarse lap is fed or card draft is reduced, the operational layers on the cylinder increases, which results in increase in the carding force due to the increased inter-fiber friction. This ultimately increases the fibre straightening and decreases the proportion of curved fibre ends [24].

Furthermore, the cylinder-to-doffer fibre transfer decreases and cylinder load increases as sliver weight is increased. At low carding rate, increased sliver weight caused smaller increase in majority hooks (trailing) but definite decrease in minority hooks (leading). Overall projected mean length decreases with increase in sliver weight. Card web neps and yarn imperfections increases with increase in carding rate. At lower carding rate, sliver weight has little effect on card web neps. However, at higher carding rate the coarse sliver appears to have fewer neps. Although the trend was not consistent, this could indicate a direct relation between neps and minority hooks. Since the heavy weight sliver had fewer minority hooks than the light weight sliver at high carding rate. Yarn imperfections increase with increase in sliver weight. Also, the increased draft necessary to process a heavy weight sliver relative to the light weight sliver into the same size yarn caused yarn imperfections to increase. The higher carding rates also improve fibre orientation, which offset the increased short term variability of the card sliver and improves drafting, resulting in a more uniform second drawing sliver. Sliver weight and carding rate had little effect on the yarn uniformity. Overall as carding rate increases strength and elongation decrease marginally. Also, yarn grade deteriorates with increase in sliver weight and carding rate [24, 29, 30, 31]. End breakage rates may increase with increase in sliver weight [31].

Furthermore, it was also reported that both fibre parallelization and fibre hooks decreases as card sliver weight increases, indicating that there were less total hooks in the heavy than in the light weight sliver, even though the fibres in the former were less parallel than in the later [32].

3.2.2. Influence of Doffer Speed

A study conducted in Japan shows that at higher card production rate the leading fibre hooks in the sliver increases and the fibre arrangements in sliver changes. A distinct rise in the number of leading hooks at higher production rates can be seen, because of the reduced peripheral speed ratio of cylinder and doffer. The number of reverse hooks decreases as the production rate increases, because of the higher tension drafts. Thus high performance carding affects not only the carding quality but also yarn quality [33].

Similarly, for bad carding (where cylinder speed is reduced and doffer speed is increased from the normal) gives better parallelization, but the rate of improvement in parallelization in the subsequent processes is better with good carding, probably due to better fibre separation. Fibre separation seems to influence carding quality more than fibre parallelization. Open end

spinning has been found to be more sensitive to carding condition both for performance and yarn quality than ring spinning. The measurement of hooks and fibre parallelization in card, drawing slivers and roving had showed that the projected mean length (PML) of fibres in sliver and roving, which measure the degree of parallelization of fibres, was higher under bad carding condition at all the stages. The values of PML with bad carding were much higher than those with good carding at card stage and subsequently as the sliver was processed through drawing and roving. This difference in PML at card stage, due to carding condition, get narrowed down as the rate of improvement of parallelization in the subsequent process was high with good carding, possibly due to better fibre to fibre separation and degree of parallelization obtained with good carding. However, the difference in PML never vanishes completely even up to roving [34]. Furthermore, with the bad carding conditions the effect of increased relative speed of doffer was reduction in majority hooks and increase in minority hooks at the card stage. Majority hooks were more under good carding, at the card stage, and this trend continues up to first and second drawing stage. Similarly, minority hooks are more under bad carding than with good carding condition at card stage and this trend continues up to first and second drawing. This indicate that the rate of unhooking the hooked fibre during drafting, at drawing, remains same irrespective of the carding condition under which hooks are formed [34].

Further, the removal of neps at carding stage significantly improved with the reduction in card production rate because of the intensive carding action. At higher card production rate, neps level tends to increase further at the drawing. Inferior quality of carding at the higher card production rate may be responsible for the generation of neps at drawing. Better carding quality at lower card production rate improves the yarn tenacity [35].

However, an increase in card production rate increases the neps in the sliver mainly due to inferior carding quality at higher production rate. But, the number of drawframe passage after carding does not influence neps generation. Thick places and neps, in ring yarn increase with increase in card production rate. The yarn unevenness (U %), however, increases marginally with increase in card production rate [36].

The above discussion reveals that decrease in the card draft and production rate not necessarily improve fibre orientation parameters in the sliver but definitely improve the yarn properties. Apart from deciding the quality parameters at various subsequent stages the carding process also significantly affects the fibre orientation in sliver and roving.

3.2.3. Carding Force

In carding operation, the force required to individualize a tuft at cylinder-flat zone is called carding force. Increase in the load on the operational layer of the cylinder, at a constant cylinder speed, linearly increases the carding force. Increase in the tuft size increases the carding force due to increase in the pressure of the tuft during carding. When the fibre stock is not well opened, increase in the coefficient of inter-fibre friction increases the carding force. When the fibres are thoroughly opened and disentangled, the carding force is influenced by the coefficient of fibre-metal friction and not by the inter-fibre friction. The changes in the carding parameters leading to an increase in the load on the operational layer of the cylinder is detrimental to the quality of carded sliver with regard to neps and regularity. The ratio between the mean carding force and the load on the operational layer of the cylinder or the mean carding force per unit load of fibre on the operational layer is a reliable index of carding

quality. Increase in carding force per unit load decreases both the neps content and the U % of the sliver [37,38,39].

3.2.5.Influence of Carding Process on Yarn Characteristics

Overall, the carding process is expected to influence the characteristics of the preparatory products and yarn quality to a considerable extent. Increase in openness by altering carding process parameters improves yarn regularity and tenacity up to a certain extent then deteriorate. Intensive opening generates short fibres, leading to uncontrolled drafting and thus rendering the yarn uneven and weak. The increase in openness of card web at lower level does not affect the yarn hairiness but at higher level of openness the hairiness increases with the increase in openness. This can be attributed to generation of short fibres [40].

Further, in case of manmades fibres, the finer and longer fibres tend to produce more neps in the yarn. Excessive beating of fibres in the blowroom, loading of licker-in or cylinder at the card, blunt wire points on various carding elements and excessive lap weight are some of the major contributory factors. The unopened fibrous neps are not only formed during opening and carding but also at all subsequent processes like drawing, roving and spinning with neps produced in blowroom and the card providing a nucleus. These neps are not only predominant but are largest among the different type of neps. These neps show a large increase as the fibre length is increased. Further the lack of fibre individualization and drafting irregularities are two distinct causes of slubs, thick places and neps in yarns. Inadequate number of doublings and/or unevenness of blending lead to clustering of similar fibre and results in thick faults [23].

Further, an insufficient degree of orientation, entanglement of fibres, hairiness and presence of fibre hooks facilitate the formation of neps. Breaking of fibre hooks may also cause the formation of neps during drafting. Generally, the unopened fibrous neps are progressively being reduced by blowroom and carding processes. But, after the blowroom and carding processes the new neps are formed because some unopened or entangled mass of fibres are still left in the material [19].

So it can be concluded from the above discussion that process of carding drastically changes the arrangement of fibres in sliver, roving and yarn. The effectiveness of carding operation is primarily dependent on the amount of material present in operational layer on cylinder. Increasing the weight of operation layer (either by feeding heavier lap or reducing card draft) sometimes improves the fibre orientation by increasing the carding force but impairs the quality of sliver and final yarn. Further, decreasing the weight of operational layer by increasing the doffer speed increases the neps in the sliver. Also, the process of carding generates lot of hooks, majority of which are trailing followed by leading and double hooks. The magnitude of these hooks decides the amount of fibre parallelization that can be achieved in subsequent processes and, in turn, the quality of sliver, roving and yarn produced. The amounts of hooks are also dependent on weight of operational layer on cylinder [19].

3.3. Importance of Drawing Process

Drafting arrangement, in particular, increase unevenness very considerably. In order to achieve usable yarn characteristics, the process must include operations, which give an equalizing effect. This can be doubling or leveling (drawing while simultaneously imparting

twist). Doubling is still the most widely used, but leveling is becoming gradually more significant in woolen spinning mill only. Doubling is infact a process of equalizing. Several products are fed in together in sliver drafting arrangement. Where the thick places generally tends to distribute and compensate each other. In principle every doubling is a transverse doubling also because the feeds are united side- by-side [41].

3.3.1. Influence of Drawframe on Fibre Straightening and Hook Removal

It is well known that the drafting process in general improves the fibre parallelization, and straightens the hooks present in the card sliver. But some time due to excessive parallelization, fibres in subsequent drawing process starts relaxing. This can be seen in the Figure 7. In the drafting arrangement the fibre hooks may be embedded in the body of fibres either as leading or as trailing hooks. A trailing hook for a certain period moves with reminder of the fibre strand at the speed of back roller towards the front roller. If the fibre tip passes into the nip region of the drawing roller, the fibre is accelerated. However, since the trailing end is moving with a relatively thick body of slowly moving fibres, the fibre is straightened before the whole fibre can reach the drawing speed-the hook is eliminated. The straightening of trailing hooks at the drawframe is shown in Fig 7. On the other hand, leading hooks are immediately caught bodily by the front roller and carried along unchanged [41, 42]. The process of straightening is improved and accelerated when the amount of draft is increased [43].

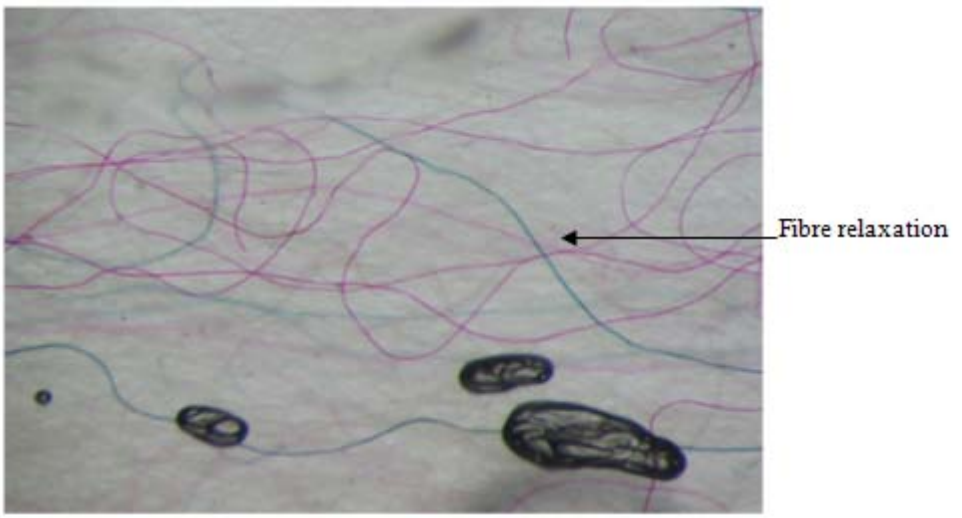

Figure 7. Fibre configuration in Finisher sliver.

However, it was also postulated that the hooks can be removed in the drafting process only through frictional contact with other fibres moving at speeds different from that of the hooked fibre. The hook removal is greater when: (i) the larger the number of such contacts at any instant and (ii) the greater the entanglement and cohesion with neighbouring fibres moving at different speeds. It was assumed that a hook is removed only if the other end of the fibre is positively gripped by a nip and that floating fibres do not take any part in removing hooks. Finally it was concluded that the probability of removal of leading or trailing hook is

same. It is probably because the total number of effective contacts from other fibres, is the density of the effective fibre fringe which brushes past a hook or through which the hook brushes. This is more at any instant for the trailing hook, which therefore is removed easily. However, the leading hooks are acted on by the fast moving fibres in the region of drafting zone (i.e. nearer the back nip) where fibre density, inter-fibre friction, and fibre entanglements are higher but due to most of the fibres in this region is fast moving and cannot therefore exercise an effective hook-removing action on the slow moving leading hooks [13].

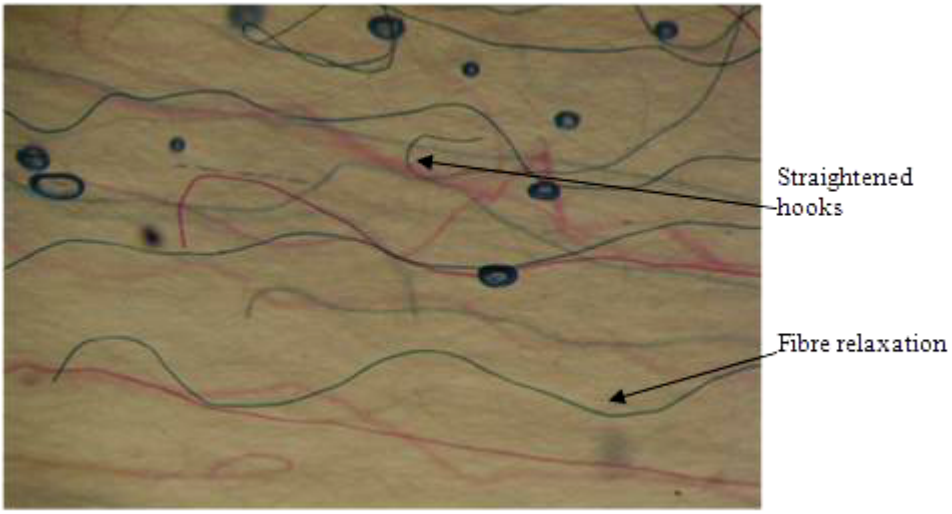

Figure 8. Straightening of hooks in the draw frame sliver.

Further, fibre parallelization decreased as sliver weight was increased, regardless of the processing stage. The improvement in fibre parallelization from card to the first drawing sliver average more than from first to second drawing, about a 3:1 ratio. This indicates that first drawing process is more critical than second drawing, since most of the fibre parallelization and reduction in hooks takes place at this process. It was shown that maximum fibre parallelization and hooks reduction could be obtained at first drawing by drafting the majority hooks in the trailing direction. This may be accomplished through use of unit carding system [13]. Also, at first drawing, the trailing (minority) hooks were reduced more than the leading (majority) hooks. At second drawing, the trailing (majority) hooks were reduced more than the leading (minority) hooks. Sliver weight had no effect on hook removal for either the majority or minority hooks in few cases [32].

Further, the proportion of curved fibre ends (ρ) decreases and relative fibre parallelization (K_{rp}) and PML increases as the number of drawframe passage increases. It is interesting to note that the decrease in the value of 'ρ' and the increase in the value of 'K_{rp}' and PML was more up to the first drawframe passage as compared to the second drawframe passage for both of the cases. But in values of degree of straightening of curved fibre ends ($E\rho$ and $E\kappa$), it was observed that the value of '$E\rho$' is more between the first and second drawframe passages. This may be due to the feeding majority of trailing hooks as trailing to the drafting system of second drawframe, which straightens out the trailing hooks during drafting [6, 24].

Further, with constant carding conditions, the ratio of majority hooks to minority hooks is constant for a wide range of fibre mean length and a moderate range of fibre fineness. During processing when majority hooks trails in first and second drawing, increase in fibre parallelization over the conventional drafting direction, is independent of mean fibre length [44]. Furthermore, the fibres in the sliver exhibit grouping behavior during drafting. The grouping behavior is directly related to the drafting performance, with optimum roller setting leading to lower grouping tendencies. Fibre orientation, fibre type and the performance of earlier processes are expected to be the major factors influencing the grouping. This grouping behaviour is responsible for the use of wider settings earlier in the process line. When comparing for breaker and finisher drawings there appeared to be longer fibre groups in the finisher drawing. The longer group sizes are attributed to the drafting process orienting the fibre groups along the axis of the strand. Effects of fibre hooks and their opening in the finisher drawing also play a part in the longer group lengths observed [45].

Significant improvements in the regularity of the roving and the yarn result from the incorporation of two additional drawings. The extent of improvement varies with the type of material processed. It is interesting to note that the improvements in the evenness are not reflected in the strength of the yarn, which is nearly unaffected by the use of additional drawing. This is contrary to earlier findings on direct sliver-to-yarn spinning frame where improved parallelization found to lead better strength. The results have clearly demonstrated that improved parallelization in the ingoing (feed) material contributes to better drafting at both speed and ring frames. The use of additional drawings, thus, offers a convenient means of upgrading the evenness of carded cotton and man made staple fibre yarns. When additional drawings were used with short staple material, it may be necessary to maintain the sliver hank on coarser side, in order to minimize the incidence of stretch and sliver breaks at the creel of the speed frame [43].

Further, the rotor yarn strength increases with the increase in drawframe passages. This is mainly due to better orientation of fibre and improvement in mean fibre length at rotor groove with the increase in drawframe passages, which is due to better fibre extent in the yarn. Yarn uniformity could be improved with the increase in number of drawframe passages. Neps and thin places do not show any trend, but thick places increase with the introduction of drawframe passages [46].

3.3.2. Influence of Draft and Doublings

Apart from number of drawframes used, amount of draft and doublings at drawframe also plays a crucial role in deciding the quality of sliver, roving and yarn. Increase in draft and doublings improve fibre parallelization, but decrease sliver uniformity. The increase in fibre parallelization over-shadowed the decrease in sliver uniformity, resulting in a decrease in spinning end breakage. Total draft and doublings had no measurable effect on percentage of hook reduction. There was a slight increase in fibre parallelization and decrease in sliver uniformity with increased draft and doublings, indicating that fibre parallelization and sliver uniformity were not directly related [32].

Furthermore, the sliver irregularity can be evened by doubling slivers together at the drawframe; however, this evening action becomes ineffective as the wavelength of the irregularity increases [47]. An 8- fold doubling, in comparison to the 6- fold doubling does not cause any improvement on drafted sliver and roving unevenness % and no significant difference in the number of hooks in sliver. However, reduction in number of hooks at roving

is more in case of 8- doubling sliver. The increase in number of doublings at drawframe does not cause any improvement in mass unevenness in the ring and rotor yarn. The tensile strength clearly increases in ring yarn with the increase in number of drawframe passage because of better parallelization of the fibres, and the related increase in fibre-fibre friction. The increase in doublings also increases the tensile strength. Whereas, in rotor spun yarn tensile strength of the yarn produced directly from the card sliver is even higher than from the yarn produced from drafted sliver. This proves that parallelization of the fibres deteriorated in rotor spinning. The increase in number of doublings decrease the breaking elongation in ring yarn but the values are unaffected in the rotor yarn. An 8-fold doubling on the drawing frame leads, for both yarn types, no detectable reduction in number of thick places [48]. However, increased number of doublings not only improves irregularity but also the mixing in the sliver. The best strength was achieved with a draft of eight and eight doublings, which gave only slight changes in yarn evenness and in imperfections [31]. It was also found that on drawing frame, the best over-all results are obtained by using light-weight slivers and a draft of eight and eight doublings [49].

In general, it can be said from the above discussion that increases in number of draw frame passages or number of doublings improves the properties of yarn. Apart from the above two factors there are other drawing parameters, which decide the fibre orientation in sliver and hence affect the quality of yarn. These factors are discussed briefly in subsequent sections.

3.3.3. Influence of Direction of Hooks in Sliver

In general, feeding majority hooks in the leading direction contributed to more irregularities and the size of the effect was not dependent upon the draft or the count spun. Direction of feed of the hooks had no significant effect on irregularities at the can fed speed frame under normal conditions.

Feeding the hooks as leading contributes to more yarn irregularity and poorer strength, but the magnitude of the effect was nearly of the same order, with the second-and third-passage slivers as regards irregularity and slightly more marked with second passage sliver as regards strength. Apart from improving the fibre parallelization, the use of additional drawing also introduces a reversal in the direction of drafting of the hooked ends at the subsequent stage, and to evaluate the effect of parallelization alone, spinning with the same feed directions must be compared. When this is done parallelization founds to contribute towards better drafting, as indicated by lesser number of irregularities and higher strengths and improvements obtained seems to be of the same order for both feed direction of the majority hooks at the ring frame. Favourable feed direction (obtained by reversal) has, in general, greater effects on drafting quality than parallelization (achieved through additional drawing,). The difference in drafting irregularities due to fibre disorder and feed direction do not vary much with the draft. Further, the draft ratio has no effect on irregularity, a lower draft at the front zone leads to slightly better yarn strength for all input slivers. The relation between relative variance and count shows that the effect of fibre arrangements in the input sliver on drafting irregularities is not sensitive to the count spun [43].

Two passages of drawing followed by can-fed speed frame are a standard processing sequence for carded counts in a modern spinning lay out. This is because of the favourable drafting direction at the ring frame and the minimum processing costs associated with this system [43]. In general, the trailing hook must be presented to the ring spinning machine.

Thus, there should be an odd number of passages between the card and ring spinning machine [41].

3.3.4. Influence of Drafting Force

The resistance met by the drafting roller when drawing a sliver is called the drafting force [50]. Basically, drafting takes place in three operating stages: straightening of the fibre, elongation of the fibres and sliding of the fibres out of the surrounding fibre strand. So the force acting on the fibre, called drafting force, which enables to move the fibre by pulling it from the restraining force due to relatively slow moving fibres in the back roller grip, first increases sharply. This causes straightening and extending of the fibres. Once the fibres start sliding drafting force drops down drastically. Overall drafting force decreases as the draft increases. Since a higher degree of draft implies fewer fibres in the cross-section. Besides this drafting force also dependent on the arrangement of the fibre in the strand (parallel or crossed), cohesion between the fibres (surface structure, crimp, finish etc.), fibre length and nip spacing [41].

Further, for a constant weight of sliver entering the drafting zone, the drafting force in one zone is inversely proportional to the draft, and thus directly proportional to the number of fibres being withdrawn by the front rollers of the zone. When this number is changed by feeding a heavier sliver, the force increases more than in proportion to the weight. This is because heavier slivers are more compact. But, considering the forces in the different zones of drawframe, it is proportional to the number of fibres under the front rollers of a zone [51]. However, for very low drafts, the drafting force increases first to a peak as the draft increases then decrease [52]. Furthermore, particularly for short fibres, a high ratio of the number of the fibres in the front roller nip to the number of fibres being delivered by the back roller at any instant will cause an increase in pulling force exerted by the faster fibres. But for apron drafting systems, this ratio can be kept low enough to prevent the bunching of the fibres dragged into the front-roller nip [53].

However, there is no relationship between the inter-fibre friction, as a measure of drafting force, and drafting irregularity. This is because the overall change in the inter-fibre friction would not affect the motion of the floating fibre; to do this it would be necessary to increase considerably the difference between static and kinetic friction [54].

3.3.5. Drafting Wave

During the roller drafting of cotton, the rollers cannot set much closer than the length of the longest fibre and consequently most of the fibres are for a time out of the control of the rollers. These fibres are called floating fibres. The undue movement of these floating fibers is responsible for generation of a periodic irregularity called drafting wave in the material [55].

The drafting wave is basically caused by the position of the change-point depending on the number of fibres held by the front rollers. The thickness of drafted sliver then tends to vary periodically. Observation shows that the drafting wave in different lengthwise strips of the sliver are formed more or less independently, so that the sliver drafts as though it were made up of number of sub-sliver, then, according to theory of drafting wave all the floating fibres in the part of the drafting zone just behind the front rollers are dragged rapidly forward by the fibres held by front rollers, so that a gap free of floating fibres is left in the sub-sliver. The fibres are held by the back rollers then move forward with back roller speed until the gap has passed into the drafted sliver. The snatching process is then repeated and caused a

periodic irregularity, called drafting wave, in the material [56, 57, 58, 59]. However, in apron drafting, it is considered that the irregularity due to the drafting wave is at a low level because of the control affected by the apron. However, the drafting wave is mainly caused by the varying acceleration of floating fibres [57].

Further, when high drafts are used without the employment of a special drafting system the resulting yarn is usually more irregular due to increase of drafting wave amplitude [55]. Overall, relative variance of the sliver or roving also increases steadily as the draft is increases. Further there are two reasons why the straightness and parallelism of the fibres affect the amplitude of the drafting wave. In the first place, the greater entanglement, which occurs when the fibres are not parallel, prevents the smooth sliding of the fibres past one another and so increases the tendency of the fibres to go forward in clumps. Secondly, in drafting, the fibres move in subgroup and the independent drafting of the lengthwise strips of the sliver is more marked when the fibres are more nearly parallel; the number of sub-slivers is therefore greater, and the coefficient of variation of the drafting wave is less. For the same cotton the irregularity of the yarn is greater as the higher the count, for the same count the irregularity is less when the fibres are finer [56]. Overall increase in amplitude of drafting wave impairs the quality of sliver and thus yarns [59].

3.3.6. Sliver Strength

The force required to slide past the fibres in a sliver is termed as sliver strength. The sliver strength can also be used as a measure of fibre-alignment in top-making. The fibre-alignment and sliver strength increase during the first and second gillings, but only a small increase during the third gilling. The principal factors determining sliver strength are: 1) fibre length and its variability, 2) intrinsic fibre strength, 3) fibre-alignment, 4) fibre-straightness and 5) sliver tension during testing. But in gilling, the major changes are those of fibre-alignment along the axis of the sliver and a reduction of fibre-hooks [60].

However, in cotton sliver, the fibre configuration mainly affects the sliver strength. As the fibre parallelization improves with the successive passages of drawing, the sliver strength drops. In the card sliver, inter fibre friction and sliver strength shows a positive correlation. But, as the fibre parallelization improves with the successive passages of drawing the sliver strength drops, and the difference in the strength of the sliver having different frictional values narrows. Thus fibre orientation affects sliver strength much more than the values of inter-fibre friction [61].

Further, the cotton slivers possess very lower strength and are liable to unexpected drafting and breakages during processing. If the sliver strength is not appropriately controlled, sliver and roving become uneven and frequent end breaks may occur. The carded sliver tenacity is halved after the two drawing passages. This is attributed to fibre-straightening and fibre parallelization activity in the card slivers. Further, fibres became more straightened and parallelized, and more intimately packed in the sliver, leading to higher sliver density, or lower sliver bulk. This means that the sliver bulkiness reflects the fibre straightening and fibre parallelization in the sliver. Increase of number of drawing process leads to decrease in sliver bulk and further reduction of sliver strength and an increase in fibre-straightening and fibre parallelization. The number of drawing passages had more influence on the sliver strength than the total draft and doublings experienced by the slivers. This was probably due to the reversal of the sliver-processing direction at each drawing passage that played an important role in the straightening and parallelization of the fibres. Increase in draft/doublings at the I

drawframe passage increases the strength of the sliver. This effect is diminished at the II drawframe passage. The increase in number of doublings at constant drawframe draft increases the tenacity and evenness. The increase in tenacity is due to reduced improvement in terms of fibre straightening and fibre parallelization. It can be deduced from the above discussion that sliver strength is affected by drafting conditions and fibre orientation in sliver [62]. Further, in viscose fibre, the tenacity of I drawframe sliver is higher than card sliver, whereas, II drawframe sliver is having the lowest value of tenacity [6]. The increase in value of 'K_{rpm}' increases the tenacity of carding and I stage of drawframe sliver whereas trend reverses in finisher sliver due to fibre relaxation, as shown in Figure 7.

Overall, the literature on drawing process reveals that the process of drafting adds to irregularity, by generation of drafting wave, in the drafted material. However, the number of doublings given on drawframe reduces the amplitude of irregularity by equalizing effect. Further, fibre straightness and parallelization improves with amount of draft but deteriorates with increase in number of doublings given at draw frame. The fibre parallelization and straightness and added irregularity in the sliver are also dependent on feed direction of the sliver to the drawframe. Thus properties of sliver are governed by counteracting effect of drafting and doublings which, in turn affects the quality of final yarn.

3.4. Effect of Roving Process

It is well known that the drafting of cotton sliver and roving is accompanied by increase in irregularity. Though in the drawframe, this increase is not apparent because it is compensated by doubling, but in the speed and spinning frames, the irregularity increases at each machine until the yarn is many times more irregular than the sliver from which it was made. Further, the relation between the variance and draft is linear and the slope of the line increases sharply, as the hank feed is finer [56].

However, for the best results from apron drafting, adequate parallelization of fibres must be obtained in the ingoing (Feed) sliver. This is the reason why concepts of apron drafting failed in the case of drawframe. The fibres become more parallel and straighten in comparison to the drawframe sliver and do not get much chance to relax after drafting system due to the presence of twist [6]. The state of fibres in the drafted roving is shown in the Figure 9. Further, in general irregularities added at the speed frame are not influenced by the feed direction of the hooks in the feed sliver especially for coarse roving. But it acquires significant importance as the roving is made finer. Where feeding the hooks as leading results in more irregularities in the case of finer roving [43].

Furthermore, the products drafted on apron drafting systems also exhibit-drafting waves like roller drafting. This suggests that the drafting wave is a feature of drafting process and could originate from factors other than uncontrolled acceleration of short fibres. With cut staple fibre in particular the drafting wave could result from acceleration of leading hooked portion of the fibre which results in too early a feed for some of the fibres or from elastic movement of fibre assembly in the drafting zone. Finally it appears that the drafting waves introduced at the speed frame are of low amplitude compared to other irregularities, and reversal and drafting at the ring frame reduce the amplitude still further so that they are not seen in the yarn. Further, the yarn produced from the roller drafting is more irregular and

weaker than that from apron drafting, the difference in uniformity is more pronounced than that in strength [63].

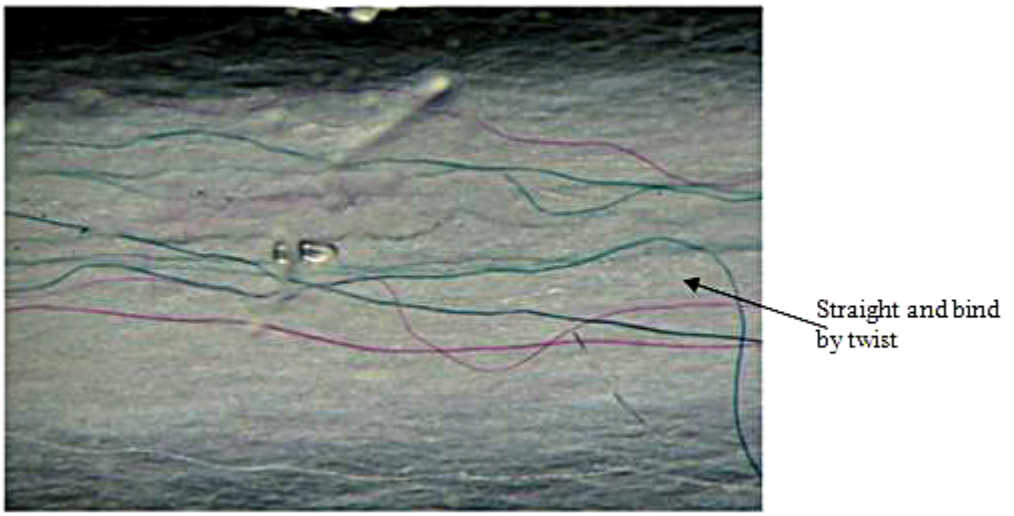

Figure 9. Fibre configuration in Roving.

3.4.1. Effect of Speed Frame Draft

Draft given at the speed frame is a crucial factor affecting quality of roving and yarn. The increase in the irregularity of a fibrous product during drafting is the result of irregular fibre movements arising from the following principal factors: 1) from the irregularity of the product entering the drafting system, 2) from an unsatisfactory technical condition of elements of the drafting system, 3) from faults in its design and 4) from structural unevenness i.e. uneven distribution of fibres of different length in cross-section of the product. The irregular movement increases with the draft and with the difference in the lengths of the fibres in the roving. It follows that the irregular movements occur at any draft and in any drafting field and that their magnitude increases with the draft [64].

However, on speed frame drafting, the irregularity added is relatively low and nearly independent of draft [63]. Contrary to the above, greater the draft at speed frame, the higher will be the level of parallelism in the roving [65, 6]. The higher roving draft required for the heavy sliver influenced parallelization more effectively than roving evenness [49]. In turn, increase in draft at speed frame improves the properties of relatively poor carded material in ring and rotor yarn [6].

Apart from the amount of draft given at speed frame, there are some other factors, which decide the quality of roving produced. These factors are described in forthcoming sections.

3.4.2. Drafting Force

In a double apron drafting system, the drafting force increased with the size of the front beard i.e. with total draft, fibre length, speed of drafting. The drafting force is decreased as break draft and apron-to-apron spacing increased. There was a difference in the force when the roving was fed in the normal direction and then in the reverse, thus showing that the effect

of fibre hooking that originated at the card still persists at the spinning frame. For good spin, a certain amount of fibre tension is necessary at the front draft zone. But an excessive tension of the front beard will not always lead to optimum conditions. Further by measuring the drafting force at the front draft zone, it was possible to detect the effect of fibre hooking that originated at the card. The force was higher when the majority of hooks are trailing. Further a certain amount of fibre tension is necessary in apron zone for optimum yarn properties. Generally, high values of drafting force are associated with the best properties of the spun yarn, but too high a fibre tension may lead to deterioration of yarn properties [66].

3.4.3. Behaviour of Hooks in the Roving Process

The relationship between the total amount of hooks in sliver and roving, for cotton, is linear. Therefore, it is sufficient to analyze hooks in sliver prior to roving as a basis for evaluating the effects on yarn properties and spinning end breakage. When converting sliver into roving the draft (approximately 8) should reduce the amount of hooks. However, when measuring hooks by the Lindsley technique, the twist in the roving is not removed, and this hides or masks the true reduction in the amount of hooks caused by the roving draft [44].

3.4.4. Roving Strength

Apart from the parameters, which decide sliver strength, the roving strength is additionally dependent on the amount of twist inserted in the roving. The inter-dependence of twist and strength in roving may be explained by two effects. Either the fibres slip, or they hold until the tension becomes too great and then break. The amount of twist determines which of these effects will occur. For small twist, parting is by fibre slippage at a low tension. As the twist increases, the strength also increases, but parting is still by slippage, up to the point where the strength is equal to the combined breaking strength of all the fibres in the cross-section. This is the maximum strength; further increases in twist beyond this value mean that the parting is by fibre breakage, but the strength does not increase and ultimately diminishes because of the increased angle at which fibres are inclined to the axis [67]. Further, stronger finisher sliver produces stronger roving [6].

3.4.5. Effect of Roving Twist and Ring Frame Break Draft

The main objective of break draft is to straighten and redistribute the roving twist to a greater length before the main draft. Further, the higher twist in the roving may exert some control over the short fibres and so reduce the amplitude of the drafting wave [68].

Also, on evaluation of the irregularity of drafting roving by its performance on the ring frame, it was revealed that as the break draft is too low, the twisted roving cannot be properly drafted thus resulting in increase in thick places in yarn. But as the draft ratio increases, the drafting force increases, and the fibre crimps and hooks are straightened, which is beneficial to improve uniformity of the drafted roving. Later, fibre slip partially, but the static friction has not yet been overcome. In this zone, the drafting force reaches a maximum value with increasing fluctuations, which results in unsteady draft behaviour and thus worsens the uniformity of the drafted roving. When passing over the peak region, the fibres begin to slip before the roving is completely drafted. In this dynamic friction behaviour, both the force and its fluctuation decrease. But it frequently causes a drafting wave in the drafted roving because of the higher draft ratio. This drafting wave remains in the yarn and tends to cause serious

thick and thin places in the spun yarn. Higher break draft ratios increase the U % of drafted roving and lower the yarn quality [69]. Further, the migration of the fibres in the cross-section of the roving impairs the mixing uniformity achieved in the proceeding operations of the spinning sector. This migration generally increases with the increase in twist in the roving [70].

Also, as the break draft increases there is an increase in the drafting tenacity (force require to slide past the fibres in dynamic condition) up to a maximum. This is followed by a decrease in the tenacity for further increase in break draft. This is because at lower break draft, in the neighborhood of 1, the fibre density in the cross section of roving, i.e., the fibre to fibre contact has not reached its maximum value. But as the break draft increases so does fibre density, until a maximum is reached, after which fibre slippage begins. On reaching this point, further increase in break draft entails a decrease in fibre contact and drafting tenacity starts to decay [71].

Furthermore, tenacity increases with the increase in roving twist multiplier. However, this characteristic of roving does not always lead to the expected increase in yarn strength [72]. Infact, the yarn tenacity increases to a maximum value then decrease as the roving twist multiplier (TM) increases. However, the yarn uniformity first increases and then decreases with increase in roving TM in majority of the cases. This is because increase in roving TM increases the inter-fibre friction due to more contact area, which creates problem during drafting and ultimately deteriorates the yarn quality. The imperfections in yarn do not show any regular trend [29]. For a given yarn count the yarn properties is superior with the medium hank (about 2^S Ne hank roving). So there is optimum draft distribution found which exists between speed and spinning frames, from the point of view of regularity and strength [63].

Overall, the process of drafting, at roving frame, adds irregularity in roving but the amplitude of drafting wave is contained to an extent by apron drafting. Further, an increase in draft at speed frame improves yarn properties by reducing the draft required at the ring frame. High strength roving produced with higher twist, produces higher tenacity yarn due to less spreading of fibres in the drafting zone. However, higher drafting force is required to draft the high strength roving which may add to the irregularity in the yarn. The increase in draft at the speed frame increases fibre parallelization and reduces number of hooks due to increased drafting force acting on the fibre.

Thus draft given at every stage of spinning preparatory plays an important role in deciding quality of the product produced on subsequent machines and ultimately the properties of the yarn.

3.5. Effect of Ring Spinning Process

Lastly, most important machine in ring yarn manufacturing is the ring frame, where the roving is drafted many times and finally twisted to form into final yarn. Majority of the fibres migrate from surface to core or vice-versa, due to tension difference arose in twisting of fibre band delivered by the drafting system. The actual migrated structure of the ring yarn is shown Figure 10.

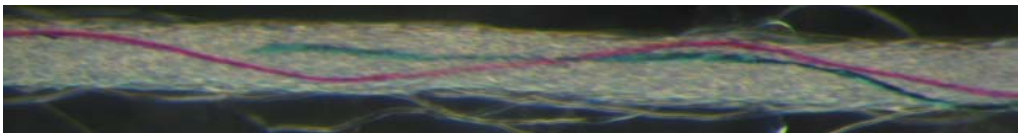

Figure 10. Uniformly twisted fibre helix in ring yarn.

Apart from that the yarn is many times irregular than the roving. There are four main causes of the irregularity in the ring frame: random arrangement of the fibres along the length of the roving; irregularities caused by random variations in the position at which the fibres change from back to front roller speed; irregularities caused by the disturbance of the drafting by the irregularity of the entering roving, and drafting wave [56]. The various important factors, which affect the fibre orientation and quality of yarn, are discussed in the next few sections.

3.5.1. Effect of Total Draft

Total spinning draft is the most important factor affecting end breakage rate, yarn strength, elongation and uniformity [73]. At modern ring frames, with the possible use of higher ranges of ring frame draft, a wider yarn count range could be covered without difficulty with relatively coarse roving. This may increase the irregularity in the yarn, neps and thick places. The use of high total drafts requires high break draft adjustment and a special measure needs to be taken against fibre flow spread due to high relative speeds of the fibres in the main zone of the drafting system. The reliable control of high total drafts and the problem-free opening of hard twist roving make necessary the use of high load pressures in ring frame drafting system [74]. Furthermore, the drafting tenacity decreases with increase in total draft. In other words, fibre to fibre contact decreases as the front draft increases. However, the drafting tenacity should be high for such good yarn properties as breaking strength and irregularity. In addition it was postulated that the yarn tenacity in turn dependent on the degree of fibre spread at the front rolls exit. The wider the front in which the fibres emerge, the more difficult for them to be assembled by the run-up twist, and the lower the strength. However, the fibre spread will be dependent on the degree of fibre tensioning in the zone between the aprons and the front draft rolls and, a high drafting tenacity bringing all the fibres to close contact is desirable at the front draft zone [71]. Further, the relative variance in the yarn increases as the finer roving is fed to ring frame. Thus making the yarn more uneven, hairy and less stronger [68].

Apart from ring frame draft, there are some other factors, which have a significant impact on the quality of final yarn. These factors are described in details in the next few sections.

3.5.2. Geometry of Spinning Triangle

The turns of twist in yarn are generated at the traveller and travel against the direction of yarn movement to the drafting arrangement. Twist must run back as close as possible to the nip line of the rollers, but it never penetrates completely to the nip because, after leaving the rollers the fibres first have to be delivered inwards and wrapped around each other. Accordingly, at the exit from the rollers there is always a triangular bundle of fibres without twist, the so-called spinning triangle. The length of spinning triangle depends upon the spinning geometry and upon the twist level in the yarn. If the spinning triangle is too short,

then the fibres on the edge must be strongly deflected to bind them in. This is not possible with all fibres. So some fibres may lose as fly. Others may be bound-in, but at one end only; one fibre end then projects from the body of the yarn, which is therefore hairy [75].

Further, the wider width of the fibre strand or the ribbon at the front roller nip makes the spinning triangle wider which affects the yarn hairiness. The wider the ribbon, the greater the difficulty for the peripheral fibres to get fully twisted and integrated into the body of the yarn thus leading to more hairiness. Higher ring frame drafts, lower roving twist multiplier and double roving feed lead to more ribbon width. Excessive draft at the ring frame can be avoided by feeding finer roving [23, 76]. Also, using a traveller that is too heavy or too light increases the hairiness of yarn [77].

However, the yarn diameter, single yarn strength and evenness are other factors related independently with hairiness indices. The yarn with higher diameter is usually more hairy. With an increase of count, yarn hairiness decreased because the same mass of cotton extends over a greater length in the finer yarn. The increase in twist reduces yarn hairiness. The correlation between Uster evenness parameters and hairiness indices show that as the U % and imperfections decrease, yarn hairiness increases. This may be because U % is influenced more by variations in the weight and shape of yarns rather than by the projecting ends. Yarn diameter influences hairiness independently irrespective of twist [78].

3.5.3. Longitudinal behaviour of Fibres in Yarn

The fibre migration is defined as movement of the each fibre between the centre and the surface of the yarn. Fibre migration in the yarn arises due to tension variation in fibre in the zone of yarn formation. Since the length of the path the fibres must follow increases from the core to the surface of the yarn, so must the tension in the fibres [80].

Further, an alternative geometric migration mechanism, either combine with or effectively replace the tension mechanism were proposed by few researchers. Yarns are often thought of as twisting in the form of cylindrical bundles of fibres, but they may also twist in the form of flat ribbons. Indeed it is probably much more common in practical twisting operations for the yarn to be present as a ribbon rather than a cylinder [80]. In addition to this, migration of fibres in yarns, was represented (a) by the mean fibre position; (b) by the root mean square deviation; (c) by the mean migration intensity;

Further, the analysis in two planes showed that there is no statistical difference in the value of the migration parameters measured in two different planes. Also, the mean fibre position and RMS deviation are only slightly affected by twist. The mean migration position falls below the value of 0.5, which would come from uniform density of packing of fibres in the yarn; and this indicates that density is greater near the centre of the yarn. This is most noticeable in the low twist yarn, with the lower value of mean fibre position. The RMS deviation is less than the value of 0.29, which would result from complete ideal migration. Overall, in ring yarn the fibres migrate rapidly though irregularly [81, 82] Further, the mean migration intensity increases rapidly as the twist increases. In that case, the fibre entanglements are more complete at higher twist factors and that longer length of the fibres is bound to the body of the yarn, which reduces the hairiness [83]. The roving twist and drafting ratio have a significant effect on the rate of fibre migration. An increase in the drafting ratio causes a postulated decrease in values of migration intensity. It is neither the roving twist nor the drafting ratio, which has any effect on fibre migration, but only the remaining amount of twist in the drafting roving. If the process particulars were so adjusted that this later factor

would not remain constant, then any induced variation in the roving twist or the drafting ratio would not have any influence on fibre migration [84].

Furthermore, in double rove feed yarn, higher the value of mean fibre position and lesser the value of mean migration intensity, better is the helical (interlocked) structure. Increases in yarn tenacity due to optimum roving spacing is mainly due to better spinning-in coefficient and mean fibre position. Also, the actual number of fibres in cross-section is continuously decreases as the roving spacing increases. This indicates more fibre inclination to the yarn axis. Further increase in roving spacing increases the fibre migration in yarn. After reaching the optimum roving spacing fibre starts inward migration. Finally, packing density was the highest at the optimum roving spacing [85].

Also, the migration of the fibres in the cross-section of the roving and yarn impairs the mixing uniformity achieved in the proceeding operations of the spinning sector. However, the fibre migration effect is at a maximum on the ring frame as a consequence of the force that come into being in the twisting operation and also as a consequence of the fact the number of fibres in the cross-section of the yarn is small [70].

Moreover, the draft distribution at ring frame and speed frame plays a crucial role in deciding the fibre migration in the yarn. Finally, it is advantageous to keep higher draft at speed frame and corresponding draft at ring frame should be lowered to achieve optimum values of the migration parameters in the yarn. High ring frame draft increases the MFP and RMSD in yarn. Further, the fibre extent in the yarn gives an idea of total projected length or indirectly gives total contacting length of fibres. But, the fibre extent is also dependent on length of fibres in the roving and hence cannot be compared in samples made from different fibre lengths. So, a new index of measuring fibre orientation named fibre overlapping index (FOI), which is comparable and gives direct information of total contact length of fibres was proposed [6]. The fibre extent increases with increase in draft at the ring frame where as, the fibre overlapping index reduces due to sliding past of the fibres [6].

Literatures on ring frame process reveals that ring yarn properties are mainly dependent on the fibre orientation parameters like fibre extent and migration parameters. These parameters primarily dependent on the dimensions of spinning triangle, which in turn is mainly governed by spreading of fibre band in the drafting zone. The draft given at the ring frame is the primary parameter, which affects the spreading of fibre band in the drafting zone.

3.6. Role of Rotor Spinning Process

Next to ring spinning, rotor spinning is the most widely accepted spinning system of yarn manufacturing in the world. In the rotor spinning, fibre ends are open to the individual level at the opening zone and redoubled in the rotor groove. The fibre band deposited in the rotor groove is twisted at low tension to form final yarn. In the next few sections the influence of various parameters, which decide the quality of rotor spun yarn, are discussed briefly.

3.6.1. Fibre Configuration in Rotor Groove

The opening, air transportation and deposition in rotor groove lead to lot of disorientation of the fibres in the rotor groove, as shown in Fig 11. In general, in rotor spinning, the direction of feeding of hooks is of little significance [41]. Similarly, in the fibre rings collected from inside the rotor there are no statistically assured difference between hooks in

reverse and forward direction. The direction of sliver feed was also without effect and original fibre orientation being irrelevant due to the effect of change in fibre orientation during opening and transportation to rotor groove [86].

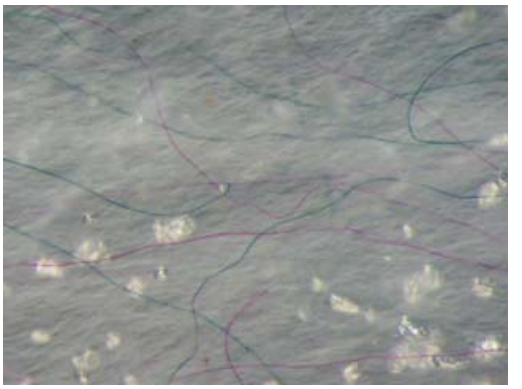

Figure 11. Fibre disorientation in rotor groves.

Apart from the above, the value of 'ρ' in forward direction is more than in the reverse direction, but the value of '$K_{гр}$' shows just the opposite trend in the fibre rings collected at rotor groove. This can be attributed to the striking effect of the leading ends of the fibre with the transport tube and rotor. This increases the leading hooks. Moreover, the brushing action, which the trailing end of the fibre experience when they are released from the feed nip will definitely be helpful in improving the fibre straightening and reducing the proportion of curved fibre ends in the reverse direction [88].

In general, in rotor spinning, fibres lie in a much straighter configuration in the yarn than in the rotor groove. This phenomenon may be attributed to the tension prevailing at the yarn formation point during the transformation process of the fibre bundle into yarn. The tension acting as a stretching force on hooked, looped, and entangled fibres present in the fibre ring, straightens them out during the transformation process. Bridging fibres also straighten out when one of their ends attached to the yarn, moves away from the rotor, while the other brushes against the rotor or fibre feed tube wall. During yarn formation, however, there is every possibility for the formation of new hooked fibres. Still the effect of tension predominates and resulting in an increase in the mean fibre extent in the yarn compared to that in the rotor fibre rings [91, 92].

3.6.2. Effect of Drawframe Passages

The introduction of drawframe passage reduces proportion of curved fibre ends and increases the value of coefficient of relative fibre parallelization in rotor yarn. The mean fibre length at rotor groove increases with the increase in the drawframe passages due to better parallelization of fibres in the sliver with the introduction of drawframe passages, which results in better fibre opening. But, there was a significant decrease in the mean fibre length at rotor groove ring, when the mean fibre length value in corresponding sliver and rotor groove ring was compared. This is due to the breakages of fibre by opening roller [46]. Similarly, satisfactory fibre parallelization and straightness leads to a stable drafting process and results in a more regular and stronger yarn. [93].

In rotor spinning, once the desired numbers of layers of fibres are deposited inside the rotor, the accumulated layers on the rotor are simply lifted and twisted to form the yarn. The configuration of fibres in the yarn body is therefore almost similar to that of fibres in the rotor groove ring. Hence, the parameters affecting the configuration of fibres in rotor groove will also influence the fibre orientation in yarn. The proportion of curved fibre ends in the corresponding sliver and rotor groove ring decreases, while coefficient of relative fibre parallelization increases, with the increase of drawframe passages. Mean fibre length at rotor groove increases with the increase of drawframe passages. Better fibre straightening, but not much improvement in fibre parallelization is achieved with the second drawing passage [90].

The number of drawing passages has a significant effect on the spinning-in coefficient and on yarn properties. Spinning directly from card sliver gives the lowest spinning-in coefficient for different sliver linear densities. The first drawframe passage sufficiently improves the fibre parallelization and straightness in the sliver, however, the increase in spinning-in coefficient is low. Introduction of the second drawframe passage does not contribute much to fibre parallelization and straightness. A significant increase in yarn tenacity occurs with the effect of the drawing passage. The improvement in the yarn tenacity is also greater in the case of first drawframe passage compared to the second one. This might be due to increase in spinning-in coefficient, which indicates a greater fibre length contribution to yarn body and increases yarn strength. The improvement in the elongation to break was also fair [90].

3.6.3. Hook Formation and Removal in Rotor Spinning

In rotor spinning, when fibres are fed to an opening roller, their trailing ends are held where as their leading ends are combed. This straightens the leading ends and tends to remove any leading hooks by opening them out or by breaking them off, and, as fibres are released by feed roller, there is slight tendency for their trailing ends to be straightened by frictional contact with other fibres. Further, the action of beater puts the fibres under tension and when they are released by the feed roller, and there are virtually no restraining forces acting upon them, they contract violently and tend to crimp and curl. In transport tube of rotor machine, contact between a fibre and inner surface of tube may straighten the fibre but depend on how the fibre contacts the tube. A hook may be straightened or increased in size or fibre can be reversed in direction in the tube. As a fibre emerges from the tube and its leading end makes contact with the rotor or with the fibre ring, there is a tendency to straighten the leading end. Then as the fibre accelerated to rotor speed, its tail end is snatched from the tube, so that friction tends to straighten the fibre and remove any trailing hook [91]. It was also postulated that the fibres are being pulled by the opening roller from the feed fringe by making hooks around its wire point. These hooks are further transmitted into the yarn structure with or without reversal [94].

3.6.4. Effect of Feeding Direction of Hooks

Feeding majority hooks in the leading direction causes more fibres to break, whereas feeding them in the trailing direction makes them less susceptible to breakage. This is because the fibres from feed sliver are constantly engaged by the wire points of the combing roller which pulls them out from the fringe by making them hook around the wire points. So, fibres undergo breakage after their leading ends hook around the wires of the combing roller. The presence of leading hooks, therefore, predisposes the fibre to breakage. It was further seen

that with the majority hooks fed in the leading direction, the losses in tenacity and breaking elongation of fibre bundle collected from rotor groove, for carded and once drawn slivers are slightly higher than with the trailing direction. The direction of feed seems to have practically no effect when twice-drawn sliver is fed. Further, it was observed that the yarn strength seems to be greatly influenced by the fibre parallelization in the material. The drawn sliver produces a stronger yarn. Sliver with majority hooks fed in the trailing direction produces a marginally stronger yarn. Yarn breaking elongation, imperfections and unevenness are hardly affected by the direction of feed or the number of drawframe passages [94, 95]. Further, the fibres in the middle layer of the feed sliver suffer maximum breakage, while those in the bottom layer suffer maximum surface damage. Further, fibre breakage is positively related to fibre reversal [96, 97].

Further, the short wave irregularity resulting from back doubling is partly or completely smoothen out and show that the limiting irregularity for a yarn produced in this manner is only three-quarters of the value used for ring-spun yarns. The lower irregularity of rotor yarns is thus inherent in the method of production, since it is directly caused by the manner of deposition of fibres on the inner wall of the rotor [98, 99].

In rotor spinning, drawing for the sake of fibre hooks formed during carding can be dispensed with, since most of these hooks are straightened by the time they reach the collecting groove in the rotor, and the rule demanding an odd number of processes between carding and spinning no longer apply [100]. Although fibre-breakage was greater when majority of the hooks lead into the opening roller, yarn properties are actually slightly better, probably owing to more efficient fibre separation and distribution to the rotor [101]. Further, the difference in sliver- feed direction (orientation) from the same process has little effect on rotor- spun yarn strength, whereas differences as a result of the number of drawing frame passage have marked effect [102, 103].

Further, the leading and trailing hooks, which correlate very well with the total number of hooks, increase with an increase in the number of passages. In ring spinning with more doublings and more drawing passages, a stronger yarn is obtained, although this is not the case with rotor-spun yarns. The number of doublings has no significant effect on the yarn elongation [104]. Also, the trends of proportion of curve ends are directly correlated with the hook extent in rotor yarn [6]. Furthermore, in rotor yarn, the leading hook extent is more than the trailing hook extent. The decrease in hook extents must increase the fibre extent in the yarn but it is not necessarily true in case of rotor yarns. This is because the hook extent in rotor yarn depends on various types of hooks and fibre buckling present in the yarn [105].

3.6.5. Effect of Fibre Length

The fibre length in rotor yarn manufacturing is a crucial parameter, which decides the yarn quality. With longer fibre length, the high incidence of the wrapper fibres and poor fibre opening and belts are counted as the neps in the rotor spinning [106]. The belts and wrapper in the rotor yarn is shown in Fig 12. Further, the optimum fibre length to produce the most regular yarn can be given by rotor diameter divided by 1.44 and optimum fibre length for getting maximum tenacity seems to be 30 mm irrespective of rotor diameter [107]. However, a value of 1.1:1 for the ratio of rotor diameter to mean fibre length is usually regarded as necessary for producing acceptable yarn [107, 108].

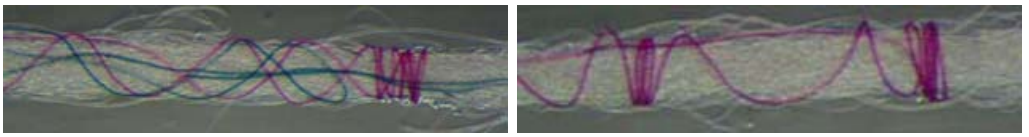

Figure 12. Belts and wrapper in the rotor yarn.

Further, the influence of longer fibres which is positive in ring spinning, for the spinning behaviour and the yarn properties, has- as already established for cotton-a deteriorating effect for rotor spun yarns. Thus length of the fibres is to be evaluated in relation to the rotor circumference [109].

Furthermore, the spinning-in coefficient in rotor yarn decreases with the increase in fibre length due to following reasons. Firstly, due to higher linear density of longer fibre they are thrown by opening roller against the wall with higher centrifugal force, so increasing the chances of fibre bending and buckling. Also, at opening roller the chances of fibre breakage are more for longer fibre. In conjunction to this, the longer the fibre used the greater the tendency towards wrapper fibre formation. Further, it is quite impossible for any fibre to integrate into yarn without its repeatedly coming under the influence of the fibre entry zone. Actually it passes the end of feed tube many times during the period that any particular fibre is being peeled off the surface. For longer fibre this frequency is still higher and if in the process the fibre emerging from the tube at the instant when yarn arm sweeps past then fibre transfer into yarn structure without being allowed to deposit in the groove and form as wrapper or belt. Secondly, for a fibre that has partly emerged when yarn tail arrives the leading part is on the surface of the rotor and the trailing end is still in the tube. The fibre is picked up at some point along its length, and such a fibre becomes folded over in the form of leading hook and also of bridging fibre. The probability of this depends on the fibre length or more precisely on the fibre extent relative to the circumference of the rotor. The longer the fibre length more is the chances of formation of such leading hooks. Also, greater is the percentage of wrapper fibres, which actually do not contribute to the yarn strength. The longer the fibre, higher the twist loss due to the higher percentage of sheath fibres [110].

3.6.6. Influence of Rotor Machine Draft

The effect of rotor draft on yarn strength does not appear to be serious at lower speeds but may well at higher speeds. Draft affects fibre orientation and its influence is greater at higher speeds and with finer yarns [111, 112].

Further, the higher linear density of feed sliver gives a lower spinning-in coefficient in yarn, and, thus does not produce adequate yarn properties. Technically, important is the opening draft between the feed roller and the opening roller. The shorter residence time of the fibres in the opening zone, the better is the fibre opening with less fibre damage. It is therefore advisable to feed lower linear density sliver in order to reduce the residence of fibres in the opening zone. Firstly, the lower the linear density of the carded sliver, the better the carding action. Second, fibre parallelizations decreases and total fibre hooks increase with increasing sliver linear density during first and second drawframe passages. The finer the sliver fed to the rotor spinning greater the spinning-in coefficient (K_f) as compared to the coarse sliver feed. The difference in 'K_f' is statistically significant too. The explanation of increased yarn tenacity can be confirmed by the increased fibre extent, which contributes more to yarn tenacity. Thus an increased spinning-in coefficient increases the yarn strength.

Elongation at break increases with the fineness of the sliver. Yarn regularity and imperfections registered a consistent improvement with the fineness of the sliver. It can be due to better separation & opening, and an improved arrangement of fibres inside the rotor groove, which improves the spinning-in coefficient too [87].

Furthermore, the increasing the draft decreases the thin places, thick places and neps and improves the yarn regularity significantly of rotor yarn. This is because fibres are exposed longer to the combing action of the opening roller. On the other hand, yarn strength is not affected much by the higher draft. This is because relative speed between the opening roller and feed roller is unaffected by halving the intake speed. This is because the opening roller surface speed is powers of ten higher than the sliver delivery speed [113].

Further, the reduction of overall draft on the rotor spinning machine led to simultaneous improvement in the breaking tenacity as well as the breaking elongation and hairiness is distinctly reduced [114]. However, few researchers have also reported that the yarn tenacity and breaking elongation decreases with increase in rotor draft. However, the effect of draft is very less. This is due to deterioration in fibre orientation at higher draft. Yarn irregularity and thick place increases with an increase in draft. This is due to more number of fibres in sliver cross-section. The upper layer of the fibres comes in contact with wire teeth but the lowermost fibre layer does not have any impact of wire teeth which is responsible for lesser opening of fibres situated at the bottom layer, thereby deteriorating yarn regularity. But it is observed that yarn uniformity improves after a draft of 148.3. This may be due to the lower feed rate at higher draft, which helps, in better fibre opening. The number of thin places increases with the increase in rotor draft. At lower opening roller and rotor speeds, the number of neps does not depend on rotor drafts [115].

Quite differently, it was also reported that the sliver linear density is not an important factor in rotor spinning, though it seems that there is rather more hairiness when yarn linear density decreases [116, 6].

Overall it can be deduced from the above discussion that rotor draft either marginally improves or does not affect the quality of yarn spun.

3.6.7. Rotor Yarn Structure

Rotor yarn has a peculiar structure, which is quite different from ring yarn structure. The rotor spun yarn mainly consists essentially of a three part structure: a densely packed core of fibres, which are substantially aligned with the axis of the yarn; more loosely packed fibres twisted round the core and lying at a considerable angle to the axis; and then fibres that are wrapped around the outside of the yarn to form belts of very small inclination. In some cases, the belts are quite loosely formed, and it was possible to slide them along the yarn, whereas, in other instances they were very tightly wrapped and formed thin places, but with a high weight per unit length due to the dense packing [95]. Further, the low strength of rotor spun yarns could be attributed to poor fibre alignment, inferior fibre migration within the yarn body, a fairly large number of folded fibres, leads to poor distribution of load over the fibres [117, 118, 6].

Further, the rotor-spun yarns exhibit minima in all the migration parameters, as the twist level is increased [119]. Whereas, the rotor-spun yarns exhibit a maxima in all migration parameters as card draft is increased and it corresponding rotor spinner draft is reduced [6]. Further, the average number of fibres in the yarn cross-section is always less than (by a factor equals to cosine of helix angle) the values calculated by using formula: linear density of yarn

to linear density of fibres. It follows as the twist increases, helix angle increases and so the value of number of fibres in the cross-section decreases by a factor cosine of helix angle. One can therefore expect an increase in fibre migration with increase in the twist of rotor-spun yarns. This has been attributed to reduced resistance to the fibre migration because of smaller numbers of fibres at the yarn formation point [120]. However, the correlation between the measured yarn twist and the physical properties of the rotor-spun yarns, such as CSP, tenacity, elongation-at-break and hairiness, is poor. Whereas, the structural parameters of rotor-spun yarn, such as incidence of wrappers per unit length of yarn, average length of wrapped portion and average number of wraps in each wrapped zone, are highly correlated with the physical properties viz. CSP, tenacity, breaking elongation and hairiness, of the rotor-spun yarns. Inclusion of TPI along with structural parameters enhances the correlation [121]. Since, the fibre migration during rotor spinning is a factor affecting the mechanism of yarn formation, which affects belt formation in rotor spinning and yarn hairiness. And the amount of hairiness can be regulated by modifying the yarn twist or by selecting the fibre fineness and fibre length [122].

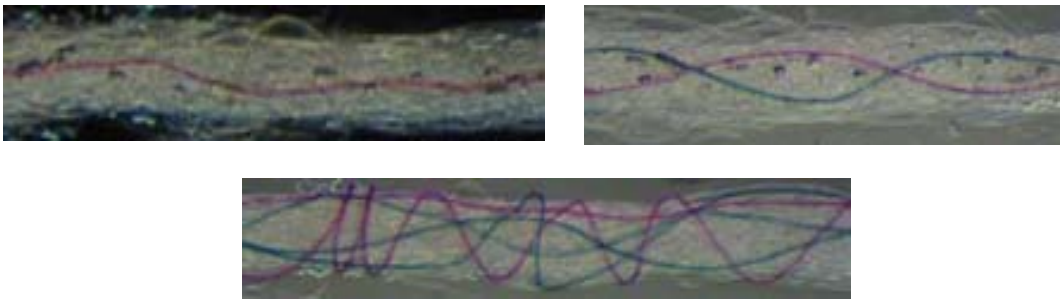

Figure 13. Three parts structure of rotor yarn.

3.6.8. Packing Density of Yarn

Furthermore, when packing density in rotor yarn was evaluated by Hearle's and Ishtiaque's formulae it was found that yarn diameter and packing coefficient have reciprocal relationship [93, 6].

Extensive literature review on rotor spinning shows that rotor yarn properties are mainly dependent on amount of fibre parallelization and straightness in sliver feed to rotor spinning. Although, the feed direction of the sliver is immaterial, factors like fibre length, sliver linear density, rotor draft and other fibre orientation parameters also play an important role in deciding the properties of rotor yarn.

3.7. Importance of Air-jet Spinning Process

The third most widely accepted system of yarn manufacturing is air-jet spinning. The method of yarn production differs significantly from ring and rotor spinning. Thus air-jet yarn structure is quite different from these two yarn structures.

3.7.1. Air-jet Yarn Structure

The structure of yarn spun from air-jet system consists of bundle of parallel fibres wound by some tight wrapper fibres. The system consists of two nozzles, which are responsible for producing false twist. During untwisting of core fibres the wrapper fibres get twisted in opposite direction and impart transverse forces towards the parallel core. Thus giving rise to a fasciated yarn structure with smallest diameter of air-jet yarn [15, 17]. The air-jet yarn structure can be understood from the Figure 14. One important requirement of air-jet yarn structure is that it should have certain minimum length to form long wrapper to give very good binding. Generally, it is being said that air-jet yarn is suited for medium and long staple fibres only, and cotton fibre and its blends difficult to be processed on the air-jet.

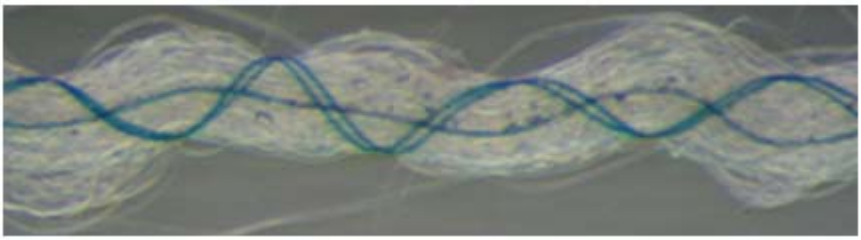

Figure 14. Fasciated structure of air-jet yarn

Further, the structure of air-jet yarn can be mainly classified into three categories: a) orderly wrapped; b) randomly wrapped; c) unwrapped. Varying the machine spinning conditions alters the relative frequency and the mean length of each class. For air-jet spun yarn, the yarn strength is attained mainly by the resultant normal force of the fibres wrapped around the parallel core fibres, which gives rise to the frictional forces necessary in the yarn assemblage to affect the transfer of tensile strength. These wrappings are caused by fibres standing out from main body of the yarn whilst false twisting the fibre assemblage, and they wrap around the yarn during untwisting [15, 123, 124]. Further, for finer fibres and coarser yarns, the fraction of wrapper fibres decreases and hence the yarn strength reduces. The influence of wrapper fibre fraction plays dominant role. However the most important fibre parameter affecting air-jet spun yarn tenacity is the extensibility and elastic recovery. This offer a potential source of improvements in yarn quality produced from man-made fibres [125]. The fasciated yarn structure is suited for the fibres having very good elastic recovery i.e. for nylon or polyester fibre. Due to lower elastic recovery of viscose fibre, it is not possible to produce stronger air-jet yarn due to insufficient binding force generated by wrapper fibres on parallel core fibres [6]. The loosening of wrappers in the air-jet yarn is shown in Figure 15. Further, it was found that majority of migration takes place in wrapper fibres in the yarn. The wrapper fibres are usually having its end embedded in parallel core fibre [6]. The yarn structure and thus their properties are influenced by several other process parameters, which decide the laying of fibres in yarn structure. These parameters are discussed briefly in next few sections.

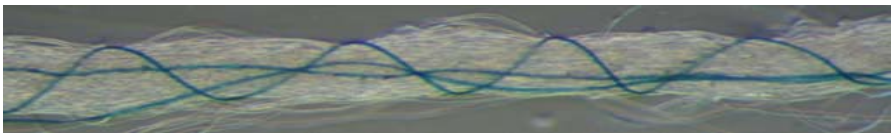

Figure 15. Loosening of viscose wrapper fibres due to permanent deformation in air-jet yarn.

3.7.2. Effect of Ribbon Width

As the width of the fibre band in the drafting system increases, more fibres go out of control of false twisting action and consequently form more wrappers [126]. But after a certain limit, the fibres get out of control completely due to the air turbulence caused by the high speed of the front drafting roller and the majority of fibres become wrappers, leaving only few as core fibres [127].

Further, with wider condenser the same number of fibres is spread over a greater width at the nip of the front roller. As a result, the inter-fibre cohesion is lower which leads to more edge and thus wrapper fibres, which makes the yarn comparatively stronger, along with some increase of unevenness [128, 129, 130]. However there were the cases in which minor improvement of the yarn tensile properties can be achieved by using a narrower condenser [131]. Further, the tenacity values increases with the decrease in yarn linear density. The change in yarn tenacity is associated with increased edge fibres, which are subjected to airflow at the nip of front roller. This would mean that as the yarn linear density decreases, there is an increase in the number of edge fibres as a result of better individualization. The airflow at the nip of the front roller causes the edge fibres to move away from the fibre bundle and thus helps produce long wrappings. Also, the trends of yarn elongation are similar to those of yarn tenacity. However, the finer yarn is more irregular and has more numbers of imperfections due to the decrease in number of fibres in the cross section [132].

3.7.3. Hook Formation and Removal in Air-jet Spinning

A prominent feature of air-jet yarn is predominance of leading hooks as observed during the microscopic study. These hooks are generated in carding process or formed in air-jet spinning due to the frictional resistance encountered by the fibres at the point of entry into the nozzles. A protruding leading end is likely to be bent back and get caught in the fibres behind it and forms a leading end. A protruding trailing hook can be expected to be straightened out at the point of entry in to the nozzle. Due to the low twist of the fibre strand, it would be very easy for an individual end to detached and bent back. Also, due to two passage of drawing, a predominance of leading hooks is to be expected in the feed sliver [124].

Contrary to the above, some researches has shown that majority of hooks are trailing in air-jet yarn. This may be due to the predominance of trailing hooks fed to the air-jet spinning in sliver. The trailing hooks may not get straightened in drafting system. This may be due to the prevailing inertia effect at higher drafting speed. If this is the case, then the theory of keeping odd number of drafting passages between card and air-jet machine may not stands true in air-jet method of yarn manufacturing [6]. Both sided hooks are very small in number. The viscose fibres having low flexural rigidity show more wrapper extent and more hooking tendency in air-jet spinning [133].

3.7.4. Effect of Main Draft

The main draft has a significant influence on the breaking load, elongation-at-break, and yarn hairiness of air-jet spun yarns. All these parameters increase with increase in main draft. This implies that the number of wrapper fibres is affected as draft changes and hence a simple change in draft can affect yarn structure also [124]. Drafts of up to 170 can be used to produce yarn with very good regularity indices, using a three-roller drafting system [134]. The mean tenacity and elongation value increase with rise in main draft. The high main draft stretches the fibre well, resulting in a high level of fibre orientation and more useful fibres for sharing the load under strain. At the same time, however, the variation of tenacity and breaking elongation can become higher. The yarn imperfections increase sharply with an increase in the main draft and, of poor consolidation the thick places lead to weak spots in the yarn [134, 6]

Further, with an increase in main draft the number of core fibres decreases and number of wrapper and wrapper-wild fibres increases. This can be attributed to the disturbance of the secondary balloon formed between the first nozzle inlet and front roller nip. Since the detached fibres are produced as a result of this disturbance, the origin of wrapper and wrapper wild fibres can be attributed to the detached fibres. The increase in main zone draft significantly increases the breaking load, breaking elongation, irregularity and hairiness of the yarns. The increases in hairiness with increase in main draft is due to the increased disturbance of secondary balloon which increases the number of fibres detached from main strand. This should increase the hairiness and number of wrapper fibres generation. But, when wrapper fibres increase beyond a certain number, they can be expected to bind the yarn and decrease the protrusion of fibre ends, which leads to reduced hairiness [134, 6]. Similarly, the increase in main draft ratio increases yarn strength up to an optimum point, after which strength decreases. Further, total draft is likely to have a major influence on evenness [135].

Overall increase in the draft, up to a certain level, in air-jet spinning improves the yarn properties but further increase in draft deteriorates the yarn properties.

The literature review on air-jet spinning reveals that the properties of air-jet yarn is decided by the proportion of core and wrapper fibres and their profile in the yarn structure. The draft given at air-jet spinning is a crucial variable affecting ribbon width of drafting material and, in turn, the proportion of core and wrapper fibres in the yarn structure. Further, other orientation parameters are also dependent on the amount of draft given on air-jet spinning machine.

Overall, the literature on all the three spinning technologies shows that the structures of the yarn spun from ring, rotor and air-jet yarn are entirely different from each other and mainly responsible for different yarn properties. Also the processing parameters at preparatory and yarn spinning stages affect the yarn spun on these three spinning technologies in a different manner. So, next few sections give a comparison of structures and properties of yarns manufactured from these three spinning technologies.

4. COMPARISON BETWEEN DIFFERENT SPINNING SYSTEMS

4.1. Ring Yarn vis –a –vis Rotor Yarn

The strength of ring and rotor yarn increases with the increase in preparatory draft and there are some advantages in presenting a majority of trailing hooks to ring spinning. Also, increase in preparatory draft results in improved regularity of ring yarn and improvement is more pronounced by feeding the majority of hooks as trailing. Also, in rotor spinning increased draft led to improved regularity but effect is less, whereas the direction of presentation has no effect on the yarn regularity. Further, the fibres in the rotor yarn show less evidence of migration than those in ring-spun yarn. Also, whatever the fibre arrangement is there in the material fed, there were always more leading hooks in the rotor yarn [91].

An analysis of packing density shows that the fibres for the rotor yarn are located most densely near the yarn centre. The ring spun yarn has a moderately uniform distribution of fibre packing density. Yarn hairiness strongly depends on mean fibre position, with an inward shifting of the packing density leading to lower yarn hairiness. That is, the higher value of the mean fibre position means that more fibres are located near the peripheral region of the yarn, so the possibility of fibre ends appearing on the outer layer of the yarn increases and more hairs can be generated in ring yarn [136, 6]. The fibres in a rotor spun yarn are neatly aligned and interlocked inside the yarn and migrate periodically, going inward and then back out, with some random features. The migratory pattern in a rotor spun yarn is more or less constricted locally, and the magnitude of fluctuation is less than that in the ring spun yarn. Further, the fibres in the ring spun yarn are spread in the middle of the yarn cross section while in rotor spun yarn the fibres are located mostly near the yarn axis. The packing density shows a trend that is very similar to the mean fibre position. The rotor spun yarn has a relatively high packing density around the yarn axis. Whereas the ring spun yarn has an intermediate packing density distribution [136].

The tenacity of rotor spun yarn is $2/3^{rd}$ of the ring spun yarn. The ring spun yarn is more even and has fewer imperfections than the rotor spun yarn. Superior yarn evenness and fewer imperfections of the ring yarn contribute to better yarn tenacity. Another reason of higher yarn tenacity was better fibre migration in ring yarn, which resists the slippage of fibres under tensile loading. The mean fibre position and root mean square deviation is the least in the rotor yarn in comparison to equivalent ring yarn [6]. Further, a higher migration factor (MMI x RMSD) corresponds with a higher yarn breaking tenacity of ring yarn. The positive contribution of the migration can be defined by the increased self-locking structure of yarn, which increases the resistance to slippage between fibres and better utilization of fibre strength for yarn tenacity. The lower breaking elongation of rotor yarn can be defined on the basis of axis-parallel alignment of fibres in the yarn center and partly by the core-sheath structural effect, in which fibre in the core region contribute to the tensile properties [136, 6].

The total yarn hairiness in rotor yarn is lower than the ring yarn. This was explained on the basis of influence of fibre distribution across the yarn cross-section or the mean fibre position. The inward shifting of the mean fibre position or the packing density leads to less yarn hairiness [136, 6].

Furthermore, the majority of the fibres in the ring yarn twists along the longitudinal axis of the yarn and thus contribute to the overall strength of the yarn and responsible for the

lower diameter of these yarn. Whereas, in rotor yarn a considerable number of fibres in the rotor yarns loosely wraps around the yarn with the some forming rings or wrappers around the yarn giving a bulky appearance. These loosely wrapped fibres did not contribute as much to yarn strength as the parallel fibres in the ring yarn. Further, the elongation to break is higher in the case of ring yarn than the rotor yarn. But rotor yarns are more uniform than the ring yarn [137].

Contrary to this, it was reported that the synthetic rotor spun yarn was somewhat similar in evenness properties, less stronger and extensible than ring-spun yarns [138, 139, 6]. Further, with increase in fibre length, rotor yarn become uneven whereas, the longer fibre leads to improvement in quality in ring yarn [140]. However, the cotton rotor yarn is comparatively less stronger but more extensible than ring yarn. Further, the rotor yarn is more even having comparatively fewer imperfections, more bulky and less hairy [141]. Also, there is a greater probability of wrapper fibres in the rotor yarn that can be counted as imperfections especially neps [91, 142].

However, in man-made yarns, the lea strength and single yarn tenacity is 20-30 % lower for rotor yarn. However the superior regularity of cotton rotor yarn is not observed in case of manmade yarn. Similarly higher breaking extension of cotton yarns is not seen in man-made yarns. The rotor yarn hairiness is also much lower due to the wrapping action of the wrapper fibres [23, 6].

Also, the evenness of the strength across the yarn length is better in rotor yarns as compared to ring yarns. However, breaking elongation % of ring yarn is less than the breaking elongation % of rotor yarn. The number of short thick places is higher for ring spun yarn than for the rotor spun yarn [48].

4.2. Ring Yarn vis –a –vis Air-jet Yarn

Polyester-viscose blended air-jet spun yarn is 14-18% weaker than the corresponding ring spun yarn [143]. Further, 100 % viscose yarn is almost 40% weaker than equivalent ring yarn [6]. The values of breaking extension for ring and air-jet spun yarn show that, in general, air-jet spun yarns are more extensible than their ring counterparts. But, it is not true for 100 % viscose yarn due to poor elastic recovery of the fibre [6]. Further, air-jet spun yarn is more evener than equivalent ring spun yarn. Yarn imperfections, in terms of thin places, thick places, and neps are lower for air-jet yarn when compared with ring yarn. Total imperfections are lower by about 70 %. If ring spun yarn irregularity is taken as 100 %, air-jet yarn irregularity lies between 65-95 % [111]. Also, the air-jet spun yarns are less hairy than ring-spun yarn [144].

Further, rotor spun yarns, which are usually considered more even than the ring spun yarns, also cannot achieve the results obtained by air-jet spun yarns [145]. The advantage of air-jet yarns is more obvious in the case of thin places, whereas air-jet yarns are significantly better than ring and rotor spun yarn. Air-jet spun yarn is less hairy when compared with ring spun yarns [146, 147, 148]. Further, total packing density is maximum for air-jet spun yarn followed by ring and rotor yarns. The rotor yarn has the lowest migration index followed by ring and air-jet spun yarns [149].

4.3. Rotor Yarn vis –a –vis Air-jet Yarn

Incase of manmade or manmade/cotton fibre blends, the MJS yarn is 22-30 % weaker and 36- 43 % less extensible than rotor yarn in comparable coarser count range. This is due to insufficient wrapping length owing to higher bending rigidity and low breaking extension and short length of cotton fibre. The higher breaking extension of rotor spun yarns, on the other hand, can be ascribed to the presence of many hooked, looped and disoriented fibres in the yarn structure. Further, rotor yarn is more even than MJS yarn [129, 6].

4.4. Comparison of Hairiness of Ring, Rotor and Air-jet Yarn

Worldwide, the hairiness of yarn is either measured by UT-3 or by Zweigle hairiness tester. UT-3 gives overall hairiness including hairs less than 1mm from yarn surface. But does not give any information about hair lengths distribution. The Zweigle G 565 detects hairiness of more than 1 mm from yarn nucleus excluding the shortest hairs. When the number of these hairs that evolve near the yarn core is of some importance and, on the contrary, the hair length is relatively short, the yarn can appear very hairy with the UT-3 and only slightly hairy with the Zweigle instrument. This occurs for bulky and open end spun yarns and when some particular fibres are present in the yarns. So the correct procedure for measuring hairiness in the yarn is both measurement of the overall hairiness including shortest hairs and also hair length distribution. However, the coefficient of correlation between hairiness values of Uster tester and Zweigle is not very high but equals to 0.7 [150, 151].

Further, the majority of a rotor spun yarn's bridging fibres emerge from the rotor with their exposed ends trailing and, on rewinding, these trailing ends become leading and easily roughed up. It is conceivable that such a rewinding effect also occurs during hairiness testing. In addition, as the yarn with majority of leading hairs traverses through the hairiness meter, the air drag acting on the leading hairs tend to open up these hairs and increase their projected lengths. Further, this is responsible for the increase in hairiness reading registered by the Zweigle hairiness meter [117].

The hairiness of the rotor yarns on an average is lower than that of ring yarns. Consideration of total length of protruding ends and loops also leads to a similar conclusion. Considering the distribution characteristics of protruding ends for each type, it is observed that the percent number of very short ends in rotor yarns is larger than that of ring yarns. The difference in the hairiness of these two types of yarns can be explained as: in ring spinning, hairiness is caused when trailing ends of fibres are preferentially thrown outside the periphery of the yarn by the intense migration in fibres that take place during spinning, but in rotor yarns, the fibres are better controlled inside the yarn structure. So in ring yarns short ends predominate over the long ends [152].

Further, when hair length distribution for ring and rotor yarn is compared. The short hairs < 3 mm and total hairs is fewer hairs in rotor yarn than the ring yarn. But, only hairs exceeding 3 mm is less in ring yarn in comparison to the rotor yarn. Further for ring spun yarn, when twist increases the number of hairs longer than 3-mm decreases rapidly. The corresponding decrease is less marked for rotor spun yarn [153, 154].

Similarly, the percentage of extremely short and long hairs (length < 0.25 mm and >3 mm) of rotor yarns are both greater than those of ring yarns. Fiber indices of ring yarn with a testing length less than 2 mm are significantly higher than rotor yarn [154].

Further, the percentage of hairs exceeding 3 mm, calculated over the total of hairs counted was influenced by spinning process. Rotor spinning process give values above the ring spinning process whereas, air-jet spinning gives lower value than the ring spun yarn [152]. Furthermore, the number of hairs longer than 1mm was highest for the air-jet spun yarns and least for the rotor spun yarns, independently of the yarn linear density, but, for the number of hairs exceeding 4 mm from the yarn core, yarn ranking depends on the yarn linear density. In coarser count range air-jet yarn is most hairy and ring yarn is the least hairy [6, 155].

An increase in yarn hairiness and neps count causes a decrease in breaking strength at high delivery rates. In general, the range in values of hairiness is lower for rotor spun yarns compared to ring spun yarn. Air-jet spun yarns are similar to ring spun yarns for 1-2 mm interval fibres, but they fall to the level of rotor spun yarn for 3-4 and 4-6 mm intervals, and finally they drop below other yarns. If ring yarn diameter is taken as 100%, the diameter of air-jet spun yarn of same linear density is 75 -100 % [156, 157].

Further, the migration of fibres in rotor yarn was only about 1/6 of ring yarn migration. Therefore, fibre ends in the inner layer or core of rotor yarn had less chance to come out of the yarn body. Also, some fibres of the outer layer of rotor yarn wrap around the yarn body, and these fibre ends rises out of the yarn body forming loops and longer hairs. Also regularity of hairiness distribution of ring yarn is much better than that of rotor yarn. Yarn diameters of the same yarn counts differed due to the difference in fibre arrangement and, hence yarn density. It was found that the rotor yarn diameter is about 9% more than ring yarn. It was also found that the diameter of rotor yarn is closely related to the structure of sliver. The better the regularity of fibre arrangement in the sliver, the better will be the regularity of fibre arrangement in the yarn. This will result in a decrease in yarn diameter [158]. Further, the air-jet yarn is having the least diameter followed by ring yarn and rotor yarn is having the highest diameter [6].

The above literature review reveals that, in case of manmades and in the coarse count range, ring yarn is better than the rotor yarn in terms of tenacity and breaking elongation and that the air-jet yarn has the least tenacity and breaking elongation. Further, rotor yarn is most even followed by ring, and air-jet yarn. However, in the fine count range, air-jet yarn is far better than rotor yarn but poorer than ring yarn in terms of all yarn properties. These differences in trends of three different yarns arise due to different yarn structures and spinnable ranges of the three spinning technologies. So a comparative study of these three yarns is required to understand which fibre orientation parameters is important for a particular yarn structure and thus responsible for deciding the properties of that yarn.

5. SUMMARY

It has been revealed from this progress that carding is the most important process stage, which affects the properties of sliver, roving and ring, rotor and air-jet yarns. The effect of drawing and doublings at subsequent stages also plays a significant role in deciding the

quality of intermediate products and yarn quality. The quality of ring spun yarns can be adjusted choosing a proper draft distribution in speed frame and ring frame. The increase in draft at the speed frame improves the fibre parallelization and ultimate yarn properties. The increase in draft at the ring frame deteriorates the properties of ring yarn. The quality of rotor yarn depends on the state of parallelization in feed sliver. The air-jet yarn properties are dependent on the amount of core and wrapper fibres. The increase in draft at the air-jet spinner tends improves the properties of air-jet yarns.

Several researchers have reported the effect of change in process parameters at individual stage in spinning process on fibre orientation parameters and yarn properties. But, only few of them have attempted to study the effect of simultaneous change in process variables at every stage of spinning process on fibre orientation and yarn properties. A number of researchers have tried to establish the interrelationship between fibre orientation parameters at different stages on sliver, roving and yarns properties. But, hardly few researchers tried to interrelate between fibre orientation parameters in sliver and roving with corresponding fibre orientation parameters in ring, rotor and air-jet yarns and their properties. Further, a comparative study involving fibre orientation parameters and properties of ring, rotor and air-jet yarns has hardly been reported due to the limitation of spinnable count ranges of these technologies.

REFERENCES

[1] Morton, W. E., and Summers, R. J., Fibre Arrangement in card sliver, *J. Text. Inst.*, 40, 106 (1949).

[2] Lindsley, C. H., Measurement of Fibre Orientation, *Text. Res. J.,* 21, 39 – 46 (1951).

[3] Leont'eva, I. S., Problem of Fibre Straightening during Sliver Preparation, *Tech. Text. Industr. U.S.S.R.,* No. 2*,* 57-63, (1964).

[4] Iyer, I. K. P., Parathasarthy, M. S., and Sundram, V., Study on Different Methods of Measuring Fibre Configuration*, Resume of Papers Twenty First Technological Conference (ATIRA/BTRA/SITRA) Bombay Textile Research Association, Bombay, India*, 12-15 (1980).

[5] Morton, W. E., and Yen, K. C., The Arrangement of Fibres in Fibro Yarns, *J. Text. Inst.,* 43, T463-T472 (1952).

[6] Kumar, A., Effect of Drafts at Different stages of Spinning Process on Fibre Orientation and Yarn Properties, Ph. D. thesis, Indian Institute of Technology, New Delhi, (2004).

[7] Hearle, J. W. S., and Gupta, B. S., Migration of Fibres in Yarns. Part III-A Study of Migration in Staple Fiber Rayon Yarn, *Text. Res. J.*, 35, 788 (1965).

[8] Hearle, J. W. S., Grosberg, P., and Backer, S., Structural Mechanics of Fibres, Yarns, and Fabrics, Wiley-Interscience of John Wiley & Sons, New York, 88 (1969).

[9] Simpson, J., and Patureau, M. A., A Method and Instrument for Measuring Fiber Hooks and Parallelization, *Text. Res. J.*, 40, 956-957 (1970).

[10] Audivert, R., The Effect of Fiber Hooks on the Digital Fibrograph Readings from Clamped Beards, *Text. Res. J.*, 41, 365-366 (1971).

[11] Balasubramanian, N., Supanekar, S. D., and Nerurkar, S. K., Estimation of Differential Fiber Hooking by Fibrograph, *Text. Res. J.*, 45, 296-302 (1975).

[12] Deluca, L. B., An Evaluation of Hooked Fibres in Cotton Sliver on a Relative Basis, *Text. Res. J.,* 35, 858 – 861 (1965).
[13] Garde, A. R., Wakankar, V. A., and Bhaduri, S. N., Fibre Configuration in Sliver and Rovings and its Effect on Yarn Quality, *Text. Res. J., 31,* 1026-1036 (1961).
[14] Ishtiaque, S. M., Distribution of Fibres in Cross-Section of Rotor- and Ring- Spun Yarns and Their Strength, *Indian J. Text. Res.*, 11, 215 (1986)
[15] Punj, S. K., Debnath, S., and Chowdhury, A., Fibre Distribution in Air-jet and Ring Yarns, *Indian J. Fibre Text. Res.*, 26, 251-254 (2001).
[16] Punj, S. K., Debnath, S., and Chowdhury, A., Radial Packing Density of MJS Yarns, *Indian J. Fibre Text. Res.*, 23, 229-232 (1998).
[17] Ishtiaque, S. M., *Selected Problems of Internal Structure of Rotor-Spun Yarn*, Ph.D. thesis, University of Mechanical and Textile Engineering, Liberec, Czechoslovakia, 1983.
[18] Ishtiaque, S. M., Chaudhuri, S., and Das A., Influence of Fibre Openness on Processibility of Cotton and Yarn Quality. Part I – Effect of Blow Room Parameters, *Indian J. Text. Res.*, 28, 399-404 (2003).
[19] Ishtiaque, S. M., Influence of Man-Made Fibres on Configuration of Neps, *Asian Text. J.*, November, 13-15 (1993).
[20] Chattopadhyay, R., Quality Considerations in Blowroom, *Advances in Technology of Yarn Production*. Edited by Chattopadhyay, R., 9-16 (2002).
[21] Bhaduri, S. N., Effect of Openness of Cotton on Subsequent Processing, *Resume of Papers First Technological Conference (ATIRA/BTRA/SITRA) Bombay Textile Research Association, Bombay, India*, (1959).
[22] Klein, W., A Short Staple Spinning Series. *A Practical Guide to Opening and Carding*, The Textile Institute, Volume 2, (1987).
[23] Salhotra, K.R., *Spinning of Manmades and Blends on Cotton Systems*, A Textile Association Publication, (1989).
[24] Ishtiaque, S. M., and Vijay, A., Optimization of Ring Frame Parameters for Coarser Preparatory, *Indian J. Fibre Text. Res.,* 19, 239-246 (1994).
[25] Ishtiaque, S. M., Present Blowroom Practices: Scope of Improvement, *Advances in Technology of Yarn Production*. Edited by Chattopadhyay, R., 23-41 (2002).
[26] Salhotra, K. R., Significance of Modern Developments in Blowroom, *Advances in Technology of Yarn Production*. Edited by Chattopadhyay, R., 50-57 (2002).
[27] Sengupta, A. K., and Chatopadhyay, R., Change in Configuration of Fibres during Transfer from Cylinder to Doffer in a Card, *Text. Res. J.,* 52, 178-181 (1982).
[28] Simpson, J., and Fiori, L. A., Effect of Mixing Cottons Differing in Micronaire Reading and Carding Variables on Cotton Sliver Quality, Yarn Properties, and End Breakage, *Text. Res. J.,* 44, 327-331 (1974).
[29] Basu, A., Effect of Carding on the Imperfections of Cotton Yarns, *Asian Text. J.*, April, 74-78 (2002).
[30] Simpson, J., Relation between Minority Hooks and Neps in the Card Web, *Text. Res. J.,* 42, 590-591 (1972).
[31] Sands, J.E., Little, H.W., and Fiori L.A., Yarn Production and Properties. *Published by Nutter, W*., *Text. Prog.*, 3, 34 (1971).

[32] Simpson, J., Sands, J. E., and Fiori, L. A., The Effect of Drawing Frame Variables on Fibre Hooks and Parallelization and Processing Performance, *Text. Res. J.,* 40, 42-47 (1970).
[33] Wolfgang, T., High Production Carding and the Quality of Combed Cotton Yarns, *Melliand Textilber.,* 65, E211-E215 (1984).
[34] Nerurkar, S. K., Detailed Analysis of Carding Quality and its Influence on Processing and Yarn Properties, *Indian J. Text. Res.,* 4, 63-70 (1979).
[35] Rakshit, A.K., and Balasubramanian, N., Influence of Carding Conditions on Rotor Spinning Performance and Yarn Quality, *Indian J. Text. Res.*, 10, 158-162 (1985).
[36] Rakshit, A.K., and Balasubramanian, N., Nep Generation with Polynosic Fibres in Relation to Surface Characteristics of Fibre, *Indian J. Text. Res.*, 8, 95-100 (1983).
[37] Sengupta, A. K., Vijayaraghavan, N., and Singh, A., Studies on Carding Force between Cylinder and Flats in a Card. Part I – Effect of Machine Variables on Carding Force, *Indian J. Text. Res.*, 8, 59 (1983).
[38] Sengupta, A. K., Vijayaraghavan, N., and Singh, A., Studies on Carding Force between Cylinder and Flats in a Card. Part II – Effect of Fibre and Process Factors, *Indian J. Text. Res.*, 8, 64 (1983).
[39] Sengupta, A. K., Vijayaraghavan, N., and Singh, A., Studies on Carding Force between Cylinder and Flats in a Card. Part III – Carding Parameters, Sliver Quality and Carding Force, *Indian J. Text. Res.*, 8, 68 (1983).
[40] Ishtiaque, S. M., Chaudhuri, S., and Das, A., Influence of Fibre Openness on Processibility of Cotton and Yarn Quality: Part II – effect of carding parameters, *Indian J. Text. Res.*, 28, 405-410 (2003).
[41] Klein, W., A Short Staple Spinning Series. *The Technology of Short- Staple Spinning*, The Textile Institute, Vol. 1, (1987).
[42] Dzhokharidze, G. V., The Straightening of Fibre Hooks on the Card, *Tech. Text. Industr. U.S.S.R.,* No. 4*,* 43-48 (1966).
[43] Balasubramanian, N., and Bhatnagar, V. K., The Effect of Disorientation of Hooks in the Input Sliver on Drafting Irregularities and Yarn Quality*, Text. Res. J.,* 41, 750-759 (1971).
[44] Deluca, L. B., Simpson, J., and Fiori, L. A., An Evaluation of Fibre Parallelization and Drafting Tenacity of Cotton Silver*, Text. Res. J.,* 38, 817- 823 (1968).
[45] Grover, G., and Lord, P.R., The Measurement of Sliver Properties on the Draw frame, *J. Text. Inst.,* 83, 560-572 (1992).
[46] Ishtiaque, S. M., and Saxena, A., Effect of Sliver Preparation on Fibre Disorder at Rotor Groove, *Indian J. Text. Res.,* 16, 233-235 (1991).
[47] Bowles, A. H., and Davies, I., The Influence of Drawing and Doubling Processes on the Evenness of Spun Yarns. Part IV: Extremely Long-Term Variations, *Text. Inst. and Industr.*, January, 38-40 (1979).
[48] Iyer, C., and Mavely, J., Influence of Doubling Number on Longitudinal and Transverse Scattering of the Yarn, Optimum Doubling Number in Modern 3-Cylinder Spinning Processes, *Melliand Textilber.* (Eng. Edition), 57, 279-287, (1976).
[49] Sands, J.E., and Fiori, L.A., Yarn Production and Properties. Published by Nutter, W., *Text. Prog.*, 3, 35 (1971).
[50] Anbinder, S. U., Fibre Straightening in the Drafting Field, *Tech. Text. Industr. U.S.S.R.,* No. 4*,* 43-47 (1969).

[51] Foster, G. A. R., Roller Slip and the Irregularity of Cotton and Rayon-Staple Drawframe Slivers. Part 2: The Nature of Roller Slip and the Theory of Draft Distribution, 44, T570-T572 (1953).
[52] El-Sharkawy, A. F., Audivert, R., Castellar, D. D., The Relation between the Drafting Force, Draft, and Setting in the Roller-Drafting of Staple-Fibre Slivers, *J. Text. Inst.*, 64, 325-327 (1973).
[53] Sengupta, A. K., and Kapoor, I. M., Yarn Evenness. Published by Slater, K., *Text. Prog.*, 14, 19 (1985).
[54] Cavaney, B., and Foster, G.A.R., Some Observations on the Drafting Forces of Cotton and Rayon-Staple Slivers, *J. Text. Inst.*, 45, T390-T404 (1954).
[55] Foster, G. A. R., Fibre Motion in Roller Drafting, *J. Text. Inst.*, 42, T335-T374 (1951).
[56] Cavaney, B., and Foster, G.A.R., The Irregularity of Materials Drafted on Cotton Spinning Machinery and its Dependence on Draft, Doubling and Roller Setting. Part I: The Speed frames, *J. Text. Inst.*, 45, T529-T549 (1954).
[57] Fujino, K., Shimotsuma, Y., and Fuji, T., A Study on Apron-Drafting. Part I: Experimental Studies, *J. Text. Inst.*, 68, 131-140 (1977).
[58] Slater, K., Yarn Evenness. Published by Slater, K., *Text. Prog.,* 14, 17 (1985).
[59] Bakhar, M. I., Yarn Evenness. Published by Slater, K., *Text. Prog.*, 14, 17 (1985).
[60] Ross, D. A., Bratt, R. L., and Story, L. F., Sliver Strength as a Measure of Fibre-Alignment in Topmaking, *J. Text. Inst*., 53, P185 (1962).
[61] Mehta, I. H., and Nanal, S. Y., The Effect of Varying Interfibre Friction on Hook Removal during Drawing, *Text. Res. J.,* 40, 1131-1132 (1970).
[62] Miao, M., Ning, F., and How, Y., Cotton Sliver Strength and Withdrawal Speed Limit, *J. Text. Inst.*, 89, 468-479 (1998).
[63] Balasubramanian, N., A Study of the Irregularities Added in Apron Drafting, *Text. Res. J.*, 39, 155-165 (1969).
[64] Nemzer, G. M., Reducing Irregularity in Sliver, Roving and Yarn, *Tech. Text. Industr. U.S.S.R.,* No. 2*,* 66-73 (1961).
[65] Sippel, A., The Relationship between Minimum Twist of Cohesion and Cutting Ratio in Cotton Rovings, *Text. Res. J.,* 35, 283-288 (1965).
[66] Audivert, R., Villaronga, M., and Coscolla, R., Drafting Force in the Front Zone of a Double Apron Drafting System, *Text. Res. J.*, 37, 1-10 (1967).
[67] Hannah, M., The Theory of High Drafting, *J. Text. Inst.*, 41, T57-T89 (1950).
[68] Anderson, S. L., and Foster, G. A. R., The Irregularity of Materials Drafted on Cotton Spinning Machinery and its Dependence on Draft, Doubling and Roller Setting. Part II: The Spinning frame, *J. Text. Inst.*, 46, T551-T564 (1955).
[69] Su, C. I., Evaluating Uniformity of Drafted Roving, *Text. Res. J.,* 69, 630-634 (1999).
[70] Tikhomirova, A. I., Investigation of Transverse Sections of Roving and Yarn, *Tech. Text. Industr. U.S.S.R.,* No. 3*,* 43-46 (1970).
[71] Audivert, R., ABC's of Drafting Tenacity, *Text. Industr.*, 133, 125-131,187-189 (1969).
[72] Barella, A., and Sust, A., Cohesion Phenomena in Rovings and Yarns. Part IV: Cohesion of Twisted Rovings, Its Effect on Yarn Properties, *Text. Res. J.*, 35, 491-496 (1965).
[73] Louis, G. L., and Firoi, L.A., Draft Zone Variables: Effect on Yarn Properties and End Breakage, *Text. Bull.,* 91, No. 8, 25-30 (1965).

[74] Bay, E., and Baier, F., Modern Drafting Systems for Improving Flexibility in Ring Spinning, *Int. Text. Bull.,* Yarn and Fabric Forming, 3, 64-70 (1996).
[75] Klein, W., A Short Staple Spinning Series. *A Practical Guide to Ring Spinning*, The Textile Institute, Volume 4, (1987).
[76] Artzt, P., and Bolze, J., Increasing the Draft on Ring Spinning Frames Improves Flexibility and Productivity in the Process Generally, *Int. Text. Bull.,* Yarn and Fabric Forming, 1, 39-42 (1998).
[77] Barella, A., and Manich, A.M., The Influence of the Spinning Process, Yarn Linear Density, and Fibre Properties on the Hairiness of Ring-Spun and Rotor- Spun Cotton Yarns, *J. Text. Inst.*, 79, 189-197 (1988).
[78] Viswanathan, G., Munshi, V. G., and Ukidye, A.V., Effects of Yarn Parameters on Hairiness, *Indian Text. J.*, March, 118-121 (1988).
[79] Morton, W. E., The Arrangement of Fibres in Single Yarns, *Text. Res. J.*, 26, 325-329 (1956).
[80] Hearle, J. W. S., and Bose, O. N., Migration of Fibres in Yarns. Part II: A Geometrical Explanation of Migration, *Text. Res. J.*, 35, 693-699 (1965).
[81] Hearle, J. W. S., and Gupta, B.S., Migration of Fibres in Yarns. Part III: A Study of Migration in Staple Fibre Rayon Yarn, *Text. Res. J.*, 35, 788-795 (1965).
[82] Hearle, J. W. S., Gupta, B.S., and Goswami, B. C., Migration of Fibres in Yarns. Part V: The Combination of Mechanisms of Migration, *Text. Res. J.*, 35, 972-978 (1965).
[83] Pillay, K. P. R., A Study of the Hairiness of Cotton Yarns. Part II: Effect of Processing Factors, *Text. Res. J.,* 34, 783-791 (1964).
[84] Gupta, B.S., Fibre Migration in Staple Yarns. Part II: The Geometric Mechanism of Fiber Migration and the Influence of the Roving and Drafting Varaibles, *Text. Res. J.*, 40, 15-24 (1970).
[85] Ishtiaque, S. M., Sharma, I. C., and Sharma, S., Structural Mechanics of Siro Yarn by Microtomy, *Indian J. Fibre Text. Res.*, 18, 116-119 (1993).
[86] Lunenschloss, J., Hoth, G., and Schusser, H., The Influence Exerted by the Number of Passages and the Direction of the Running Sliver on the Number of Hooks in the Fiber Ring of the OE Rotary Spinning Machine, *Melliand Textilber*. (Eng. Edition), 55, May, E289-E292 (1974).
[87] Ishtiaque, S. M., Longitudinal Fibre Distribution in Relation to Rotor Spun Yarn Properties, *Text. Res. J.,* 59, 696-699 (1989).
[88] Ishtiaque, S. M., and Sharma, N., Fibre Disorder in Rotor Spinning, *Text. Asia,* November, 45-47, (1986).
[89] Ishtiaque, S. M., and Sharma, N., Spinning of Synthetic Fibres and Blends on Rotor-Spinning Machine, *Indian J. Text. Res.*, 20, 6-10 (1995).
[90] Valdimirov, B. M., The Sci. Res. Inst. of the Cotton Indian of the Central Board of the Cotton Indian of the Ivanovo Industrial Region, Bull. No. 5, (1935).
[91] Nield, R., *Monograph on Open-End Spinning*, The Textile Institute, Manchester, 1976.
[92] Chattopadhyay, R., Influence of Yarn Formation Process on Fiber Configuration in Rotor Spun Yarn, *Text. Res. J.,* 58, 674-676 (1988).
[93] Saxena, A. K., *Internal and Surface Structure of Rotor-Spun Yarn,* Ph. D. thesis, Indian Institute of Technology, New Delhi, (1991).
[94] Chattopadhyay, R., *Fibre Breakage in Rotor Spinning during Opening by the Combing Roller*, Ph. D. thesis, Indian Institute of Technology, New Delhi, (1983).

[95] Salhotra, K.R., and Chattopadhyay, R., Loss in Fiber Tenacity during Separation in Rotor Spinning, *Text. Res. J.*, 54, 194-197 (1984).
[96] Ishtiaque, S. M., and Bhortakke, M. K., Study of Fibre Damage in Different Layers of Feed Sliver in Rotor Spinning, *Asian Text. J.*, March, 38-40 (1995).
[97] Ishtiaque, S. M., and Bhortakke, M. K., Study of Fibre and Machine Parameters on Fibre Damage and Reversal in Rotor Spinning, *Asian Text. J.*, July, 52-56 (1995).
[98] Krause, H. W., and Soliman, H. A., Yarn Evenness. Published by Slater, K., *Text. Prog.,* 14, 20 (1985).
[99] Krause, H. W., and Soliman, H. A., Yarn Evenness. Published by Slater, K., *Text. Prog.*, 14, 20 (1985).
[100] Siegl, R., The Production and Properties of Staple-Fibre Yarns made by Recently Developed Techniques. Published by Hunter, L., *Text. Prog.,* 10, 58 (1978).
[101] Simpson, J, The Production and Properties of Staple-Fibre Yarns made by Recently Developed Techniques. Published by Hunter, L., *Text. Prog.,* 10, 58 (1978).
[102] Cripps, H., The Production and Properties of Staple-Fibre Yarns made by Recently Developed Techniques. Published by Hunter, L., *Text. Prog.,* 10, 59 (1978).
[103] Simpson, J., and Louis, G. L., The Production and Properties of Staple-Fibre Yarns made by Recently Developed Techniques. Published by Hunter, L., *Text. Prog.,* 10, 61 (1978).
[104] Iyer, C., and Mavely, J., The Production and Properties of Staple-Fibre Yarns made by Recently Developed Techniques. Published by Hunter, L., *Text. Prog.,*10, 62 (1978).
[105] Ishtiaque, S. M., and Kumar, P., Impact of Rotor and Opening Roller Speeds on Configuration of Fibres in Yarn, *Indian J. Fibre Text. Res.*, 19, 71-75 (1994).
[106] Salhotra, K. R., and Balasubramanian, P., An Approach to the Optimization of Rotor-Spinning-Machine Parameters, *J. Text. Inst.*, 77, 128-137 (1986).
[107] Salhotra, K. R., and Alaiban, T. S., Optimization of Fibre Length in Relation to Rotor Diameter, *Indian J. Text. Res.*, 10, 7-9 (1985).
[108] Ishtiaque, S. M., Spinning of Synthetic Fibres and Blends on Rotor-spinning Machine, *Indian J. Text. Res.*, 17, 224-230 (1992).
[109] Lunenschloss, J., Siersch, E., and Phoa, T. T., Influence of Fiber Length and Fiber Length Distribution on the Properties of OE Rotor Spun Synthetic Fibres, *Melliand Textilber.* (Eng. Edition), 57, 387-395 (1976).
[110] Ishtiaque, S. M., and Chattopadhyay, S., Fibre Length Factors, *Text. Asia.*, 21, 64-68 (1990).
[111] Bowen, D. A., The Production and Properties of Staple-Fibre Yarns made by Recently Developed Techniques. Published by Hunter, L., *Text. Prog.,*10, 65 (1978).
[112] Warlick, S. J., The Production and Properties of Staple-Fibre Yarns made by Recently Developed Techniques. Published by Hunter, L., *Text. Prog.,* 10, 65 (1978).
[113] Landwehrkamp, H., and Pridohi, H. P., Fine Rotor Yarns from Manmades Fibres-Quality and Economics, *Text. Praxis Int.,* 49, May, 303-307, EII- EIV (1994).
[114] Landwehrkamp, H., Influence Exerted by the Preparatory Operations and the Sliver Weight on the Production of Fine Rotor-Spun Yarns , *Melliand Textilber*. (Eng. Edition), 59, November, E919-E924 (1974).
[115] Ishtiaque, S. M. and Singh, C. P., Spinning of Synthetic Fibres and Blends on Rotor-Spinning Machine, *Indian J. Fibre Text. Res.*, 20, 73-78 (1995).

[116] Manich, A. M., Barella, A., and Vigo, J. P., A Contribution to the Study of the Hairiness of Rotor-Spun Yarns by Means of the Digital Hairiness Meter. Part II: The Influence of Process Parameters on the Hairiness of Open-End-Spun Polyester-Fibre, Cotton, and Blended-Fibre Yarns, *J. Text. Inst.*, 72, 131-140 (1981).
[117] Lord, P. R., The Structure of Open-End Spun Yarn, *Text. Res. J.,* 41, 778-784 (1971).
[118] Hearle, J. W. S., Lord, P. R., and Senturk, N., Fiber Migration in Open-End Spun Yarns, *J. Text. Inst.*, 63, 605-617 (1972).
[119] Salhotra, K.R., Dutta, B., and Sett, S. K., Influence of Twist on Fiber Migration in Rotor-Spun Yarns, *Text. Res. J.*, 51, 360-363 (1981).
[120] Neelaketan, P., and Subramanian, T. A., An Attempt to Quantify the Translation of Fiber Bundle Tenacity into Yarn Tenacity, *Text. Res. J.*, 46, 822-827 (1976).
[121] Basu, A., Objective Measurement of Structural Parameters of Rotor-Spun Yarns, *Indian J. Fibre Text. Res.*, 26, 358-365 (2001).
[122] Minh, H. V., The Hairiness of Yarns. Published by Barella, A., *Text. Prog.*, 24, 20 (1993).
[123] Lawerence, C. A., and Baqui M. A., Effects of Machine Variables on the Structure and Properties of Air-jet Fasciated Yarns, *Text. Res. J.,* 61, 123-130 (1991).
[124] Chasmawala, R. J., Hansen, S. M., and Jayaraman, S., Structure and Properties of Air-jet Spun Yarn, *Text. Res. J.,* 60, 61-68 (1990).
[125] Oxenham, W., Influence of Fibre Properties in Air-jet Spinning, *Indian J. Text. Res.*, 17, 194-200 (1992).
[126] Basu, A., *Influence of Fibre Type on Properties of Jet-spun Yarns*, Doctoral Thesis, Department of Textile Industries, University of Leeds, UK, 1991.
[127] Miao, M., *The Insertion of Twists into Yarns by Means of Jets*, Doctoral Thesis, Department of Textile Industries, University of Leeds, UK, 1986.
[128] Tyagi, G. K., and Dhamija, S., Bulk and Related Properties of Acrylic-Cotton Jet Spun Yarns, *Indian J. Fibre Text. Res.*, 23, 13-18 (1998).
[129] Shah, R. N., *Effect of Some Variables on Structure and Properties of 100% Acrylic MJS Spun Yarn and Comparison with Ring Spun Yarn*, M. Tech. Thesis, The Technological Inst. of Textiles and Sciences, Bhiwani, India, (1995).
[130] Tyagi, G. K., Kaushik, R. C. D., and Salhotra, K. R., Properties of OE Rotor and MJS Yarns Spun at High Spinning Speeds, *Indian J. Fibre Text. Res.*, 22, 8-12 (1997).
[131] Kampl, R., and Leitner, J., Use of Viscose and Modal Fibres in Unconventional Spinning Process, *Melliand Textilber*. (Eng. Edition), 70, E134-E135 (1989).
[132] Tyagi, G. K., and Salhotra, K. R., Bulk and Related Properties of Acrylic-Cotton Jet Spun Yarns, *Indian J. Fibre Text. Res.*, 21, 184-188 (1996).
[133] Punj, S. K., Ishtiaque, S. M., and Dhingra, L. K., Influence of Spinning Conditions on Structure and Properties of Polyester-Viscose Blended MJS Yarns, *Indian J. Fibre Text. Res.*, 22, 73-83 (1997).
[134] Artzt, P., Dallman, H., and Zeigler, K., Effect of Draft and Blend Ratio on the Properties of Air-jet Spun Yarns, *Chemifasern/Textilindustr.*,December, E104 (1985).
[135] Venktapathi, T. M., and Nishimura, T., Resume of Papers, 33rd Joint Technological Conference of BTRA, SITRA, NITRA and AITRA, 203 (1992).
[136] Huh, Y. R., Kim, Y. R., and Oxenham, W., Analyzing Structural and Physical Properties of Ring, Rotor, and Friction Spun Yarns, *Text. Res. J.,* 72, 156-163 (2002).

[137] Louis, G. L., Salaun, H. L., and Kimmel, L. B., Comparison of Properties of Cotton Yarns Produced by the DREF-3, Ring and Open-End Spinning Methods, *Text. Res. J.*, 55, 344-351 (1985).
[138] Godek, J. W., The Production and Properties of Staple-Fibre Yarns made by Recently Developed Techniques. Published by Hunter, L., *Text. Prog.,* 10, 115 (1978).
[139] Shaw, H. V., The Production and Properties of Staple-Fibre Yarns made by Recently Developed Techniques. Published by Hunter, L., *Text. Prog.,* 10, 116 (1978).
[140] Lunenschloss, J., Siersch, E., and Phoa, T. T., Influence Exerted by Fiber Length and the Distribution of Fiber Lengths on the Properties of Open-End Synthetic Fiber Yarns, *Melliand Textilber*. (Eng. Edition), 57, April, E267-E269 (1974).
[141] Barella, A., Manich, A.M., Castro, L., and Hunter, L., Diameter and Hairiness of Ring and Rotor Polyester-Cotton Blended Spun Yarns, *Text. Res. J.,* 54, 840-843 (1984).
[142] Manohar, J.S., Rakshit, A.K., and Balasubramanian, N., Influence of Rotor Speed, Rotor Diameter, and Carding Conditions on Yarn Quality in Open-End Spinning, *Text. Res. J.*, 53, 497-503 (1983).
[143] Kaushik, R. C. D., Salhotra, K. R., and Tyagi, G. K., Response of Polyester-Viscose Blends to Air-jet Spinning, *Indian J. Fibre Text. Res.*, 17, 219-223 (1992).
[144] Mohamed, M. H., Faria, C. A., and Barker, R. L., Proceedings of 7th SIET, Mulhosue, France, 1986.
[145] Artzt, P., and Conzelmann, M., Processing of Viscose and Modal Blended with Cotton on Air-jet Spinning Systems, *Melliand Textilber*., 70, E354 (1989).
[146] Stalder, H., New Spinning Methods, their Applications and Possibilities for Developments, *Int. Text. Bull.,* Yarn and Fabric Forming, 1, 27-39 (1988).
[147] Wang, K. Y., and Jordan, G., Air-jet Spun Yarn-Its Properties and Effects on the End Product, *Melliand Textilber.*, (Eng. Edition), 64, 344 (1984).
[148] Lord, P.R., Air-jet and Friction Spinning, *Text. Horizons*, 7, 10 (1987).
[149] Ishtiaque, S. M., and Khare, S. K., Study of Internal Structure of Ring, Rotor and Air-jet Spun Blended Yarn by Cross-Sectional View, *Text. Asia*, 24, 36-38 (1993).
[150] Barella, A., Bardi, X., Coll-Tortosa, and Segura, G., Proceedings of 34th Hungarian Textile Conference, Budapest, Hungary 1991; *Text. Praxis*, 47, 1116 (1992).
[151] Zachert, J., Private Communication, R.W.T.H., Aachen, Germany (1990).
[152] Pillay, K. P. R., Viswanathan, N., and Parathasarathy, M. S., Open-End Yarns. Part I: A Study of Fibre Configurations and Migration , *Text. Res. J.,* 45, 366-372 (1975).
[153] Barella, A., Alvarez Vega, P. A., and Castro, L., The Hairiness of Yarns. Published by Barella, A., *Text. Prog.*, 24, 23 (1993).
[154] Sirang, Y., Dinfon, G., and Behery, H. M., A Study of Hairiness and Diameter of Open-End Yarn Processed Through Single- and Double-Cylinder Carding Machines and Its Comparisons with Ring Yarn, *Text. Res. J.,* 51, 274-279 (1982).
[155] Stalder, H., The Hairiness of Yarns. Published by Barella, A., *Text. Prog.*, 24, 25 (1993).
[156] Nishimura, T., Shigeyma, M., and Venktapathi, T. M., Yarn Hairiness Update. Published by Barella, A., and Manich, A. M., *Text. Prog.*, 26, 10 (1997).
[157] Barella, A., Bardi, X., Castro, L., Manich, A. M., and Castellar, M.D., Approach to the Study of Yarn Hairiness Variability, *Melliand Textilber*., (Eng. Edition), 74, E85-E86 (1993).

[158] Hearle, J. W. S., Lord, P. R., and Senturk, N., Fiber Migration in Open-End Spun Yarns, *J. Text. Inst.*, 63, 605-617 (1972).

In: Chemistry and Chemical Engineering Reserch Progress ISBN: 978-1-61668-502-7
Editor: A.K. Haghi

Chapter 9

Y_2O_3-ND_2O_3 DOUBLE STABILIZED ZRO_2-TICN (60/40) NANO-COMPOSITES

S. Salehi, K. Vanmeensel, B.Yüksel, O. Van der Biest, and J. Vleugels
Department of Metallurgy and Materials Engineering, Katholieke Universiteit Leuven, Kasteelpark Arenberg 44, B-3001 Heverlee, Belgium

ABSTRACT

Yttria-neodymia double-stabilized electro-conductive ZrO_2-TiCN ceramic nano-composites were shown higher hydrothermal stability and fracture toughness than yttria stabilized composites with the same total amount of stabilizer. Therefore a set of double-stabilized electro-conductive ZrO_2-TiCN ceramic composites were processed using Pulsed Electric Current Sintering (PECS) to optimize the composition and sintering process. All the composites contained 40 vol% of electrically conductive, nano-sized TiCN phase. The Y_2O_3 stabilizer content was fixed at 1 mol % while the Nd_2O_3 stabilizer content was varied between 0.75-2 mol% with step size of 0.25 mol%. The sintering temperature was varied between 1400°C and 1500 °C, applying a heating rate of 400°C/min below 1050°C and 200°C/min up to the sintering temperature. The pressure was gradually increased towards 62 MPa.

The mechanical (Vickers hardness, fracture toughness and bending strength), electrical (electrical resistivity) as well as the microstructural properties were investigated. The neodymia stabilizer content and sintering temperature were optimized to get the best mechanical properties and EDM performance.

Composites, containing a content of 1 to 1.75 mol% Nd_2O_3, sintered at a temperature of 1400°C and 1450°C, combined excellent mechanical properties (a toughness of about 8 $MPa.m^{0.5}$, a hardness of about 13 GPa and a bending strength of 1.1-1.3 GPa) with a low electrical resistivity ($1.6\text{-}2.2\times10^{-5}\Omega m$). To avoid problems with zirconia destabilization during electro discharge machining (EDM), the compositions with more than 1.5 mol% Nd_2O_3 stabilizer are preferred.

The grain size is in the range of 100 ± 30 nm. A combination of good mechanical properties, low electrical resistivity and high hydrothermal stability makes these materials a proper candidate for cutting tool applications and facilitates their machining by EDM, respectively.

I. INTRODUCTION

ZrO_2-TiCN (60/40) composites were investigated in the framework of the research at K.U. Leuven into EDM doable ceramics [1-5] with good mechanical properties. TiCN is an electro-conductive phase (ρ: 2.28×10^{-6} Ωm) [6], but the brittleness and high sintering temperature of the material as a pure phase are the two most important factors preventing its widespread use [7]. Non-conductive ZrO_2 (ρ:10^9 Ωm) [8] on the other hand is well-known for its high toughness, because of stress-induced transformation of tetragonal to monoclinic ZrO_2 phase in the stress field of propagating cracks, known as transformation toughening [9, 10]. In the present study, 40 vol% TiCN was added to zirconia matrix to make a composite with highest possible toughness combined with enough electro-conductivity to be EDM doable [11]. By using EDM machining, the aim is to avoid the expensive grinding operation for final shaping and surface finishing of components, therefore increasing the possibility of mass production and manufacturing cost reduction.

Destabilization in vicinity of humidity in low temperature (RT to 400°C) is one of the biggest draw backs of ZrO_2 ceramics [12, 13]. In the earlier works, it was shown that the hydrothermal stability and in the same time fracture toughness of 1mol% Y_2O_3 + 1 or 2 mol% Nd_2O_3 stabilized ZrO_2 are higher than 2 or 3 Y_2O_3 stabilized ZrO_2 [14] respectively.

The goal of the present work is therefore to investigate the privilege of yttria-neodymia double stabilized zirconia based composites compare to yttria stabilized one from hydrothermal stability point of view and optimizing stabilizer content and sintering temperature to have an optimum balance of properties (high toughness, high hardness and good electrical conductivity).

II. EXPERIMENTAL PROCEDURE

A) Sample Preparation

17 discs with composition of ZrO_2-TiCN (60/40), diameter of 30mm and a thickness of 5mm were fabricated by means of the PECS. The commercial powders used were yttria-free monoclinic ZrO_2 and nano size TiCN. Details on the commercial starting powders are given in Table 1. 0.8 wt % Al_2O_3 powder was added as a ZrO_2 grain growth inhibitor and sintering aid.

Zirconia powder was stabilized with neodymia and yttria, before mixing with titanium carbo-nitride and alumina by means of a coating method. For this purpose a proper amount of neodymia (Chempur, Germany) and yttria (ACROS, Belgium) was dissolved in nitric acid at about 100°C using magnetic stirring. The resulting nitrate solution was applied to the monoclinic zirconia powder (TZ-0) via a suspension drying process [15]. The nitride coating was exposed to oxidation at 800°C for 20 minutes. Yttria stabilizer content was kept fixed at 1 mol % while the neodymia stabilizer content was varied between 0.75-2 mol percent with a step size of 0.25 mol%.

Table 1. Starting powder composition (based on supplier information)

Powder	Grade	Supplier	Crystal size*
ZrO_2	TZ-0	Tosoh (Japan)	27 nm
TiCN	50/50	HTNMC*	<100 nm
Al_2O_3	SM8	Baikowski (France)	0.60 µm

*HTNMC: Hebei Sinochem, China Shijiazhuang High-tech Nanometer Ceramic Material Factory.

50 grams of fully formulated powder mixture was mixed on a multidirectional Turbula mixer (type T2A, Basel, Switzerland) in ethanol in a polyethylene container of 250 ml during 48 h at 60 rpm. 250 grams of hardmetal milling balls (Ø = 4-5 mm, CERATIZIT grade MG15) were added to the container to break the agglomerates in the starting powder and to enhance powder mixing. The ethanol was removed after mixing using a rotating evaporator.

Resulting powder after sieving (315 mesh), was sintered on a PECS device (Type HP D 25/1, FCT system, Rauenstein, Germany), equipped with a 250 kN uniaxial-press. Details about the apparatus are given somewhere else [16]. The sintering temperature was varied between 1400°C to 1500 °C, applying a heating rate of 400°C/min below 1050°C and 200°C/min up to the sintering temperature. The pressure was gradually increased towards 62 MPa. Dwell time at maximum temperature and pressure was set at 2 minutes.

The sintering cycle for the samples sintered at 1400°C is shown in Figure 1. Relative piston movement also is added to give an idea about shrinkage rate during sintering.

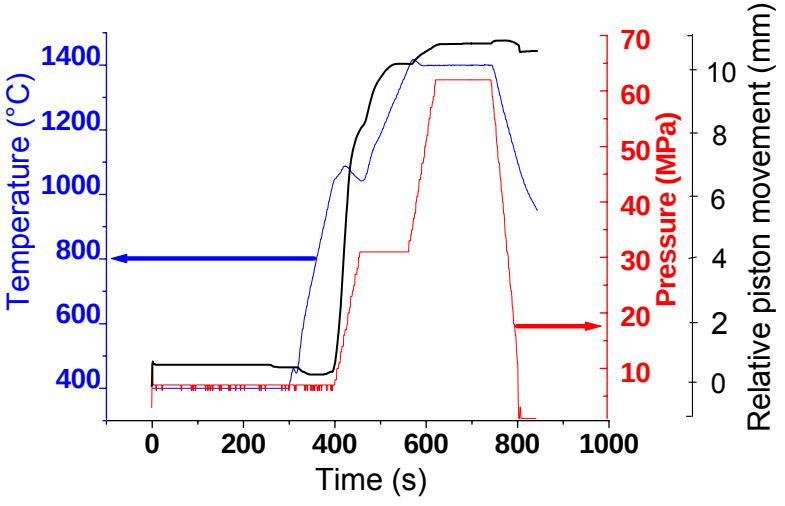

Figure 1. Sintering cycle and relative piston movement during sintering (for sintering cycle with maximum temperature of 1400°C).

B) Sample Characterization

The density of the samples was measured in ethanol, according to the Archimedes method (BP210S balance, Sartorius AG, Germany). The Vickers hardness ($HV_{0.3}$ and HV_{10}) was measured on a Zwick hardness tester (model 3202, Zwick, Ulm, Germany) with an indentation load of 0.3 kg, respectively 10 kg for a dwelling time of 10 s. The indentation toughness, K_{IC}, was calculated according to the formula of Anstis et al. [17] based on crack length measurements of the radial crack pattern produced by Vickers HV_{10} indentations. The flexural strength was measured for three samples with optimum toughness and hardness. Measurements were done by a 3-point bending test (Instron 4467, PA**,** USA) on rectangular samples (25.0 × 5.4 × 2.1 mm), with a span length of 20 mm and a cross-head displacement of 0.2 mm/min. The reported values are the mean with standard deviation of 4 measurements. Sample surfaces were ground with a diamond grinding wheel (type MD4075B55, Wendt Boart, Brussels, Belgium) on a Jung grinding machine (JF415DS, Göppingen, Germany). The elastic modulus (E) of the ceramic specimens was measured using the resonance frequency method [18]. The resonance frequency was measured by the impulse excitation technique (Model Grindo-Sonic, J. W. Lemmens N.V., Leuven, Belgium). The test was done on bar shape samples with dimensions of 25.0 × 5.4 × 2.1 mm^3 (prepared samples for bending strength test). The reported values are the mean and standard deviation of 10 measurements. Microstructural investigation was performed by scanning electron microscopy (SEM, XL-30FEG, FEI, Eindhoven, The Netherlands). X-ray diffraction (Seifert 3003 T/T, Ahrensburg, Germany) analysis was used for phase identification and calculation of the relative phase content of monoclinic and tetragonal ZrO_2. Grain size of samples was measured using Image pro plus software, based on measuring of about 50 grains in each SEM picture of fractured surface. The electrical resistance of the samples was measured according to the 4-point contact method using a Resistomat (TYP 2302 Burster**,** Gernsbach, Germany).

Low temperature degradation (LTD) tests were performed at 200°C under a saturated H_2O pressure of 1.55 MPa. For this purpose, rectangular bars (20 × 5 × 2 mm) were polished and inserted in a stainless steel autoclave. The autoclave was placed in a salt bath to establish an internal temperature of 200°C, as monitored by a thermocouple in the autoclave. Details of experiment is explained somewhere else [14]. The amount of m-ZrO2 on the exposed sample surface was measured by X-ray diffraction. The m-ZrO2 volume fraction is calculated according to the method of Toraya et al.[19].

III. RESULTS AND DISCUSSION

For simplicity, a sample code will be used in all the text from now on. The composition (ZrO_2-TiCN-Al_2O_3 (60/40) and amount of yttria stabilizer (1 mol% Y_2O_3) is the same for all the samples. The differences are the amount of neodymia stabilizer and the sintering temperature. The used code consists of two numbers, the first is the mol% of Nd_2O_3 which is variable between 0.75 to 2 mol% with a step size of 0.25 mol% and the second number is the sintering temperature.

A) Microstructural Investigation

A micro-structural image of polished cross-sectioned ZrO_2-TiCN (60/40) composite is shown in figure 2. Three phases can be observed: yttria-neodymia stabilized ZrO_2 (bright grey), TiCN (dark) and some WC impurity coming from the milling balls (white). Based on the micro-structural investigation, all the samples were fully densified, since no pores were found on the cross-sections (Figure 2a). Moreover, homogeneous ZrO_2-TiCN microstructures were obtained, indicating that the powder mixing procedure was appropriate.

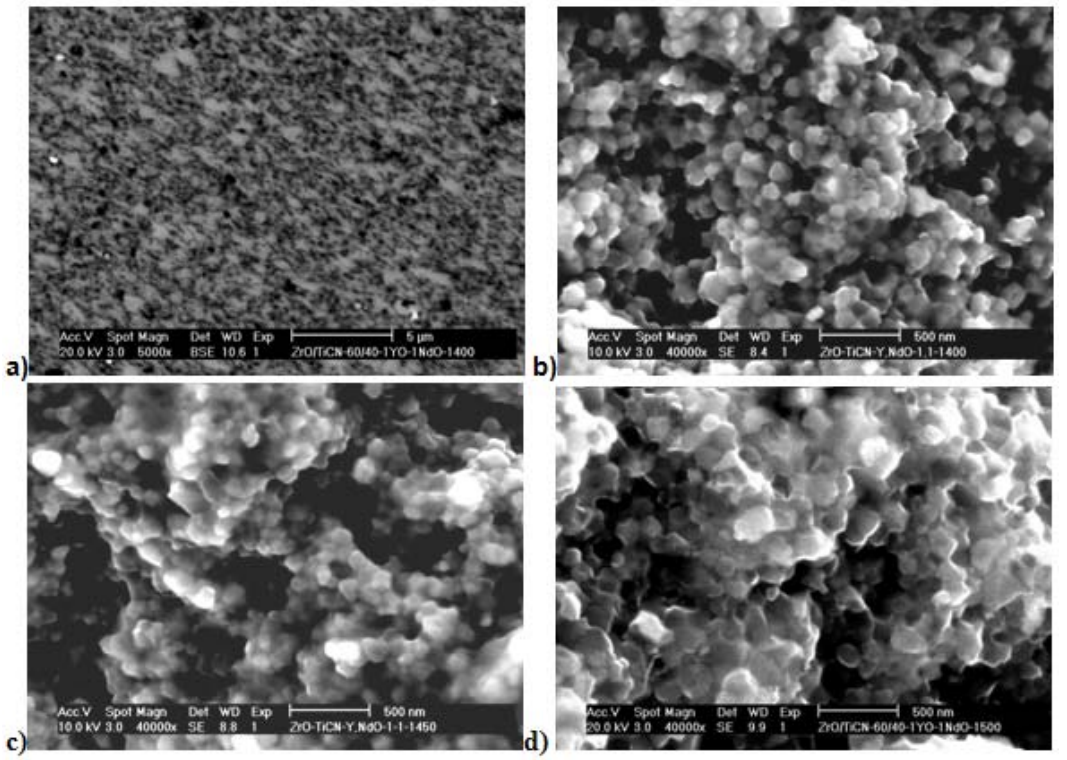

Figure 2. SEM picture of polished cross-section of sample 1-1400 (a) and fracture surfaces of sample 1-1400 (b), 1-1450 (c) and 1-1500 (d). In fig (a) the grey matrix is ZrO_2 and the dark phase is TiCN; the white particles are WC coming from the milling ball.

Due to the nano-size form of the structures, it is nearly impossible to measure the grain size on polished surfaces; therefore grain size measurement was done on fracture surfaces of samples. As is shown in figure 2 (b, c and d) and in figure 3, grain size increases as sintering temperature increases. On the other hand, it decreases when stabilizer amount increases (Figure 3).

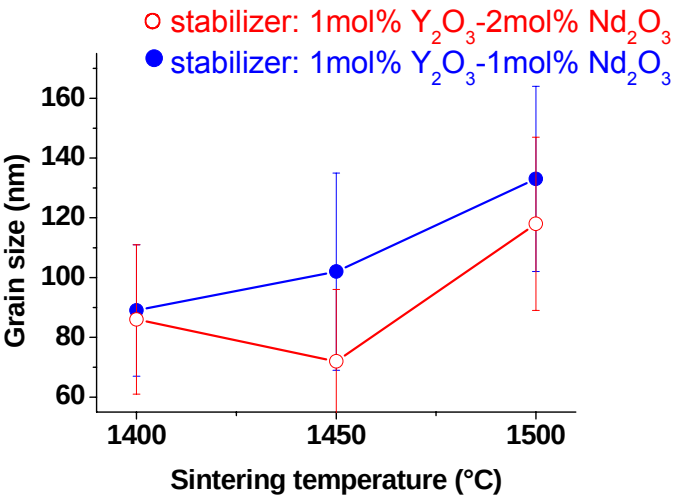

Figure 3. Measured grain size of ZrO_2-TiCN-Al_2O_3 (60/40/0.8) stabilized with 1 mol% yttria plus 1 mol% neodymia (blue line) or 2 mol% neodymia (red line); sintered at 1400°C, 1450°C and 1500°C.

Based on a literature review, the optimum grain size for yttria stabilized zirconia, to realise highest fracture toughness, is about 2 micron (for 2% yttria stabilized zirconia) [20]. When the grain size is big, a lower amount of yttria will segregate at grain boundaries and more yttria can distribute throughout the grain itself. Also, bigger tetragonal grains result in a thicker transformation zone and consequently in higher toughness [20]. Furthermore, cracks tend to deflect around larger particles, instead of cleaving through smaller ones; hence the crack deflection mechanism is more effective in samples with larger grain size. Notwithstanding the above facts, it is possible to achieve high toughness (17-18 MPa.$m^{0.5}$) in nano-crystalline ceramics (about 100nm grain size) by choosing a very precise dopant/grain size combination that places the ceramic very near the phase transformation boundary [21]. In the current study it is shown that a high toughness of about 8 MPa.$m^{0.5}$ is achievable for a ZrO_2-TiCN (60/40) composite with a zirconia grain size of about 90 nm (sample 1-1400) (Figure 3 and table 2).

The XRD patterns of polished cross sections of samples sintered at 1400°C (a), 1450°C (b) and 1500°C (b) are shown in figure 4. For all the discs, after sintering, no cracks were observed. Sample 1-1500 showed a significant monoclinic peak and low fracture toughness and hardness, indicating premature tetragonal to monoclinic transformation; hence composition 0.75-1500 was not made. Some small monoclinic peaks can be seen in the XRD patterns of the samples stabilized with 1.5 mol% Nd_2O_3 or less. This insignificant amount of premature transformation is not enough to cause micro-cracks, as can be concluded from acceptable hardness values found (table 2). Because of high transformability of the samples (table 3), the small monoclinic amount detected on the polished surface of sample also can be due to polishing.

Despite the above facts, samples with 1.5% Nd_2O_3 or less encounter crack formation during EDM machining when exposed to water and electrical discharge. So it seems that very high transformability or in other words small amount of monoclinic phase on polished surface

of sintered samples can be an indicator of ZrO_2 degradation during EDM. Therefore, compositions with more than 1.5 mol% Nd_2O_3 are preferable.

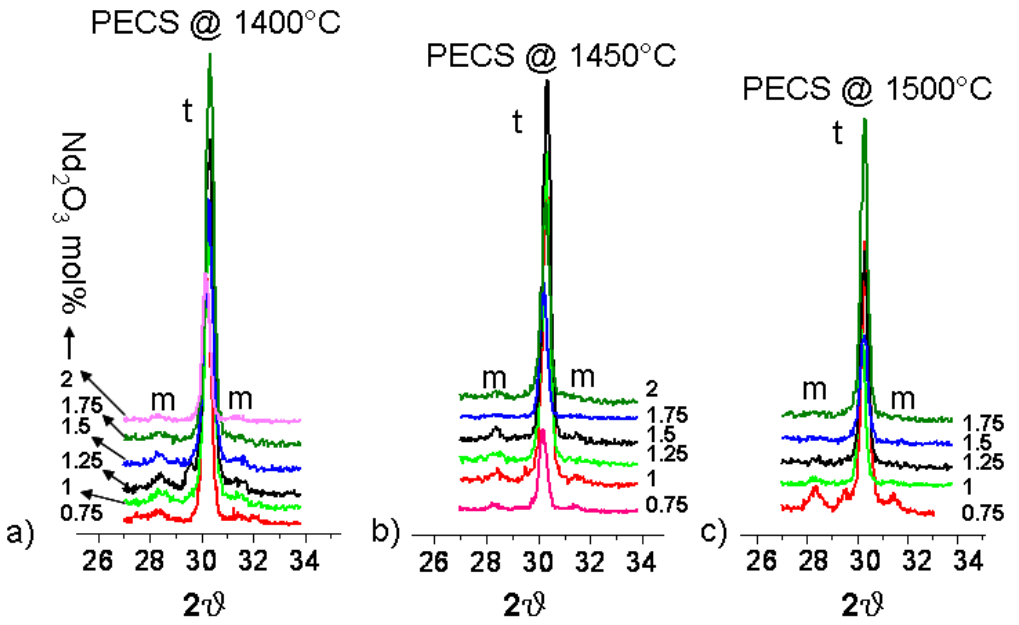

Figure 4. XRD patterns of ZrO_2-TiCN (60/40) nano-composites, stabilized with 1 mol% Y_2O_3 and 0.75 to 2 mol% Nd_2O_3, sintered at 1400°C (a) and 1500 (b)°C; m: monoclinic ZrO_2, t: tetragonal ZrO_2.

B) Mechanical Properties

For further extension of a plastic zone during a hardness test, multiplication of pre-existing elements of plasticity is easier than generation of new dislocations in the virgin material around the indentation site. With increasing testing load (size of the indent), there is a decrease in hardness due to a multiplication of dislocations created in the earlier stages of indentation (cracks at the corner of indentation) [22]. In the current research, indentation hardness was measured by applying 0.3 Kg as well as 10 Kg load. A 0.3 Kg load was chosen to avoid crack (elements of plasticity) appearing around the indentation site. A 10 kg load was chosen to allow comparison with previous results [2, 3, 23, 24]. Hardness of all the samples is given in table 2.

The maximum achieved hardness (HV_{10}) for composites is about 13 GPa. The measured density of the composites is about 98% of the theoretical density although no porosity is observed at SEM microstructures (Figure 2). The theoretical density was calculated using a density of 6.05, 5.18 and 2.90 g/cm^3 for ZrO_2, TiCN and Al_2O_3 respectively. It is reported that the existence of about 2-3% porosity can cause a decrease of about 1-2 GPa in hardness values of ZrO_2 and ZrO_2-nano TiCN (60/40) composites [25]. In order to investigate the effect of porosity, yttria stabilized ZrO_2-TiCN (60/40) was exposed to HIPing (Hot Isostatic Pressing) (Bodycote, Sheffield, UK) at 1390°C for 20 minutes, under 140 MPa. After HIPing,

the density and hardness values were increased only 0.2 to 0.4% and about 0.2 GPa respectively. This means that the lower than expected values for density are not because of porosity. An in depth study [nano ZrO2-TiCN article] was revealed that a nano ZrO_2 most probably react with nano TiCN powder during PECS. The low hardness of sample 1-1500 is due to premature tetragonal to monoclinic transformation (Figure 4c) which results in micro-cracks appearing in the sample (LTD).

Table 2. Mechanical and electrical properties of (Nd,Y)-stabilised ZrO_2- TiCN-Al_2O_3 (60-40-0.8) composites stabilized with 1 mol % Y_2O_3 and 0.75-2 mol% Nd_2O_3 (plus one more sample stabilized with 2mol% yttria), sintered at 1400,1450 and 1500°C for 3 min

Composition	E GPa	ρ g/cm^3	HV_{10} GPa	$HV_{0.3}$ GPa	K_{IC10} MPa.m$^{0.5}$	[ii]K_{IC10} MPa.m$^{0.5}$	Resistivity Ohm.m
[i]0.75-1400	255	5.56	13.23 ± 0.09	14.38 ± 0,28	8,17 ± 0,22	9.14	-
1-1400	253	5.56	12.80 ± 0.15	12.97 ± 0.97	8.67 ± 0.20	9.75	1.6E-05
1.25-1400	251	5.54	12.96 ± 0.12	14.24 ± 0.35	7.64 ± 0.49	8.71	1.85E-05
1.5-1400	263	5.55	12.81 ± 0.10	13.83 ± 0,57	8.42 ± 0.10	9.38	2.13E-05
1.75-1400	258	5.54	13.12 ± 0.08	13.74 ± 0.54	7.85 ± 0.18	8.77	2.19E-05
2-1400	254	5.57	13.03 ± 0.17	13.91 ± 0.63	5.49 ± 0.45	6.53	1.95E-05
0.75-1450	255	5.60	13.22 ± 0.13	14.75 ± 0.44	8.37 ± 0.41	5.31	-
1-1450	256	5.53	13.04 ± 0.08	14.58 ± 0.26	8.34 ± 0.35	9.33	-
1.25-1450	255	5.54	12.72 ± 0.21	14.13 ± 0.12	8.42 ± 0.30	9.41	1.7E-05
1.5-1450	253	5.54	12.71 ± 0.11	13.76 ± 0.47	7.50 ± 0.20	8.37	1.71E-05
1.75-1450	248	5.53	12.30 ± 0.15	13.09 ± 0.49	8.35 ± 0.41	9.34	1.92E-05
2-1450	251	5.58	13.23 ± 0.18	14.57 ± 0.55	6.81 ± 0.14	7.72	1.84E-05
1-1500	263	5.57	12.01 ± 0.21	12.81 ± 1.04	5.69 ± 1.22	6.62	1.64E-05
1.25-1500	246	5.54	12.71 ± 0.10	14.26 ± 0.25	7.21 ± 0.15	8.08	1.63E-05
1.5-1500	254	5.56	12.90 ± 0.05	14.27 ± 0.31	7.13 ± 0.37	8.00	1.75E-05
1.75-1500	251	5.57	12.80 ± 0.09	13.46 ± 0.41	7.65 ± 0.18	8.54	1.87E-05
2-1500	255	5.59	12.71 ± 0.09	13.93 ± 0.18	6.50 ± 0.12	7.38	1.81E-05

i: Nd_2O_3 mol% stabilizer – PECS temperature (The amount of Y_2O_3 stabilizer is constant (1 mol%) in all the compositions)

ii: Palmqvist formula

The diagonal mark resulting from Vickers indentation on sample 2-1400 (a) and 1-1500 (b) is shown in figure 7. When the c/a ratio is high (L/a $\leq$ 2.5, when L = c-a), the radial

cracks have the geometry of Palmqvist cracks (Fig 7a), whereas at the lower c/a ratios (Figure 7b), the radial cracks take the form of median cracks and obey Anstis condition [26]. The length of the cracks in high toughness samples (e.g. 1-1400 with Anstis toughness of $K_{IC\ 10}$: 8.67 ±0.20 MPa.$m^{0.5}$) is short and does not satisfy the conditions of the Anstis formula [17]. Hence, the fracture toughness was measured also with the Palmqvist formula. The obtained data was 9.75 MPa.$m^{0.5}$ for the same sample (1-1400).

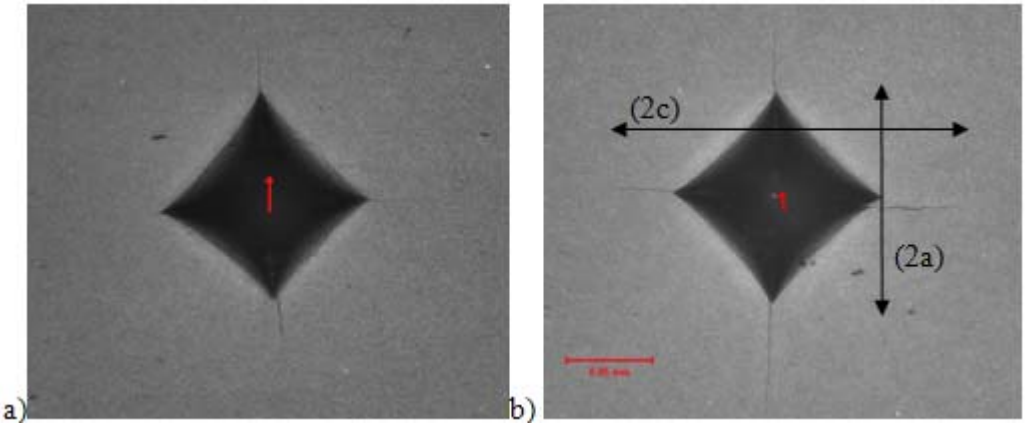

Figure 7. Vickers indentation mark (10Kg) on sample (a): 2-1400 and (b): 1-1500.

The Anstis technique is suited for toughness evaluations on a comparative basis. With reference to previous work at KU Leuven [1, 3, 23, 24, 27] , toughness in this study was calculated based on Anstis formula as well. The measured toughness values are shown in figure 8.

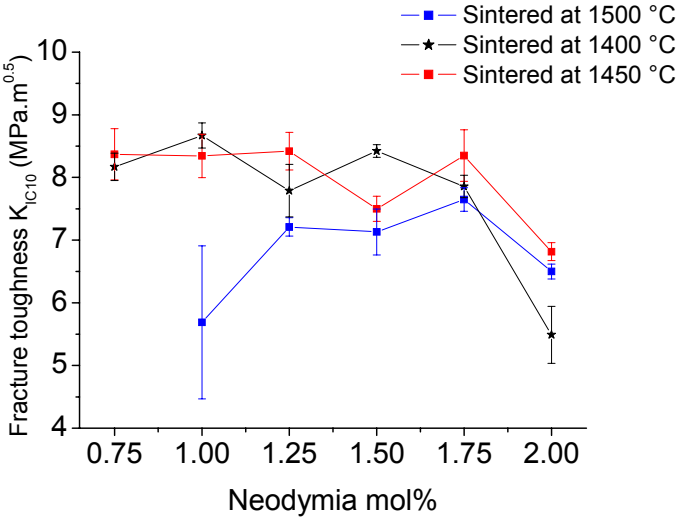

Fig 8. Fracture toughness of ZrO_2-TiCN (60-40) nano-composites stabilized with 1 mol % Y_2O_3 plus 0.75-2 mol% Nd_2O_3, sintered at 1400 °C,1450 °C and 1500°C, calculated according to Anstis formula.

The samples sintered at 1500°C, with a range of 1.25 till 1.75 mol% Neodymia stabilizer, are fully tetragonal at room temperature (see Figure 4c). The sample with 1 mol% neodymia suffered from premature tetragonal to monoclinic transformation, resulting in lower toughness.

For all samples, at more than 1.75 mol% neodymia a decrease in fracture toughness is observed. This is due to a decrease in transformability due to over-stabilization of zirconia phase or reduction in grain size (see Figure 3).

For the samples sintered at 1400 °C and 1450 °C with 0.75 to 1.5 mol% neodymia stabilizer, it is possible to have samples without cracks at room temperature with a very good zirconia transformability and toughness, although there is some monoclinic phase present initially. The presence of monoclinic phase can result in cracks appearing during an EDM procedure. Therefore, systems at 1.75% neodymia seem optimal.

There are several fracture toughness mechanisms participating in final toughness of a composite (e.g. crack deflection, transformation toughening and toughness coming from compressive residual stress due to difference in thermal expansion coefficient of components). For a zirconia based composite containing 40 vol% secondary phase, the major toughening mechanism is typically transformation toughening [2]. Transformation toughening is directly related to zirconia transformability. The ZrO_2 phase transformability is defined as the difference in the percentage of monoclinic and tetragonal zirconia phase, obtained from XRD patterns of smoothly polished and fractured surfaces. The volume fraction of the m-ZrO_2, V_m, is calculated by measuring the intensities of the (111) and $(11\bar{1})$ reflections of the monoclinic ZrO_2 phase and the (111) peak of the tetragonal ZrO_2 phase according to the formula of Toraya et al [19]. .The m-ZrO_2 fraction measured on both polished and fractured surfaces as well as the ZrO_2 phase transformability of all samples sintered at 1450°C are summarized in Table 3. A ZrO_2 transformability of about 54% could be obtained for the sample 1-1450.

Table 3. Calculated transformability for ZrO_2-TiCN (60/40) nanocomposites stabilized with 1 mol % Y_2O_3 plus 0.75-2 mol% Nd_2O_3, sintered at 1450°C for 3 min

Sample code	1-0.75	1-1	1-1.25	1-1.5	1-1.75	1-2
ZrO_2 transformability	53	54	47	39	36	22

The calculated transformability largely explains the toughness results in figure 8. Towards higher neodymia content, the toughness starts to decrease due to less transformation (over-stabilization of tetragonal phase).

Anée et al. reported a transformability of 46% for 2mol% yttria stabilized ZrO_2-WC (60/40) [4].. A zirconia transformability of 40% is reported by Salehi et al. for ZrO_2-TiN (60/40) [2]. Basu et al. reported a transformability of 57% for 2 mol% (mixing method) yttria stabilized zirconia with a grain size of about 500 nm [28]. The highest transformability was reported by Tao et al. who reported a transformability of 83% for pure zirconia stabilized with 1 mol% yttria plus 1 mol% Nd_2O_3 for a sample sintered for 1h at 1450°C with a grain size of about 320nm [29].

It should be mentioned that the thermal expansion coefficient of zirconia ($10\times10^{-6^\circ}K^{-1}$) is higher than for TiCN ($8\times10^{-6^\circ}K^{-1}$) [30], TiN ($9.4\times10^{-6^\circ}C^{-1}$) [31] and WC ($5.2\times10^{-6^\circ}C^{-1}$) [32]

Therefore, the zirconia phase of the ZrO_2-TiCN, ZrO_2-TiN and ZrO_2-WC composites is exposed to tensile stress during cooling and is expected to have higher ZrO_2 transformability compared to pure zirconia. On the contrary, a stiffer matrix, constrains the transformation more than does ZrO_2, decreasing the extent of the transformation zone and consequently toughness [33]. The stiffness of TiN (600 GPa) [29], TiCN (416 GPa) [31], and WC (620-720GPa) [34] is higher than stabilized zirconia (200GPa)**Error! Bookmark not defined.**. Therefore, addition of these phases to zirconia matrix increases the stiffness of the composite and as a result decreases zirconia transformability. Most probably the latest explanation is more valid given the above mentioned highest observed transformability in pure zirconia.

C) LTD Resistance

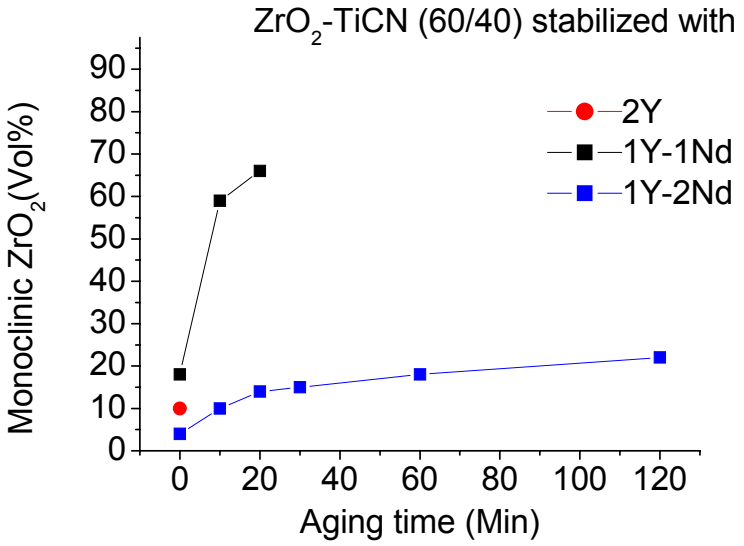

Figure 2. LTD resistance of ZrO_2-TiCN.

Table 1. Mechanical properties of ZrO_2- TiCN (60/40) composites, stabilized with 2 mol % Yttria (2Y) or 1 mol % Yttria + 1 or 2 mol% Neodymia (1Y-1Nd or 1Y-2Nd)

	P (g/cm^3)	E (GPa)	HV_{10} (Kg/mm^2)	K_{IC} ($MPa*m^{1/2}$)	Transform…
TiCN, 1Y-1Nd	5.65	248	1262 ±15	9.07± 0.16	54
TiCN, 1Y-2Nd	5.59	250	1273 ±17	5.24± 0.29	22
TiCN, 2Y	5.5	218	1206±16	3.8±0.1	2

* second phase of ZrO_2 based composites (60/40)

REFERENCES

[1] Bikramjit. Basu, T. Venkateswaran and Doh-Yeon Kim, Microstructure and properties of Spark-Plasma-sintered ZrO_2-ZrB_2 Nanoceramic composites, *Journal of The American Ceramic Society*, 2006,

[2] Sedigheh Salehi, Omer Van der Biest and Jef Vleugels, Electrically conductive ZrO_2–TiN composites, *journal of European society*, ….

[3] B. Basu, J. Vleugels and O. Van Der Biest, Processing and Mechanical properties of ZrO_2-TiB_2 composites, *J. Europ. Ceram. Soc.*, In Press

[4] Guy Anné, Stijn Put, Kim Vanmeensel, Dongtao Jiang, Jef Vleugels and Omer Van der Biest, Hard, tough and strong ZrO_2–WC composites from nanosized powders, Journal of the European Ceramic Society , Volume 25, Issue 1 , January 2005, Pages 55-63

[5] J. Vleugels, O. Van Der Biest, Development and characterization of Y_2O_3-stabilized ZrO_2 (Y-TZP) composites with TiB_2, TiN, TiC, and $TiC_{0.5}N_{0.5}$, *Journal of The American Ceramic Society*, 1999, 82(10), 2717 -2720.

[6] J. Zdanowski , J. Kozłowski, J. Markowski and A. Prajzner, Properties of carbides, nitrides and carbonitrides based on Ti and Mo multicomponent layers, Surface and coatings technology, Vol. 98, Issue 1-3, Jan 1998, pages 1440-1443.

[7] E. barbier & F. Thrvrnot, Titanium carbonitride-zirconia composites: formation and characterization, , *J. of the europian society*, 8 (1991) 263-269

[8] R. Morrell, handbook of properties of technical & engineering ceramics, part1., 1985, 95-166.

[9] Garvie, R. C., Hannink, R. H. J., and Pascoe, R. T., Ceramic steel? *Nature*. 1975, 258, 703-704.

[10] Rühle, M. and Evans, A. G., High toughness ceramics and ceramic composites. Prog. Mater. Sci., 1989, 33, 85-167.

[11] Sedigheh Salehi, Omer Van der Biest , Karel Brans and Jef Vleugels, ZrO2-NbC composites, submitted to J. Am. Ceram. Soc at Feb. 2008.

[12] S. Lawson, ‘’Environmental degradation of zirconia ceramics, ‘’ J. Eu. Ceram. Soc., 15, 485-502 (1995).

[13] J. Chevalier, B. Cales, J. Drouin, ‘’Low temperature aging of Y-TZP ceramics,’’ *J. Am. Ceram. Soc*., 82, 2150-4 (1999).

[14] Sedigheh Salehi, Kim Vanmeensel, Omer Van der Biest and Jef Vleugels, Hydrothermal stability of yttria and neodymia co-stabilized ZrO2, submitted for J. Am. Ceram. Soc. May 2008

[15] Yuan, Z. X., Vleugels, J and Van der Biest, O., preparation of Y_2O_3-coated ZrO_2 powder by suspension drying. *J. Matter. Sci. Lett.*, 2000, 19, 359-361.

[16] K. Vanmeensel, A. Laptev, S. Huang, D. Jiang, S.A. Salehi, G. Anné, J. Vleugels, O. Van der Biest, ECRES 2005

[17] Anstis, G. R., Chantikul, P., Lawn, B. R. and Marshall, D. B., A critical evaluation of indentation techniques for measuring fracture toughness, *Journal of The American Ceramic Society*, 1981, 64, 533-538.

[18] ASTM Standard E 1876-99, Test Method for Dynamic Young’s Modulus, Shear Modulus, and Poisson’s ratio for Advanced Ceramics by Impulse Excitation of Vibration, ASTM Annual Book of Standards, Philadelphia, PA, 1994.

[19] H. Toraya, M. Yoshimura and S. Somiya,'' Calibration curve for quantitative analysis of the monoclinic-tetragonal ZrO2 system by X-ray diffraction'', J. Am. Ceram. Soc., 67 [6] C119–C121 (1984).

[20] P. F. Becher and M. V. Swain, J. Am. Cerm. Soc., Vol. 75, 493-502, 1992.

[21] Alfonso Bravo-leon, Yuichiro Morikawa, Masanori Kawahara and Merrilea, Fracture toughness of nanocrystalline tetragonal zirconia with low yttria content, J. Mayo, Acta materialia 50 (2002) 4555-4562.

[22] A. Krell, A new look at grain size and load effects in the hardness of ceramics, *Material science and Engineering*, A 245 (1998) 277-284.

[23] D. Jiang, J. Vleugels, O. Van der Biest, W. Liu, R. Verheyen, B. Lauwers, Electrical conductive and wear resistant Si_3N_4-based composites with $TiC_{0.5}N_{0.5}$ particles for electrical discharge machining., Materials Science Forum, 492-493 (2005) 27-32.

[24] K. Vanmeensel, K.Y. Sastry, J. Hennicke, G. Anné, D. Jiang, A. Laptev, J. Vleugels, and O. Van der Biest, Microstructure and Mechanical Properties of Spark Plasma Sintered ZrO_2-Al_2O_3-$TiC_{0.5}N_{0.5}$ Nanocomposites., Solid State Phenomena, 106 (2005) 153-160.

[25] Porosity-dependence of elastic moduli and hardness of 3Y-TZP J. Luo and R. Stevens , Volume 25, Issue 3 , April 1999, Pages 281-286.

[26] K. Niihara, R. Morena and D. P. H hasselman, Indentation fracture toughness of brittle materials for palmqvist cracks, *Journal of Materials Science Letters*, Volume 1, Number 1, January 1982 , 13 – 16.

[27] Xu, Jef Vleugels, Omer Van der Biest and Peiling Wang, fabrication and characterization of (Nd,Y)-TZP ceramics from stabilizer coated nanopowders; materials letters 58 (2004) 3353-3357.

[28] Bikramjit basu, Jef Vleugels and Omer van der Best, Toughness tailoring of yttria-doped zirconia ceramics, Matreial Science and Engineering A 380 (2004) 215-221.

[29] Tao Xu, Jef Vleugels, Omer Van der Biest, Yanmei Kan and Peiling Wang, Phase stability and mechanical properties of TZP with a low mixed Nd_2O_3/Y_2O_3 stabiliser content, Journal of the European Ceramic Society, Volume 26, Issue 7, 2006, Pages 1205-1211.

[30] Materials science forum Vols. 429-493 (2005)pp. 705-710.

[31] Peter J. Hardro, selected material system and comparison of their predicted properties to H13 Tool steel, Sep 1999, P5.

[32] Pedzich Z., Haberko K., Faryna M., Sztwiertnia K., Interphase boundary in zirconia-carbide particulate composites, *Key Engineering Materials,* 223 (2002), pp. 221-226.

[33] Transformation toughening in Zirconia-Containing Ceramics, Richard H. J. Hannink, *J. Am. Ceram. Soc*., 83 [3] 461-87 (2000).

[34] Pierson, H. O., Handbook of Refractory Carbides and Nitrides. Properties, Characteristics, Processing and Applications. Noyes Publications, Westwood, New ey, USA, 1996, p. 106.

In: Chemistry and Chemical Engineering Reserch Progress ISBN: 978-1-61668-502-7
Editor: A.K. Haghi

Chapter 10

Y_2O_3 AND Nd_2O_3 CO-STABILIZED ZrO_2-WC COMPOSITES

Sedigheh Salehi, Omer Van der Biest and Jef Vleugels*
Department of Metallurgy and Materials Engineering, K.U.Leuven, Kasteelpark Arenberg 44, B-3001 Leuven, Belgium

ABSTRACT

Y_2O_3+Nd_2O_3 co-stabilized ZrO_2-based composites with 40 vol % WC were fully densified by pulsed electric current sintering (PECS) at 1350°C and 1450°C. The influence of the PECS temperature and Nd_2O_3 co-stabiliser content on the densification, hardness, fracture toughness and bending strength of the composites was investigated. The best combination of properties was obtained for a 1 mol % Y_2O_3 and 0.75 mol % Nd_2O_3 co-stabilized composite densified for 2 minutes at 1450°C under a pressure of 62 MPa, resulting in a hardness of 15.5 ± 0.2 GPa, an excellent toughness of 9.6 ± 0.4 MPa.$m^{0.5}$ and an impressive 3-point bending strength of 2.04 ± 0.08 GPa. The hydrothermal stability of the 1 mol% Y_2O_3+ 1 mol% Nd_2O_3 co-stabilized ZrO_2-WC (60/40) composites was compared with that of the equivalent 2 mol% Y_2O_3 stabilized ceramic. The double stabilized composite did not degrade in 1.5 MPa steam at 200°C after 4000 minutes whereas the yttria stabilized composite degraded after less than 2000 minutes. Moreover, the (1Y,1Nd) ZrO_2-WC composites have a substantial higher toughness (~9 MPa.$m^{0.5}$) than their 2Y stabilized equivalents (~7 MPa.$m^{0.5}$).

I. INTRODUCTION

Yttria stabilized tetragonal ZrO_2 polycrystalline (Y-TZP) ceramics are favourable because of their high toughness [1]. Addition of about 40 vol% of electro-conductive carbide or nitride ceramic phases to a Y-TZP matrix allows to further improve the hardness, toughness and strength and enables electrical discharge machining (EDM) as a cost effective machining technique for producing complex ceramic parts [2,3]. Amongst the investigated ZrO_2-based composites with WC, TiN, TiCN, TiC, TiB_2 and NbC as secondary phase [4-7],

ZrO_2-WC [8-10] shows the best combination of hardness, strength and toughness. The reciprocating sliding wear resistance against WC-Co of EDM ZrO_2-WC (60/40) composites is also reported to be higher than for ZrO_2 based composites with 40 vol% TiN or TiCN [2]. Earlier reports on ZrO_2-WC composites revealed that the optimum composition from a mechanical point of view as well as EDM behaviour contain 40 vol% of WC phase in combination with an Y_2O_3 stabilizer content of 2 mol % [8-10].

The main drawback of ZrO_2 is the possible degradation in aqueous environments or ambient humidity at low temperature (RT to 400°C) [11,12], a phenomenon commonly known as low temperature degradation (LTD) that is expressed as a spontaneous transformation of the metastable tetragonal ZrO_2 phase into the monoclinic phase, accompanied with a volume expansion, microcrack formation and complete material degradation. Double yttria+neodymia stabilized ZrO_2 however has a higher hydrothermal stability than yttria stabilized ZrO_2 with the same overall amount of stabilizer [13].

In this work, the hydrothermal stability of 2 mol% yttria stabilized ZrO_2-WC (60/40) is compared with that of 1 mol% yttria + 1 mol% neodymia co-stabilized composites. Furthermore, a range of Y_2O_3+Nd_2O_3 co-stabilized ZrO_2-WC (60/40) ceramic composites were processed using pulsed electric current sintering (PECS) at 1350 and 1450°C. The Y_2O_3 stabilizer content was fixed at 1 mol % while the Nd_2O_3 stabilizer content was varied between 0.75-1.5 mol%. The Vickers hardness, fracture toughness, bending strength, electrical resistivity as well as the microstructural properties were investigated. The neodymia stabilizer content and PECS temperature were optimised in order to obtain the best combination of mechanical properties.

II. EXPERIMENTAL PROCEDURE

Commercial ZrO_2 (TZ-0, Tosoh, Japan), mechanomade WC (grade J300, MBN, Italy) and Al_2O_3 (SM8, Baikowski, France) starting powders were used for the composite preparation. As shown in Figure 1A, the WC powder is highly agglomerated with an agglomerate size range of 0.1 to 10 μm, although the primary crystal size is claimed to be about 20 nm (Supplier information), whereas the ZrO_2 powder is nanometric with a particle size of about 50 nm (Figure 1B). The Al_2O_3 powder has an average grain size of 0.4 μm.

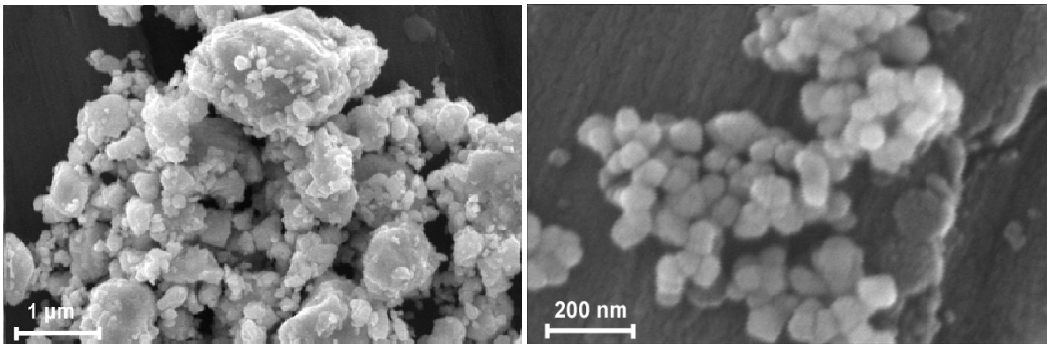

Figure 1. Scanning electron micrograph of WC (a) and ZrO_2 (b) starting powder.

The neodymia and yttria were applied by a stabiliser coating technique on the ZrO_2 starting powder prior to mixing with the WC powder. For this purpose, the proper amount of neodymia (99.9 %, Chempur, Germany) and yttria (99.9 %, ACROS, Belgium) was dissolved in nitric acid (65 %, Sigma-Aldrich, Germany) at 100°C on a magnetic stirrer. The resulting nitrate solution was applied to the monoclinic zirconia powder via a suspension coating process [14]. The nitrate-coated powder was calcined for 1 hour at 800°C. The yttria stabilizer content was fixed at 1 mol % whereas the neodymia content was varied between 0.75 to 1.5 mol %. 0.8 wt % Al_2O_3 was added as a ZrO_2 grain growth inhibitor and sintering aid. Moreover the addition of 0.8 wt% Al_2O_3 was claimed to improve the hardness [8].

50 grams of ZrO_2-WC with 40 vol% of WC was mixed on a multidirectional Turbula mixer (type T2A, Basel, Switzerland) in ethanol in a polyethylene container of 250 ml during 48 h at 60 rpm. 250 grams of cemented carbide milling balls (Ø = 4-5 mm, Ceratizit grade MG15) were added to the container to break the agglomerates in the starting powder and to enhance powder mixing. The ethanol was removed after mixing using a rotating evaporator. The dry powder mixture was sieved (315 mesh) to remove the agglomerates, prior to densification.

The powder was densified into 30 mm diameter discs by means of pulsed electric current sintering (Type HP D 25/1, FCT Systeme, Rauenstein, Germany) at 1350 or 1450°C in a graphite tool set-up. Details on the equipment, die/punch set-up and temperature control are given elsewhere [15]. A heating rate of 400°C/min was applied up to 1050°C with a dwell time of 1 min and subsequent heating at 200°C/min up to the sintering temperature. The initial pressure was increased from 7 to 30 MPa during the 1 minute dwell time at 1050°C and from 30 to 62 MPa during the first minute at the sintering temperature. The total dwell time at maximum temperature was 3 minutes.

Microstructural investigation was performed by scanning electron microscopy (SEM, XL-30FEG, FEI, Eindhoven, The Netherlands). X-ray diffraction (Seifert 3003 T/T, Ahrensburg, Germany) was used for phase identification and calculation of the relative monoclinic and tetragonal ZrO_2 phase content. The m-ZrO_2 volume fraction is calculated according to the method of Toraya *et al*. [16]. The transformability of a ceramic is defined as the difference in m-ZrO_2 content of a fractured and polished surface, whereas the transformability during hydrothermal aging is the % m-ZrO_2 difference between the steam treated and pristine polished surface. The average grain size of the phases in the densified composites was measured according to the linear intercept method. The reported values are the average of about 200 grains measured by means of Image Pro software on SEM micrographs. The electrical resistivity of the composites was measured according to the 4-point contact method using a Resistomat (TYP 2302 Burster**,** Gernsbach, Germany).

The density of the samples was measured in ethanol, according to the Archimedes method (BP210S balance, Sartorius AG, Germany). The Vickers hardness (Model FV-700, Future-Tech Corp., Tokyo, Japan), HV_{10}, was measured with an indentation load of 98 N with a dwell time of 10 s. The indentation toughness, K_{IC}, was calculated according to the formula of Anstis *et al*. [17] based on crack length measurements of the median crack pattern produced by Vickers HV_{10} indentations. The elastic modulus of the ceramic specimens was measured using the resonance frequency method [18], measured by the impulse excitation technique (Model Grindo-Sonic, J.W. Lemmens N.V., Leuven, Belgium). The test was done on 25.0×5.4×2 mm samples. The reported values are the mean and standard deviation of 10 measurements. The sample surfaces for E-modulus and strength testing were ground with a

diamond grinding wheel (type MD4075B55, Wendt Boart, Brussels, Belgium) on a Jung grinding machine (JF415DS, Göppingen, Germany).

Low temperature degradation (LTD) tests were performed at 200°C under a saturated H_2O pressure of 1.55 MPa. For this purpose, rectangular bars (20×5×2 mm) were polished and inserted in a stainless steel autoclave. The autoclave was inserted in a molten salt bath to establish an internal temperature of 200°C as monitored by a thermocouple in the autoclave.

III. Results and Discussions

A) Hydrothermal Stability

The results of the hydrothermal stability testing, performed on 2 mol% yttria (2Y) and 1 mol% yttria + 1 mol% neodymia (1Y,1Nd) stabilized ZrO_2-WC (60/40) composites PECS at 1450°C, are summarised in Figure 2. The 2 mol % yttria stabilized composite completely degraded after 2000 minutes in 1.5 MPa saturated water vapour at 200°C, while the 1Y-1Nd stabilized ZrO_2-WC composite sample remained intact even after 4000 minutes. In general, the mechanisms which increase the hydrothermal stability of ZrO_2 ceramics, such as a reduction in ZrO_2 grain size or an increased stabilizer content, etc. [1,19], decrease the t-ZrO_2 phase transformability and concomitant fracture toughness. Beside the higher hydrothermal stability, the (1Y,1Nd) stabilized ZrO_2-WC composite also has a higher fracture toughness than the 2Y stabilized ZrO_2-WC (see Table 1). The reason for the superior hydrothermal stability of double stabilized yttria + neodymia ZrO_2 over yttria stabilized ZrO_2 was reported to be the larger lattice parameter of double stabilized ZrO_2 as a result of the incorporation of Nd^{3+} ions and the absence of a thermally activated martensitic transformation above room temperature [13]. The same mechanism applies to the ZrO_2-based composite systems.

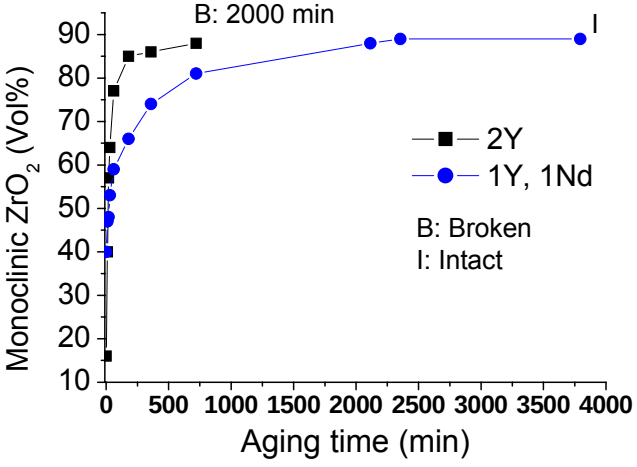

Figure 3. Hydrothermal stability of 2 mol% Y_2O_3 and 1 mol% Y_2O_3 + 1 mol% Nd_2O_3 stabilized ZrO_2-WC (60/40) composites.

Table 1. Mechanical and electrical properties of 1 mol% Y_2O_3 + 0.75-1.5 mol% Nd_2O_3 and 2 mol% yttria stabilized ZrO_2-WC (60/40) composites, PECS at 1350 or 1450°C

Tempe-rature (°C)	Nd_2O_3 (mol%)	transfor-mability (%)	Density (g/cm^3)	E (GPa)	HV_{10} (GPa)	K_{IC-10} ($MPa.m^{0.5}$)	Strength (MPa)	Resistivity (Ω.m)
1350	0.75	30	9.79	356	15.24 ± 0.19	9.2 ± 0.4	1513 ± 64	1.3E-05
	1	45	9.76	350	15.38 ± 0.29	10.1 ± 0.2	1486 ± 164	1.0E-05
	1.25	52	9.68	349	15.62 ± 0.17	10.0 ± 0.5	1561 ± 165	1.6E-05
	1.5	29	9.81	344	15.78 ± 0.16	9.0 ± 0.4	1497 ± 200	1.2E-05
1450	0.75	31	9.77	359	15.52 ± 0.23	9.6 ± 0.4	2045 ± 80	6.9E-06
	1	44	9.75	356	15.48 ± 0.26	9.7 ± 0.4	1808 ± 139	1.5E-05
	1.25	41	9.78	356	15.92 ± 0.23	9.9 ± 0.5	1849 ± 101	1.2E-05
	1.5	26	9.76	362	15.79 ± 0.27	9.1 ± 0.4	1863 ± 4	9.6E-06
	0* [9]	44	9.78	372	16.20 ± 0.15	7.3 ± 0.1	1873 ± 90	/

*: 2 mol% yttria stabilized ZrO_2-WC (60/40)

B) Mechanical Properties

The microstructure of a polished cross-section and fracture surface of the (1Y,1.25Nd) stabilized composite, PECS at 1450°C is shown in Figure 3. The fracture surface shows that the ZrO_2 grain size is in the of 100-150 nm range while the WC particle size ranges from 20 nm up to 2 µm. Three phases can be differentiated on the atomic number contrast image of the polished cross-section, i.e. ZrO_2 (dark), WC (white) and Al_2O_3 (black). Assuming a density of 6.0, 15.8 and 3.9 g/cm^3 for (1Y,1-1.5Nd) stabilized ZrO_2 [13], WC and Al_2O_3 respectively, a theoretical density of 9.80 g/cm^3 is calculated for ZrO_2-WC (60/40) composites. The relative density of the ceramic grades is about 99 % of the theoretical density and hardly changes with sintering temperature.

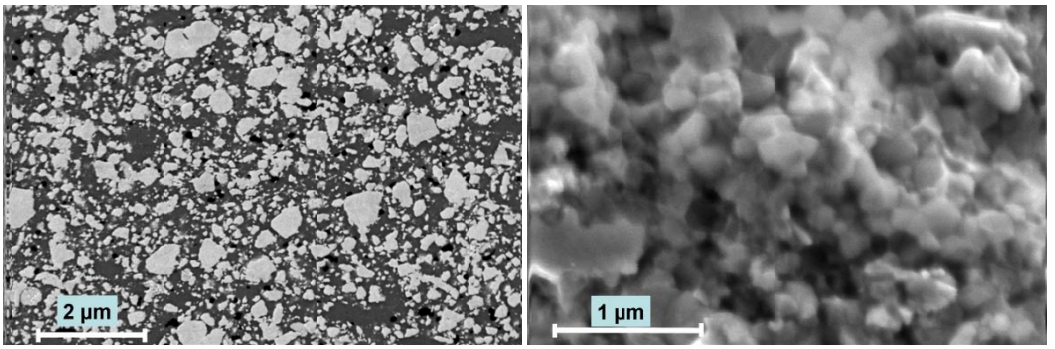

Figure 4. SEM micrograph of polished and fracture surface of (1Y,1.25Nd) stabilized ZrO_2-WC (60/40), PECS for 2 min at 1450°C and 60 MPa. ZrO_2 (dark), WC (white) and Al_2O_3 (black).

The strength of the ceramics PECS at 1450°C is substantially higher than for those sintered at 1350°C, although the density is comparable (see Table 1). ZrO_2 and WC have a very good high temperature chemical stability below 1500°C [20]. Hence, the ZrO_2-WC grain-boundaries should be comparable for the ceramics PECS at 1350 and 1450°C. The higher PECS temperature however could result is a stronger ZrO_2-WC interphase strength explaining the higher strength of the composites PECS at 1450°C. The bending strength of the 2 mol % yttria stabilised composite is comparable with that of the Nd_2O_3 co-stabilised ceramic (see Table 1).

Only a minor amount of monoclinic ZrO_2 (m-ZrO_2) could be detected by means of X-ray diffraction on the polished surfaces of the ceramic composites, as shown in Figure 4. A small amount of m-ZrO_2 could be present in the bulk of the lowest stabiliser content grade, whereas the small amount of m-ZrO_2 on the 1 and 1.25 mol % Nd_2O_3 co-stabilised grades could also have been generated during polishing, due to the higher transformability of the latter grades.

Different toughening mechanisms are active in ZrO_2-based composites [10]. The main toughening mechanism is ZrO_2 transformation toughening [4,10], whereas crack deflection is clearly operational as shown in Figure 5.

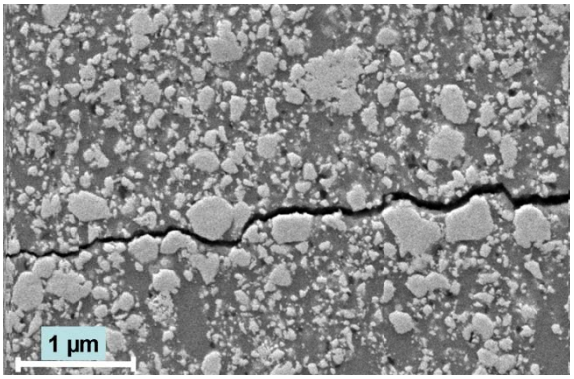

Figure 4. Crack path initiated from the corner of a Vickers indentation on a (1Y-0.75Nd) stabilized ZrO_2-WC (60/40) composite PECS at 1350°C.

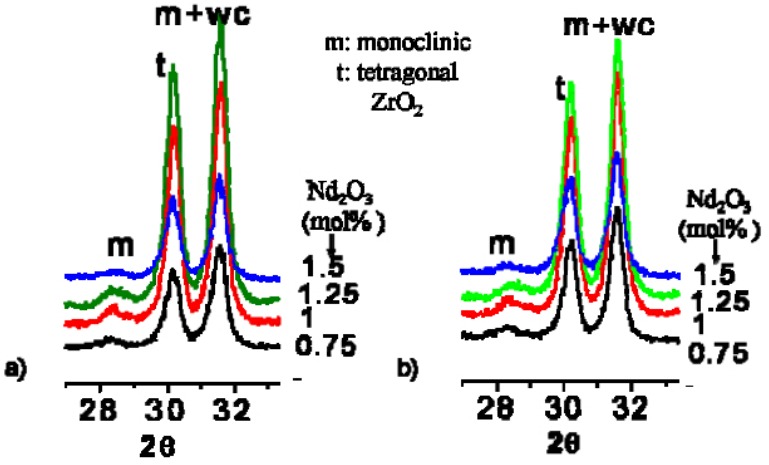

Figure 5. XRD pattern of (1Y,1-1.5Nd) stabilized ZrO_2-WC (60/40) PECS at 1350 (a) and 1450°C (b).

All ZrO_2-WC (60/40) composites stabilized with 1 mol% Y_2O_3 + 0.75-1.5 mol% Nd_2O_3, have a toughness of 9-10 MPa.$m^{0.5}$, despite a substantial difference in ZrO_2 phase transformability varying from 30 to 52 % (Table 1). The toughness of the 1.5 mol % Nd_2O_3 co-stabilised composite is statistically slightly lower, whereas the toughness of the other grades is the same, which could be attributed to the higher stabiliser content in agreement with a lower phase transformability. Although the transformability of the 0.75 mol % Nd_2O_3 co-stabilised composite is also lower and comparable to that of the 1.5 mol % Nd_2O_3 grade, the toughness is as high as for the other grades. The loss in ZrO_2 transformation toughening in the lower stabiliser content grade might be compensated by a higher tendency for the formation of microcracks resulting in crack tip shielding by microcracking.

The transformability is hardly influenced by the PECS temperature what can be attributed to the high heating rate of 200°C/min and short dwell time of 3 minutes, which does not allow to establish a substantial difference in ZrO_2 grain size that would strongly influence the ZrO_2 phase transformability. The comparable grain size is also reflected in a comparable hardness and stiffness.

The toughness and hydrothermal stability of the (1Y,1-1.5Nd) stabilized ZrO_2-WC (60/40) composites, PECS at 1450°C, is higher than for the 2 mol % yttria stabilised equivalent (see Table 1 and Figure 3), whereas the strength and hardness are comparable.

The toughness of the 1 and 1.25 mol % Nd_2O_3 co-stabilised composites is higher than for the 2 mol % yttria stabilised equivalent, although the ZrO_2 phase transformability is comparable. Since the Nd^{3+} ionic radius (0.110 nm) is larger than for Y^{3+} (0.102 nm) [21,22], the co-stabilised t-ZrO_2 phase has a larger lattice parameter [13]. This is confirmed by the peak shift of the t-ZrO_2 phase towards a lower 2 θ angle (Figure 6.a) whereas the m-ZrO_2 phase shows no peak shift (Figure 6.b). At the same t-ZrO_2 phase transformability, the volume expansion resulting from the t-ZrO_2 phase transformation in doubled stabilized ZrO_2 composites will therefore be larger than in the yttria-stabilized equivalent implying a higher residual compressive stress on the propagating crack tip and concomitantly higher fracture toughness.

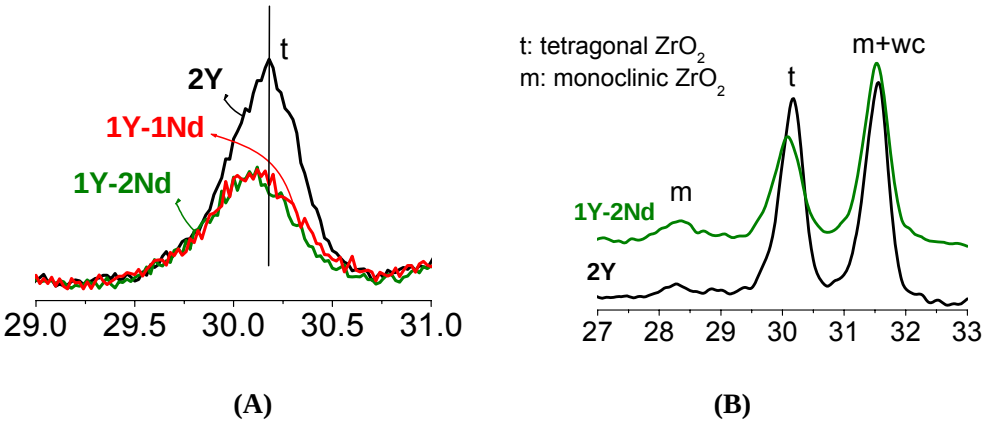

Figure 6. XRD patterns of (1Y,1Nd)-, (1Y,2Nd)-, and 2Y-stabilized ZrO_2-WC (60/40) composites, PECS at 1450°C.

IV. CONCLUSION

ZrO_2-based composites with 40 vol % WC and stabilized with 1 mol% yttria and 0.75-1.5 mol% neodymia were pulsed electric current sintered (PECS) to full density at 1350 and 1450°C. The (1Y,0.75Nd) co-stabilized composite densified for 2 minutes at 1450°C under a pressure of 62 MPa combines a hardness of 15.5 ± 0.2 GPa, an excellent toughness of 9.4 ± 0.4 $MPa.m^{0.5}$ and impressive 3-point bending strength of 2.04 ± 0.08 GPa.

A very high fracture toughness of about 9-10 $MPa.m^{0.5}$ was measured for all the composites irrespective of the neodymia stabilizer and PECS temperature. The toughness was hardly influenced by the PECS temperature and a Nd_2O_3 co-stabiliser content ranging from 0.75-1.25 mol %. The excellent bending strength of about ~1900 MPa for the double stabilized composites PECS at 1450°C was substantially higher than for the grades PECS at 1350°C (~1500 MPa).

The 1 mol% yttria + 1 mol% neodymia co-stabilized ZrO_2-WC (60/40) composites have a higher fracture toughness, hardness as well as hydrothermal stability in steam at 200°C than the equivalent 2 mol% yttria stabilized composites, whereas the bending strength and stiffness is comparable.

ACKNOWLEDGEMENTS

S. Salehi thanks the Research Council of K.U.Leuven for a doctoral scholarship (DB/07/012). This work was supported by the Commission of the European Communities within the 6th Framework Program under project No. STRP 505541-1.

REFERENCES

[1] Hannink RHJ, Kelly PM, Muddle BC (2000) J Am Ceram Soc 83:461.
[2] Bonny K, De Baets P, Vleugels J, Salehi A, Van der Biest O, Lauwers B, Liu W (In press) J Mat Proc Tech.
[3] Lauwers B, Brans K, Liu W, Vleugels J, Salehi S, Vanmeensel K (2008) CIRP Annals Manu Tech 57: 191.
[4] Salehi S, Van der Biest O and Vleugels J (2006) J Eu Ceram Soc 26:3173.
[5] Salehi S, Van der Biest O, Brans K, Vleugels J (2008) submitted to J Am Ceram Soc.
[6] Vleugels J, Van Der Biest O (1999) J Am Ceram Soc 82:2717.
[7] Basu B, Vleugels J, Van der Biest O (2005) *J Eu Ceram Soc*. 25:3629.
[8] Jiang D, Van der Biest O, Vleugels J (2007) *J Eu Ceram Soc***.** 27:1247.
[9] Huang SG, Vanmeensel K, Van der Biest O, Vleugels J (2007) *J Eu Ceram Soc***.** 27:3269.
[10] Anné G, Put S, Vanmeensel K, Jiang D, Vleugels J, Van der Biest O (2005) J Eu Ceram Soc 25:55 .
[11] Lawson S (1995) *J Eu Ceram Soc.* 15:485.
[12] Chevalier J, Cales B, Drouin J (1999) *J Am Ceram Soc*. 82:2150.
[13] Salehi S, Vanmeensel K, Van der Biest O, Vleugels J (2008) submitted to J Am Ceram Soc.
[14] Yuan Z X, Vleugels J, Van der Biest O (2000) *J Matter Sci Lett.* 19:359.
[15] Vanmeensel K, Laptev A, Hennicke J, Vleugels J, Van der Biest O (2005) *Acta Mater*. 53:4379 .
[16] Toraya H, Yoshimura M, Somiya S (1984) *J Am Ceram Soc*. 67:C119 .
[17] Anstis GR, Chantikul P, Lawn BR, Marshall DB (1981) *J Am Ceram Soc*. 64:533.
[18] ASTM Standard E 1876-99 (1994) ASTM Annual Book of Standards, Philadelphia, PA
[19] Lawson S (1995) J Eu Ceram Soc 15:485.
[20] Moskała N, Pyda W, (2006) *J Eu Ceram Soc*. 26:3845.
[21] Shannon RD (1976) *Act. Crystall*. 32:751.
[22] Rey JFQ, Muccillo ENS (2004) *J Eu Ceram Soc*. 24:1287.

In: Chemistry and Chemical Engineering Reserch Progress ISBN: 978-1-61668-502-7
Editor: A.K. Haghi

Chapter 11

ELECTRO-CONDUCTIVE ZRO_2-NBC-TIN COMPOSITES USING NBC NANOPOWDER MADE BY CARBO-THERMAL REACTION

S. Salehi, J. Verhelst, O. Van der Biest, J. Vleugels*
Department of Metallurgy and Materials Engineering, Katholieke Universiteit Leuven, Kasteelpark Arenberg 44, B-3001 Heverlee, Belgium

Niobium carbide (NbC) is known for its good physical properties, such as high melting point (~ 3600°C), good electrical conductivity (~ 2.8 $\times 10^6$ S/m) and high hardness (~ 19 GPa). These properties encourage the investigation of zirconia-based niobium carbide composites aiming at achieving a composite with good fracture toughness, high hardness and at the same time a sufficient electrical conductivity to allow electro discharge machining (EDM).

Since all commercially available NbC powders are relatively coarse (d_{50} = 1-3 μm), a NbC nanopowder was prepared by carbo-thermal reduction of Nb_2O_5. The synthesis time, temperature, and C/Nb_2O_5 ratio have been optimized to obtain a NbC powder with minimum grain size and minimum residual carbon and oxide impurities. To achieve that, carbon black and niobium pentoxide were mixed in a different ratio (1.25 to 2.12) and thermally treated at 1000-1450°C for 0.5-10 h. NbC powder with a grain size of d_{50}:185 nm, was obtained from a powder mixture with a carbon to niobium oxide ratio of 1.88, thermally treated in vacuum (10^{-5} to 10^{-3} Pa) at 1350°C for 5 hours.

ZrO_2-NbC-TiN (65:35:5 vol %) composites could be fully densified by means of hot pressing at 1450°C for 1 hour at 28 MPa, resulting in a composite with an excellent hardness of 16 GPa, a fracture toughness of 5 $MPa.m^{0.5}$ and an electrical resistivity of 0.8 mΩ.cm. The composites could be machined by EDM.

I. INTRODUCTION

The Y-TZP matrix offers enhanced toughness and an acceptable strength but the hardness and conductivity of this compound is rather limited. On the other hand the ultra finely divided carbides and nitrides of various (transition) metals have high melting points and high

chemical stability combined with a low electrical resistivity. Therefore, with a combination of the two, it is expected to obtain a ceramic composite with high hardness, toughness and enough electrical conductivity to be EDM doable. By doing EDM, it is tring to avoid the expensive grinding operation for final shaping and surface finishing of components, thus increasing the possibility of mass production and manufacturing cost reduction.

NbC has an excellent hardness of about 20 GPa and a low resistivity of 35×10^{-3} mΩ.cm [4], and usually, it is used as reinforcing particles in tool steels [1-3]. In the frame work of making ZrO_2 based electro-conductive ceramic composite, ZrO_2 -TiN, TiB2, WC, TiCN [22-25] and …have been already investigated in our department. For this reason and with due attention to good electro-mechanical properties of NbC, It has been chosen as second phase for ZrO_2 based composite in this study.

Nowadays, commercially available NbC powders are relatively coarse (d_{50} = 1-3 μm). In this work, it is has been tried to obtain a NbC powder with minimum grain size and impurities by the mean of carburizing. The convenient methods for NbC synthesis are high-temperature (oxide above 1000°C) solid-state reactions of metal or metal such as direct combination of niobium metal or niobium oxides with carbon [13, 15, 17] or solid-gas reaction like reaction of NbCl5 with hydrocarbon or carburizing of oxide by methane–hydrogen mixtures [14, 16]. Among theses convenient methods, carburizing from Nb_2O_5 is chosen, because its simplicity and enforceability in situ. Afterward a zirconia based composite made by optimum self-synthesized NbC powder and the mechanical properties have been compared to the composites made by commercial NbC powders.

II. EXPERIMENTAL PROCEDURE

In carburizing method, a mixture of Nb_2O_5 and carbon black react in high temperature in non-reactive atmosphere and result to NbC formation (equation 1 & 2) [7].

$$½\ Nb_2O_5 + 7/2\ C \longleftrightarrow NbC + 5/2\ CO \quad (1)$$

$$½\ Nb_2O_5 + 9/4\ C \longleftrightarrow NbC + 5/4\ CO_2 \quad (2)$$

Table 1. Starting powders plus reference NbC (based on supplier information - *: grain size measured based on SEM micrograph

	Producer	**Impurities**	**Prticle size (μm)**
NbC	Treibacher-Austria	0.25% O – 0.13% free* carbon	Ave: 1.18 (FSSS)
Nb_2O_5	CBMM –Brazil	1.5% mainly Ta and Ti (2000 & 1500ppm)*	0,5-5 - (d_{50}:1.04 *)
C	Degussa-germany Noir special 4	Acclaimed to be pure!	Grain size: Few nano-meter Agglomerate size:1-50 (porous and weak)

In view of equation 1 and 2, Nb_2O_5 (CBMM, Brezil) and Carbon (Degussa, Germany) were mixed together with a C/Nb ratio of 2.5-4.25. An overview of starting powders and C:Nb ratio in starting powder mixtures are shown in Table 1 and 2.

Table 2. Codes and related C:Nb ratio of starting powder mixtures

Mixture code	A	B	C	D	E	F	G	H
C:Nb ratio	2.5	3	3.33	3.5	3.76	3.9	4	4.25

To make a homogeneous powder mixture, 50 grams of fully formulated powder mixtures were mixed on a multidirectional Turbula mixer (type T2A, Basel, Switzerland) in ethanol in a polyethylene container of 250 ml for 48 h at 60 rpm. 250 grams WC–Co milling balls (Ø: 3mm, Ceratizit grade MG15) were added to the containers to break the agglomerates in the starting powders and to enhance powders mixing. The suspensions were dried in a rotating evaporator at 80 °C. After 3h staying at oven (70°C), the dried powders were sieved trough a 315 µm sieve. An SEM micrograph of starting powder mixture before carburizing is shown in Figure 1. The Nb_2O_5 particle size measured based on SEM pictures was d_{50}:1.04 µm.

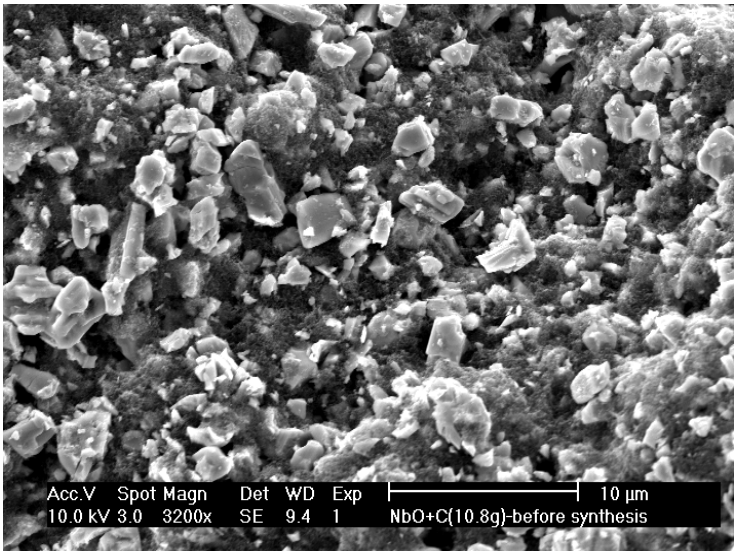

Figure 1. SEM picture of starting Nb_2O_5 and carbon mixture (C/Nb:3).

3 grams of the sieved powder was placed on a SiC crucible (Haldenwanger, germany-Ø:30 mm, h:20 mm) which covered with a SiC lid. The container was inserted on a hot press (Model W100/150-2200-50 LAX, FCT Systeme, Rauenstein, Germany) in vacuum (~10^{-3} to 10^{-5} Pa). Heating and cooling rates were 50°C/min and 20°C/min respectively. It has been tried to optimized three parameters, C/Nb ratio, maximum temperature and dwell time. Different combinations have been tried and the details are shown in Table 3.

Table 3. Variant parameters in carburizing procedure

Temperature	Time			
	30min	2 hr	5 hr	10 hr
1000 °C				A,
1150 °C	A, B	A, B, D	A, D	A, B, D
1250 °C	D	D		
1350 °C	D, E	D, E	D, E	
1450 °C	D, E , F , G, H			

Minimum temperature has been chosen based on the Gibbs free energy of the equations 1 and 2 (3 & 4). Based on the ΔG's, at a pressure of 10^{-3} Pa (atm), we can expect NbC formation (equation 1) at 648°C. NbC can forms in the same pressure from equation 2, at 845°C. Since the vacuum is not perfect at hot press device and can vary from 10^{-3} atm and also kinetic of reaction did not taken in to account, the minimum temperature which is used was 1150°C.

$$\Delta G_1 = 521.2 - 421.84 \times 10^{-3} T + 20.78 \times 10^{-3} T \times \ln(P_{CO}) \text{ [7]} \quad (3)$$

$$\Delta G_2 = 313.0 - 208.10 \times 10^{-3} T + 10.39 \times 10^{-3} T \times \ln(P_{CO_2}) \quad (4)$$

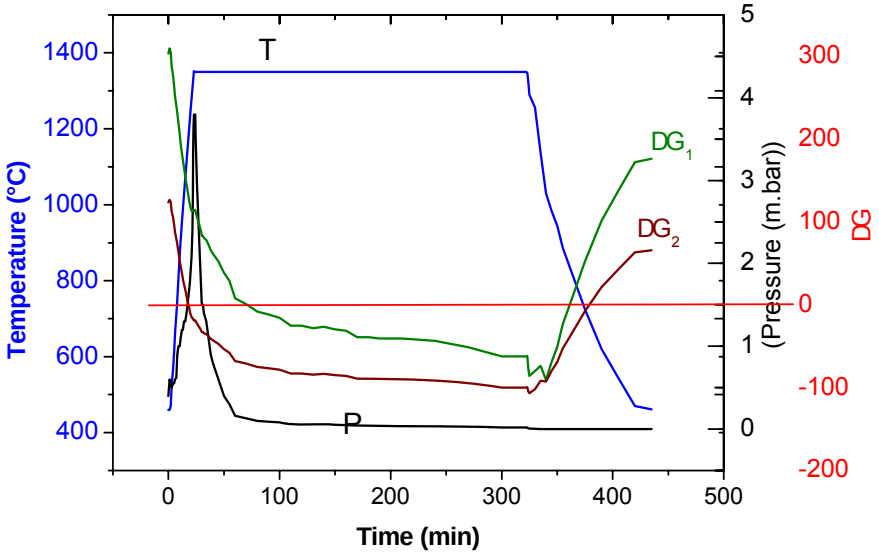

Figure 2. Monitored temperature and pressure inside the furnace during a carburizing cycle (1350°C for 5h on mixture powder E) plus calculated DG_1 and DG_2 using reported temperature and pressure during synthesizing process.

In Figure 2, ΔG's of reactions 1 and 2 are monitored based on the pressure and temperature which has been read during synthesizing process. As it can be seen, reaction 1 starts at 1350°C after about 45 minutes and reaction 2 starts at about 1150°C. Vacuum pomp in furnace is soaked all the air out, so it has been consumed that the pressure inside the chamber can be used as P (CO) or P (CO_2). It is difficult to differentiate P (Co) from P (CO_2), so calculations repeated considering P (CO) or P (CO) are half of the pressure inside the chamber. In this case, both reactions can happen at about 1200°C.

The oxidizing temperature of NbC varies from 200°C to 800°C depending to grain size [5]. Hence after carburizing the powder cooled down till room temperature and studied by SEM (XL-30FEG, FEI, Eindhoven, The Netherlands) equipped with an X-ray energy dispersive analysis system (EDS, EDAX, Tilburg, The Netherlands) for compositional analysis and X-ray diffraction (Seifert 3003 T/T, Ahrensburg, Germany). This machine has a Cu Kα radiation source (40 kV, 40 mA) that operates with a wavelength of 1,540598 nm. The XRD profiles for powders were scanned in step increments of 0.04° from 20° to 90°, and with dwell times of 1 second. The average grain size of powders was determined from SEM micrographs according to the linear intercept method [18], using Image-pro Plus software (version 4, Media Cybernetics, Silver Spring, Maryland). A minimum of 200 grains was counted for each material grade.

Two NbC powders with different Nb/C ratio (D and E, table 2) have been synthesized with optimum synthesis path way (1350°C, 5h) in larger scale (35 grams of initial powders in a bigger crucible (Ø:50mm, h: 50mm). The self-synthesized NbC powders mixed with proper amount of ZrO_2 (TOSHOH, Japan, TZ-0, TZ-3Y and TZ-8Y, d:37 nm) and TiN (Kennametal, USA, Jet milled, d:1.03 μm) to make 6 discs with 5 mm height and and 30 mm diameter. TiN was added to some of the compositions to exclude residual carbon which remains from carburizing process in the NbC powder by forming TiCN. Al_2O_3 powder (Baikowski grade SM8, Annecy, France) was added as a ZrO_2 grain growth inhibitor and sintering aid to all composite grades. The Y_2O_3-stabiliser content of the powder mixtures was adjusted by mixing the appropriate ratio of ZrO_2 starting powders. The powders were mixed in the same way that Nb_2O_5 and C mixed before carburizing. The powder compact was inserted in to a graphite die with 30 mm internal diameter. The graphite die was coated with BN to separate the powder mixture from the graphite die/punch setup. The temperature was monitored using a pyrometer.

The discs were sintered at 1450°C or 1500°C for 1 hour under 30 MPa pressure using the same Hot press which was used for carburizing. Using heating and cooling rates were 50°C/min and 20 °C/min respectively. After sintering, the samples were cross-sectioned and mirror polished to 1 μm finish, for hardness and toughness measurement. Microstructure was studied by SEM and XRD (details was explained before). The Vickers hardness, HV_{10}, was measured (Model FV-700, Future-Tech Corp., Tokyo, Japan) with an indentation load of 10 Kg. The indentation toughness, K_{IC}, was calculated from the length of the radial cracks originating in the corners of the Vickers indentations according to the formula proposed by Anstis et al. [19]. The density of the samples was measured in ethanol, according to the Archimedes method (BP210S balance, Sartorius AG, Germany). The reported hardness and toughness values are the mean with standard deviation obtained from five indentations.

The electrical resistance of the samples was measured on grounded bars ($20 \times 2.5 \times 4.95\ \mathrm{mm}^3$) according to the 4-point contact method using a Resistomat (TYP

2302 Burster**,** Gernsbach, Germany). The bars were cut from sintered discs by the mean of EDM and then were grounded to exact dimensions.

The elastic modulus (E) of the ceramic specimens was measured using the resonance frequency method [10]. The same bars used for electrical resistivity measurement, were used for E modulus measurement as well. The resonance frequency was measured by the impulse excitation technique (Model Grindo-Sonic, J. W. Lemmens N.V., Leuven, Belgium). The reported values are the mean and standard deviation of 10 measurements.

III. RESULTS AND DISCUSSION

A) NbC Powder Synthesis

Different powders with C/Nb ratio of 2.5 till 4.25 treated at different temperature from 1000°C to 1450°C and the resulted powders studied with SEM and XRD. SEM micrographs of some carburized powders are shown in Figure 3. The phases are mentioned on the pictures were defined by EDAX analysis. Figures 3a, 3b and 3c shows the result of carburizing of powder B (C/Nb:3) after 0.5, 5 and 10h heating at 1150°C. Theoretically reactions 1 and 2 can happen at this temperature (under 10^{-3} atm), but at practice, even after 10h dwell time, still graphite and NbO_x are present at powder mixture. This can be due to alternation of pressure in heating camper or kinetic of reaction. In Figure 3d, it is shown that NbO_x remains in powder D after 30min treating at 1350°C, but the powder treating at the same temperature for 5h shows no left over oxide. Figure 3f shows NbC grain growth in powder D treated at 1450°C for 30 minutes. This grain growth can be seen at Table 4 and figure 4. Finally at figure 3g and 3h, Treibacher commercial NbC powder is compared with optimum self-synthesized NbC_x (C/Nb:3.5 treated at 1350°C for 5h). As it can be seen, the grain size is more homogeneous and much smaller. The results of grain size measurements are shown graphically at figure 4. It is clear from the picture, that in 1450°C, NbC faces grain growth, but at 1350°C most of the grain sizes are in the range of 100-200 nm. XRD pattern of the most optimum carburizing powders and commercial NbC powder are shown in Figure 5. The most similar XRD pattern to commercial NbC is XRD pattern for powder E (C/Nb: 3.76) treated at 1350°C for 5h. There is not much NbO_x or carbon left over at this powder. The effect of Carbon left over is much more inferior for mechanical properties of composite compare to NbO_x. Hence two starting powder E (the best resulted powder and D, similar with less C amount in starting powders) treating at 1350°C for 5h were chosen for producing at higher amount for making composite.

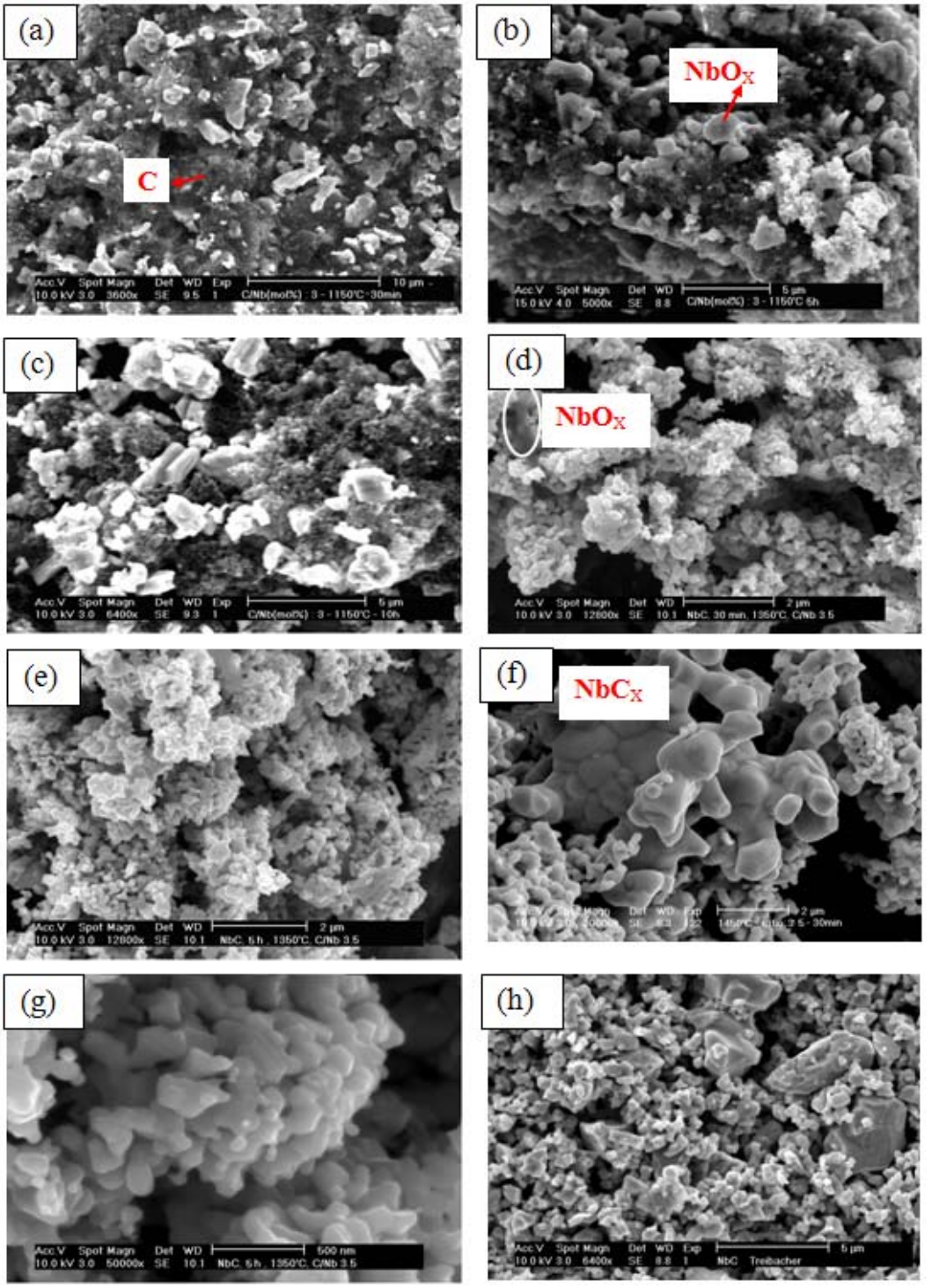

Figure 3. SEM micrograph of Nb_2O_5+C with C/Nb ratio of 3 heated at 1150°C for 30 min (a), 5h (b) and 10h (c) and C/Nb ratio of 3.5 heated at 1350°C (for 30 min (d) and 5h (e,g)) and 1450°C (for 30 min (f)) and commercial NbC powder (h).

Table 4. Grain size measurement for optimum synthesized NbC powders and Nb_2O_5 staring powder

Powder	1350-D-5h	1350-D-30min	1450-D-30min	Nb_2O_5
Grain size (nm)	Ave: 198 – d_{50}:185-d_{90}:335	Ave: 213 – d_{50}:225, d_{90}:490	Ave: 474 d50:339,d90:1	Ave: 1.24 d50:1.04,d90:2.08

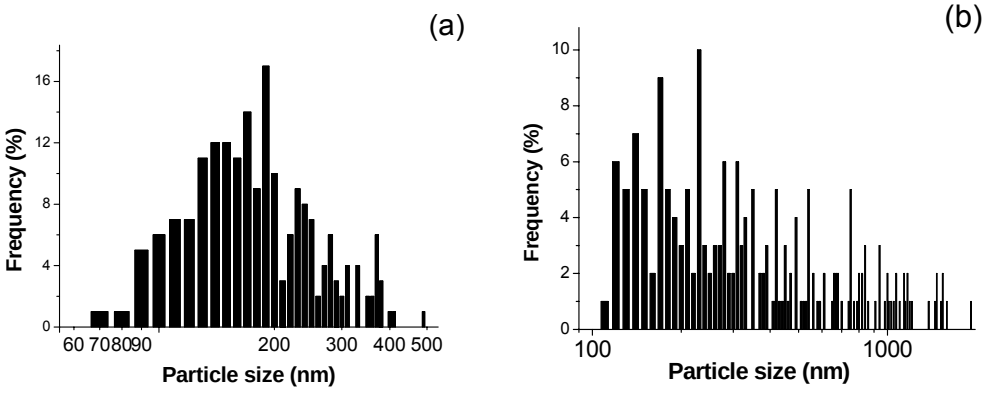

Figure 4. Grain size measurement results of Powder E synthesized at 1350°C-5h (a) and 1450°C-30 min (b).

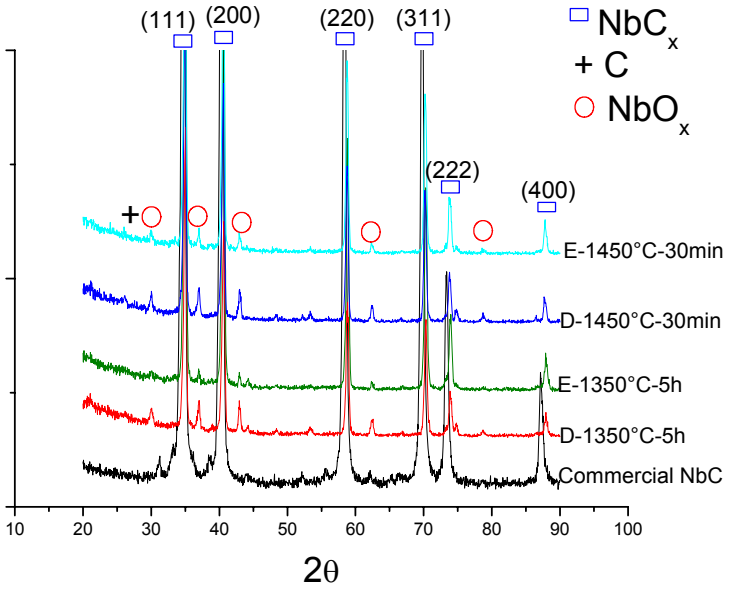

Figure 5. XRD pattern of commercial NbC and Nb_2O_5 + C with C/Nb ratio of 3.5 (D) and 3.76 (E) heat synthesized at 1350°C and 1450°C for 5h and 30 min respectively.

The importance of the stoichiometry on the mechanical properties of the ceramics is shown in Pierson work. Pierson was showed that some carbide like NbC and TaC have maximum hardness at certain stoichiometry, for example NbC shows maximum hardness (~25GPa) at $Nb_{0.8}C$ and hardness decrease till about 21 GPa at NbC [4]. Therefore stoichiometry of optimum carburized powders was calculated and was compared to commercial NbC. For non-stochiometric NbC_x, it was postulated and proved by D. Brown [10], that a number of carbon vacancies in the NbC lattice introduce a corresponding change in the inter-plane distance. This distance is reflected in the value of the lattice parameter (a). The ratio of (C:Nb) can be calculated, starting from the lattice parameter (a), with the use of below formula [Li et al, [9,10]].

$$a = 4.09847 + 0.71820\ (\mathrm{C:Nb}) - 0.34570\,(\mathrm{C:Nb})^2$$

Relation between NbC reflective planes and bragg angles, and the results of lattice parameter calculation and (C:Nb) determination is shown in Table 5.

Table 5. Relation between NbC reflective planes and bragg angles, the results of lattice parameter calculation and (C:Nb) determination

Miller Indiches			**Commercial NbC (Treibacher)**	**Mixture D 1350° 5 hours**	**Mixture E 1350° 5 hours**
h	k	L			
1	1	1	34.72	35.35	35.01
2	0	0	40.32	40.65	40.65
2	2	0	58.36	58.80	58.82
3	1	1	69.75	70.30	70.27
2	2	2	73.35	73.89	73.96
4	0	0	87.12	87.91	87.88
$(\alpha)_{ave}$			4.47	**4.43**	**4.44**
(C:Nb) ratio			0.96	**0.70**	**0.72**

The lattice parameters were calculated according to the method suggested by Suryanarayana and Grant [11].

$$a = \frac{\lambda * (h^2 + k^2 + l^2)^{0.5}}{2 * \sin\theta_{hkl}}$$

C/Nb ratio in powder D and E synthesized for 5h at 1350°C calculated to be 0.7. The maximum hardness can be achieved for $NbC_{0.8,}$ so it is expected that the hardness of composite made by optimum self-synthesized NbC powder should be more than the one made by commercial powder (with C/Nb ratio of 0.96).

B) Composite

The SEM micrograph of composites ZrO_2-NbC-TiN (65:30:5) stabilized with 3 mol% yttria, ZrO_2-NbC-TiN (50:45:5) stabilized with 4 mol% yttria and ZrO_2-NbC (50:50) stabilized with 4.5 mol% yttria is shown in Figure 6 a, b and c respectively. The name of phases which are written in the picture, were defined by EDAX analysis. The existence of TiCN phase in Figure 6a, confirms the formation of TiCN by TiN addition. The white phase in Figure 6a is WC which comes from Wc-Co milling ball in 48 h mixing step. The grey phase is yttria stabilized ZrO_2 and the bright phase is NbC_x. Residual carbon can be seen at figure 6b, although 5 vol% TiN added to composition to exclude residual carbon. It seems that 5 vol% TiN is enough to exclude carbon from a composition with 30 vol% NbC (6a), but is not enough to exclude carbon from a composition with 45 vol% NbC. Figure 5c shows that even 4.5 mol% yttria can not stabilized 50 vol% ZrO_2 in a composition without TiN addition. It seems that carbon existence act as a barrier for ZrO_2 stabilization. This fact can be also seen in XRD pattern of sintered samples (Figure 7). ZrO2 phase could not be stabilized in the samples without TiN addition even with 4 - 4.5 mol% Yttria addition.

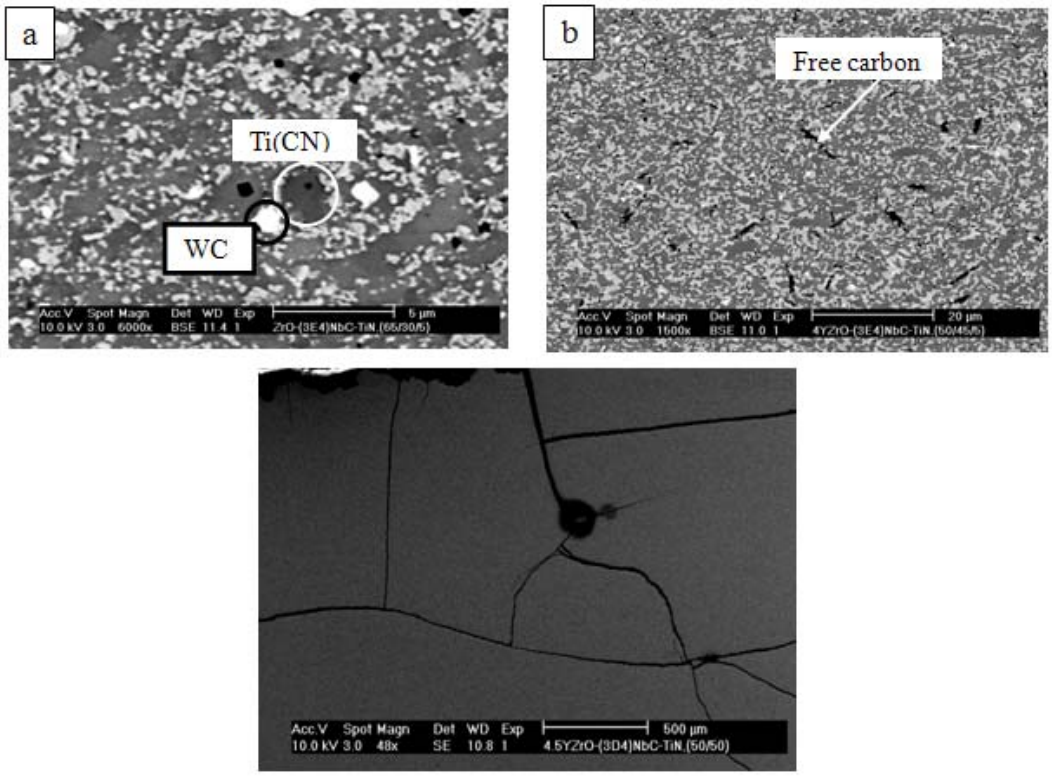

Figure 6. SEM photograph of sintered ceramic discs with ZrO_2-NbC-TiN 65:30:5 vol% (a) – and ZrO_2-NbC-TiN 50:45:5 vol% (b) and ZrO_2-NbC 50:50 vol% (c). The grey phase is ZrO_2 – the bright phase is NbC, the white and black phases are WC and AlO_x respectively.

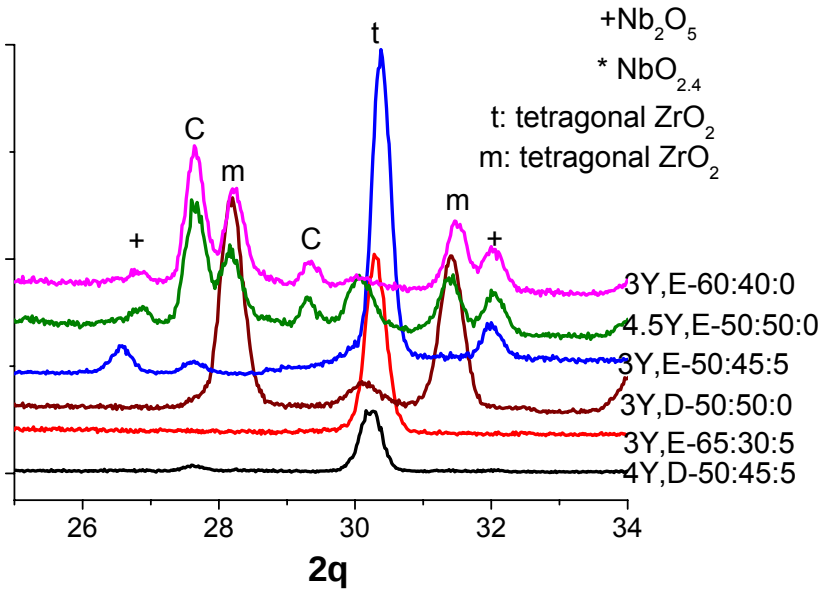

Figure 7. XRD pattern of sintered ceramic discs.

The mechanical properties of the discs made by self-synthesised powder are shown in Table 6. For comparative reasons a ZrO_2-NbC (60/40) vol% disc was made by commercial NbC powder (treibacher). The mechanical properties of this sample also are shown in this Table.

Table 6. (calculated) Young module, Hardness and Toughness of different compounds. The name of the compounds consists of mol% ytria - NbC code (table 2) ZrO:NbC:TiN Vol% -

Name	Relative density	H_v [Gpa]	K_{IC} [Mpa.m$^{0.5}$]	E [Gpa]
3Y - E 60:40:0	Cracked	8,78 + 0.11	5,2 + 0.3	260
3Y - E 65:30:5	0,99	15,82 + 0.13	4,9 + 0.2	257
3Y - E 50:45:5*	0,99	16,15 + 0.08	2,9 + 0.2	277
3Y - D 50:50:0	Cracked	10,89 + 0.04	6,1 + 0.1	273
4Y - D 50:45:5	0.99	15,99 + 0.1	3,7 + 0.3	277
4,5Y - E 50:50:0	Cracked	10,89 + 0.05	5,9 + 0.1	273
TTM2 – 60:40	99.59	13.64 + 0.07	5.4 ± 0.1	284

*: sample sintered at 1450°C while all the rest sintered at 1500°C.

The hardness of samples without TiN addition is so low. It is because the residual graphite in the sintered sample Figure 6b. In figure 6 a & b, It is shown that, 5 vol% TiN is enough to exclude carbon from a sample with 35 Vol% TiN but, it is not enough for a sample with 45 vol% NbC. The hardness of composites made by self-synthesis powder is higher than

the one made by commercial powder. The reason can be the smaller grain size of the self-synthesis powder, or the stoichiometry which is more suitable for having higher hardness.

The relative density of all the composite has been made was measured to be about 0.99% Theoretical density considering a density of 6.05, 7.85, 5.43 and 2.90 g/cm^3 for ZrO_2, NbC,TiN and Al_2O_3 respectively.

The resistivity of two discs 3Y-E 65:30:05 and 3Y-E 50:45:05 were measured. The measured datas are 0.81 and 2.49 $m\Omega.cm$ which is in the range of EDM machining [20,21]. This was confirmed by the fact that the blank specimens used for the the E modulus measurement were machined by means of wire-EDM (Robofil 240cc, Charmilles, Switzerland).

IV. SUMMARY

A carbothermal synthesis-method to produce nanosized NbC powder was developed. The optimal synthesis parameters were found to be a vacuum environment and a temperature of 1350°C, a reaction time of 5 hrs and a starting C:Nb ratio of 3,75. Higher synthesis temperatures results to NbC grain growth. The powder, generated by the carbothermal reduction of Nb_2O_5 was determined not to be stochiometric NbC, but it has a Nb:C ratio of 0.7. The measured grain size for optimum self-synthesized NbC powder is d_{50}:185 nm.

The addition of the self-synthesised NbC powder to an Y-ZrO_2 matrix , resulted in an insufficiently stabilised ZrO_2 matrix phase containing 66-100 vol% monoclinic zirconia. However, when 5 vol% TiN, acting as a carbon receptor, was added to the reaction mixture, the zirconia matrix could be stabilised, which was confirmed by XRD measurements on polished surfaces. The resulting ZrO_2-NbC-TiN composites combined an excellent Vickers hardness of 16 GPa (which is much higher than hardness of composite made with commercial NbC powder) and with a moderate toughness of 3-5 Mpa.m$^{1/2}$.

All processed ZrO_2-NbC-TiN composite materials had a sufficiently high electrical conductivity enough for being EDM machinable.

REFERENCES

[1] Abrasive wear of metallic matrix reinforced materials, R. Colaso, R.Vilar, *Wear*, (225) -2003 -643, 650

[2] Microstructural investigation of NbC-doped vacuum-sintered tool-steel-based composites, B. Sustarisc, M. jenko, M. Godec, L. Kosec; *Vacuum*, 71 (2003) 77-82

[3] Wear mechanisms in high speed steel reinforced with (NbC)p and (TaC)p MMECs, E. Gordo et al, Wear 239 (2000) 251-259

[4] Hugh O.Pierson,Noyes Publications, ISBN 0-8155-1392-5: "Handbook of Refractory carbides and nitrides"-page 67 & 70

[5] CAS #:12069-94-2, Hazardous data sheet, 1991

[6] A co-reduction synthesis of supersonducting NbC nanorods, Liang Shi et al., J. Phys. Candens. Matter 16 (2004) 8459-8464

[7] Jian-Bao Li; Gui-Ying Xu; Sun, E.Y.; et al. Synthesis and morphology of niobium monocarbide whiskers, *Journal of the American Ceramic Society*, vol.81, no.6 : 1689-91, June 1998

[8] Maitre, D. Tetard and P.Leford, Journal of the European Ceramic Society 20(2000) 15-22 (1999): "Role of some technological parameters during carburising titanium oxide"

[9] Storms.E.K.1967 Refractory materials Vol 2,ed J.L.Margrave (new York: Academic) P 65

[10] D. Brown, ''The chemistry of Niobium and Tantalum'' pp. 553-622 in Comprehensive Inorganic chemistry, Vol. 3, Edited by J. C. Bailer Jr., H. J. Edeleus, R. Nyholm, and A. F. Trotman-Dickenson. Pergamon Press, London, U.K., 1975

[11] Suryanarayana and M.G. Norton, X-ray Diffraction: A Practical Approach, Plenum Press, New York/London (1998).P 157.

[12] K. Niihara, R. Morena and D. P. H hasselman, Indentation fracture toughness of brittle materials for palmqvist cracks, Journal of Materials Science Letters, Volume 1, Number 1, January 1982 , 13 - 16

[13] Naumenko VY 1970 *Poroshk. Metall.* **10** 20

[14] Crayton H H and Gridly M C 1971 *Powder Met. Bull.* **14** 78

[15] Masumoto O and Saito M 1974 *High Temp. Sci.* **6** 135

[16] Oyama S T, Schlatter J C, Metcalfe J E and Lambert J M 1988 *Indust. Eng. Chem. Res.* **27** 1639

[17] Formation of NbC and TaC by solid-state reaction, Shiro shimada, Tadashi Koyoma, Kohei Kodaira and Taru Mastushita; Journal of material science 18 (1983) 1291-1296.

[18] M.I. Mendelson, Average grain size in polycrystalline ceramics, Journal of The American Ceramic Society , 1969, 52, 443-446.

[19] Anstis, G. R., Chantikul, P., Lawn, B. R. and Marshall, D. B., A critical evaluation of indentation techniques for measuring fracture toughness, Journal of The American Ceramic Society, 1981, 64, 533-538.

[20] König, W., Dauw, D.F., Levy, G., U. Panten, EDM - future steps towards the machining of ceramics, *Annals of the CIRP*, 1988, 37, 623-631.

[21] R.F. Firestone, Ceramic Applications in Manufacturing, SME, Michigan, 1988, 133.

[22] Electrically conductive ZrO_2-TiN composites, S. Salehi, O. Van der Biest and J. Vleugels, *J. Europ. Ceram. Soc.*

[23] Processing and Mechanical properties of ZrO_2-TiB_2 composites, B. Basu, J. Vleugels and O. Van Der Biest, *J. Europ. Ceram. Soc*., 25 (2005) 3629-3637

[24] Hard, tough and strong ZrO_2-WC composites from nanosized powders. G. Anné, S. Put, K. Vanmeensel, D. Jiang, J. Vleugels, O. Van der Biest, *J. Europ. Ceram. Soc*., 25, [1] (2005) 55-63.

[25] Development and characterization of Y_2O_3-stabilized ZrO_2 (Y-TZP) composites with TiB_2, TiN, TiC, and $TiC_{0.5}N_{0.5}$, J. Vleugels, O. Van Der Biest, *Journal of The American Ceramic Society*, 82 (10) (1999), 2717–2720.

In: Chemistry and Chemical Engineering Reserch Progress ISBN: 978-1-61668-502-7
Editor: A.K. Haghi

Chapter 12

ON THE PYROLYSIS OF POLYMERS AS A PETROCHEMICAL FEEDSTOCK RECOVERY ROUTE

S.M. Al-Salem [1,2]* and P. Lettieri[1]

[1] Centre for CO_2 Technology, Department of Chemical Engineering, University College London, Torrington Place, London WC1E 7JE, UK

[2] Petrochemical Processes Program Element, Petroleum Research and Studies Centre, Kuwait Institute for Scientific Research, P.O. Box: 24885, Safat 13109, Kuwait

ABSTRACT

The main reason behind the success of the petrochemicals industry is not only due to the vast array of products that it provides and are considered beneficial to our daily functions, but also in the added value that it brings to the value of the crude oil barrel, making it an unmistaken venture to any concerned party. Yet, the industry is faced with a fluctuating market and an unstable economy, which makes it imperative to find a more abundant and sustainable feedstock. Of all petrochemicals, polymers and their related industry posses the major share. This alternatively, makes the plastic industry a growing sector in processing and conversion terms. Both, virgin and waste plastic present themselves as an advantageous source of energy and product recovery. In this communication, the pyrolysis process is investigated as a product recovery process via both two modes of operation, *i.e.* isothermal and dynamic. Plastic solid waste (PSW) as a feed to thermo-chemical (in general) and pyrolysis (in particular) is a very promising alternative, either treated solely or via co-treatment with other municipal solid waste (MSW) streams. We also present an extensive review on the up-to-date literature related to the subject matter, presenting the four main routes of PSW treatment and recycling. Finally, we present two experimental case studies on the pyrolysis processes that reveal the main products, operation modes and specifications that could be utilized in reactor engineering and design. It is concluded that: (i) pyrolysis as a thermolysis process is a very promising way to treat virgin and waste polymers, which on the other hand illustrates a viable route of PSW recovery; (ii) the pyrolysis design is highly sensitive to the mathematical and numerical treatment of the obtained data in a laboratory scale;

* Author for correspondence (Current Address): Sultan Al-Salem, Department of Chemical Engineering, University College London (UCL). Tel: +44(0)207-679-7868, Fax: +44(0)-207-383-2348, e-mail: s.al-salem@ucl.ac.uk

finally (iii) micro studies (demonstrated by the case studies presented) still lack proper end-product process design, which is reflected on the current status of the process on an industrial scale.

1. INTRODUCTION

Polymers are the most versatile material in our modern day and age. With certain plasticizers and additives (*e.g.* pigments, concentrates, anti-blockers, light transformers (LTs), UV-stabilizers, etc.), they become what we know as plastics. Being a crude oil derivative, polymers present themselves as an advantageous option for a number of treatments. Polymers and polymeric articles converted and engineered for multi-purpose use have solely replaced classical construction materials in many sectors, namely wood and metals. Polymers and plastic reinforced composites also contribute to our daily functions in many aspects and applications, from packaging, automobiles, clothing, appliances and electrical and vehicle equipment, to insulations, industrial applications, greenhouses, automotive parts, aerospace and mulches.

Over the past seventy years, the plastic industry has witnessed a drastic growth, namely in the production of synthetic polymers represented by polyethylene (PE), polypropylene (PP), polystyrene (PS), polyethylene terephthalate (PET), polyvinyl alcohol (PVA) and polyvinyl chloride (PVC). Plastic materials production have reached global maximum capacities levelling at 150 million tonnes per year, where in 1990 production capacity was estimated at 80 million tonnes (Valavanidis et al., 2008). In 1996 the total plastics consumption in Western Europe was 33.4 million tonnes, whereas in the USA and in Japan 33.9 and 11.3 million tonnes; respectively. In the year 2004 the consumption of plastic material in Western Europe was 43.5 million tonnes, increasing by 4% per year. It is estimated that the production of plastics worldwide is growing at a rate of about 5% per year (APC, 2008). This results in high estimates of almost 60% of plastic solid waste (PSW) being discarded in open space or landfilled in many developing and developed countries (APM EU, 2008).

1.1. Polymers, Polymerization Technology and Plastic Solid Waste (PSW)

A track record of the innovations in the plastic conversion industry has driven a global average increase in production and consumption of about 9% every year since 1950. The total world production of plastics grew to 260 million tonnes in 2007 from a mere 1.5 tonnes in 1950 (Figure 1). An analysis of plastic materials consumption on a per capita basis shows that this has now grown to approximately 100 kg in the North America Free Trade Agreement (NAFTA) countries and Western Europe, with the potential to grow towards 140 kg per capita by 2015. The highest potential for growth can be found in the rapidly developing parts of Asia (excluding Japan), where currently the consumption per capita is only around 20 kg. In the European context, it is the new member states which are expected to see the biggest percentage increase as their economies develop. Their current average per capita consumption between 50 and 55 kg is a little more than half of that of the old Member States (Figure 2). The EU_{27}+Norway and Switzerland represent 25% of the world plastic production with about

65 million tonnes/year, slightly above the NAFTA states at 23%. With the EU, plastic production lines are well spread. Germany is the major producer, accounting for 7.5% of the world production capacity. Whilst France, Italy, Spain and the UK account for 3, 2, 1.5 and 1.5%, respectively.

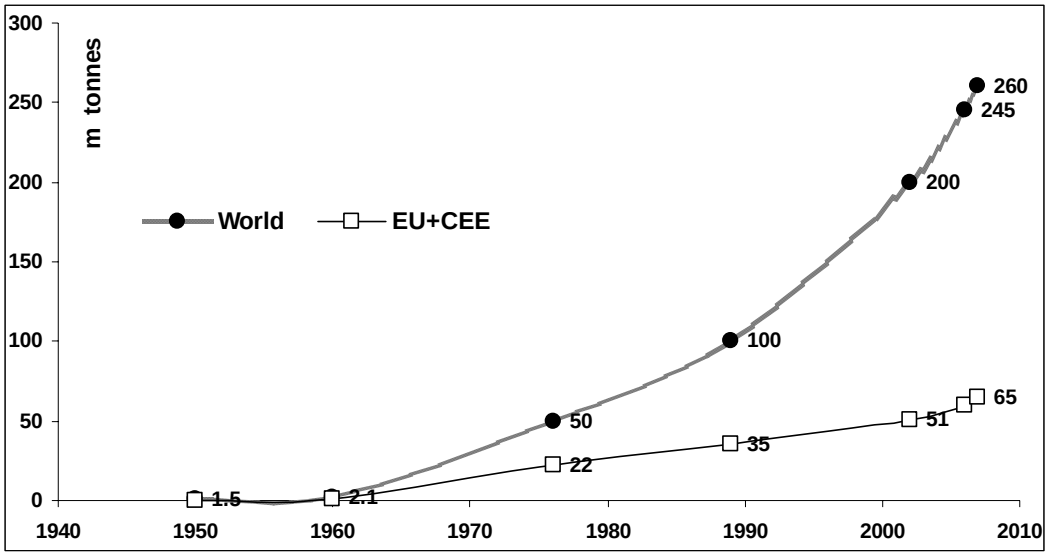

Figure 1. World and Europe plastic production (1950-2007). Source: PEU, 2008. Includes thermoplastics, PU, thermosets, elastomers, adhesives, coatings, sealants and PP fibres. PET, PA and polyacryl-fibres were excluded.

Latin America accounts for 4% of the global production capacity, whilst the Middle East and Africa account for 8%. Plastics demand by converters in EU_{27} + Norway and Switzerland was 52.5 million tonnes in 2007. The demand expressed as tonnage of virgin resin processed by European converters by country shows that Germany and Italy account for 40% of the EU conversion capacity. Of the new Member States, Poland has the highest plastic conversion, currently at about 2.35 million tonnes of the European total. The Czech Republic and Hungary are each at about half this level. It is expected that the converting industries in most of the new Member States will grow strongly in the coming years (PEU, 2008). In 2008, a revised waste framework directive (WFD) was introduced in the EU. The WFD provides a framework to drive waste management practices in the EU. The revision was badly needed to bring legal clarity in a number of important areas. In summary the revised WFD provides a strong drive for resource efficiency and diversion of waste from landfill. A landmark change introduced by the WFD is that efficient energy from waste (efw) will now be classified as recovery rather than disposal, and as it is above landfilling it will create strong drivers in society. Also, a climate correction factor will be defined to ensure that countries with warmer climates will still have a good opportunity to meet the energy efficiency criteria. Broadly-speaking, the revised WFD will provide a framework which will enable improved recycling of plastics (both mechanical and chemical) via innovative, eco-efficient technologies. High-calorific waste plastics will be important to help *efw* plants meet the efficiency criteria set for classification as recovery. Innovative new plastics-enabled solutions will save resources through applications such as packaging, both by reducing waste and by light-weighting the

packaging itself. Plastics are resource-efficient materials and will play a key role in driving a resource-efficient Europe.

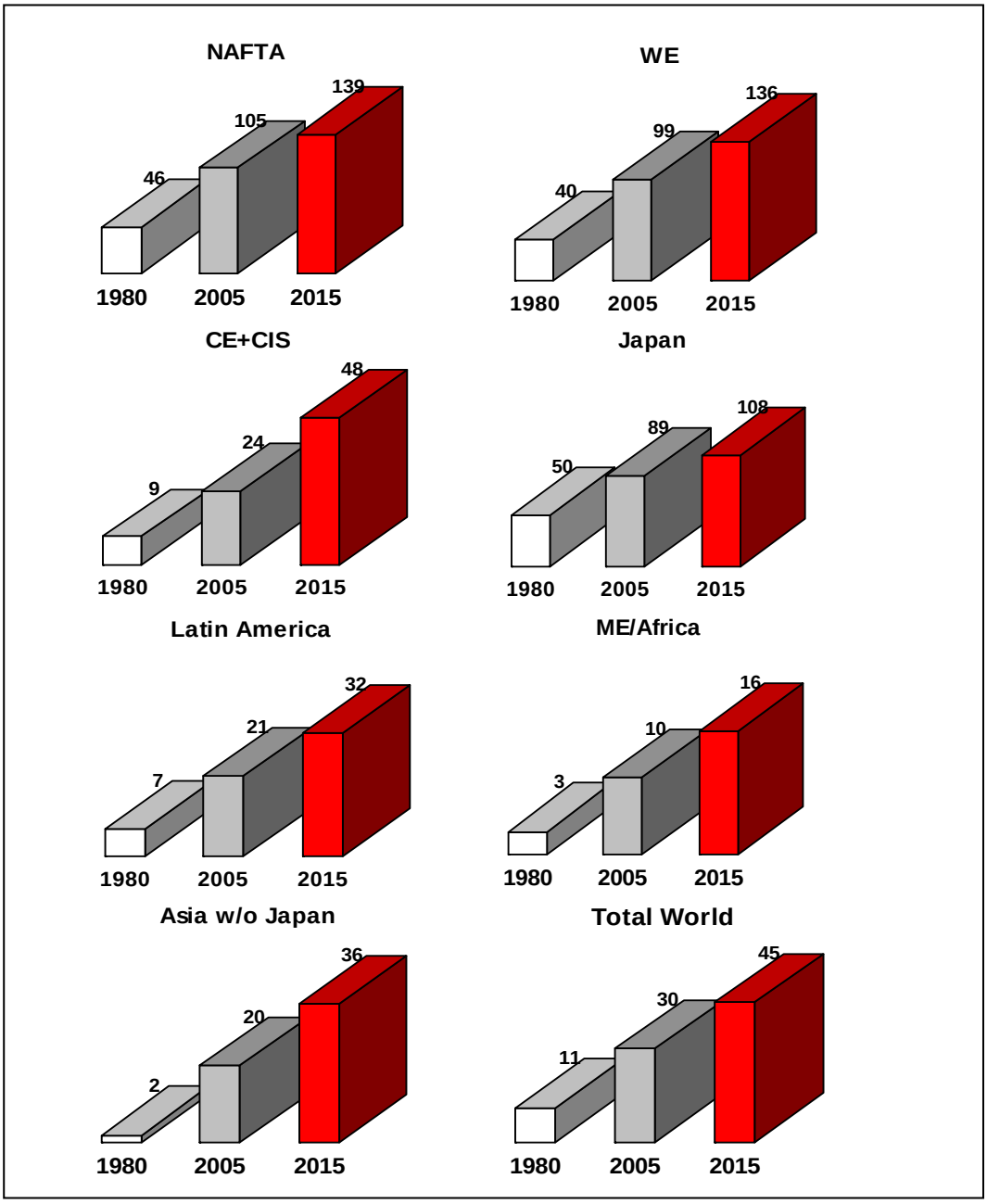

Abb. NAFTA, North American Free Trade Agreement; CIS, Commonwealth of Independent States; WE, West Europe; ME, Middle East.

Note: 2015 data used are projection figures from the same source.

Figure 2. Plastic demand by converters per capita per region. Source: PEU, 2008.

Another aspect of the revised WFD was the enforcement of the waste hierarchy and its implementation within the EU states. The hierarchy for improving resource efficiency is (in descending priority order): reduce, reuse, recycle, recover and disposal. Plastics save energy and CO_2 emissions during the use phase. If we were to substitute all plastics in all applications with the prevailing mix of alternative materials, and look from a life cycle perspective, then 24 million additional tonnes of crude oil would be required every year. The corresponding greenhouse gas emissions are equivalent to 30% of the EU_{25} Kyoto target for 2000-2012 (PEU, 2008). Plastics contribute to waste minimisation by offering more and more resource-effective solutions, including lower energy consumption during production, a reduction in the plastics material needed to do a particular job and less waste of the packaged goods, whether it is food or water or a computer. Examples include ever-lighter bottles for water, soft drinks or detergents or thinner film for packaging. Plastics are re-used in a number of areas. Plastics bottles are re-used in deposit systems in a number of member states, many of us reuse the carrier bag for a variety of needs, and plastics trays used in supermarkets offer a clean, robust and cost-effective way of moving vegetables, bread or fish from producer to customer. The recycling of plastics is increasing year by year. In addition to the well known applications such as bottles and industrial packaging film, new important developments are ongoing, like the Recovinyl initiative under the Vinyl 2010 programme of the PVC industry (covering pipes, window frames, roofing membranes, and flooring). Another stream which is explored in a number of member states is the "*mixed packaging plastics*". This important development must continue and we must drive towards realising the full potential of existing recycling streams as well as opening up new eco-efficient streams for recycling.

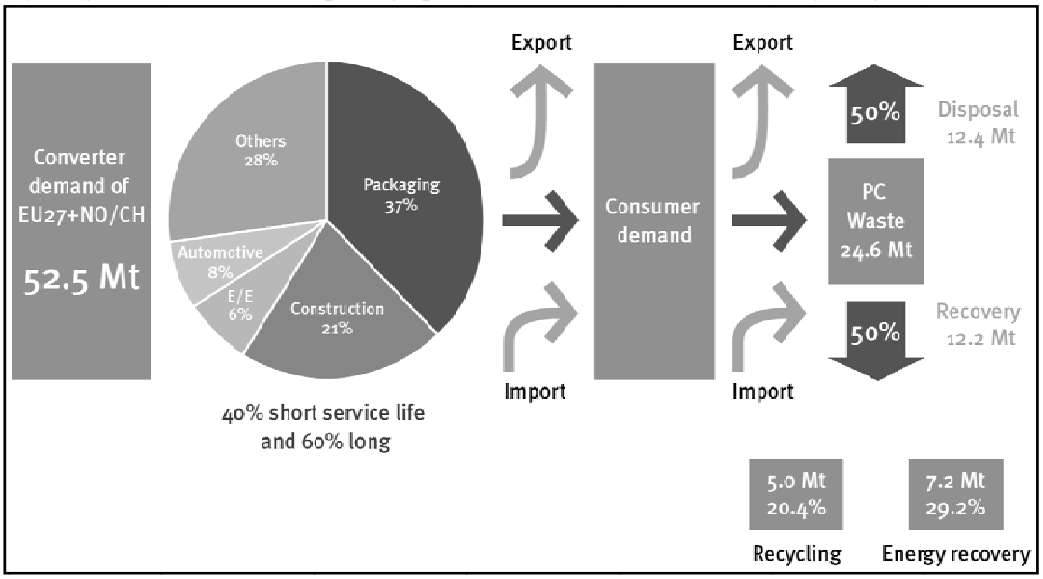

Source: PEU, 2008. Abb. PC, Petrochemical.

Figure 3. Plastic materials from cradle to grave in the EU_{27}+Switzerland and Norway.

However even after including these growing applications there will be residual streams which are not appropriate to mechanically recycle in an eco-efficient way. For these streams plastics offer an additional recovery option, i.e. energy recovery and thermolysis. As long as we use fossil fuels for energy production, plastics will offer an additional value to society as

plastics enable many vital applications during the life cycle of these hydrocarbon molecules on their journey from oil well to energy source. Landfill or disposal must be minimised as it wastes a valuable resource and contributes to greenhouse gas formation. Figure 3 illustrates the flow of plastics from conversion to the end-of-life phase. The data is valid for EU_{27}+Norway and Switzerland.

Converters used 52.5 million tonnes of plastics in 2007, with an increase of 3% compared to 2006. Of all plastics used by consumers, 24.6 million tonnes ended up as post-consumer waste, up from 23.7 million tonnes in 2006. 50% of the post-consumer used plastic was recovered and 50% went to disposal. Of the quantity recovered, 5 million tonnes were recycled (as material and feedstock) and 7.2 million tonnes were recovered as energy. The overall material recycling rate of post-consumer plastics in 2007 was 20.4%, with mechanical recycling at 20.1% (up 1.2% points from 2006) and feedstock recycling at 0.3% (down 0.3% points from 2006). The energy recovery rate remained stable at 29.2% reflecting how the sensitivity and planning complexity of this resource management technology has led to slow progress in society. In 2007, 12.4 million tonnes of plastics were wasted in landfill. Despite a 3 % per year growth over the past decade for post-consumer waste the quantity going to landfill has remained stable.

The growth of post-consumer plastic waste is the result of several drivers. Plastics continue to substitute alternative materials, economic growth drives greater consumption, smaller households require more packaging per person and more ready-made single-portion meals are consumed. Over the last decade the average annual growth rate of plastics in the EU has been about 10%. Mechanical recycling quantity saw another good increase of 1% in 2007 which is explained by higher plastic prices and improved collection and sorting technology. Growth in energy recovery quantity slowed to 3% as very little capacity was added in 2007. More investment in monomer, valuable chemicals and energy recovery facilities is needed to divert streams which cannot be eco-efficiently recycled from landfill. The material recycling and energy recovery of post-consumer plastics waste varies significantly by country. In some countries like Switzerland, Germany, Sweden and Denmark there is very little landfill -these countries are very close to completing their diversion-from-landfill strategy. A recent study by the Swiss consultancy Prognos showed that 27% of the EU Kyoto target for greenhouse gas (GHG) emissions could be saved if all waste currently going to landfill was to be diverted flexibly to recycling and energy recovery. The best results were achieved without specific targets but with full flexibility to explore recycling and energy recovery where it best served the specific waste stream. In addition to saving GHG emissions, diversion from landfill contributes to increased resource efficiency and energy security while reducing littering. One major observation from recent estimates is that countries with high recovery rates do well on both recycling and energy recovery. Therefore, it can be assumed that a strategy including energy recovery is not contradictory to achieving good recycling results. It simply illustrates that a complete resource management strategy needs to address both, as no country will be able to recycle all post-consumer waste. The other observation that could be withdrawn from recent estimates is that recycling performance is fairly similar across most of the EU_{27}+NO/CH countries there are huge differences in the utilisation of energy recovery. Countries which have high dependence on landfill must not only exploit their full recycling potential but rapidly expand their energy-from waste network. The progress of the diversion from landfill is slow on average with recycling (mechanical and chemical) across EU_{27}+NO/CH increasing from 19.5% in 2 006 to 20.4% in 2007 while

energy recovery remained stable at 29.2%. Strong efforts will be required in many Member States to capture the full potential offered by a diversion from landfill strategy, namely GHGs emission savings, enhanced resource efficiency and energy security and the avoiding of landfill penalties.

1.2. Routes of Recycling, Recovery and Treatment

Plastics, as waste articles, are found in all major municipal solid waste (MSW) categories. PSW in found to be comprised mainly of a number of articles, namely containers and packaging plastics (bags, sacks, and wraps, other packaging, other containers, and soft drink, milk, and water containers). These articles represent the highest percentage in the final assessed stream of MSW (USEPA, 2002; USEPA, 2008). In durable goods, plastics are found in appliances, furniture, casings of lead-acid batteries, and other products. In the UK, recent studies show that PSW make up 7% of the final waste stream (Parfitt, 2002). In the European Union countries, over 250 x 10^6 tonnes of MSW is produced each year, with an annual growth of 3%. In 1990, each individual in the world produced an average of 250 Kg of MSW generating in total 1.3 x 10^9 tonnes of MSW (Beede and Bloom, 1995). Ten years later, this amount almost doubled levelling at 2.3 x 10^9 tonnes. In US, PSW found in MSW has increased from 11% in 2002 (USEPA, 2002) to 12.1 % in 2007 (USEPA, 2008).

Increasing cost and decreasing space of landfills are forcing considerations of alternative options for PSW disposal. Years of research, study and testing have resulted in a number of treatment, recycling and recovery methods for PSW that can be economically and environmentally viable (Howard, 2002). The plastic industry has successfully identified workable technologies for recovering, treating, and recycling of waste from discarded products. In 2002, 388,000 tonnes of PE were used to produce various parts of textiles, of which 378,000 tonnes were made from PE discarded articles (Gobi, 2002).

The continued development of recycling and recovery technologies, investment in infrastructure, the establishment of viable markets and participation by industry, government and consumers are all considered priorities of the highest order (Scheirs, 1998). A Life Cycle Assessment (LCA) approach to MSW technologies will assist in identifying environmental impacts associated with the alternatives in a '*cradle to grave'* fashion identifying the most sustainable options. 90% of plastics used today are synthesized using non-renewable fossil resources. It is essential to integrate waste management schemes in the production cycle of plastics and treatment schemes of PSW. Whilst recycling is considered a sustainable practice, implying an integrated waste management (IWM) scheme provides a more sustainable developed use of energy and supplies. PSW treatment and recycling processes could be allocated to four major categories (Mastellone, 1999), re-extrusion (primary), mechanical (secondary), chemical (tertiary) and energy recovery (quaternary). Each method provides a unique set of advantages that make it particularly beneficial for specific locations, applications or requirements. Mechanical recycling (*i.e.* secondary or material recycling) involves physical treatment, whilst chemical recycling and treatment (*i.e.* tertiary encompassing feedstock recycling) produces feedstock chemicals for the chemical industry. Energy recovery involves complete or partial oxidation of the material (Troitsch, 1990), producing heat, power and/or gaseous fuels, oils and chars besides by-products that must be disposed of, such as ash.

Primary recycling, better known as re-extrusion, is the re-introduction of scrap, industrial or single polymer plastic edges and parts to the extrusion cycle in order to produce products of the similar material. This process utilizes scrap plastics that have similar features to the original products. Primary recycling is only feasible with semi-clean scrap, therefore making it an unpopular choice with recyclers. A valid example of primary recycling is the injection moulding of out of specification LDPE crates (Barlow, 2008). Crates that do not meet the specifications are palletised and reintroduced into the recycling loop or the final stages of the manufacturing. Currently, most of the PSW being recycled is of process scrap from industry recycled via primary recycling techniques. In the UK, process scrap represents 250,000 tonnes of the plastic waste and approximately 95% of it is primary recycled (Parfitt, 2002). Primary recycling can also involve the re-extrusion of post consumer plastics. Generally, households are the main source of such waste stream. However, recycling household waste represents a number of challenges, namely the need of selective and segregated collection. Kerbside systems are required to collect relatively small quantities of mixed PSW from a large number of sources. This poses a resource drain and involves significant operating costs in many countries, especially considering the current market situation. Taking into account current market prices for virgin resins, a 0.45 $ is the return on average from every converted Kg of polyolefin (EEC, 2009, Al-Salem et al., 2009a).

Mechanical treatment, also known as secondary recycling, is the process of recovering PSW for the reuse in manufacturing plastic products via mechanical means (Mastellone, 1999). It was promoted and commercialized all over the world back in the 1970s. Separation, washing and preparation of PSW are all essential to produce high quality, clear, clean and homogenous end products. Due to the previously stated reasons, it is very important to have a customer ready to purchase the product to achieve a sensible economical and environmental practice. Nevertheless, mechanical recycling opens an economic and viable route for PSW recovery, especially for the case of foams and rigid plastics (Zia et al., 2007). A number of products found in our daily lives come from mechanical recycling processes, such as grocery bags, pipes, gutters, window and door profiles, shutters and blinds, etc. The quality is the main issue when dealing with mechanically recycled products. The industrial PSW generated in manufacturing, processing, and distribution of plastic products is well suited for the use as a raw material for mechanical recycling due to the clear separation of different types of resins, the low level of dirt and impurities present, and their availability in large quantities.

In the European Union, collection rate for mechanical recycling of post-consumer plastics waste increased 1% over 2006 to 20.1% in 2007. This represents an increase of 0.5 million tonnes, giving EU_{27}+NO/CH a total of 4.9 million tonnes. This increase is fuelled by higher polymer prices and improved collection and sorting technology. The recycling capacity of the European recycling industry is estimated to be still higher to enable all collected material to be treated in Europe. A big part of this increase was achieved through the increase in packaging streams such as PET bottles, industrial packaging film and PVC products via the programme Vinyl 2010. As there is still the potential to collect more from these streams across Member States, it is important to continue efforts to drive these streams towards their full potential. Crates and pallets are two streams where recycling is well above 90%. This successful "*closed loop*" is threatened by changes in the EU legislation linked to the heavy metal content of these products. Without the derogation extension to continue to recycle and keep the heavy metals safely in the plastic. A huge quantity of recyclable plastics could become obsolete. Industry is working towards a controlled scheme to monitor the renewal of

the derogation. In addition, countries like the UK are seeking increased recycling from the mixed plastics stream (*i.e.* the household plastics stream excluding bottles). The plastics industry is engaged in this initiative and supports extended eco-efficient recycling. However, infrastructure and demography varies across Member States, and therefore solutions will not be the same in different countries. For example Austria and the Netherlands have taken the opposite decision to the UK and decided not to collect mixed plastics but instead to recover this stream through energy recovery.

Chemical (tertiary) treatment is a term used to refer to advanced technology processes which convert plastic materials into smaller molecules, usually liquids or gases, which are suitable for use as a feedstock for the production of new petrochemicals and plastics (Mastellone, 1999). Almost no argument exist that the best utilization of PSW is via tertiary treatments, *i.e.* chemical recycling. The term chemical is used; due to the fact that an alteration is bound to occur to the chemical structure of the polymer. Products of chemical recycling have proven to be useful as fuel. The technology behind its success is the depolymerization processes that can result in a very profitable and sustainable industrial scheme, providing a high product yield and minimum waste. Under the category of chemical recycling advanced process (similar to those employed in the petrochemical industry) appear, *e.g.* pyrolysis, gasification, liquid-gas hydrogenation, viscosity breaking, steam or catalytic cracking and the use of PSW as a reducing agent in blast furnaces. Recently, much attention has been paid to chemical recycling (mainly non catalytic thermal cracking (thermolysis), catalytic cracking and steam degradation) as a method of producing various fuel fractions from PSW.

By their nature, a number of polymers are advantageous for such treatment. PET and certain polyamides (nylon 6 (PA 6) and nylon 66) can be efficiently depolymerised. In particular, PE has been targeted as a potential feedstock for fuel (gasoline) producing technologies. There is also a growing interest in developing value added products such as synthetic lubricants via PE thermal degradation. The development of value added recycling technologies is highly desirable as it would increase the economic incentive to recycle polymers (Horvat, 1996). Several methods for chemical recycling are presently in use, such as direct chemical treatment involving gasification, smelting by blast furnace (Asanuma and Ariyama, 2004) or coke oven (Kato et al., 2004), and degradation by liquefaction (Steiner et al., 2002). Condensation polymers such as polyethylene terephthalate (PET) and nylon undergo degradation to produce monomer units, *i.e.* feedstock or monomer recycling (Yoshioka et al., 2004), while vinyl polymers such as polyolefins produce a mixture containing numerous components for use as a fuel. Various degradation methods for obtaining petrochemicals are presently under investigation, and conditions suitable for pyrolysis and gasification are being researched extensively (Aguado et al., 2007). Catalytic cracking and reforming facilitate the selective degradation of waste plastics. The use of solid catalysts such as silica-alumina, ZSM-5, zeolites, and mesoporous materials for these purposes has been reported. These materials effectively convert polyolefins into liquid fuel, giving lighter fractions as compared to thermal cracking.

The main advantage of chemical recycling is the possibility of treating heterogeneous and contaminated polymers with limited use of pre-treatment. If a recycler is considering a recycling scheme with 40% target or more, one should deal with materials that are very expensive to separate and treat. Thus, chemical recycling becomes a viable solution (Scheirs, 1998). Petrochemical plants are much greater in size (6-10 times) than plastic manufacturing

plants. It is essential to utilize petrochemical plants in supplementing their usual feedstock by using PSW derived feedstock.

Last route of recycling and recovery is energy recovery, which by definition, implies burning waste to produce energy in the form of heat, steam and electricity. This is only considered a very sensible way of waste treatment, when material recovery processes fail due to economical constrains. Plastic materials possess a very high calorific value (when burned); especially when considering that they are derived from crude oil. Table 1 illustrates the calorific value of a number of single polymer plastics, compared to oil and PSW. Since the heating value of plastics is high, they make a convenient energy source. Producing water and carbon dioxide upon combustion make them similar to other petroleum based fuels (Dirks, 1996).

Table 1. Calorific value of major polymers in comparison to common fuels

Item	Calorific value (MJ Kg^{-1})
Polyethylene (PE)	43.3-46.5
Polypropylene (PP)	46.50
Polystyrene (PS)	41.90
Kerosene	46.50
Gas oil	45.20
Heavy oil	42.50
Petroleum	42.3
Household PSW mixture	31.8

Source: Williams and Williams, 1997; Mastellone, 1999.

In general, it is considered that incineration of PSW results in a volume reduction of 90-99%, which reduces the reliability and burden on landfilling. In the process of energy recovery, the destruction of foams and granules resulting from PSW also destroys CFCs and other harmful blowing agents present (Zia et al., 2007). Yet again, the presence of FRs complicates the technical aspects of energy recovery receiving much of the attention nowadays.

2. PYROLYSIS MODES, OPERATION AND ADVANTAGES

Thermal degradation processes allow obtaining a number of constituting molecules, combustible gases and/or energy, with the reduction of landfilling as an added advantage (Mastral et al., 2007). The pyrolysis process is an advanced conversion technology that has the ability to produce a clean, high calorific value gas from a wide variety of waste and biomass streams. The hydrocarbon content of the waste is converted into a gas, which is suitable for utilisation in either gas engines, with associated electricity generation, or in boiler applications without the need for flue gas treatment. This process is capable of treating many different solid hydrocarbon based wastes whilst producing a clean fuel gas with a high calorific value. This gas will typically have a calorific value of 22-30 MJ m^{-3} depending on the waste material being processed. The lower calorific value is associated with biomass

waste, the higher calorific value being associated with other wastes such as sewage sludge. Gases can be produced with higher calorific values when the waste contains significant quantities of synthetic materials such as rubber and plastics. Solid char is also produced from the process, which contains both carbon and the mineral content of the original feed material. The char can either be further processed onsite to release the energy content of the carbon, or utilised offsite in other thermal processes. Pyrolysis has been investigated as a viable route of recycling by a number of researchers for the case of PSW treatment, or other waste including biomass (Ray et al., 2004) and rubbers (Yang et al., 2004; Al-Salem et al., 2010).

The development and expansion of the petrochemical industry in recent years have been characterized by a concentration of production and an increase in the size of individual process units and process sections. Along with the use of larger process units, came an improvement in the production economics, with more favourable conditions for the combined utilization of raw material resources, including by-products and wastes. At the same time, the concentration of petrochemical production has led to problems in raw material supplies. Only the largest petroleum refineries can serve as a stable source of feedstock. However, the lack of any such refineries in many districts has created a need for setting up an autonomous raw material base equipped with specialized production units or refineries for primary crude oil processing with the specific purpose of producing petrochemical feedstocks. It is difficult to produce large amounts of naphtha from pyrolysis (cracking) within the ranks of the existing fuel profile refineries. Integrating upstream, downstream and end of stream processing in many production cycles will, evidently, aid in the supply chain and demand coverage. Many products from thermo-chemical (in general) and pyrolysis (in particular) can serve the industry in a number of refinery cut replacement.

Pyrolysis provides a number of other advantages, such as (i) operational advantages, (ii) environmental advantages and (iii) financial benefits. Operational advantages could be described by the utilization of residual output of char used as a fuel or as a feedstock for other petrochemical processes. An additional operational benefit is that pyrolysis requires no flue gas clean up as flue gas produced is mostly treated prior to utilisation. Environmentally, pyrolysis provides an alternative solution to landfilling and reduces greenhouse gas (GHGs) and CO_2 emissions. Financially, pyrolysis produces a high calorific value fuel that could be easily marketed and used in gas engines to produce electricity and heat. Several obstacles and disadvantages do exist for pyrolysis though, mainly the handling of the char produced (Ciliz, 2004) and the treatment of the final fuel produced, if specific products are desired**.** In addition, there is not a sufficient understanding of the underlying reaction pathways, which has prevented a quantitative prediction of the full product distribution.

2.1. Pyrolysis in Literature: Depolymerization Processes and Weight Loss Kinetics

Understanding the behaviour of polymeric and lignocellulosic materials during their thermal decomposition in the presence of inert (i.e. nitrogen, helium, etc.) and partial oxidative atmospheres is important because this knowledge can be applied to pyrolysis, combustion and other thermal processes studies. The thermal decomposition of polymeric and lignocellulosic materials is a complex process which involves a number of chemical reactions as well as physical stages such as heat and mass transfer (Bilbao et al., 1997a). The presence

of oxygen can cause an oxidative degradation of the material and the subsequent oxidation of the volatile released during this degradation and of the char residue. These reactions add further complexity to the already complex process of thermal decomposition, hence the need of a better understanding of thermal decomposition behaviour under inert atmospheres. On the whole, similar results were obtained for samples with different densities, *i.e.* 25 kg m^{-3} was chosen as a representative sample discarding the effect of density. Significant differences were observed between the degradation in air and nitrogen atmospheres. Higher solid conversion (x_s) was obtained with gasification experiments than pyrolysis, which was attributed to the low heating rate (β = 5 ^{o}C min^{-1}) used. The evolution of solid conversion, in terms of x_s, and dx_s/dt, with temperature in a nitrogen atmosphere was also investigated. Two temperature ranges for which significant solid conversion variation occurs can be appreciated. The first range corresponds to a conversion of a value of about 0.30, starting at about 200 °C and extending to 310 °C with the maximum conversion variation occurring at about 280 °C. There is a subsequent temperature range for which the solid conversion variation is low. But this conversion starts to increase again from 325 °C. This increase extends until 400 ^{o}C, the maximum variation of solid conversion occurring at about 370 °C. In a follow up study, Bilbao et al. (1996b) investigated the influence of moisture content on the thermal decomposition of wood under pyrolysis conditions. Using experimental results of temperature profiles and solid conversion for different moisture contents, the heat fluxes have been obtained. An acceptable agreement was found by the results obtained and the mathematical model proposed by the authors investigating the behaviour of the samples in nitrogen atmosphere. Bilbao et al. (1997b) have also investigated the pyrolysis and partial oxidation behaviour of pine samples under dynamic conditions with a β value of 12 ^{o}C min^{-1}. As many previous researchers did (Bilbao et al., 1996a, 1996b, 1997a, 1997b, Ceamanos et al., 2002), they have defined the solid conversion of the material (x_s) as follows:

$$x_s = \frac{W_i - W_t}{W_i} \tag{1}$$

where W_t is the solid weight at a time t and W_i is the initial solid weight, dry basis.

Bilbao et al. (1996a) obtained values of the overall kinetic rate constant for the dynamic thermal decomposition of PU in a wide temperature range. The k_β values have been calculated from the following equation:

$$k_\beta = \frac{dx_s / dt}{A_s - x_s} \tag{2}$$

where A_s is the solid weight fraction, t is time (min), x_s is the solid conversion, β is the heating rate (^{o}C min^{-1}) and k_β is the dynamic rate constant (min^{-1}).

The variation of k_β with the temperature corresponding to a β = 5°C min^{-1} showed three distinct peaks corresponding to temperatures ranging between 200 and 240 ^{o}C, 240 and 282 °C and 315 and 393 °C respectively. The kinetic constant values have been fitted to an

Arrhenius equation of the 1st order. Therefore the kinetic constants obtained for a heating rate of 5 °C min^{-1} are as follows:

$$k_\beta = 39.\exp(-\frac{6860}{RT}) \qquad ; 200 < T < 240\,^oC \tag{3}$$

$$k_\beta = 1.07\times10^5.\exp(-\frac{15066}{RT}) \qquad ; 240 < T < 282\,^oC \tag{4}$$

$$k_\beta = 9.4\times10^{13}\exp(-\frac{43070}{RT}) \qquad ; 315 < T < 393\,^oC \tag{5}$$

It was observed that, for a given temperature, the kinetic constant obtained from a dynamic experiment is higher than that calculated from an isothermal experiment.

2.2. Current Industrial Status

An engineering approach to improve the overall waste incineration efficiency is to separate pyrolysis from actual combustion and burnout processes of the waste (Malkow, 2004). In industrial scale schemes, external separation is required whilst pyrolysis reactor products are fired (e.g. char, waxes, etc). One of the main technologies incorporated by a number of plants in Austria, Germany, Korea, Italy and Switzerland, is the PYROPLEQ® process. This technology (dominant in the period between 1978 to1996) is based on pyrolysis at 450-500 ^oC in an externally heated rotary drum and gas combustion at 1200 ^oC. Typical feed to the process is PSW (post consumer mixtures), although the process was proven successful for other MSW streams.

A different process which has proven to be successful for PSW, rich in PVC, is the Akzo process (Netherlands) (Tukker et al., 1999). With a capacity of 30 kg/hour, this fast pyrolysis process is based on a circulating fluidised bed system (two reactors) with subsequent combustion. Input to the process is shredded mixed waste including a high percentage of PVC waste. The main outputs consist of HCl, CO, H_2, CH_4 and, depending on the feedstock composition, other hydrocarbons and fly ash. The ConTherm® technology treats MSW and automotive shredder residues (ASR) as well as up to 50% PSW at 500–550 ^oC in 100 kt/year rotary kilns supplied by TECHNIP and combusts the gas directly in a pulverised coal (PC)-fired boiler (Malkow, 2004). Residues from the process are screened and sorted to recover materials, mainly metals. The NRC (National Research Council of Canada) process is another successful pyrolysis scheme. This process is based on the pyrolysis with subsequent metal extraction technology. The aim is to produce purified calcium chloride instead of HCl. The input to the process is PVC waste (cables, flooring, profiles, etc.). No other PSW type is fed to the processing, which results in calcium chloride, coke, organic condensate (for use as fuels) and heavy metals for metal recycling, as products. PKA pyrolysis is another type of pyrolysis process technology, described previously by Malkow (2004). The technology comprises a modular pyrolysis and gasification concept at high temperatures. The process

starts with a pre-processing step involving separation, screening and shredding of different kind of wastes such as MSW, ASR, ELTs, industrial and plastic waste as well as contaminated soil. The pyrolysis takes place at 500 to 550 ^{o}C for about 45 to 60 min in an externally heated rotary kiln. The yield is a de-dusted and homogenised CO/H_2 rich fuel gas. Char containing minerals and metals are conditioned by separating ferrous and non-ferrous metals, reduced in moisture to <10% and ground to < 2 mm before being used as a fuel, a sorbent (*i.e.* activated carbon) or a raw material in brick production (Malkow, 2004). The PyroMelt process (developed by ML Entsorgungs und Energieanlagen GmbH) combines pyrolysis and slagging combustion yielding an eluation-resistant, recyclable granulated slag (Juniper, 2005). The feed to the process consists of MSW, hazardous waste, ASR and post consumer plastic waste. Pyrolysis takes place prior to the combustion process and the resulting gas is subjected to multiple scrubbing steps using pyrolysis oil. This process cools the gas from the range of 500 to 600 ^{o}C down to 120 to 150 ^{o}C. However, the char is cooled to 50 ^{o}C and jointly combusted with a slurry composed of dust and heavy pyrolysis oils in a melt furnace.

One of the most important pyrolysis processes is the BP polymer cracking process (Tukker et al., 1999). After a series of pilot trails (between 1994 to 1998), a plant was established in Scotland with a capacity of 25,000 tonnes/year. Size reduction is required for the feed, which is then fed to a heated fluidized bed reactor (operating at 500 ^{o}C) in the absence of air. Plastics crack thermally under such conditions to hydrocarbons which vaporise and leave the bed with the fluidising gas. PSW decomposition leads to HCl formation (from PVC), which is neutralized by bringing the hot gas into contact with a solid lime absorbent. 85% by weight of the plastic that enters the process is passed on as hydrocarbon liquid, and the remaining 15% is gas at ambient temperature. The gas has a high content of monomers (ethylene and propylene) and other useful hydrocarbons with only some 15% being methane (Brophy et al., 1997). Total solids produced are typically up to 0.2 kg/kg of total solids feed.

One of the main pyrolysis technologies ever commissioned is the BASF process. The process started with a pilot plant capacity of 15,000 tonnes/year (Ludwigshafen, Germany) in 1994. As it is the case with many recycling thermo-chemical schemes, the process starts with a pre-treatment step. Mixed PSW is grinded, and separated from metals and agglomerated materials (Heyde and Kremer, 1999). The conversion of the PSW into valuable petrochemicals takes place in a multi-stage melting and reduction process. The hydrogen chloride separated out in this process is absorbed and processed in the hydrochloric acid production plant. Hence, the major part of the chlorine present in the input (e.g. from PVC) is converted into saleable HCl. Minor amounts come available as NaCl or $CaCl_2$ effluent (Heyde and Kremer, 1999).

3. CASE STUDIES

The objective of this section is twofold; (i) to demonstrate the validity of the pyrolysis process in experimental conditions and therefore obtain the best design parameters for reactor design and engineering; (ii) to illustrate the methodology and up-to-date results in determining the kinetics of such thermal cracking processes. In two case studies, we will

investigate the pyrolysis of a number of virgin and recyclate grades of polymers, and then a number of conclusions and recommendations will be drawn.

3.1. Case Study no.1: Comparative study of LDPE and HDPE in Dynamic and Isothermal Modes of Pyrolysis

3.1.1. Introductory Remark

In this case study, 15 mg samples of virgin low and high density polyethylene (LDPE and HDPE) were milled and pyrolysed using a micro thermobalance reactor (TGA set-up) to study their thermal degradation under both isothermal and dynamic conditions. Moderate to elevated temperature range (500-600 ^{o}C) was utilized in the isothermal runs, identifying five major pyrolysis lumped products (i.e. gases (C_1-C_4), liquids (non-aromatic C_5-C_{10}), aromatics (single ring structures) and waxes (> C_{11}). The data obtained enabled us to assess the thermal cracking mechanism and introduce a kinetic model based on primary to tertiary depolymerisation reactions. Four constant heating rates (β = 5, 10, 25 and 50 ^{o}C min^{-1}) were used in the dynamic assessment. The Ozawa-Flynn-Wall (OFW) and the general kinetics theory (GKT) were both used to determine the kinetic rate constants and apparent activation energies (E_a). Results obtained were compared with previously published reports on the pyrolysis of polyethylene, and it was concluded that such mechanisms and processes are robust enough to warrant further investigation on an industrial scale.

The importance of reaction kinetics comes directly from the benefits they provide, in terms of unit operation and design. Dahiya et al. (2008) stated that the kinetics of dynamic (non-isothermal) depolymerization can be obtained by utilizing the following general kinetic expression:

$$dx_s / dT = (A/\beta).\exp(-E/RT).x_s \tag{6}$$

where β is the heating rate (^{o}C min^{-1}) expressed as dT/dt. E is the apparent activation energy (kJ mol^{-1}), A is the Arrhenius pre exponential or frequency factor (min^{-1}), T is the temperature in K, x_s is the polymer solid conversion, and R is the universal gas constant. There are several methods for deriving kinetic parameters from eq.(6), such as: (i) the differential method, *i.e.* direct application of the equation; (ii) the difference-differential method, *i.e.* the Freeman and Carroll method; (iii) the integral method using a simple approximation of the exponential temperature integral, *i.e.* the Coats–Redfern method; and (iv) model-independent methods, *i.e.* isoconversional methods based on heating rate (such as the Ozawa–Flynn–Wall (OFW) method, the Friedman method or the Kissinger method). Table 2 reviews the major methods and states their drawbacks and applications using TGA data.

Table 2. Review of main dynamic derived expressions utilized in polymer degradation studies

Method	Expression(s)	Notes	Reference
Differential	$\ln(\frac{dx_s/dt}{f(x_s)}) = \ln(A/\beta) - E/RT$; (7) β is the heating rate ($^oC\ min^{-1}$), E is the apparent activation energy ($kJ\ mol^{-1}$), A is the Arrhenius pre exponential factor (min^{-1}), and x_s is the polymer solid conversion. Thus, a plot of the left-hand side vs. $1/T$ yields both E and A from the slope and intercept, respectively. For order-based models, *i.e.* those involving $(1-x_s)$, the reaction order (n) has to be determined by an independent method as such: $1 - x_{s,\max} = n^{1/(1-n)}$; (8) $x_{s,max}$ is the fraction reacted at the maximum rate of decomposition.	The suppression of errors due to the logarithmic form of dx_s/dT and need for data filtration and smoothing to obtain bias parameters are amongst its major drawbacks.	Dahiya et al., 2008
Freeman and Carroll	$\frac{\Delta\log(dx_s/dT)}{\Delta\log(1-x_s)} = \frac{E}{2.3RT}\left[\frac{\Delta(1/T)}{\Delta\log(1-x_s)}\right] + n$; (9) Where the function withdrawn from the TGA curve is: $f(x_s) = (1-x_s)^n$ (10)	Widely used in literature, but eliminates the evolution of data, and inaccurate in maximum decomposition regions	Liu and Fan, 1999; Caykara et al., 1999; Park et al., 2000; Budrugeac, 2005; Paik and Kar, 2008; Dahiya et al., 2008
Integral method	$\log g(x_s) = \log(\frac{AE}{\beta R}) + \log p(x)$ (11) $g(x_s) = \frac{AE}{\beta R}p(x)$ (12) $p(x) = \frac{\exp(-x)}{x^2}(1-\frac{2}{x})$ (13)	The main controversy is around the p(x) expression were a number of authors have tried to adapt simpler and more representative expressions.	Agrawal, 1992a; Junmeng et al., 2006; Junmeng et al., 2007; Dahiya et al., 2008
Single heating rate isoconversion OFW method	$\ln(\beta) + 5.33 + \ln(1-x_s) = \ln(k_o E/R) - 1.05(E/R.T)$ (14)	The major disadvantage is that multi-step process during the course of reaction cannot be dictated	Ceamanos et al., 2002

Ideally, it would be desirable to convert polymers (waste) using isothermal pyrolysis into a high value refinery cut for the utilization in a petrochemical process, e.g. light gases. In the case of PE waste, a desired product would be synthetic lubricants (poly-α-olefin based) and heavy waxes (> C_{11}). This means that the product of the thermal cracking should be close to 1-decene in both chain length and molecular structure. This was the basis of McCaffrey et al. (1995) work in PE thermolysis in an inert atmosphere. The thermolysis of LLDPE was studied at moderate temperatures (425-450 °C) in a 500 ml Pyrex kettle-type reactor. The major reaction products obtained was a liquid at room temperature with a yield of 82.5% of the initial charge to the reactor (60 gm). The balance of the reaction products was in two parts: a residue and a non-condensable gas fraction, with yields of 9.5 and 8.0%, respectively. The thermolysis of 60/40 mixtures of PE and PS was investigated at temperatures below 440 °C and published in a follow up study by McCaffrey et al. (1996). Liquid yield from the mixture, 84.1%, was comparable to yields obtained with the individual polymers. The yields of styrene monomer, 57.1%, and α-olefins, 27.7%, increased over those obtained when the polymers were processed individually.

In micro scale pyrolysis, only random initiation and intermolecular transfer were reported to be important steps in the polymers thermal degradation mechanism. Conversely, on milligram scale of polyethylene charges and samples, intermolecular transfer of hydrogen atoms via abstraction by free radicals was considered to be the predominant transfer mechanism to produce volatiles. A simple mechanistic kinetic model able to describe the radical chain pyrolysis taking place in the liquid phase was presented by Ranzi et al. (1997), assuming, thermal degradation of polyolefins to be a typical radical chain mechanism: initiation, H-abstraction, β-scission and radical recombination. Bockhorn et al. (1999) suggested a mechanism for the thermal cracking of PE that starts with a random scission to give primary radicals. The propagation is carried out: (1) by scission in β of these radicals, (2) by intramolecular hydrogen transference, followed by scission, and (3) by intermolecular hydrogen transference. The termination is carried out by a recombination of radicals. The kinetic equation obtained is a function of the polymer amount to the power of 0.5 and 1.5. Ceamanos et al. (2002) considered the following scheme, presented in equation (15):

$$
\begin{aligned}
& P \xrightarrow{k_1} 2R_P + R_{p'} \\
& R_P \left[\begin{array}{l} \xrightarrow{k_2} G_1 \\ \xrightarrow{k_3} R_s \xrightarrow{k_5} R_p + G_2 \\ \xrightarrow{k_4} R_s + G_3 \end{array} \right] \\
& 2R_p + R_{p'} \xrightarrow{k_6} P
\end{aligned}
\qquad (15)
$$

Only the relevant reactions and species involving weight loss have been included. Initially, the polymer degrades to form primary radicals (R_p). This degradation generates a relatively low number of long radical chains at low temperatures and a high number of relatively short radical chains at high temperatures. If the random scission generates radicals with chain length lower than 72 carbon atoms, they are volatile at 400 °C. The weight loss

kinetic equation would follow an apparent order of one, regardless of the secondary steps that these radicals can suffer in the gas phase. The radicals of higher chain length, remaining in the liquid phase, can generate relatively higher amounts of volatile products at temperatures around 500 °C: ethene by β-scission (G_1) and alkanes from intermolecular hydrogen transfer (G_3). However, if temperature or heating rate is low, the primary radicals react to generate mainly secondary radicals by intramolecular hydrogen transfer. This step and the subsequent β-scission of these secondary radicals and the intermolecular hydrogen transfer constitute the propagation steps of the mechanism. The intramolecular hydrogen transfer is favoured in the case of the 1,5 hydrogen shift, given the favourable ring transition step. The β-scission generates either alkenes (G_2) and a shorter primary radical (being this the predominant path) or non-volatile matter and primary radical (not shown in the scheme). High temperatures increase the concentration of short radicals, increasing the rate of this step and favouring vaporisation of relatively long chains. In the gas phase, the radicals may suffer subsequent β-scission with higher rate than that in the liquid phase, where the *'cage effect'* can modify the apparent pre-exponential factor for the reaction. This effect decreases as temperature increases. Taking this into account, volatiles can be generated from different steps of the mechanism, although some of them are clearly predominant. Unlike previous reports on thermal degradation of the polymer cracking, this study considers a novel lumped product mechanism of degradation based on the isothermal runs data obtained from the pyrolysis of HDPE and LDPE. The dynamic investigation was carried out by using the OFW and General Kinetics Theory (GKT) methods. The kinetic parameters and methodology reported in this work could be utilized primarily in industry, since it obeys an engineering analysis and approach, rather than an abstract chemistry one.

3.1.2. Materials and Methods

HDPE (ρ = 0.952 gm cc^{-1}; T_m = 131 ^oC) extrusion resin grade EGDA-6888 was secured form EQUATE Petrochemicals Co. (Kuwait). LDPE film grade (ρ = 0.92 gm cc^{-1}) was secured from Qatar Petrochemicals Co. Ltd. (QAPCO). All the virgin polymers were supplied in pellet form and were milled to below 0.1 mm before experimentation, to avoid mass and heat transfer resistance. 15 mgs were weighted and used in all experiments. HDPE and LDPE samples were subjected to dynamic pyrolysis in a thermobalance reactor (TG-CHAN 131, Combustion Lab, UCL) with a 1.5 bar inlet gauge pressure. Four constant heating rates (β) were used, 5, 10, 25 and 50 $^oC\ min^{-1}$. Pure nitrogen gas (British Oxygen Co.) was used as an inert pyrolysis medium. Figure 4 shows a schematic representation of the thermobalance reactor used.

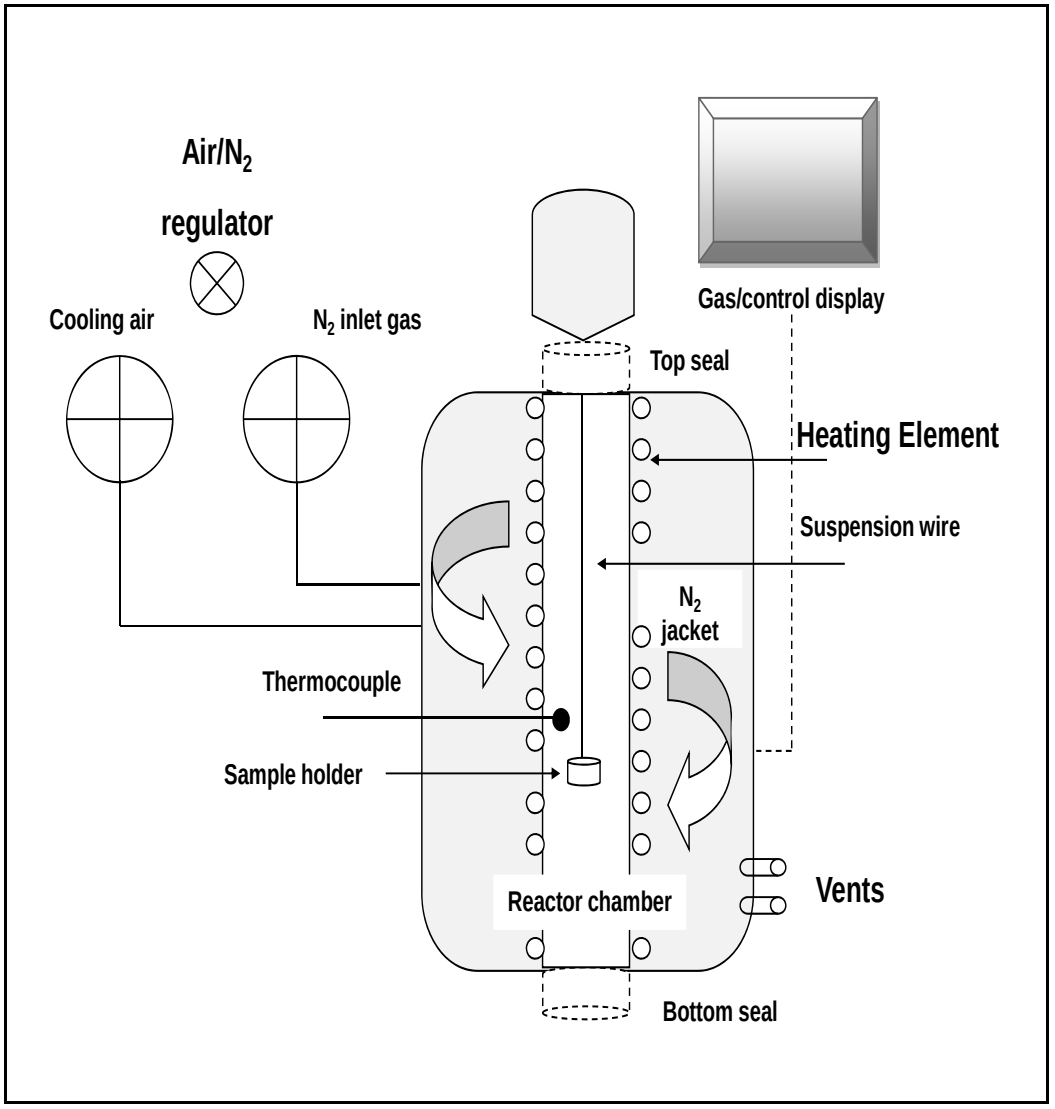

Figure 4. Thermobalance reactor (TGA set-up) schematic showing main parts.

The isothermal runs were conducted under the following temperatures using the set-up shown in Figure 4: 500, 550 and 600 ^{o}C. Product analysis has been carried out by means of a Hewlett Packard 6890 chromatograph provided with thermal conductivity (TCD) and flame ionization (FID) detectors, being connected online to the balance by means of a thermostated line. Furthermore, lump product identification has been carried out by means of a mass spectrometer (Shimadzu *GC*MS-QP20 I OS). 99.9% pure nitrogen was used in the pyrolysis process with a flow of 50 ml min^{-1}. Pyrolysis products were lumped into gases (C_1-C_4), liquids (*non-aromatic* C_5-C_{10}), *single ring* aromatics (C_5-C_{10}) and waxes *(*$> C_{11}$).

3.1.3. Results and Discussion

Pyrolysis produces three different phases: a solid phase (char, 5-25 wt %), a liquid phase (tars, 10-45 wt %) and a gas phase (Aznar et al., 2006, Zia et al., 2007). First products yielded

are usually in the range of C_{20} to C_{50}. These products are cracked in the gas phase to obtain lighter hydrocarbons, as ethene and propene, which are unstable at high temperatures and react to form aromatic compounds as benzene or toluene. If the residence time is long, coke, methane and hydrogen form (Westerhout et al., 1998). In thermo-chemical treatment of polyolefins, products obtained mainly depend on cracking reactions in the gas phase. Long residence times of volatiles in reactors and high temperatures decrease tar production but increase char formation (Cozzani et al., 1997). The main disadvantage of plastic pyrolysis and gasification is that it is necessary to control the chloride content in the feedstock and the risk of bad fluidization because of particle agglomeration (Kaminsky et al., 1995). It is believed that increasing temperatures above 500 ^{o}C and prolonging the gas residence time, result in a reduction in tar content of the gas product from both pyrolysis and gasification of PSW, ASR, MSW and even mixtures of coal, biomass and PSW (Stiles and Kandiyoti, 1989; Pinto et al., 2003; Zolezzi et al., 2004; Miscolczi et al., 2004; Ciliz et al., 2004). In fact, at temperatures above 800 ^{o}C larger paraffines and olefins produced from decomposition of plastics are cracked into H_2, CO, CO_2, CH_4 and lighter hydrocarbons (Ponzio et al., 2006). As a result of methyl-group abstraction from aromatics and decomposition of paraffines, C_2H_4 and C_2H_2 are typically reported to increase with temperature (Ledesma et al., 2000). The abstraction methyl groups and hydroxyl groups from aromatic structures imply that the aromatic fraction does increase with temperature even though the total amount of tar decreases. H_2-abstraction from light hydrocarbons and crosslinking reactions may also produce PAH.

Figure 5. shows the solid conversion (x_s) of HDPE as a function of temperature at 500, 550 and 600 ^{o}C. The effect of the temperature was very clear on the performed runs and conversion time (t_c), described as the time to reach 99.5% of the polymer conversion. In the case of LDPE, x_s showed a similar response to higher temperatures (Figure 6). At a temperature of 600 ^{o}C, both polymers converged to a value approximately equal to 1 in 80 s. Ceamanos et al. (2002) reported an isotherm of less than 50 s in their study in HDPE with a maximum temperature of 470 ^{o}C. It is very important to note that in the case of HDPE, the reaction was very rapid and reached a conversion of 1. Both polymers yielded pyrolysis products that were lumped into rich gases (C_1-C_4), liquids (C_5-C_{10}), heavy residue waxes (> C_{11}) and aromatics. Table 3 shows the products obtained for both polymers under the operating temperature range. As observed, increasing the operating temperature yields more rich gas cut (in both polymers), but decreases the waxy residue in the same time. In a previous study by Al-Salem et al. (2009b), the pyrolysis products of a European commercial grade of HDPE were analyzed in a temperature range between 450 to 700 ^{o}C. The conversion time ranged between 510 to 66.3 s for temperatures between 500 to 600 ^{o}C. A better conversion was reached in this study in a lesser time (8 s) for both polymers (HDPE and LDPE). The products recovered in this study exceeded the past analysis reported by Al-Salem et al. (2009b), in terms of recovered heavy residues (oil and waxes), and char recovered in a very minimal quantities (< 0.01 wt%).

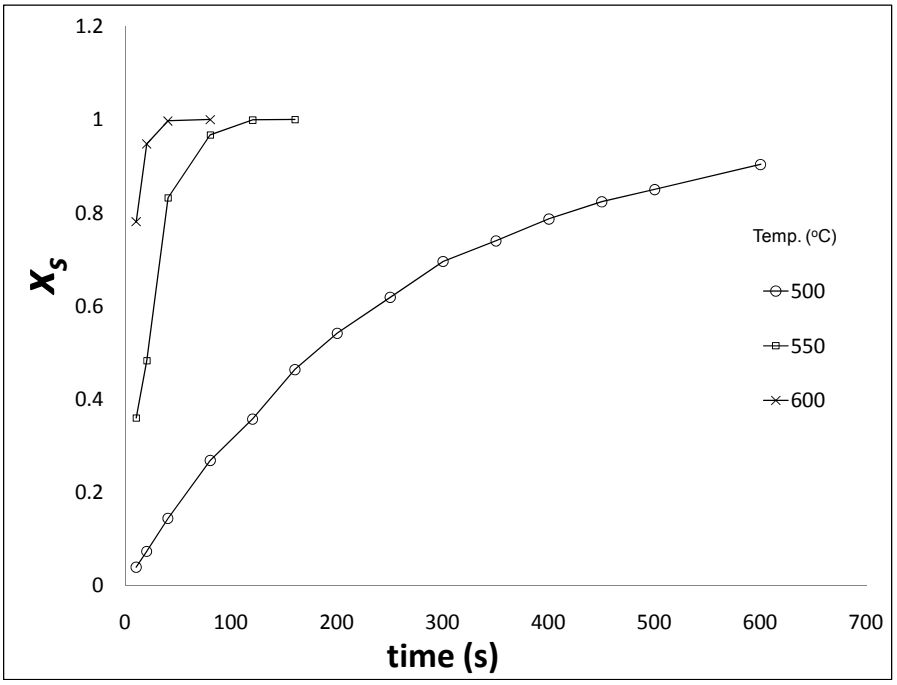

Figure 5. Isothermal run. HDPE solid conversion (x_s) as a function of time (s).

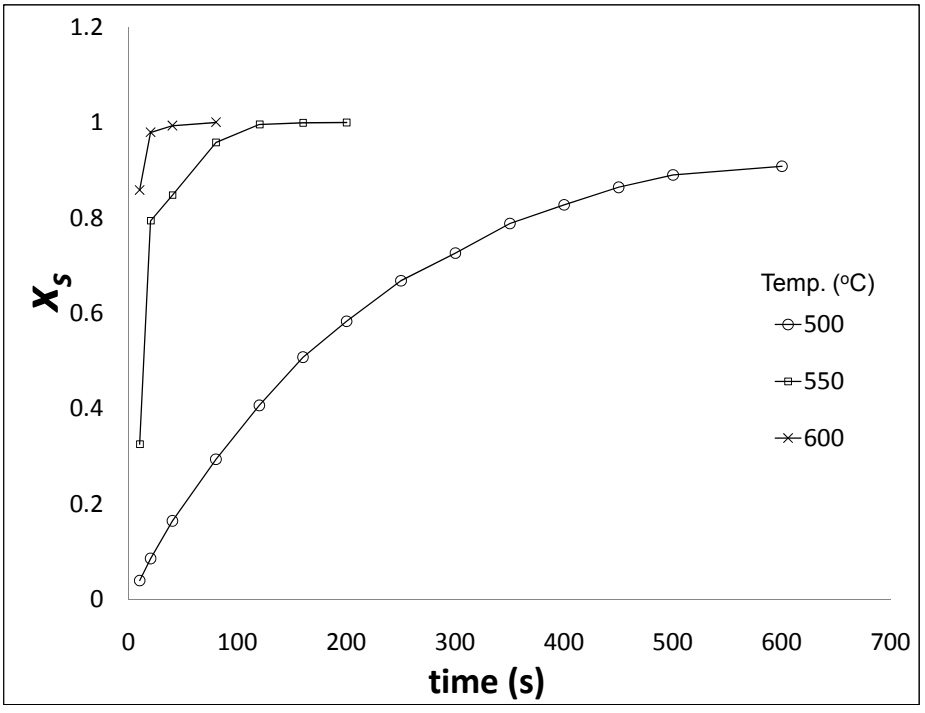

Figure 6. Isothermal run. LDPE solid conversion (x_s) as a function of time (s).

Table 3. Pyrolysis products in wt% of HDPE and LDPE at 500, 550 and 600 °C under isothermal conditions

	Gases (C_1-C_4)		Liquids (C_5-C_{10})		Aromatics		Waxes (> C_{11})	
Temperature (°C)	HDPE	LDPE	HDPE	LDPE	HDPE	LDPE	HDPE	LDPE
500	20.7	19.2	10.9	11.1	1.1	0.9	68.3	68.8
550	32.4	32	6.3	10.2	0.9	0.6	60.4	57.2
600	40.1	36.8	10.8	12.4	0.4	0.4	48.7	50.4

Numerous attempts have been undertaken to develop a thermal degradation scheme, usually via a simple approach of parallel reactions from polymer to product lumps (McCaffrey et al., 1995; Williams and Williams, 1997; Williams and Williams, 1999a; Williams and Williams, 1999b; Horvat and Ng, 1999; Mastellone, 1999; McCaffrey et al., 1998). Yet differences are always present due to variations in polymer's characteristics (molecular weight, presence of weak links, additives, etc.) and differences in experimental conditions from which kinetic data are calculated (McCaffrey et al., 1995). In this work, a model of the first order (*n=1*) is proposed based on the experiments conducted on HDPE and LDPE thermal degradation. The model determines the amount of liquids, gases, waxes and aromatics produced by wt%. The mechanism employed in the current study is illustrated below in Eqs.(16-17) for HDPE and LDPE, respectively. The scheme for HDPE thermal degradation is proposed as follows: primary conversion of HDPE to liquids, gases, waxes and aromatics; and then secondary conversion of waxes to liquids and aromatics. As for LDPE: Primary conversion of the polymer to an intermediate state (waxes), which converges to liquids and gases (secondary cracking reactions), and finally gases form the aromatics detected. Certain elements determine the validity of mechanisms proposed, which are: (i) physical characterization and behaviour of the polymers studies, i.e. gases typically evaporate to light cuts and aromatics, etc, (ii) the mathematical breakdown of the problem and its kinetic soundness, and finally (iii) the regressions obtained between the products found experimentally and the normalized solutions obtained from solving the complex systems obtained.

$$[HP]\begin{bmatrix} \xrightarrow{k_1}[G] \\ \xrightarrow{k_2}[L] \\ \xrightarrow{k_3}[W] \\ \xrightarrow{k_4}[A] \end{bmatrix}[W]\begin{bmatrix} \xrightarrow{k_5}[L] \\ \xrightarrow{k_6}[A] \end{bmatrix} \tag{16}$$

$$[LP] \xrightarrow{k_1} [W]\,[W]\begin{bmatrix} \xrightarrow{k_2} [L] \\ \xrightarrow{k_3} [G] \end{bmatrix} [G] \xrightarrow{k_4} [A] \tag{17}$$

where HP, LP, G, L, W and A stand for the fractions of high and low density polyethylene, gases, liquids, waxes and aromatics fractions, respectively. In the case of HDPE thermal degradation, k_1, k_2, k_3, k_4, k_5 and k_6, respectively stand for the rate constant (s^{-1}) of thermal degradation of (primary reactions): polymer to gases, liquids, waxes, aromatics and chars; (secondary reactions): waxes to liquids and aromatics. In the case of the proposed model of LDPE, k_1, k_2, k_3 and k_4, respectively stand for the rate constant (s^{-1}) of thermal degradation of (primary reaction): polymer to waxes, (secondary reactions): waxes to liquids and gases, and (tertiary reaction): gases to aromatics. In the case of HDPE, the secondary reaction is proposed to be an interaction one between the products. All reactions were assumed to be irreversible ones and initiate at a time equal to zero simultaneously.

The mathematical breakdown of the mechanism proposed in this work was solved using MatLab version 9.0. Assuming that initial conditions were at time = 0, the fractions of the polymer and products would be as follows:

$$@\, t = 0; \qquad x_p = 1 \text{ and } x_g = x_l = x_w = x_{ac} = 0 \tag{18}$$

Where t is the time (s), x_p is the polymer mass fraction, and x_g, x_l, x_w, *and* x_a are the mass fractions of gases, liquids, waxes, and aromatics, respectively.

The second conditions would be at time t (s), described as follows:

$$@\, t = t; \qquad x_p < 1 \text{ and } x_g, x_l, x_w \;\&\; x_a = f(t, x_p) \tag{19}$$

The derivation of the model was based on Bockhorn et al. (1999) and Fogler (2005), mass concentrations and balances, and rate equation analysis. Eqs. (20-24) show the balances derived for the mechanism proposed, in the case of HDPE. Eqs. (25-28) show the derived model for LDPE.

$$dx_p/dt = -x_p[k_1 + k_2 + k_3 + k_4] \tag{20}$$

$$dx_g/dt = x_p[k_1] \tag{21}$$

$$dx_l/dt = x_p[k_2] + x_w[k_5] \tag{22}$$

$$dx_w/dt = x_p[k_3] - x_w[k_5 + k_6] \tag{23}$$

$$dx_a/dt = x_p[k_4] + x_w[k_6] \quad (24)$$

$$dx_p/dt = -x_p[k_1] \quad (25)$$

$$dx_w/dt = x_p[k_1] - x_w[k_2 + k_3] \quad (26)$$

$$dx_l/dt = x_w[k_2] \quad (27)$$

$$dx_g/dt = x_w[k_3] - x_a[k_4] \quad (28)$$

It was also assumed that all reactions were irreversible with 99.5% conversion. At a certain temperature, the polymer thermally decomposes as a function of time. A high regression coefficient; correspondent to the relation typically represented by a power law or an exponential equation, is chosen. The relationship is descriptive of the weight loss (in terms of polymer fraction, x_p). Once such an equation is set, with initial conditions and a breakdown of the model, the predicted values of both the products and polymer (with time) are evaluated, based on normalized results. Time of initial guess set up in MatLab program was equal to 0.001 s, solved by Runga-Kutta 4th order method.

Pyrolysis was previously carried out on HDPE in a fluidized bed reactor by Mastral et al. (2003). Their work showed great compatibility with our experimental results. Gases were produced at a higher yield with higher temperatures whereas waxes were minimal at severe high operating temperatures (i.e. 850 ^{o}C). Most types of thermal degradation (thermolysis) follow a similar basic pattern as previously stated in the report by ZEUS (2005). The conventional model for thermal degradation is that of an autoxidation process which involves the major steps of initiation, depropagation, branching, and termination. The initiation step involves the loss of a hydrogen atom from the polymer chain as a result of energy input from heat or light. This creates a highly reactive and unstable polymer free radical (usually denoted by R*) and a hydrogen atom with an unpaired electron (H*). The process can therefore accelerate depending on how easy it is to remove the hydrogen from the polymer chain. The termination of thermal degradation is achieved by *'mopping up'* the free radicals to create inert products. This can occur naturally by combining free radicals or it can be assisted by using stabilizers in the plastic. In some polymers it is also possible to get branching of the polymer chains; this is where two polymer chains become linked together and results in cross-linking and embrittlement of the polymer.

From the data obtained in this work and the proposed mechanisms of thermal degradation, the predicted polymer fraction (x_p) was calculated. Three fitting equations were obtained at the three given temperatures for both HDPE and LDPE. The form of the equation is not related to the occurring mechanism, but represents the best fit of the data (Al-Salem et al., 2009c). Previous work on HDPE and ELTs showed high regressions with diffusion type equations and power law fits. Other authors also report exponential fits (Khan et al., 2001;

2002; Mathew et al., 2005). In the case of isothermal runs under moderate and elevated temperatures, the polymer loss occurs very rapidly and in our case is best represented by an exponential equation for each temperature to base the solution on. Table 4 shows the equations obtained for the polymer loss and their regression coefficients against the experimental data. Exporting the previous equations to the MatLab program combined with Eqs. (15-23), enabled determining the kinetic parameters for each degradation path. The models developed had a high fit with respect to experimental results obtained by TGA analysis. Figs.7 and 8 show the experimental and modelled values. Table 5 shows the kinetic rate constants estimated for both degradation mechanisms at the three different temperatures.

Table 4. Isothermal runs. HDPE and LDPE obtained polymer loss expression as a function of time and the regression coefficients (R^2) obtained against the experimental data of the polymer fraction (x_p)

Material	Temperature (^oC)	Expression	R^2
HDPE	500	$x_p = 0.99.\exp(-0.001t)$	0.99
	550	$x_p = 1.34.\exp(-0.01t)$	0.90
	600	$x_p = 0.1.45.\exp(-0.01t)$	0.89
LDPE	500	$x_p = 0.973.\exp(-0.001t)$	0.994
	550	$x_p = 1.65.\exp(-0.01t)$	0.90
	600	$x_p = 1.89.\exp(-0.01t)$	0.89

Table 5. Isothermal runs. Kinetic rate constants (s^{-1}) determined for the degradation of both HDPE and LDPE in Eqs.(16-17)

Material	Temperature (^oC)	k_1	k_2	k_3	k_4	k_5	k_6
HDPE	500	4×10^{-3}	1.1×10^{-3}	6.6×10^{-4}	2.0×10^{-4}	2.0×10^{-4}	2.0×10^{-4}
	550	5.5×10^{-3}	4.2×10^{-3}	7.0×10^{-3}	3.7×10^{-3}	2.1×10^{-3}	9.0×10^{-4}
	600	6.8×10^{-3}	1.0×10^{-2}	9.0×10^{-3}	3.0×10^{-2}	2.9×10^{-3}	9.0×10^{-4}
LDPE	500	6.7×10^{-3}	1.1×10^{-3}	1.6×10^{-4}	1.1×10^{-4}	-	-
	550	8.9×10^{-3}	4.2×10^{-3}	1.7×10^{-3}	1.2×10^{-3}	-	-
	600	10.8×10^{-3}	1.0×10^{-2}	2.3×10^{-3}	1.3×10^{-2}	-	-

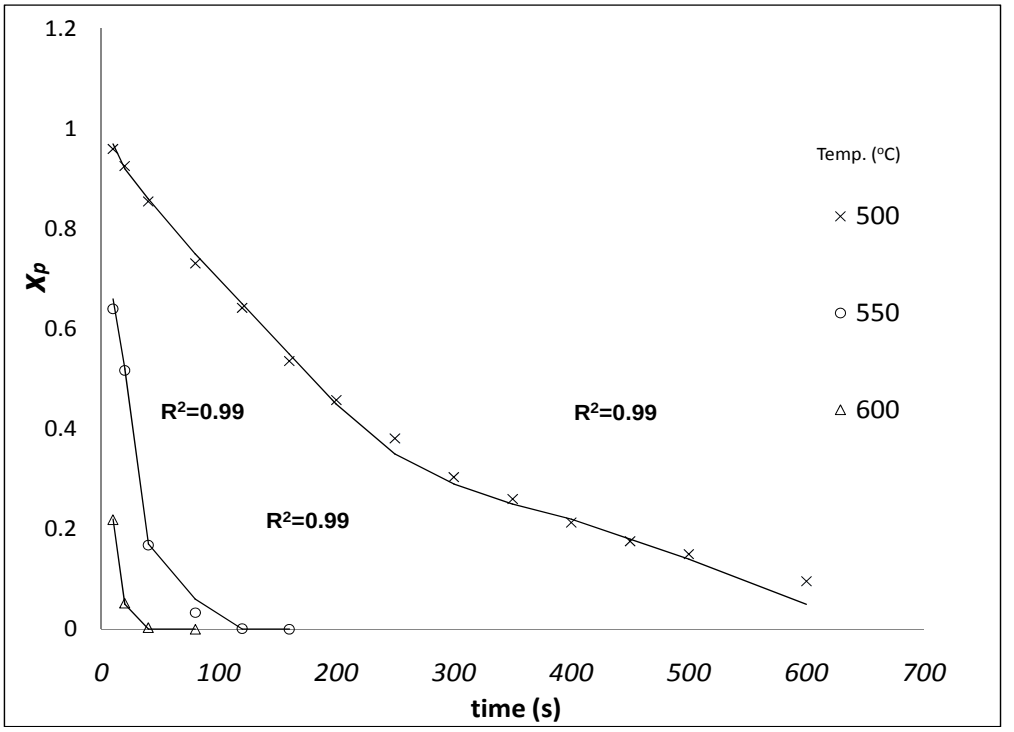

Figure 7. Isothermal run. HDPE polymer fraction (x_p) experimental and modelled values (straight line) as a function of time (s).

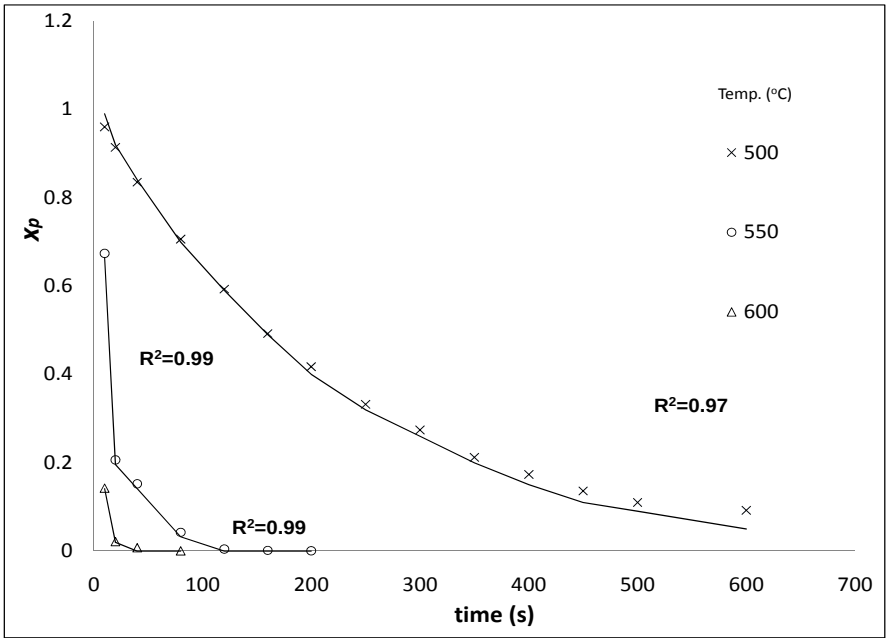

Figure 8. Isothermal run. LDPE polymer fraction (x_p) experimental and modelled values (straight line) as a function of time (s).

A high match was obtained from the experimental and modelled cases at temperatures of 500, 550 and 600 ^{o}C. Pyrolysis starts occurring at temperatures as low as 400 ^{o}C (Ceamanos et al., 2002). Previous researchers have reached a final temperature above 700 ^{o}C, especially when working with circulating bed reactors (Mastellone, 1999). Apparent overall kinetic rate constants (k_o) were estimated by summing the k values of the primary reactions (Al-Salem et al., 2009c), resulting in 0.005, 0.0204 and 0.0558 s^{-1}, at temperatures of 500, 550 and 600 ^{o}C, respectively for HDPE. And in the case of LDPE, k_o (s^{-1}) values were 0.0067, 0.0089, 0.0108 at 550 and 600 ^{o}C, respectively. The activation energies (absolute) and pre-exponential factors were estimated for every primary product (Table 6) by *1st* order Arrhenius equation fitting according to Figs.9 and 10.

Table 6. Isothermal runs. HDPE and LDPE activation energies and pre-exponential factors of primary lumped products

Material	Primary products	Waxes	Liquids	Gases	Aromatics
HDPE	E_a (kJ mol^{-1})	14.87	12.42	29.84	12.92
	P_o (s^{-1})	8.88	2.86	2.37	15.88
LDPE	Ea (kJ mol^{-1})	14.87	12.42	15.16	12.92
	Po (s^{-1})	8.88	2.86	1.10	6.60

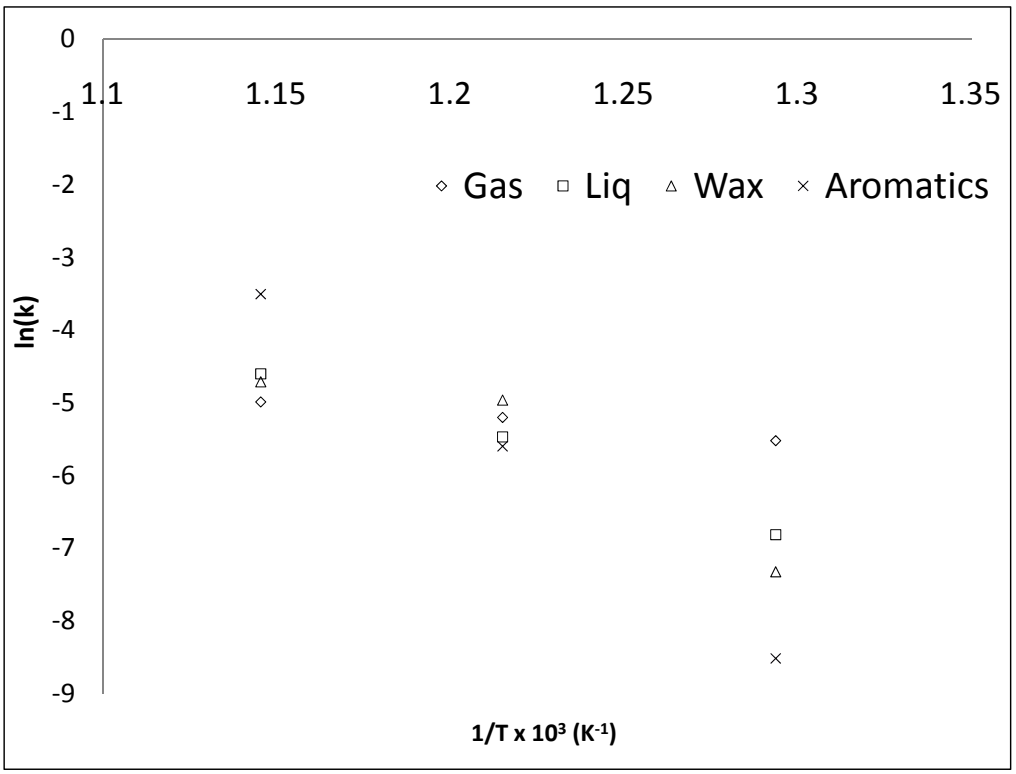

Figure 9. Isothermal run. Arrhenius equation fittings for primary products (HDPE).

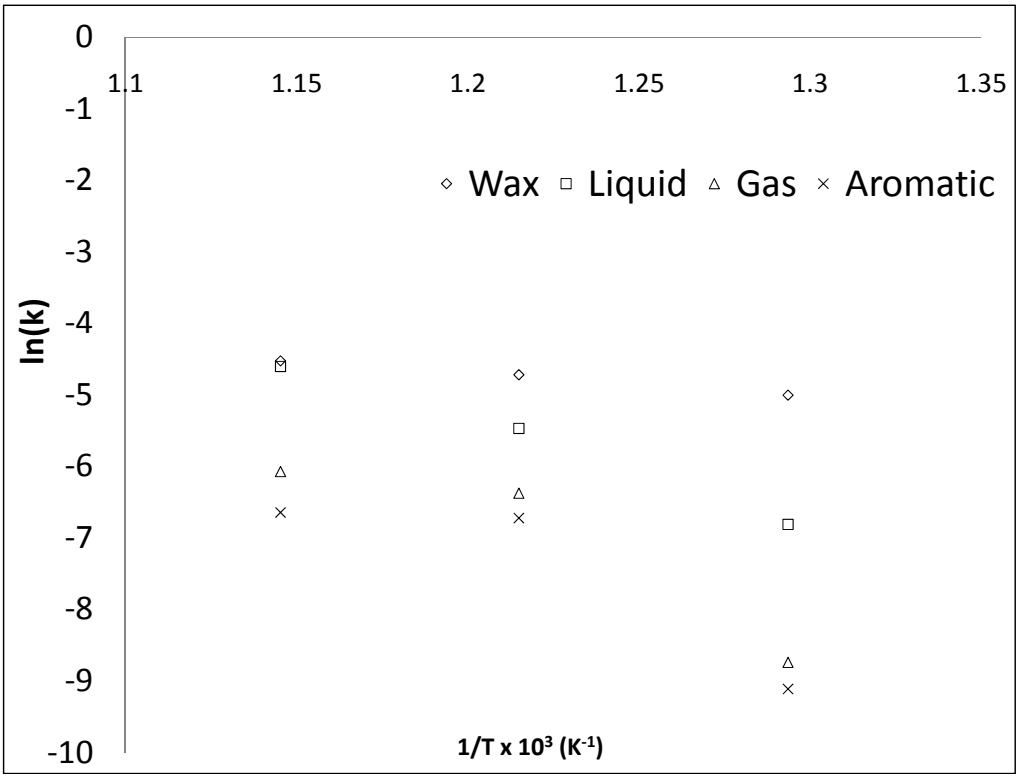

Figure 10. Isothermal run. Arrhenius equation fittings for primary products (LDPE).

By comparing the results reported in this work, an agreement with previously reported estimations is observed (Ranzi et al., 1997; Horvat and Ng, 1999; Bockhorn et al., 1999). The gases category show very interesting estimations in our work. Other than having the highest apparent activation energies (E_a), they also have the highest kinetic rate constant amongst yielded products. This shows the influence of this product within the mechanism proposed. This, combined with the contribution from secondary reactions, influences the thermal degradation of HDPE and LDPE to a large extent. Our model presented in this work is of the first order (n=1). Previous attempts reported in the literature show conversion orders between 0.86-1 with an overall kinetic rate constant between 0.0008 to 0.009 s^{-1} in a moderate temperature range of 390-470 ^{o}C (Ceamanos et al., 2002). It was also reported that operating temperatures have a proportional effect on overall rate constant, which our results confirm. Earlier work by Mastellone (1999); reports the total activation energy (E_o) of a number of polymer after thermal degradation by pyrolysis. For PE, it was reported that E_o ranged between 192-301 kJ.mol^{-1}. Whilst Horvat and Ng (1999) reported E_a to be in the range of 237-279 kJ.mol^{-1}, in the range of 450-470 ^{o}C. Other authors reported total activation energy (E_o) in the range of 188-293 kJ mol^{-1} (Ranzi et al., 1997; Bockhorn et al., 1999). Conesa et al. (1994a; 1994b; 1996) proposed a very simple yet effective thermal degradation mechanism based on isothermal TGA runs carried on HDPE samples. The behaviour has been modelled according to the mechanism presented in Eq.(29).

$$P \xrightarrow{k1} G1$$
$$P \xrightarrow{k2} P* \xrightarrow{k3} G2 \quad (29)$$

where P is the virgin polymer, P^* is the polymer free radical and G_1 and G_2 are the gas phase products of the primary reactions alone, respectively.

Both the model by Conesa et al. (1994a; 1994b; 1996) and the model presented in this study are based on experimental TGA runs, and serve the same purpose of finding a realistic mechanism for HDPE thermal degradation. Yet, our model is based on a novel complex engineering approach. The previous attempts were based on simple decomposition schemes and radical concentration estimation that will not serve in industrial schemes and reactor design. The model presented by Conesa et al. (1994a; 1994b; 1996) also estimated the E_a for each of the three reactions (Eq.29) and found it to be 185, 271.1 and 221.5 kJ mol^{-1}. In our work, the overall activation energy (E_o) was estimated at 125.59 kJ mol^{-1} (HDPE) and 110.75 kJ mol^{-1} (LDPE), according to the fitting in Figure 11.

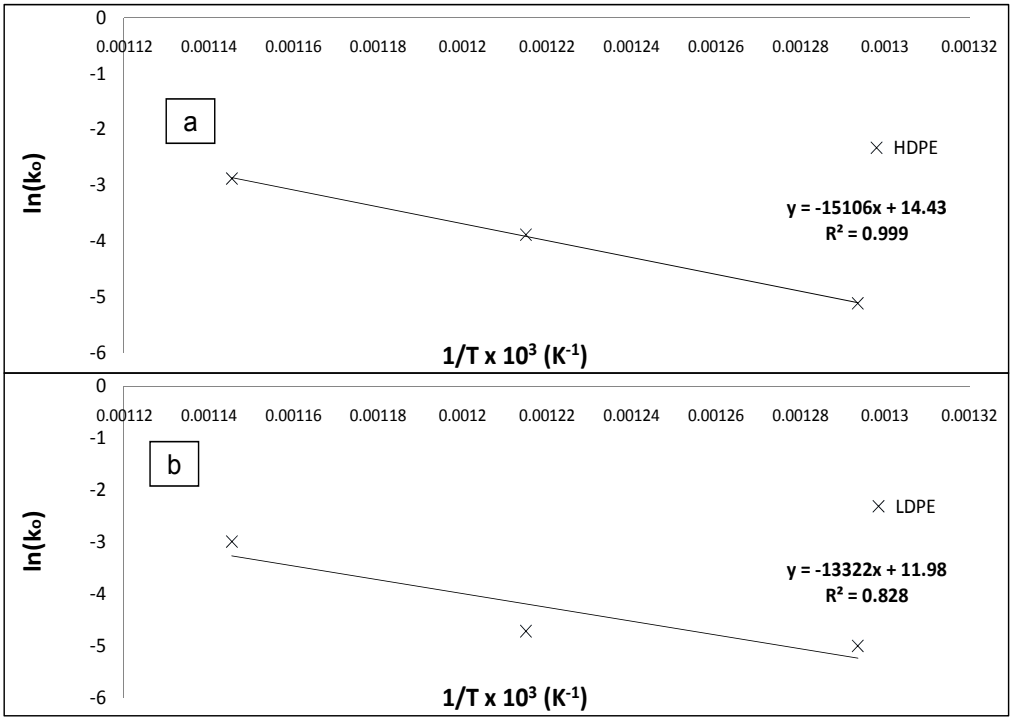

Figure 11. Isothermal run. Overall fitting of HDPE (a) and LDPE (b) activation energy determination by Arrhenius equation of 1st order.

Al-Salem et al. (2009c) determined the *Eo* value of HDPE using isothermal pyrolysis to be 147.25 kJ mol^{-1}. The E_o resulted from data fitted (R^2=0.986) after estimating the overall rate constant (k_o) at 500, 550 and 600 ^oC, which was found slightly lower than previous

reports. This can be attributed to the pyrolysis process used in this study (TGA with an elevated pre-set temperature), resulting in a low residence time and achieving high operating temperatures. The low E_o also points to the direction of achieving industrial fast and flash pyrolysis in reactors of full-industrial scale. Bockhorn et al. (1999) obtained values around 250 kJ mol^{-1} (HDPE) from isothermal experiments and around 360 kJ mol^{-1} from non-isothermal experiments. This important discrepancy can be explained by a detailed description of the reaction. The value of activation energy obtained from the isothermal experiments was described as an apparent value (Ceamanos et al., 2002).

As for the dynamic runs, four different heating rates were utilized in the case of HDPE and LDPE (β = 5, 10, 25 and 50 $^oC\ min^{-1}$). The objective was to reach a β value of 50 $^oC\ min^{-1}$ in the case polymers subjected to dynamic thermogravimetry known to be optimum for product recovery (rich gases and liquids) (Ceamanos 2002; Cunliffe and Williams, 2003). Figure 12 shows the solid conversion (x_s) vs. temperature in the case of HDPE for different heating rates. The experimental results show the typical S-curve until x_s values practically equal to 1 were reached. As observed, the increase of the heating rate delays the conversion, so the same value of conversion is obtained for higher temperatures of the experimental system, also called the reference temperature (T_{ref}). Reference temperature of the experimental system, obtained over the temperature range was 441 ^oC. At β=50 °C min^{-1}, the polymer was showing a delayed response to reach the optimum conversion rate. This behaviour was witnessed on all runs of HDPE, especially after crossing the $T_{1/2}$ point. The polymer lost half of its initial weight at 415 ^oC, on all the runs conducted with the four heating rates used.

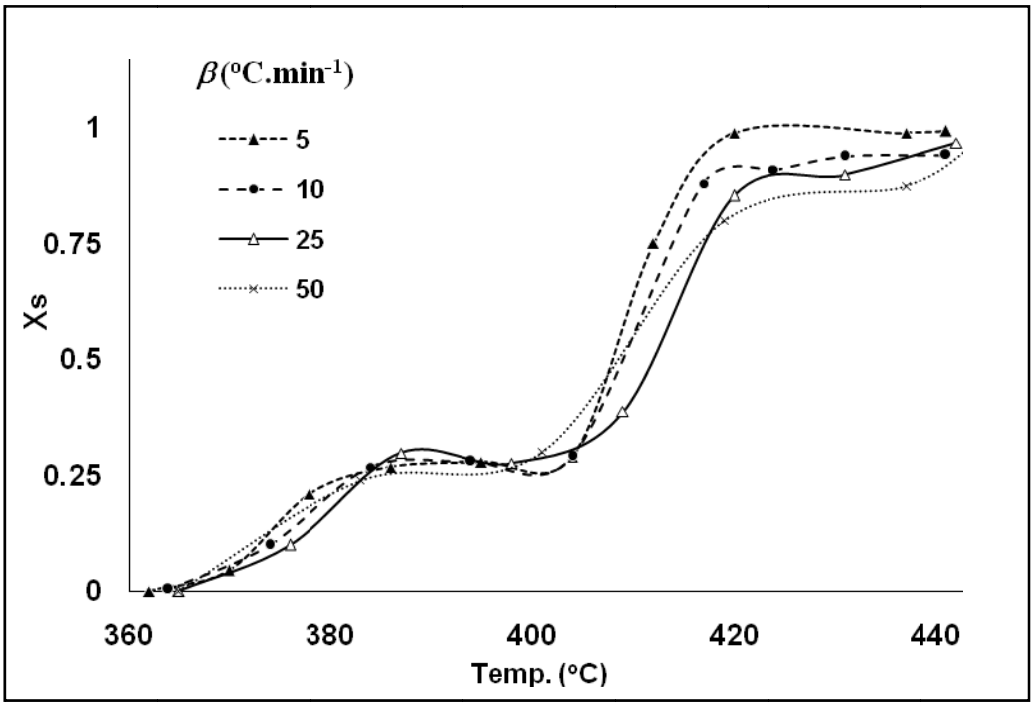

Figure 12. Dynamic run. Solid conversion as a function of temperature (^oC) for different heating rates on high density polyethylene (HDPE).

The effect of the increase of β is clear for 25 °C min^{-1} and is less significant for β=50 °C min^{-1}. The same behaviour was previously reported by Ceamanos et al. (2002). In order to explain these results, the values of dx_s/dT versus T for the differenț β values are shown in Figure 13. It can be observed that the maximum x_s data point is shifted to higher temperatures when the heating rate increases from β = 5 to 25 °C min^{-1}, and it remains approximately equal to 400 °C for β= 50 °C min^{-1}. The peak heights coincide for β=5 and 10 °C min^{-1}, and decrease for higher β. Agrawal (1992a) suggests that the values of dx_s/dT versus T obtained at different β values can indicate whether the process can be described as a simple reaction or not. The width of the peak indicates the range of temperatures for which the reaction takes place, and an increase of this range therefore indicates a decrease in the apparent activation energy. The process as illustrated in Figure 13 shows; in fact three distinct peaks. The second peak (corresponding with the pyrolysis reaction talking place in the reactor chamber) is the one of interest. The first and third peaks are consistent with the degradation of the additives in the polymer grade. Unlike pure polymeric materials, such initial degradation of stabilizers and additives is expected in the case of commercial grades, which typically contain trace amounts of stabilizers and plasticizers. The highest peak was observed for β = 10 °C min^{-1}, with β = 5 °C min^{-1} having the least wide reaction peak curve.

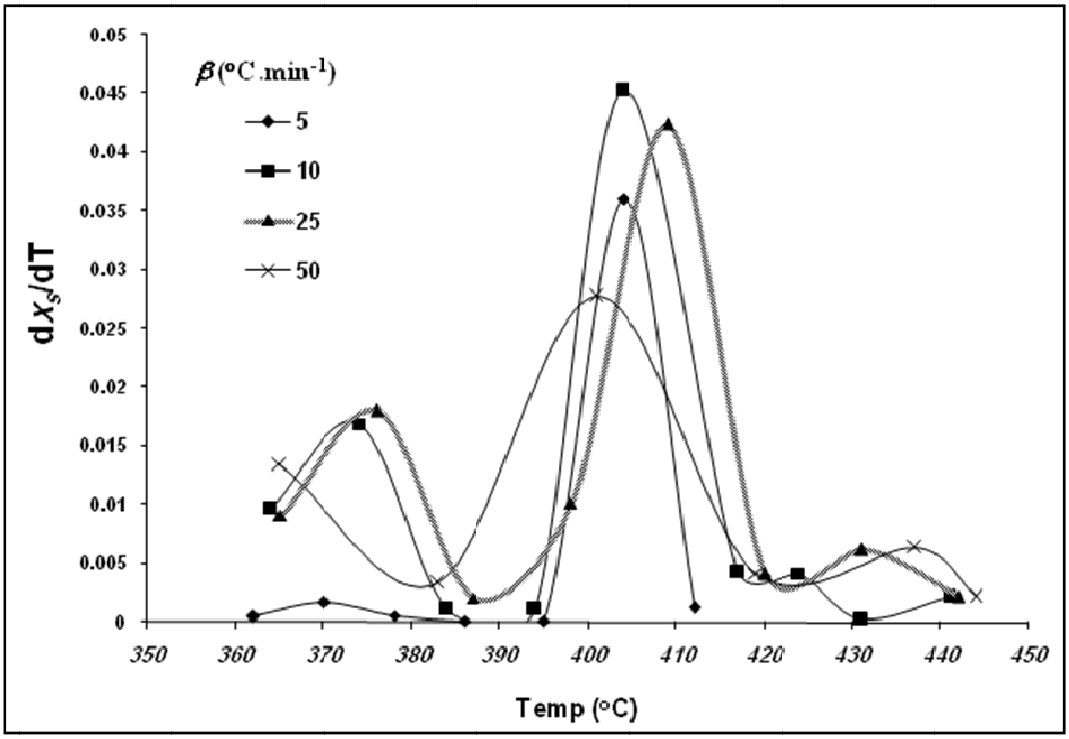

Figure 13. Dynamic run. Values of dx_s/dT as a function of temperature (°C) for different heating rates on high density polyethylene (HDPE).

In the case of LDPE, Figure 14 shows the solid conversion (x_s) vs. temperature for different heating rates. The typical S-curve was clear in the case of low heating rates (β = 5 and 10 °C min^{-1}). But it shrivels with higher ramps, making it very hard to identify (β = 25

and 50 ^{o}C min^{-1}). It was also observed that the behaviour of the material was found to be very similar to the previous case in terms of delay of conversion with higher values of β. T_{ref} was 375 ^{o}C for LDPE. Figure 15 shows the values of the first derivative (dx_s/dT) versus T obtained at different β values. The maximum variation was observed with a β = 10 ^{o}C min^{-1}. Whilst the range of the reaction temperature was clearly greater for β = 25 and 50 ^{o}C min^{-1}, covering the full span of the pyrolysis reaction temperature range. With low heating rates (especially in the case of β = 5 ^{o}C min^{-1}), it was observed that two distinct peaks occurred in an oscillatory behaviour after the reaction peak. This is attributed to the UV stabilizer in the polymer disintegrating in the reactor chamber. This effect is less observed with higher heating rates. The polymer had a wide range of $T_{1/2}$, varying between 260 ^{o}C (β = 5 ^{o}C min^{-1}) to 305 ^{o}C (β = 50 ^{o}C min^{-1}). The widest curve was obtained for the pyrolysis reaction at (β = 50 ^{o}C min^{-1}. This was on the other hand coherent with the activation energy estimates presented later on.

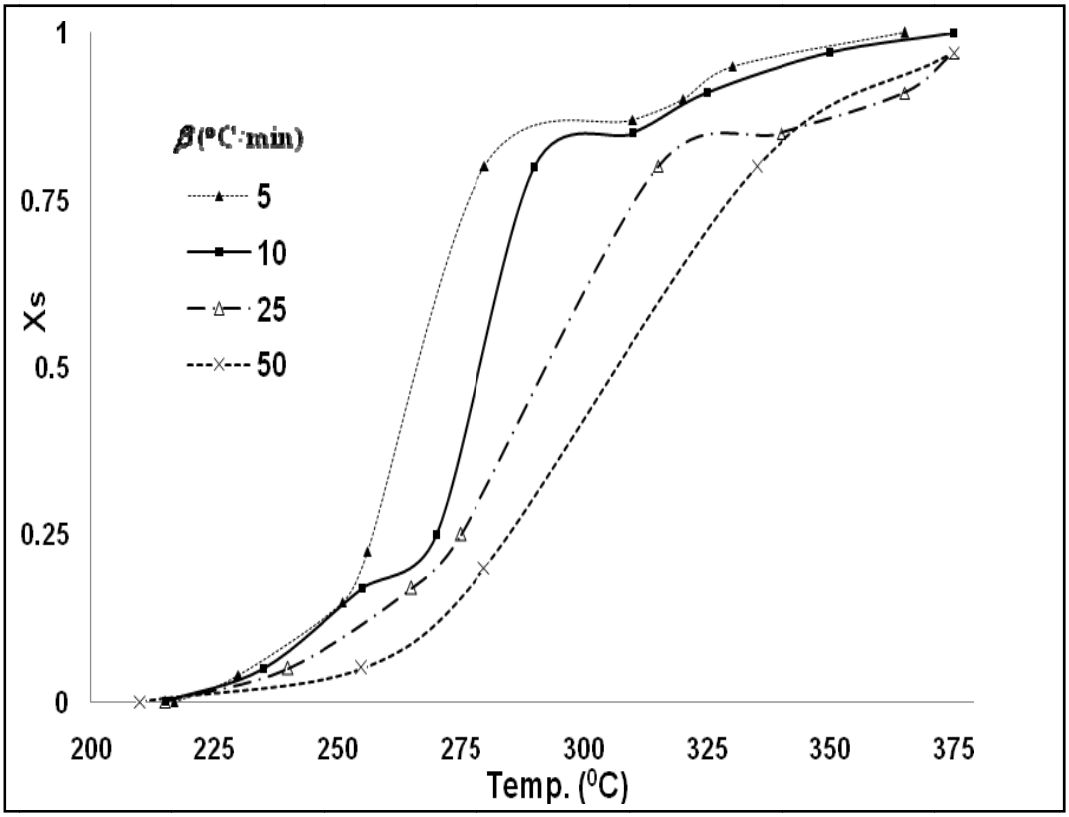

Figure 14. Dynamic run. Solid conversion as a function of temperature (^{o}C) for different heating rates on high density polyethylene (LDPE).

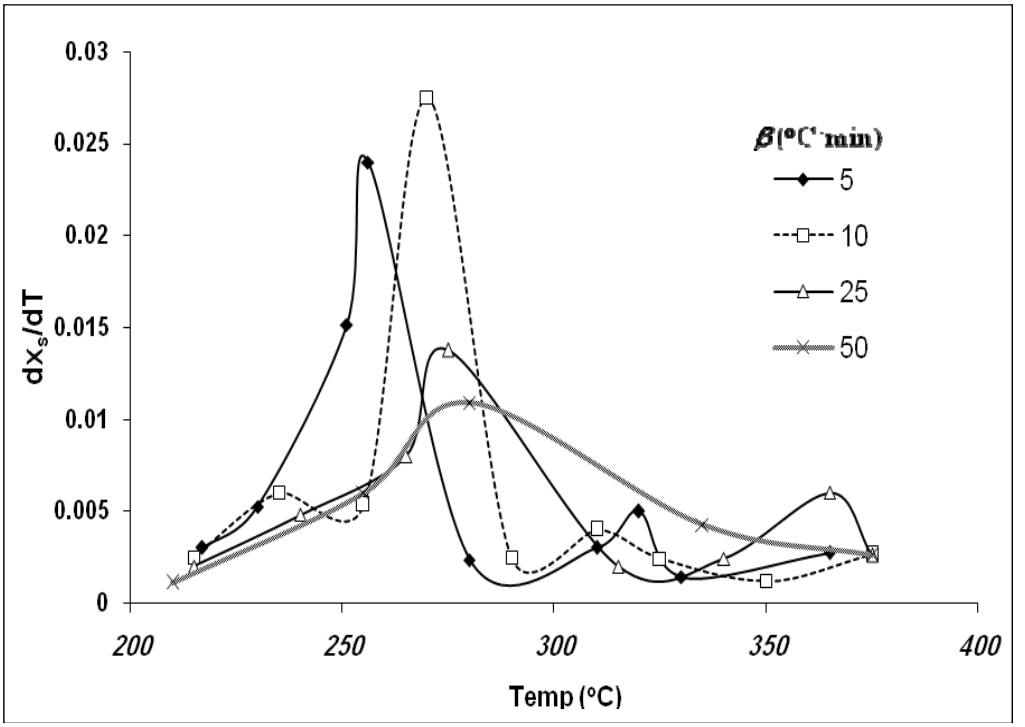

Figure 15. Dynamic run. Values of dx_s/dT as a function of temperature (^oC) for different heating rates on high density polyethylene (LDPE).

Polymers subjected to thermal cracking, mainly under the influence of a fixed heating rate, undergo complicated processes, such as random chain scission, end chain scission, chain stripping, cross linking and coke formation. Apparent dynamic kinetics, useful for engineering design, is the focus of this section. In this study, we have determined the apparent activation energy (E_a) and the overall activation energy (E_o) using two methods. Dynamic kinetic rate constants are dependent not only on factors such as atmosphere, sample weight, shape and type, heating rate and flow rate, etc., but also upon the mathematical treatment used to evaluate certain parameters. Dynamic kinetic studies utilize the basic rate equation of the General Kinetics Theory (GKT). The weight loss of a polymer is described as follows:

$$dx_p/dt = A.(1-x_p)^n.\exp(-E_a/RT) \tag{30}$$

where x_p is the polymer fraction pyrolysed (loss) of a polymer, A is the Arrhenius fitting pre-exponential factor (min^{-1}), n is the reaction order and E_a is the activation energy (apparent) of a single path reaction ($J\ mol^{-1}$).

If the temperature rises with a constant ramp or a heating rate (β) and the kinetic parameters at any weight loss fraction are approximately equal to those of neighbouring weight loss fraction, then by differentiating Eq.(30) with respect to temperature (T) to obtain the second derivative, we can employ the ramp expression described by Oh et al. (2003) as $\beta = dT/dt$, resulting in the following equality expression:

$$-E/RT = \ln\left(\left[\frac{dx_s}{dT}\right].\frac{1}{A_o T^{1/2}.(1-x_s)^n}\right) \tag{31}$$

where E is the apparent activation energy (J mol^{-1}), x_s is the polymer solid conversion fraction, T is the temperature (K) at time (t, s), n is the polymer conversion order and A_o is the collision theory dependant variable (s^{-1} K$^{-1/2}$). Eq.(26) gives the estimate of the activation energy at each data point corresponding to solid fraction and temperature range, and the average activation energy could be determined using the Coats and Redfern (1964) approximation:

$$E_{avg} = \frac{\sum_{i=1}^{n} E_i(\alpha_i - \alpha_{i-1})}{\alpha_f} \tag{32}$$

where E_i is the activation energy corresponding to point i and time (t), α_i is the weight loss fraction at point i and α_f is the weight loss fraction at the final status of maximum degradation.

A valid approximation at maximum, non-catalytic thermal degradation cracking has been presented by Oh et al. (2003), combining the heating rate (β) and the 1^{st} order Arrhenius fitting equation. Eq.(32) shows the Oh et al. (2003) equation used for maximum degradation estimates as a function of β:

$$\ln\beta = \ln A_o + \frac{3}{2}\ln(T_m) - \ln\left(\frac{E_m}{RT_m} + \frac{1}{2}\right) - \frac{E_m}{RT_m} \tag{33}$$

where E_m is the activation energy at maximum degradation conditions (J mol^{-1}) and T_m is the final temperature (maximum degradation temperature), (K).

In order to estimate kinetic parameters over a range of temperatures, the Ozawa-Flynn-Wall (OFW) method is still widely applied and used especially in elevated heating rates. Ceamanos et al. (2002) has expressed the OFW equation in terms of heating rate (β) and solid conversion (x_s) as follows:

$$\ln(\beta) + 5.33 + \ln(1-x_s) = \ln(k_o E/R) - 1.05(E/R.T) \tag{34}$$

By combining $\ln(\beta)$ and 5.33 to a common expression (κ) and rearranging Eq.(34), we can evaluate the activation energy from a plot of $\kappa+\ln(1-x_s)$ vs. 1/T.

The abetment of kinetic coefficients from dynamic experiments has been a matter of controversy for various authors, mainly due to the deficiencies in the Arrhenius equation, i.e. kinetic compensation effect. However, it is clear that the influence of the heating rate (β = dT/dt) must be considered in some processes that do not operate at constant temperatures. The

results obtained from non-isothermal experiments cover a greater range of temperatures of decomposition, exceeding 600 °C.

In order to calculate the kinetic parameters of polymer thermal cracking reactions, two methods were used. First, the Ozawa-Flynn-Wall (OFW) method was used. OFW method is considered one of the exact methods, since it depends solely on the accuracy of the results obtained experimentally. By plotting the $\kappa + \ln(1-x_s)$ vs. 1/T, one obtains a set of points that the linear fit to it corresponds to the 1^{st} order Arrhenius fit. Overall kinetics rate constants (k_o) and apparent activation energies (E_a) were also determined. The activation energy was increasing proportionally with the heating rate. This behaviour was previously witnessed on polymeric materials (Ceamanos et al., 2002; Mastral et al., 2002; Mastral et al., 2003; Oh et al., 2003; Mastral et al., 2007). Table 7 shows the activation energy (E_a) and overall kinetic rate constants obtained from the OFW method for HDPE. The overall activation energy (E_o) for HDPE thermal cracking reaction was also determined (by Arithmetic mean) to be 171 kJ mol^{-1}. Mastral et al. (2002) used the OFW method to verify their modelling approach and obtained E_a values (163-273 kJ mol^{-1}) over a range of heating rates (5-50 $^oC\ min^{-1}$).

Table 7. Overall kinetic rate constants (k_o) and apparent activation energies (E_a) obtained using the OFW method on HDPE dynamic runs

β ($^oC\ min^{-1}$)	Overall kinetic rate constant (k_o), min^{-1}	Apparent activation energy (E_a), kJ mol^{-1}
5	0.013×10^6	103.33
10	0.186×10^9	160.16
25	0.187×10^9	164.90
50	1.40×10^{14}	256.71

The general kinetics theory (GKT) expression previously adapted by Oh et al. (2003) was also used to determine the overall activation energy (E_o). An objective function was set to be minimized (maximizing the correlation coefficient between experimental and calculated values) to solve the equality reported in Eq.(31). The objective function corresponds to the sum of absolute errors (%) calculated between the $-E/RT$ and the rest of the expression as follows:

$$OF = Minimize \sum_{i=1}^{n} \frac{\left|(E/R.T) - \ln(C)\right|}{E/RT}$$

,i = 1, 2, 3, …. n (Maximum degradation temperature) (35)

With OF as the objective function, E is the activation energy (J mol^{-1}) obtained at a given temperature (K), R is the universal gas constant (8.314 J $mol^{-1}K^{-1}$) and C is the equality expression given below:

$$C = \ln\left(\left[\frac{dx_s}{dT}\right].\frac{1}{A_o T^{1/2}.(1-x_s)^n}\right) \quad (36)$$

Table 8 shows the estimated parameters (*i.e.* E_a, A_o and corresponding errors) obtained from (*i.e.* E_a, A_o and corresponding errors) obtained from Eqs.(35-36). The overall activation energy was estimated to be 204 kJ mol^{-1} with a reaction order equal to 1. Overall activation energy estimation has always been dependant on the numerical methods used to determine the value. Order of magnitude is always of desire when such calculations are executed (Oh et al., 2003). The same approach was undertaken for LDPE. The overall activation energy (E_o) for LDPE thermal cracking reaction was also determined (by Arithmetic mean) to be 198.74 kJ mol^{-1}. The overall activation energy (LDPE) was estimated to be 131.062 kJ mol^{-1} with a reaction order equal to 1.

It is of paramount importance to express obtained sets of kinetics parameters with a comprehensive model that could be utilized in future studies. This was the main objective when the experimental and kinetics assessments were conducted. The General Kinetics Theory (GKT) was used to verify the model and re-calculate the apparent activation energy and other parameters based on results obtained. The main equation utilized in this research is based on modelling of the weight loss (in terms of solid conversion) against temperature. No reported literature carries out similar methodology, in fact, most dynamic modelling is concerned with the estimation of kinetic parameters rather than the behaviour of the polymer in a reactor chamber, hence the temperature element. Obtained models could be coupled with the basic kinetic rate equations to predict product yields and evolution of the polymer under a number of conditions. The main equation used in solid conversion (x_s) prediction in the reactor chamber could be expressed as follows:

$$x_s = a + \left[\frac{(b-a)}{1+\exp(-(T_d - c)/d)} \right] \tag{37}$$

where at a given time (t, s) in the reactor chamber, x_s and T_d are the polymer's solid conversion and dynamic temperature (K), and a, b, c, and d are optimized numerical constants obtained based on the reaction range and heating rate (β).

In the case of HDPE, an expression (optimised) was determined for the case of lower heating rates (β = 5, 10, 25 $^oC\ min^{-1}$), and a different one with higher regressions was obtained for the case of $\beta \geq 50\ ^oC\ min^{-1}$. In fact, such behavioural changes at elevated heating rates ($\beta \geq 50\ ^oC\ min^{-1}$) was previously witnessed by Ceamanos et al. (2002), when they developed their model expressions based on the Arrhenius (1st order) equation. Eqs.(38-39) shows the expressions obtained based on the optimised fitting of HDPE weight loss (expressed as solid conversion, x_s):

$$x_s = 0.039 + \left[\frac{0.96}{1+\exp(-(T_d - 681)/3.84)} \right]; \quad \beta < 50\ ^oC\ min^{-1} \tag{38}$$

$$x_s = 0.002 + \left[\frac{0.88}{1+\exp(-(T_d - 678)/6.34)}\right]; \quad \beta \geq 50\ ^{o}\text{C min}^{-1} \tag{39}$$

The overall activation energy (E_o) estimated from the modelled results was 207.20 kJ mol^{-1}, with a 1.47% error from the value estimated from experimental results. The same range of heating rates was used to develop the expressions of LDPE shown below. A very similar behaviour was witnessed in terms of heating rates on LDPE. High regressions were estimated for $\beta < 50\ ^{o}$C min^{-1} (in terms of optimised parameters) resulting in regression coefficients > 0.90. Eqs.(35-36) shows the expressions obtained based on the optimised fitting of LDPE weight loss (expressed as solid conversion, x_s):

$$x_s = 9.9\times10^{-5} + \left[\frac{0.93}{1+\exp(-(T_d - 538.67)/3.34)}\right]; \quad \beta < 50\ ^{o}\text{C min}^{-1} \tag{35}$$

$$x_s = -3.5\times10^{-5} + \left[\frac{1}{1+\exp(-(T_d - 580.13)/19.88)}\right]; \quad \beta \geq 50\ ^{o}\text{C min}^{-1} \tag{36}$$

This analysis shows that a first-order equation with a reaction order equal to 1 can predict the solid conversion in reactor chambers and is very robust and worth of further investigation, as a standardized method for reactor design. The observed differences can be explained taking into account the variation of the reaction order derived from the complex mechanism of degradation, which is compensated with the variation of the pre-exponential factor when the first-order equation is used in the dynamic fits (Ceamanos et al., 2002). The value of the activation energy remains approximately constant due to the mathematical method used in the data analysis.

3.1.4. Conclusion

The thermal degradation and weight loss kinetics of high and low density polyethylene in an inert atmosphere has been studied by thermogravimetry. Isothermal and dynamic experiments using different heating rates have been carried out with small samples (15 mg) in order to avoid diffusional, heat and mass resistance problems. The kinetic parameters from both types of experiments have been determined, showing similar values to those suggested by other authors. The pyrolysis products from the isothermal runs were analyzed and lumped into four categories: rich gases (C_1-C_4), liquids, waxes and aromatics (single ring structure). The increase of the operating temperature had an inverse effect on the aromatics product yield. A novel kinetics model based on the thermal degradation mechanism and thermal cracking reactions (primary to tertiary), was also proposed in this study. Results of kinetic parameters and activation energies were obtained by experimental and model means. With respect to the dynamic runs, two methods were used to study the kinetics of the complex degradation mechanism, namely the Ozawa-Flynn-Wall (OFW) and the GKT method. A simple yet appropriate equation has been obtained for its subsequent application to non-isothermal processes, based on the polymer weight loss in the reactor chamber. This equation is coherent with the mechanism of thermal degradation for polyethylene when only the steps involving weight loss are considered. However, it is necessary to define the limit conditions

for using the equation suggested, i.e. range of heating rates and operating pre-set temperature. In our work, the overall activation energy (E_o) determined from isothermal experiments was estimated at 125.59 kJ mol^{-1} (HDPE) and 110.75 kJ mol^{-1} (LDPE). The value of activation energy obtained from the isothermal experiments at low temperatures agrees with previous reports, especially when considering the value of the C - C bond energy. The dynamic methodologies followed in this work result in similar order of magnitude for activation energy estimations. This analysis shows that a first-order equation with a reaction order equal to 1 can predict the solid conversion in reactor chambers and is very robust and worth of further investigation, as a standardized method for reactor design.

3.2. Case Study no.2: Kinetics of Dynamic Pyrolysis in a Micro Reactor of Two MDPE Recyclate Grades

3.2.1. Introductory Remarks

In the following section, two recyclate grades of medium density polyethylene (MDPE) were subjected to pyrolysis in dynamic conditions. The pyrolysis of materials in industry is normally performed in dynamic mode with a constant heating ramp (rate) that subjugates the materials of mixed origins together in the unit operation. Two methods were used to determine the kinetics of the material and a simple model based on the fitting of the data obtained is also reported.

3.2.2. Materials and Methods

Two MDPE recyclate grades were supplied from Metals & Recycling Co. (MRC, Kuwait). Grade 1 originated from carrier bags and municipal pipes and grade 2 was recovered from TV frames (LG Company, Kuwait). Both MDPE polymers were supplied in pellet form (3x3 mm granules). In order to verify the density and type of polymer, a density gradient column test was carried out at the time of sample delivery. De-aired water and isopropanol were used to calibrate the column using standardized floats in accordance with ASTM D-1505-96 (1990). Figure 16 shows the calibration curve obtained for the density gradient column (Polymer Characterization Lab, KISR). Grade 1 had a density of 0.9445 gm cc^{-1} and grade 2 had a density of 0.9361 gm cc^{-1}. Both grades of MDPE were not exposed to any weathering, but directly recovered by the company to the processing line. All samples were milled to below 0.1 mm before experimentation, to avoid mass and heat transfer resistance. 15 mgs were weighted and used in all experiments. The TGA set-up previously described was used in the experimentation.

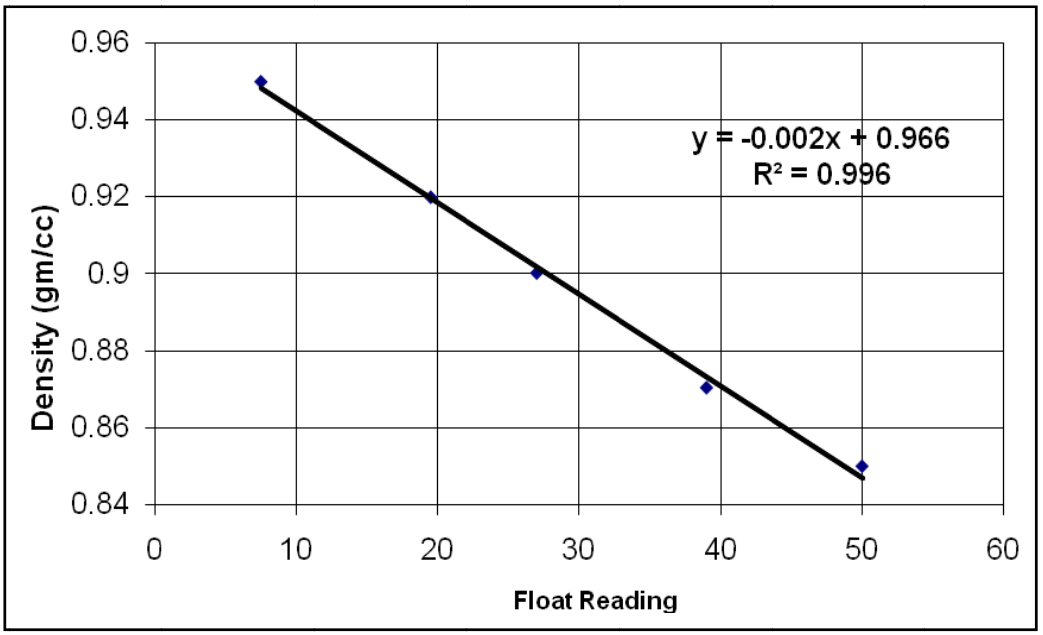

Figure 16. Density gradient column calibration curve used for the density determination of MDPE recyclate grade 1 and 2.

3.2.3. Results and Discussion

Figs.17 and 18 show the solid conversion as a function of temperature; and the first derivative (dx_s/dT) versus T obtained at different β values for MDPE recyclate grade 1, respectively. As it can be observed, the solid conversion was at a maximum value at about 550 ^oC (T_{ref}) but never seems to reach a value of 1. This is attributed to the residual amount of polymer (unpyrolysed) in the case of this recyclate grade. The high content of plasticizer initially present in the plastic is the cause of such behaviour. A significant residual amount of the materials was visible after each run. Yet still, the values of dx_s/dT showed a classical trend in polymer behaviour under inert atmosphere decomposition. The curvature peak was gradually increasing, levelling around 500 ^oC for $\beta = 25$ and 50 $^oC\ min^{-1}$. The reaction range was similar for $\beta = 25$ and 50 $^oC\ min^{-1}$. In the case of MDPE recyclate grade 2, a higher solid conversion was reached. The value of x_s was virtually equal to 1 in the case of $\beta = 5$ $^oC\ min^{-1}$ (Figure 19). Lower conversions were reached in the case of $\beta = 10$, 25 and 50 $^oC\ min^{-1}$. The '*delay effect'* of conversion with higher heating rates was very clear in the case of MDPE recovered from recyclate grades. The first derivative of solid conversion with temperature is shown in Figure 20. dx_s/dT showed a peak shift in the case of higher heating rate (50 $^oC\ min^{-1}$) very similar to previous reports on PE (Ceamanos et al., 2002). In fact, reaction peak and range were changing noticeably with the change of β.

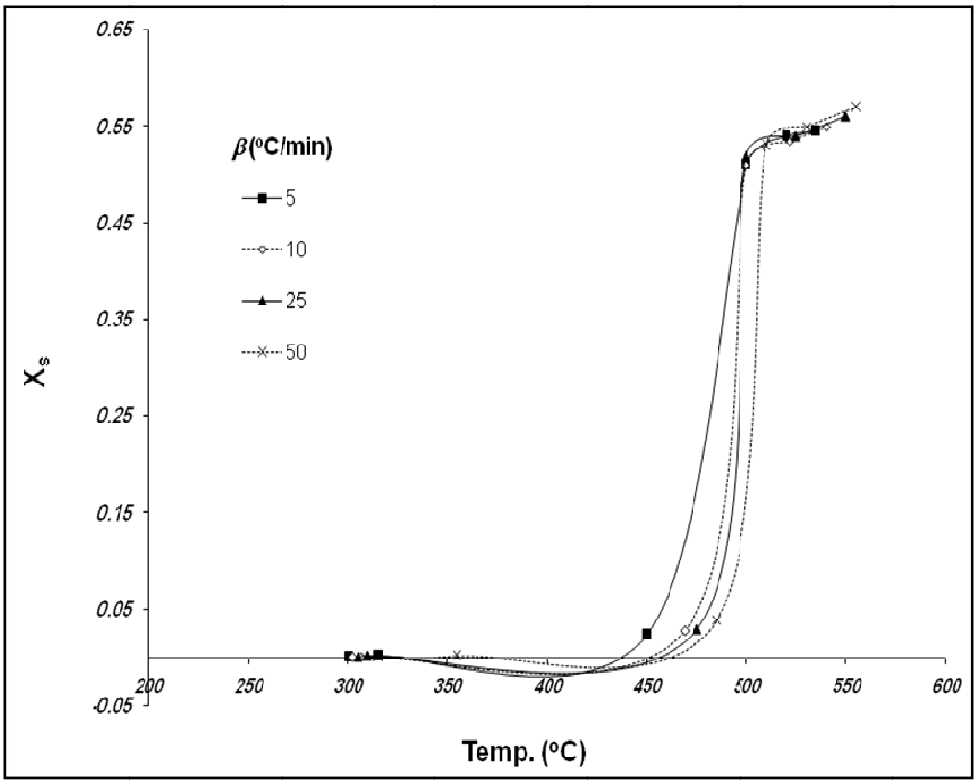

Figure 17. Dynamic run. Solid conversion as a function of temperature (°C) for different heating rates on medium density polyethylene (MDPE) recyclate grade no.1.

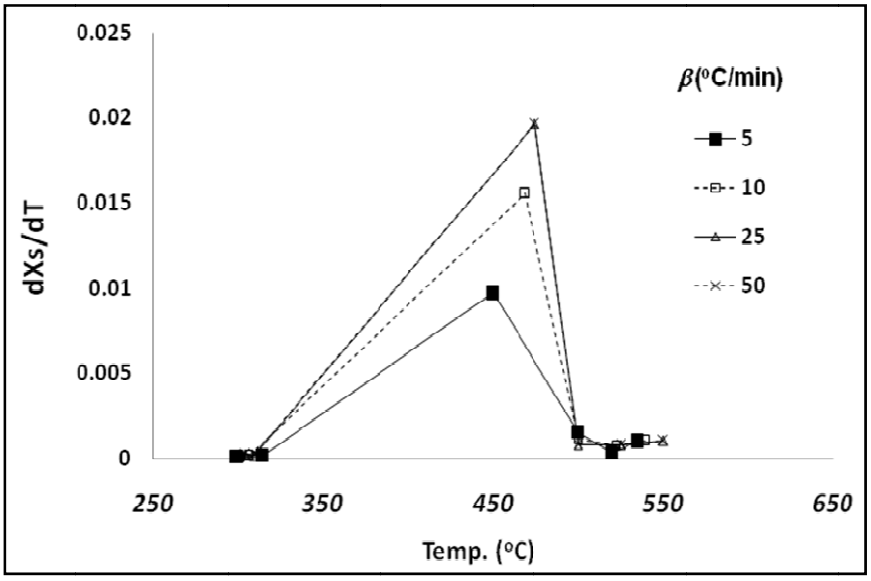

Figure 18. Dynamic run. Values of dx_s/dT as a function of temperature (°C) for different heating rates on medium density polyethylene (MDPE) recyclate grade no.1.

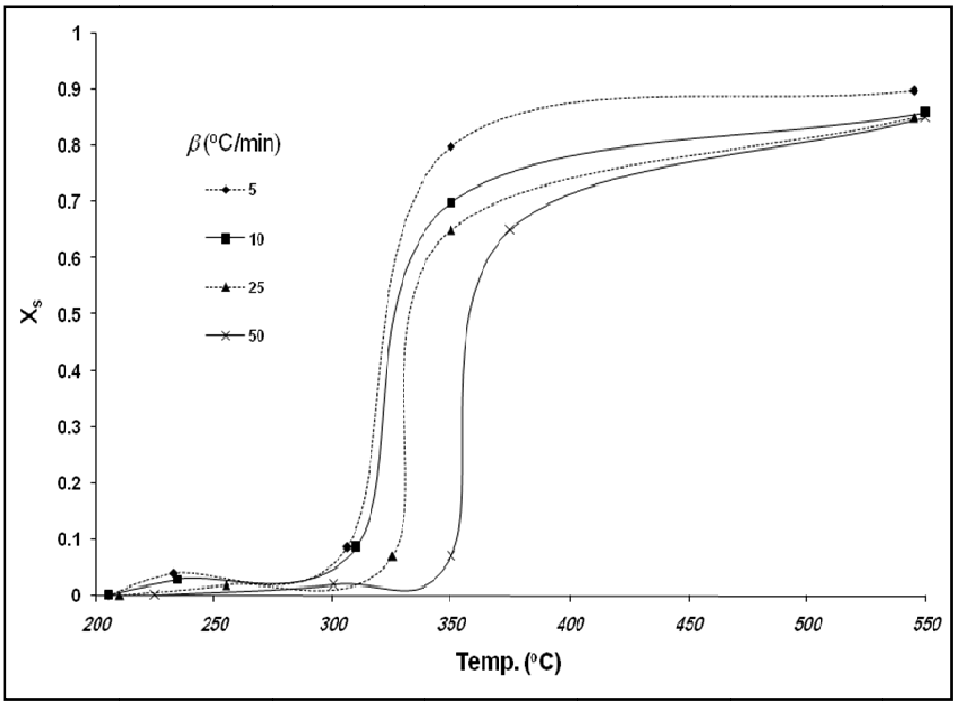

Figure 19. Dynamic run. Solid conversion as a function of temperature (°C) for different heating rates on medium density polyethylene (MDPE) recyclate grade no.2.

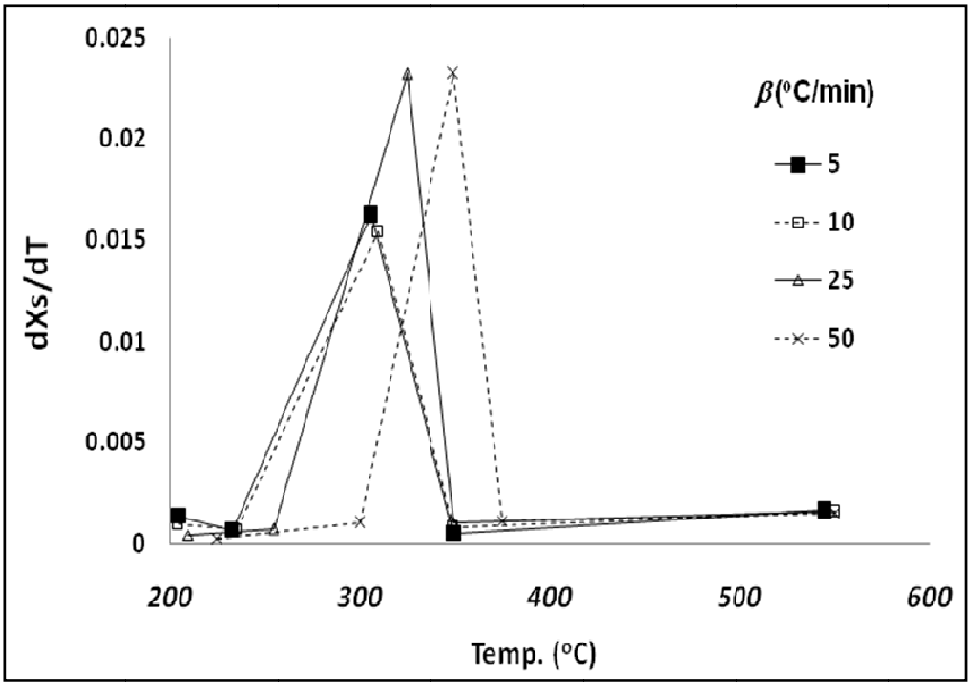

Figure 20. Dynamic run. Values of dx_s/dT as a function of temperature (°C) for different heating rates on medium density polyethylene (MDPE) recyclate grade no.2.

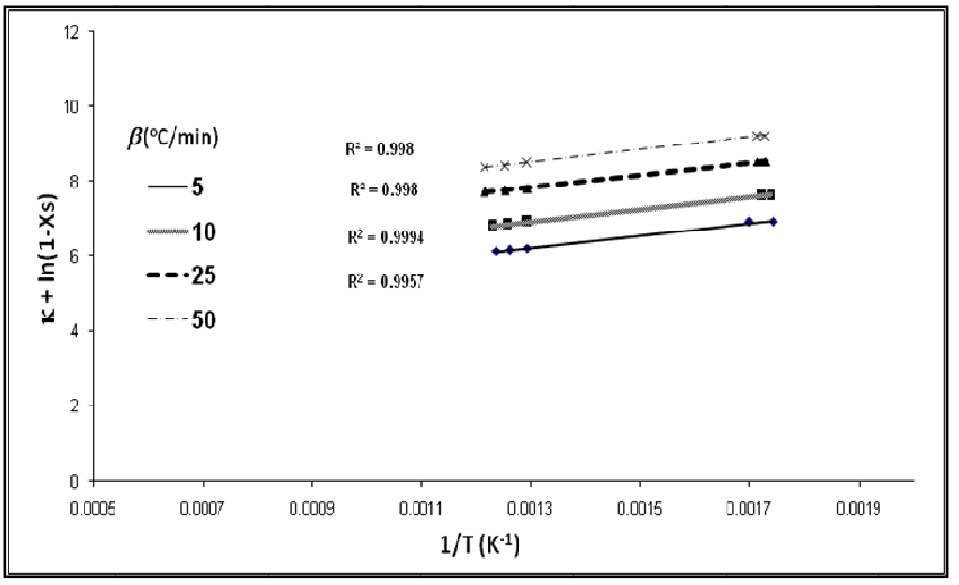

Figure 21. Ozawa-Flynn-Wall (OFW) fitting results showing regression and fitting equations used in activation energies estimation for different heating rates (HR = β) on MDPE recyclate grade no.1 dynamic runs.

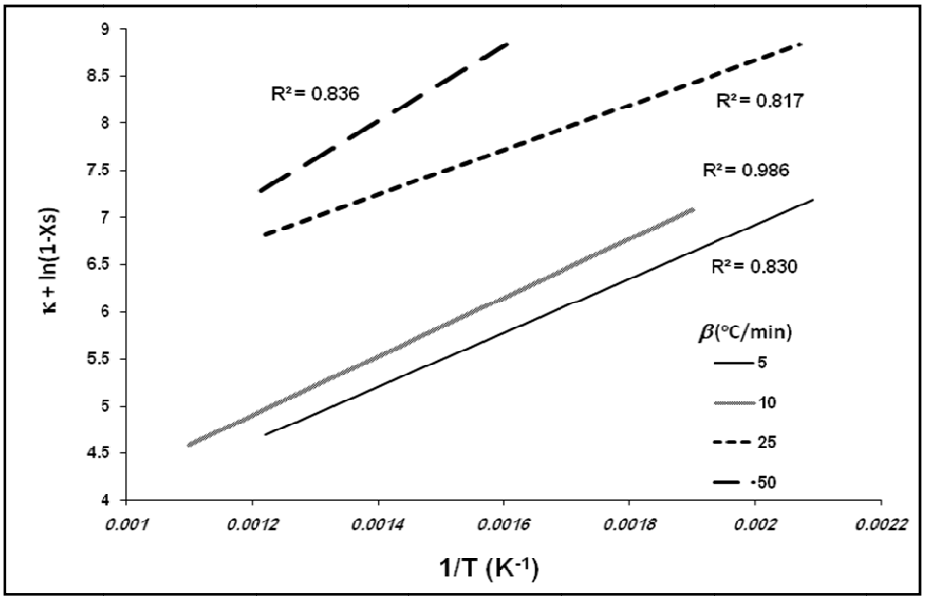

Figure 22. Ozawa-Flynn-Wall (OFW) fitting results showing regression and fitting equations used in activation energies estimation for different heating rates (HR = β) on MDPE recyclate grade no.2 dynamic runs.

Figs. 19 and 20 show the OFW fittings developed from the four different heating ratesused for the TGA experiments on MDPE grades 1 and 2. Tables 8 and 9 show the activation energy (E_a) and overall kinetic rate constants obtained from the OFW method on both MDPE grades. The overall activation energy (E_o) for MDPE recyclate grade nos.1 and 2

were determined to be 203.75 and 143 kJ mol^{-1}, respectively. Tables 10 and 11 show the estimated parameters (*i.e.* E_a, A_o and corresponding errors) obtained from eqs.(2.25.-2.26.) of the GKT for both grades of MDPE. The overall activation energy for MDPE grades no.1 and 2 were estimated to be 205.50 and 146.26 kJ mol^{-1}, respectively.

Table 8. Overall kinetic rate constants (k_o) and apparent activation energies (E_a) obtained using the OFW method on MDPE grade no.1 dynamic runs

Heating rate (β), $^oC\ min^{-1}$	**Overall kinetic rate constant (k_o), min^{-1}**	**Apparent activation energy (E_a), kJ mol^{-1}**
5	1.011×10^6	166.65
10	1.23×10^6	189.00
25	3.50×10^9	220.32
50	4.45×10^{12}	240.01

Table 9. Overall kinetic rate constants (k_o) and apparent activation energies (E_a) obtained using the OFW method on MDPE grade no.2 dynamic runs

Heating rate (β), $^oC\ min^{-1}$	Overall kinetic rate constant (k_o), min^{-1}	Apparent activation energy (E_a), kJ mol^{-1}
5	1.12×10^6	137.71
10	1.1×10^5	139.91
25	3.21×10^9	144.93
50	2.22×10^{12}	147.66

The same range of heating rates previously used for HDPE and LDPE in dynamic modes was used to develop the expressions of MDPE no.1, as shown below. A very similar behaviour was witnessed in terms of heating rates on MDPE. High regressions were estimated for $\beta < 50\ ^oC\ min^{-1}$ (in terms of optimised parameters) resulting in regression coefficients > 0.90. Eqs.(37-38) show the expressions obtained based on the optimised fitting of MDPE no.1 weight loss (expressed as solid conversion, x_s):

$$x_s = 0.001 + \left[\frac{0.549}{1+\exp(-(T_d - 760)/7.6)}\right]; \quad \beta < 50\ ^oC\ min^{-1} \tag{37}$$

$$x_s = 0.009 + \left[\frac{0.5491}{1+\exp(-(T_d - 760)/4.7)}\right]; \quad \beta \geq 50\ ^oC\ min^{-1} \tag{38}$$

Table 10. General kinetics theory parameters, collision theory parameter (A_o), %error between the equation equality and activation energies estimated at each heating rate (β) for medium density polyethylene (MDPE) recyclate grade no.1

Heating rate (β), ^oC/min	Temperature (K)	- E/RT	Error	Mean error (%), A_o and activation energy (kJ mol^{-1})
	573	43.34	0.173	
	588	42.24	0.173	
	723	34.35	0.099	%ME = 0.95%
5	773	32.13	$3.75x10^{-7}$	$A_o = 9.9 \times 10^{+9}$ $K^{-1/2}$ s^{-1}
	793	31.32	0.072	E_a = 206.5 kJ/mol
	808	30.74	0.056	
	575	40.47	0.182	
	580	40.12	0.187	
	742	31.33	0.101	%ME = 7.1%
10	773	30.10	$2.84x10^{-7}$	$A_o = 1 \times 10^{+10}$ $K^{-1/2}$ s^{-1}
	795	29.27	0.038	E_a = 193.47 kJ mol^{-1}
	813	28.62	0.053	
	578	37.63	0.199	
	583	37.31	0.188	
	748	29.08	0.118	%ME = 0.98%
25	773	28.14	$3.24x10^{-7}$	$A_o = 9.99 \times 10^{+7}$ $K^{-1/2}$ s^{-1}
	798	27.26	0.031	E_a = 180.86 kJ mol^{-1}
	823	26.43	0.053	
	578	37.45	0.199	
	583	37.13	0.198	
	748	28.94	0.118	%ME = 1.06%
50	773	28.00	$1.12x10^{-7}$	$A_o = 8.99 \times 10^{+9}$ $K^{-1/2}$ s^{-1}
	798	27.12	0.031	E_a = 179.98 kJ mol^{-1}
	823	26.30	0.052	

Table 11. General kinetics theory parameters, collision theory parameter (A_o), %error between the equation equality and activation energies estimated at each heating rate (β) for medium density polyethylene (MDPE) recyclate grade no.2

Heating rate (β), ^oC/min	Temperature (K)	- E/RT	Error	Mean error (%), A_o and activation energy (kJ mol^{-1})
	478	36.62	0.107	
	506	34.59	0.032	%ME = 0.95%
5	579	30.23	$1.65x10^{-6}$	$A_o = 1.0 \times 10^{+10}$ $K^{-1/2}$ s^{-1}
	623	28.10	0.146	E_a = 145.55 kJ mol^{-1}
	818	21.40	0.424	
	478	34.01	0.099	
	508	32.00	0.034	%ME = 0.14%
	583	27.88	$4.93x10^{-8}$	$A_o = 9.0 \times 10^{+9}$ $K^{-1/2}$ s^{-1}
10	623	26.09	0.140	E_a = 135.17 kJ mol^{-1}
	823	19.75	0.441	
	483	31.46	0.069	
	528	28.77	$2.47x10^{-8}$	%ME = 0.12%
25	598	25.41	0.004	$A_o = 9.99 \times 10^{+9}$ $K^{-1/2}$ s^{-1}
	623	24.39	0.126	E_a = 126.33 kJ mol^{-1}
	818	18.57	0.417	
	498	27.47	0.08	
	573	23.87	$1.68x10^{-8}$	%ME = 0.10%
50	623	21.96	0.05	$A_o = 1.00 \times 10^{+6}$ $K^{-1/2}$ s^{-1}
	648	21.11	0.07	E_a = 113 kJ mol^{-1}
	823	16.62	0.30	

Figs. 23 and 24 show experimental and modelled results as a function of temperature range; Table 12 shows the model performance against experimental results obtained at different heating rates on MDPE no.1 dynamic pyrolysis. Table 13 shows the GKT parameters estimated using the predicted values from the model and %error between experimental and modelled results.

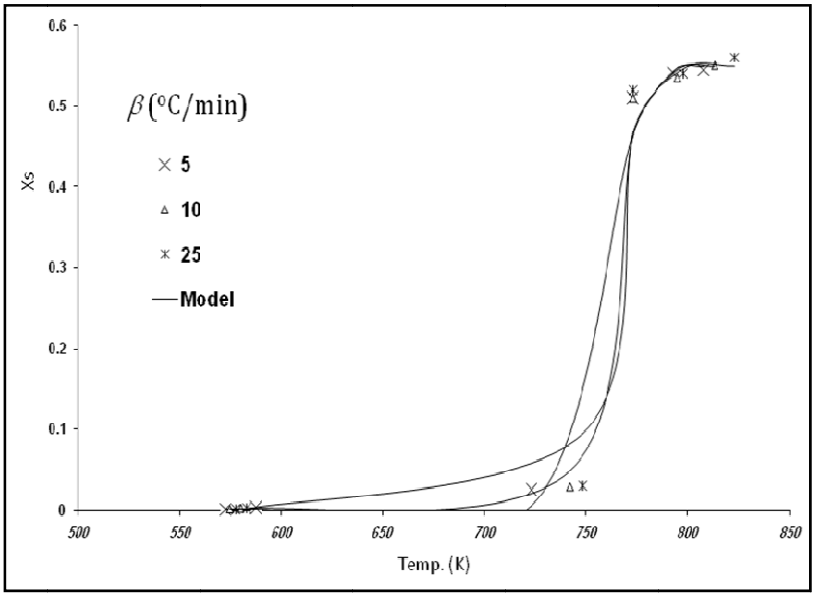

Figure 23. Model and experimental solid conversion as a function of temperature (K) for β = 5, 10 and 25 ^{o}C min^{-1}.

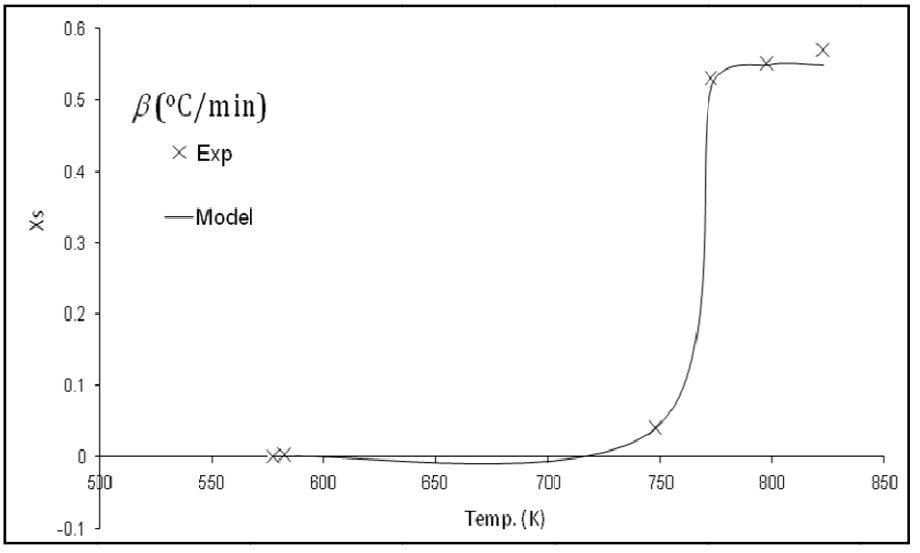

Figure 24.Model and experimental solid conversion as a function of temperature (K) for β = 50 ^{o}C min^{-1}.

Table 12. Model performance against experimental results obtained at different heating rates on MDPE no.1 dynamic pyrolysis

β = 5 °C min^{-1}					β = 10 °C min^{-1}				
Temp. (K)	x_s (Exp)	Model	Error		Temp. (K)	x_s (Exp)	Model	Error	
573	0.001	0.001	5 x	SE=1.38	575	0.001	0.001	5.12 x	SE=1.13
588	0.002	0.001	10^{-5}	ME=0.23	580	0.001	0.001	10^{-5}	ME=0.18
723	0.02	0.005	0.49	R^2=0.997	742	0.02	0.04	0.33	R^2=0.997
773	0.50	0.46	0.78		773	0.50	0.465	0.69	
793	0.54	0.54	0.08		795	0.53	0.54	0.08	
808	0.54	0.549	0.005		813	0.55	0.54	0.01	
			0.007					0.0009	
β = 25 °C min^{-1}					β = 50 °C min^{-1}				
Temp. (K)	x_s (Exp)	Model	Error		Temp. (K)	x_s (Exp)	Model	Error	
			5.12 x	SE= 2.79					SE=0.72
578	0.001	0.001	10^{-5}	ME= 0.46	578	0.001	0.0009	0.1	ME=0.12
583	0.002	0.001	0.49	R^2= 0.993	583	0.002	0.0009	0.55	R^2=0.999
748	0.03	0.09	2.16		748	0.04	0.04	0.01	
773	0.52	0.46	0.10		773	0.53	0.51	0.02	
798	0.54	0.54	0.01		798	0.55	0.54	0.0003	
823	0.56	0.54	0.01		823	0.57	0.54	0.03	

Table 13. GKT parameters using modeled results for dynamic TGA on MDPE no.1

Heating rate (β), °C/min	**Temperature (K)**	**- E/RT**	**Error**	**Mean error (%), A_o and activation energy (kJ mol^{-1})**
	573	43.34	0.20	
	588	42.24	0.13	
	723	34.35	0.09	%ME = 0.58%
5	773	32.13	0.02	A_o= 9.9 x 10^{+9} K$^{-1/2}$ s^{-1}
	793	31.32	0.06	E_a = 206.50 kJ/mol
	808	30.74	0.05	
	575	40.47	0.24	
	580	40.12	0.20	
	742	31.33	0.09	%ME = 7.1%
10	773	30.10	0.03	A_o= 1 x 10^{+10} K$^{-1/2}$ s^{-1}
	795	29.27	0.07	E_a = 193.47 kJ mol^{-1}
	813	28.62	0.05	
	578	37.63	0.27	
	583	37.31	0.22	
	748	29.08	0.11	%ME = 0.79%
25	773	28.14	0.04	A_o= 9.99 x 10^{+7} K$^{-1/2}$ s^{-1}
	798	27.26	0.09	E_a = 180.86 kJ mol^{-1}
	823	26.43	0.05	
	578	37.45	0.64	
	583	37.13	0.19	
	748	28.94	0.11	%ME = 2.07%
50	773	28.00	0.01	A_o= 8.99 x 10^{+9} K$^{-1/2}$ s^{-1}
	798	27.12	0.20	E_a = 179.98 kJ mol^{-1}
	823	26.30	0.05	

The overall activation energy (E_o) estimated from the modelled results was 205.59 kJ mol^{-1}, with a 0.04% error from the value estimated from experimental results (205.501 kJ mol^{-1}). The same range of heating rates was used to develop the expressions of MDPE no.2 shown below. A very similar behaviour was witnessed in terms of heating rates on MDPE. High regressions were estimated for β < 50 ^{o}C min^{-1} (in terms of optimised parameters) resulting in regression coefficients > 0.90. Eqs.(39-40) show the expressions obtained based on the optimised fitting of MDPE no.2 weight loss (expressed as solid conversion, x_s):

$$x_s = 0.0009 + \left[\frac{0.88}{1+\exp(-(T_d - 608)/10)}\right]; \quad \beta < 50\ ^{o}\text{C min}^{-1} \tag{39}$$

$$x_s = 0.0002 + \left[\frac{0.9}{1+\exp(-(T_d - 640)/6.7)}\right]; \quad \beta \geq 50\ ^{o}\text{C min}^{-1} \tag{40}$$

Figs. 25 and 26 show experimental and modelled results as a function of temperature range and Table 14 shows the model performance against experimental results obtained at different heating rates on MDPE no.2 dynamic pyrolysis. Table 15 shows the GKT parameters estimated using the predicted values from the model and %error between experimental and modelled results.

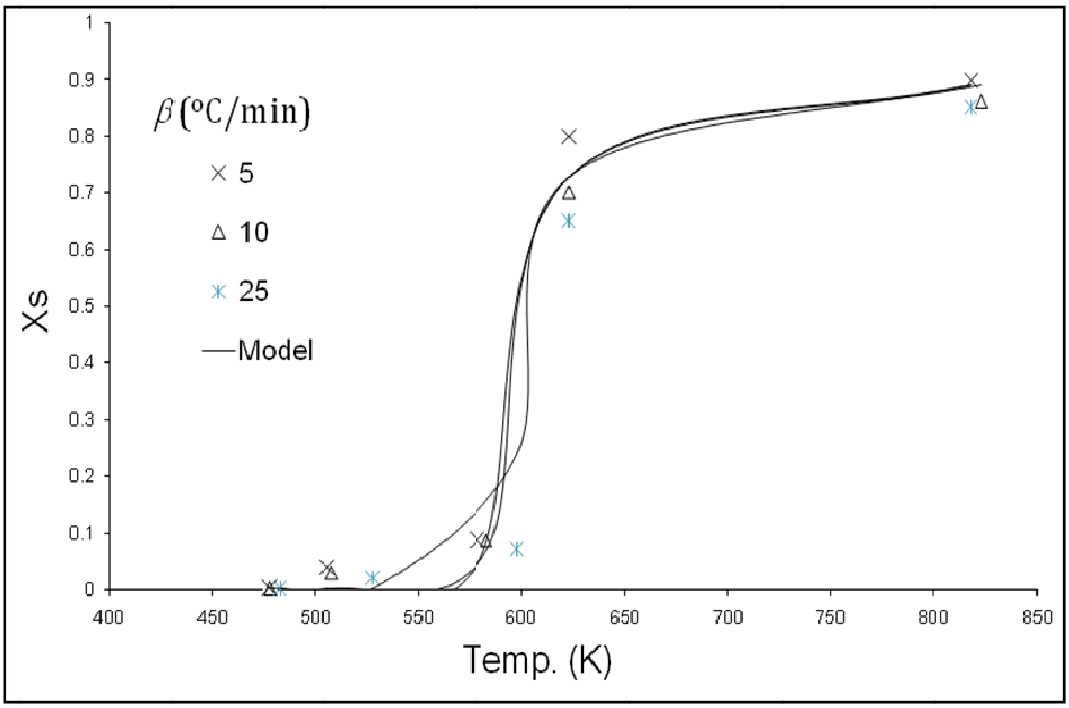

Figure 25. Model and experimental solid conversion as a function of temperature (K) for β = 5, 10 and 25 ^{o}C min^{-1}.

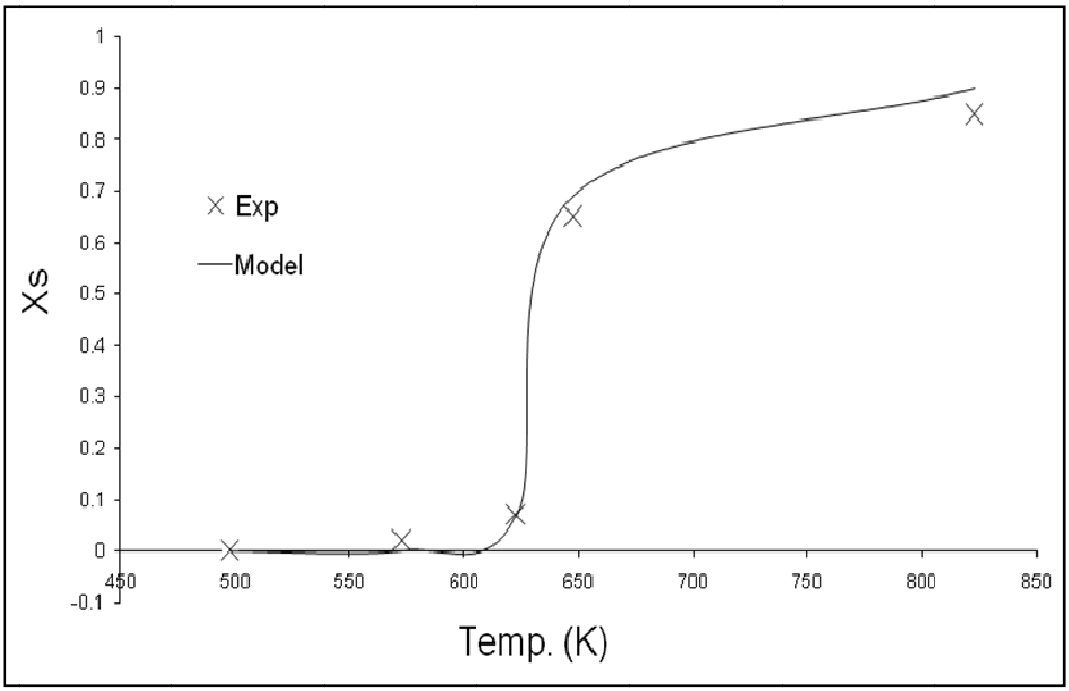

Figure 26. Model and experimental solid conversion as a function of temperature (K) for $\beta = 50\ ^{o}C\ min^{-1}$.

Table 14. Model performance against experimental results obtained at different heating rates on MDPE no.2 dynamic pyrolysis

$\beta = 5\ ^{o}C\ min^{-1}$					$\beta = 10\ ^{o}C\ min^{-1}$				
Temp. (K)	x_s (Exp)	Model	Error		Temp. (K)	x_s (Exp)	Model	Error	
478	0.001	0.0009	0.09	SE=1.62	478	0.001	0.0009	0.09	SE=1.34
506	0.04	0.0009	0.97	ME=0.32	508	0.03	0.0009	0.96	ME=0.26
579	0.08	0.04	0.44	R^2=0.998	583	0.08	0.06	0.20	R^2=0.999
623	0.8	0.72	0.09		623	0.70	0.72	0.03	
818	0.89	0.89	0.01		823	0.86	0.89	0.03	
$\beta = 25\ ^{o}C\ min^{-1}$					$\beta = 50\ ^{o}C\ min^{-1}$				
Temp. (K)	x_s (Exp)	Model	Error		Temp. (K)	x_s (Exp)	Model	Error	
483	0.001	0.0009	0.09	SE= 3.63	498	0.001	0.0002	0.79	SE=1.96
528	0.02	0.001	0.94	ME=	573	0.02	0.0002	0.98	ME=0.39
598	0.07	0.24	2.42	0.72	623	0.07	0.06	0.05	R^2=0.999
623	0.65	0.72	0.11	R^2=	648	0.65	0.69	0.06	
818	0.85	0.89	0.04	0.983	823	0.85	0.90	0.05	

Table 15. GKT parameters using modeled results for dynamic TGA on MDPE no.2

Heating rate (β), ^{o}C/min	Temperature (K)	- E/RT	Error	Mean error (%), A_o and activation energy (kJ mol^{-1})
5	478 506 579 623 818	36.62 34.59 30.23 28.10 21.40	0.08 0.03 0.002 0.13 0.42	%ME = 1.3% A_o= 1.0 x 10^{+10} K$^{-1/2}$ s^{-1} E_a = 145.55 kJ mol^{-1}
10	478 508 583 623 823	34.01 32.00 27.88 26.09 19.75	0.09 0.03 0.001 0.13 0.42	%ME = 0.14% A_o= 9.0 x 10^{+9} K$^{-1/2}$ s^{-1} E_a = 135.17 kJ mol^{-1}
25	483 528 598 623 818	31.46 28.77 25.41 24.39 18.57	0. 06 0.05 0.005 0.12 0.39	%ME = 0.12% A_o= 9.99 x 10^{+9} K$^{-1/2}$ s^{-1} E_a = 126.33 kJ mol^{-1}
50	498 573 623 648 823	27.47 23.87 21.96 21.11 16.62	0.14 0.01 0.05 0.07 0.28	%ME = 0.10% A_o= 1.00 x 10^{+6} K$^{-1/2}$ s^{-1} E_a = 113 kJ mol^{-1}

The overall activation energy (E_o) estimated from the modelled results was 145.20 kJ mol^{-1}, with a 0.54% error from the value estimated from experimental results (146.26 kJ mol^{-1}).

3.2.4. Conclusion

Dynamic TG pyrolysis was performed on two grades of recyclate grades MDPE. Different heating rates were utilized in this study. The high content of plasticizer and impurities initially present in the plastic is the cause of such behaviour. In the case of MDPE no.2, a higher solid conversion was reached. The value of x_s was virtually equal to 1 in the case of β = 5 ^{o}C min^{-1}. Lower conversions were reached in the case of β = 10, 25 and 50 ^{o}C min^{-1}. The '*delay effect'* of conversion with higher heating rates was very clear in the case of MDPE recovered from recyclate grades. The kinetics parameters were determined using two methods, the OFW and the GKT. Order of magnitude is always of desire when such calculations are executed. Nonetheless, the deviation in results could be expressed by mathematical treatment method and order of reaction, which was taken as one in both cases. In the case of MDPE no.1, the k_o ranged between 1.011 x 10^6 to 4.45 x 10^{12} min^{-1} depending on the heating rate. The apparent activation energy (E_a) was estimated in the range of 166.65 to 240.01 kJ mol^{-1}. As for MDPE no.2, k_o ranged between 1.12 x 10^6 to 2.22 x 10^{12} min^{-1} corresponding to an activation energy (E_a) in the range of 137.71 to 147.66 kJ mol^{-1}. The overall activation energy (E_o) for MDPE recyclate grade nos.1 and 2 were determined to be

203.75 and 143 kJ mol^{-1}, respectively (OFW). The overall activation energy for MDPE grades no.1 and 2 were estimated to be 205.50 and 146.26 kJ mol^{-1}, respectively (GKT).

4. FINAL AND CONCLUDING REMARKS

In this chapter, we have demonstrated the variability of pyrolysis as a petrochemical feedstock recovery route. Not only rich cut products were retrieved by the process, but major reactor and reaction engineering parameters were estimated. After reviewing the industrial status of the process, one can withdraw the following conclusions:

- The pyrolysis process *per se*, is in need of an end product design. This will target certain products and yield higher amounts of said products that can cover the demand of the petrochemical markets.
- More pilot and industrial scale operations are necessary to demonstrate the process validity depending on the materials treated.

As for the design and its numerous approached undertaken in the past few years, weight loss kinetics are in need of more in depth studies to ascertain the optimum designs of thermolysis reactors. Polyolefins were tested in this study and proven a high source of rich product cuts that integrated processes can benefit from.

REFERENCES

Aguado, J., Serrano, D.P., Miguel, G.S., Escola, J.M., Rodriguez, J.M., 2007. Catalytic activity of zeolitic and mesostructured catalysts in the cracking of pure and waste polyolefins, *J Anal App Pyrolysis*, 78(1); 153-61.

Al-Salem, S.M., Lettieri, P., Baeyens, J., 2009a. Recycling and recovery routes of plastic solid waste (PSW): A review. *Waste Manage*, 29(10): 2625-2643.

Al-Salem, S.M., Lettieri, P. and Baeyens, J., 2009b. Thermal treatment of different grades and types of polyethylene (PE) wasted articles, In: Proc 8th World Congress of Chemical Engineering, Montreal (Quebec), Canada, 23-27 August.

Al-Salem, S.M., Lettieri, P. and Baeyens, J., 2009c. Thermal pyrolysis of High Density Polyethylene (HDPE), In: Proc 9th European Gasification Conference: Clean energy and chemicals, Düsseldorf, Germany, 23-25 March.

Al-Salem, S.M., Lettieri, P. and Baeyens, J., 2010. Kinetics and product distribution of end of life tyres (ELTs) pyrolysis: A novel approach in polyisoprene and SBR thermal cracking, J Hazard Mat (In Press, DOI: 10.1016/j.jhazmat.2009.07.127)

APC, 2008. American Plastics Council, Facts and figures. Arlington VA 22209, Technical paper.

APM EU, 2008. Association of Plastic Manufacturers in Europe, An analysis of plastics consumption in Europe. Code: 2002 APME.

Asanuma, M., Ariyama, T., 2004. Recycling of waste plastics in blast furnace, *J Japan Inst Energy*, 83(4); 252–256.

Aznar, M.P., Caballero, M.A., Sancho, J.A., Francs, E., 2006. Plastic waste elimination by co-gasification with coal and biomass in fluidized bed with air in pilot plant, *Fuel Process Tech*, 87(5); 409 – 420.

Barlow, C., 2008. Intelligent recycling, Presented at the Department of Engineering, Institute for Manufacturing, University of Cambridge, England (UK).

Beede, D.N., Bloom, D.E., 1995. Economics of the generation and management of MSW. NBER working papers 5116, National Bureau of Economic Research, Inc.

Bilbao, R., Mastral, J.F., Aldea, M.E., Ceamanos, J., 1997a. Kinetic study for the thermal decomposition of cellulose and pine sawdust in an air atmosphere. *J Anal App Pyrolysis*, 39(1); 53-64.

Bilbao, R., Mastral, J.F., Aldea, M.E., Ceamanos, J., 1997b. The influence of oxygen in atmosphere on the thermal decomposition of lignocellulosic materials. *J Anal App Pyrolysis*, 42(2); 189-202.

Bilbao, R., Mastral, J.F., Ceamanos, J., Aldea, M.E., 1996a. Kinetics of the thermal decomposition of polyurethane foams in nitrogen and air atmospheres. *J Anal App Pyrolysis*, 37(1); 69-82.

Bilbao, R., Mastral, J.F., Ceamanos, J., Aldea, M.E., 1996b. Modelling of the pyrolysis of wet wood. *J Anal App Pyrolysis*, 36(1); 81-97.

Bockhorn, H., Hornung, A., Hornung, U., Schawaller, D., 1999. Kinetic study on the thermal degradation of polypropylene and polyethylene. J Anal App Pyrolysis, 48(2); 93-109.

Brophy, J.H., Hardmann, S., Wilson, D.C., 1997. Polymer Cracking for Feedstock Recycling of Mixed Plastic Wastes. In: Chemical Aspects of Plastics Recycling, Hoyle, W., D.R. Karsa (eds). The Royal Society of Chemistry Information Services, Cambridge, England (UK).

Budrugeac, P., 2005. Some methodological problems concerning the kinetic analysis of non-isothermal data for thermal and thermo-oxidative degradation of polymers and polymeric materials. *Polym Degrad Stab*, 89(2); 265-273.

Caykara, T., Eroglu, M.S., Güven, O., 1999. Thermal and oxidative degradation of vinyl triethoxy silane – methyl methacrylate copolymers. *Polym Degrad Stab*, 63(1); 65-70.

Ceamanos, J., Mastral, J.F., Millera, A., Aldea, M.E., 2002. Kinetics of high density polyethylene: Comparison of isothermal and dynamic experiments. *J Anal App Pyrolysis*, 65(2); 93-110.

Ciliz, N.K., Ekinci, E., Snape, C.E., 2004. Pyrolysis of virgin and waste polyethylene and its mixtures with waste polyethylene and polystyrene. *Waste Manage*, 2(24); 173–81.

Coats, A.W., Redfern, J.P., 1964. Kinetic parameters from thermogravimetric data. *Nature*, 201(4914); 68-69.

Conesa, J.A., Font, R., Marcilla, A., Garcia, A.N., 1994a. Pyrolysis of polyethylene in a fluidized bed reactor. *Energy Fuels*, 8(6); 1238-1246.

Conesa, J.A., Marcilla, A., Font, R., 1994b. Kinetic model of the pyrolysis of polyethylene in a fluidized bed reactor. *J Anal App Pyrolysis*. 30(1); 101-120.

Conesa, J.A., Marcilla, A., Font, R., Caballero, J.A., 1996. Thermogravimetric studies on the thermal decomposition of polyethylene. *J Anal App Pyrolysis*, 36(1); 1-15.

Cozzani, V., Nicolella, C., Rovatti, M., Tognotti, L., 1997. Influence of gas phase reactions on the product yields obtained in the pyrolysis of polyethylene. *Ind Eng Chem Res*, 36(2); 342– 348.

Cunliffe, A.M., Jones, N., Williams, P.T., 2003. Recycling of fibre-reinforced polymeric waste by pyrolysis: thermo-gravimetric and bench-scale investigations. J Anal App Pyrolysis, 70(2); 315-338.

Dahiya, J.B., Kumar, K., Muller-Hagedorn, M. , Bockhorn, H., 2008. Kinetics of isothermal and non-isothermal degradation of cellulose: model-based and model-free methods. Polym Int, 57(5); 722-729.

EEC, 2009. Recycling plastic waste: Recommendation action, AR no.5, Oregon State University, Technical report.

Fogler, H.S., 2005. Elements of Chemical Reaction Engineering, 4th ed, Prentice Hall.

Gobi, 2002. New Forecasts for Polypropylene, Polystyrene and Polyurethane. Gobi International, May 20.

Heyde, M., Kremer, S., 1999. LCA Packaging Plastics Waste. LCA Documents Vol. 2, No. 5, EcoMed, Landsberg, Germany.

Horvat, N., 1996. Tertiary polymer recycling: Study of polyethylene thermolysis and polyethylene oil hydrogenation, PhD Thesis, Chemical Engineering Department, University of Waterloo, Canada.

Horvat, N., Ng, F.T.T., 1999. Tertiary polymer recycling: study of polyethylene thermolysis as a first step to synthetic diesel fuel, *Fuel*, 78(4); 459-470.

Howard, G.T., 2002. Biodegradation of polyurethane: A review. Int Biodeter Biodegr, 49(1); 245–252.

Juniper, 2005. Pyrolysis and gasification fact sheet. Juniper consultancy group report, Gloucestershire, England (UK).

Junmeng, C., Fang, H., Weiming, Y., Fusheng, Y., 2006. A new formula approximating the Arrhenius integral to perform the nonisothermal kinetics. *Chem Eng J*, 124(1-3); 15-18.

Junmeng, C., Liu, R., Wang, Y., 2007. Kinetic analysis of solid-state reactions: A new integral method for nonisothermal kinetics with the dependence of the pre-exponential factor on the temperature ($A = A_0T^n$). *Solid State Sci*, 9(5); 421-428.

Kaminsky, W., Schlesselmann, B., Simon, C., 1995. Olefins from polyolefins and mixed plastics by pyrolysis. J Anal App Pyrolysis, 32; 19-27.

Kato, K., Fukuda, K., Takamatsu, N., 2004. Waste plastics recycling technology using coke ovens, J Japan Inst Energy, 83(4); 248–251.

Khan, A.R., Al-Roomi, Y.M., Mathew, J., Sari, M., 2001. Kinetic evaluation of an oligomeric amidation reaction. J App Polym Sci, 82(10); 2534-2543.

Khan, A.R., Mathew, J., Al-Shayji, K., Sari, M., 2002. Copolyesteramides: synthesis and kinetic analysis. Euro Polym J, 38(5); 1013-1023.

Ledesma, E.B., Kalish, M.A., Nelson, P.F., Wornat, M.J., Mackie, J.C., 2000. Formation and fate of PAH during pyrolysis of fuel-rich combustion of coal primary tar. *Fuel*, 79(14); 1801–1814.

Liu, N.A., Fan, W.C., 1999. Critical consideration on the Freeman and Carroll method for evaluating global mass loss kinetics of polymer thermal degradation. *Thermochim Acta*, 338(1-2); 85-94.

Malkow, T., 2004. Novel and innovative pyrolysis and gasification technologies for energy efficient and environmentally sound MSW disposal. Waste Manage, 24(1); 53-79.

Mastellone, M.L., 1999. Thermal treatments of plastic wastes by means of fluidized bed reactors. PhD thesis, Department of Chemical Engineering, Second University of Naples, Italy.

Mastral, F. J., Esperanza, E., Berrueco, C., Juste, M., Ceamanos, J., 2003. Fluidized bed thermal degradation products of HDPE in an inert atmosphere and in air–nitrogen mixtures. *J Anal App Pyrolysis*, 70(1); 1-17.

Mastral, J.F., Berrueco, C., Ceamanos, J., 2007. Theoretical prediction of product distribution of the pyrolysis of high density polyethylene. J Anal App Pyrolysis, 80(2); 427-438.

Mathew, J., Khan, A.R., Ahmed, A.S.M., 2005. Kinetics of co-polyesters of hydroquinone diacetate and its methyl derivative with terephthalic acid. *Des Monom Polym*, 8(4); 365-381.

McCaffrey W.C., Brues, M.I., Cooper, D.C., Kamal, M.R., 1996. Thermolysis of polyethylene/polystyrene mixtures. *J App Polym Sci*, 60(12); 2133-2140.

McCaffrey W.C., Kamal, M.R., Cooper, D.G., 1995. Thermolysis of polyethylene. *Polym Degrad Stab*, 47(1); 133-139.

Miscolczi, N., Bartha, L., Dea´k, G., Jo´ver, B., 2004. Thermal degradation of municipal solid waste for production of fuel-like hydrocarbons. *Polym Degrad Stab*, 86(2); 357– 366.

Oh, S.C., Jun, H.C., Kim, H.T., 2003. Thermogravimetric evaluation for pyrolysis kinetics of styrene-butadiene rubber, *J Chem Eng Japan*, 36(8); 1016-1022.

Paik, P., Kar, K., 2008. Kinetics of thermal degradation and estimation of lifetime for polypropylene particles: Effects of particle size. Polym Degrad Stab, 93(1); 24-35.

Parfitt, J., 2002. Analysis of household waste composition and factors driving waste increases, Waste and Resources Action Programme (WRAP) for strategy unit, Government Cabinet Office, London, England (UK).

Park, J.W., Oh, S.C., Lee, H.P., Kim, H.T., Yoo, K.O., 2000. A kinetic analysis of thermal degradation of polymers using a dynamic method. Polym Degrad Stab, 67(3); 535-540.

PEU, 2008. Plastics Europe, The compelling facts about plastics 2007: An analysis of plastics production, demand and recovery for 2007 in Europe. Published by the Association of Plastics Manufactures (Plastics Europe), October.

Pinto, F., Franco, C., Andre, R.N., Tavares, C., Dias, M., Gulyurtlu, I., 2003. Effect of experimental conditions on co-gasification of coal, biomass and plastics wastes with air/steam mixture in a fluidized bed system. Fuel, 15–17(82); 1967–1976.

Ponzio A, Kalisz S, Blasiak W., 2006. Effect of operating conditions on tar and gas composition in high temperature air/steam gasification (HTAG) of plastic containing waste, *Fuel Process Tech*; 87(3); 223-233.

Ranzi, E., Dente, M., Faravelli, T., Bozzano, G., Fabini, S., Nava, R., Cozzani, V., Tognotti, L., 1997. Kinetic modelling of polyethylene and polypropylene thermal degradation. *J Anal App Pyrolysis*, 40-41, 305-319.

Ray, R., Bhattacharya, P., Chowdhury, R., 2004. Simulation and modelling of vegetable market wastes pyrolysis under progressive deactivation condition. *Can J Chem Eng*, 82(3); 566-579.

Scheirs, J., 1998. Polymer recycling: Science, technology and application, Wiley-Blackwell, 1st edition.

Steiner, C., Kameda, O., Oshita, T., Sato, T., 2002. EBARA's fluidized bed gasification: Atmospheric 2x225 t/d for shredding residues recycling and two-stage pressurized 30 t/d for ammonia synthesis from waste plastics, In: Proc 2nd int sym feedstock recycle plastics innov plastics recycl tech, 8–11 September, Ostend, Belgium.

Stiles, H.N., Kandiyoti, R., 1989. Secondary reactions of flash pyrolysis tars measured in a fluidized bed pyrolysis reactor with some novel design features. Fuel, 68(3); 275– 282.

Troitsch, J., 1990. International Plastics Flammability Handbook, Hanser Publishers, Munich, Germany.

Tukker, A., de Groot, H., Simons, L., Wiegersma, S., 1999. Chemical recycling of plastic waste: PVC and other resins. European Commission, DG III, Final report, STB-99-55 Final; Delft, the Netherlands.

USEPA, 2002. Municipal Solid Waste in the United States: 2000 Facts and Figures. Executive summary. United States Environmental Protection Agency, Office of solid waste management and emergency response (5305W), EPA530-S-02-001, June.

USEPA, 2008. Municipal Solid Waste in the United States: 2007 Facts and Figures. Executive summary, United States Environmental Protection Agency, Office of solid waste management and emergency response (5306P), EPA530-R-08-010, November.

Valavanidis, A., Iliopoulos, N., Gotsis, G., Fiotakis, K., 2008. Persistent free radicals, heavy metals and PAHs generated in particulate soot emissions and residue ash from controlled combustion of common types of plastic. *J Hazard Mater*, 156(1-3); 277–284.

Westerhout, R.W.J., Kuipers, J.A.M., van Swaaij, W.P.M., 1998. Experimental determination of the yield of pyrolysis products of polyethylene and polypropylene. Influence of reaction conditions. *Ind Eng Chem Res*, 37(3); 841–847.

Williams, E.A., Williams, P.T., 1997. The pyrolysis of individual plastics and plastic mixture in a fixed bed reactor. *J Chem Tech Biot*, 70(1); 9-20.

Williams, E.A., Williams, P.T., 1999a. Product composition from the fast pyrolysis of polystyrene. *Environ Tech*, 20(11); 1109-1118.

Williams, E.A., Williams, P.T., 1999b. Fluidized bed pyrolysis of low density polyethylene to produce petrochemical feedstok. *J Anal App Pyrolysis*, 51(1-3); 107-126.

Yang, J., Gupta, M., Roy, X., Roy, C., 2004. Study of tire particle mixing in a moving and stirred bed vacuum pyrolysis reactor**,** *Can J Chem Eng*, 82(3); 510-519.

Yoshioka, T., Gause, G., Eger, C., Kaminsky, W., Okuwaki, A., 2004. Pyrolysis of poly (ethylene terephthalate) in a fluidized bed plant, Polym Degrad Stab, 86(3); 499–504.

ZEUS, 2005. Thermal degradation of plastics, ZEUS Industrial Products, Technical whitepaper.

Zia, K.M., Bhatti, H.N., Bhatti, I.A., 2007. Methods for polyurethane and polyurethane composites, recycling and recovery: A review. *React Funct Polym*, 67(8); 675–692.

Zolezzi, M., Nicolella, C., Ferrara, S., Iacobucci, C. and Rovatti, M., 2004. Conventional and fast pyrolysis of automobile shredder residues (ASR). *Waste Manage*, 24(7); 691– 699.

INDEX

A

B

C

D

E

F

G

H

I

J

K

L

M

N

O

P

Q

R

S

T

U

V

W

X

Y

Z